DE MONTFORT
UNIVERSITY
LEICESTER

MODELLING OF DISTORTION PROBLEMS IN OMT SUPER-CONDUCTING MAGNETIC FIELDS

PhD Thesis
De Montfort University

Xianri Huang

2003

Abstract

Magnetic Resonance Imaging (MRI) is the most precise technology to date to obtain images inside of human body in a non-invasive way for diagnostic purposes. In the development of new types of commercial super-conductive MRI system, the structural vibration of the MRI system becomes significant in causing degradation of high-quality imaging. There is now an urgent need for an understanding of the mechanism between image degradation and structural vibration, which can be applied within the design of a cryostat of the MRI system to improve image quality and to reduce production costs.

This research consists of theoretical and experimental developments for image distortion problems (or MR phase-angle distortion problems) due to structural vibrations, including: (1) any possible structural vibrations which may cause the phase-angle distortions; (2) the characteristics of structural vibrations of a cryostat; (3) the relationship between the magnetic disturbance and structural vibrations; (4) the relationship between the phase-angle distortion and magnetic disturbance; (5) the phase-angle distortions in existing products in Oxford Magnet Technology(OMT); (6) reliability of a traditional instrument applied in the measurement of phase-angle distortions and magnetic disturbances; (7) the novel methods of measurement which are effective in evaluating the phase-angle distortions.

To provide the groundwork for this research, mathematical models of NMR and MRI are presented. They form the fundamental work to uncover the reason of the image or phase-angle distortions in a MRI system. The mechanical structure of a generic MRI cryostat is discussed to indicate the main components and suspensions through which vibrations could be transmitted. The components of an MRI system are also illustrated to give a complete view of a MRI system. The principle of a NMR spectrometer and a generic model of MR phase-angle measurement are explained. They are a fundamental

part to explain or analyse the many experiments. A generic surface harmonic is formulated in spherical polar coordinates. It is used by engineers both in calculation of magnetic field homogeneity and in the design of a MRI magnet with specific homogeneous magnetic field, although the latter one is not covered in this thesis. Maxwell's equations and the Biot-Savart Law are presented to explain the interaction between eddy-currents and magnetic fields. Generic methods of vibration isolation and control are also summarized to assess and recommend possible modifications of the cryostat structure.

The problem of phase-angle distortion is analysed systematically considering various possible sources of the distortion and the mechanism. The analysis results in focuses on several main aspects of vibration modals and their relationship to the magnetic field disturbances and phase-angle distortions. Two major modals of vibration, the translation of Helium Can (the super-conductive magnet) and the relative rotations between the Helium Can and the highly conductive shields, are investigated theoretically and experimentally.

For the problems of magnetic disturbances, the effect of magnetic inhomogeneity and the effect of eddy-current are considered separately to isolate the complexity and uncertainty of quantitative estimation of eddy-current from assessing the effect of magnetic inhomogeneity. The distribution of the magnetic field produced by eddy-currents is investigated in analytical methods. The rate of change of magnetic field generated by the eddy-currents is calculated with computer simulation and compared with the rate of change of phase-angle distortions measured in several types of cryostats, to determine which one of the eddy-current and the magnetic inhomogeneity is the main source of the phase-angle distortions. The magnetic gradients (a representation of magnetic inhomogeneity) are calculated using coefficients of surface harmonic, which are available for most of OMT's magnets. The phase distortion due to the motion of these inhomogeneous magnetic fields are calculated at specific positions and compared

to the phase-angle distortions measured at the equivalent positions to determine how much of the phase-angle distortions is contributed by the magnetic gradients.

Experiments are set up and carried out for measurements of magnetic disturbance, phase-angle distortions and structural vibrations under normal excitations of Cold Heads of cryostats and under swept sine excitations of the Cold Heads respectively. A novel experiment, referred to as the probe beam excitation, is employed to measure the phase-angle distortion under relative vibrations between a NMR probe and the magnetic field without introducing any eddy-currents in the conductors of the cryostat. The phase-angles are compared to the phase-angles tested under the same frequency and magnitude of relative vibrations, which are excited by a shaker on the Cold Head.

The reliability and sensitivity of a search coil sensor, which is widely used in former experiments, are investigated by creating its mathematical model of measurement and by computer simulations. A mathematical model is created for magnetic spectrum measurements from under-sampled phase-angles with a NMR probe. An improved method of the measurement is developed based on this model, with which the magnetic spectrum, which causes the phase angle distortion, can be detected more precisely.

Computer programs are developed for simulation of the mathematical models created in this thesis, for transformation of experiment data, for off-line synchronization of measurements and for analysis of the vibration modals, magnetic disturbance and phase-angle distortions.

This research has resulted in the mathematical modelling of the distortion problems for overall property prediction and has provided a software package to assist designing new products. It is concluded from both analytical and experimental investigations that magnetic inhomogeneity is a significant factor of phase distortion, while eddy current has limited influence on the phase angle.

Contents

Acknowledgements

Many thanks to my supervisors, Dr. Weiji Wang, Professor Jeffrey Knight and Dr. Mingsheng Yao for their constant support in the research.

I am most grateful to Dr. Weiji Wang to provide me the opportunity to fulfil my dreams. His constant encouragement and invaluable guidance have accompanied the research work from the beginning to the end.

This thesis was only possible because of the support of Professor Jeffrey Knight, to whom I am deeply indebted not just for his scientific contribution but also for his understanding, day after day, his help, essential financial support and his friendship.

I am very grateful to Dr. Mingsheng Yao, for his friendship, his guidance and help in the laboratory of Oxford Magnetic Technology. My thanks go to Mr. Edward Kershaw, Dr. Marcel Kruip and all other people who provided assistance in this project at Oxford Magnet Technology.

This research was made possible by the research studentship from De Montfort University and Oxfort Magnet Technology.

Last, I would like to pay tribute to the constant support of my family and my friends, without their love none of this would have been possible. Their sacrifice I can never repay.

Symbols

α	Magnetization flip angle or precession angle
γ	Gyromagnetic or magnetogyric ratio ($\gamma = 2.6752196 \times 10^8$ /Tesla/s)
μ	Magnetic moment or micron
$\hbar$	Planck's constant
θ	Colatitude angle of a spherical coordinate system
$\theta(t)$	Rotation angle of a rigid body on a plane at time t
ϕ	Longitude angle of a spherical coordinate system
φ	Magnetic flux
μ	Magnetic permeability or mass ratio
ε	Electric potential
δ_{st}	Static deflection of a mass-spring system
σ	Conductivity
ω	Angular velocity of Larmor frequency
ω_0	Angular velocity of static Larmor frequency
$\vec{\omega}_e$	Vector of angular velocity of rotating coordinate system

ω_a	Natural angular velocity of absorber mass
ω_n	Natural angular velocity of main mass
ξ	Damping ratio of structural vibration
Ω	Angular velocity of structural vibration or magnetic field disturbance
$\vec{\Omega}$	Vector of angular velocity
Σ	sum
$\Delta\Phi$	MR phase angle distortion
$\Delta\Phi_{pk-pk}$	Peak-to-peak value of MR phase angle distortion
Ψ	Initial phase angle of structural vibration or magnetic field disturbance
$\rho(\mathbf{r})$	Proton density at position pointed by the space vector **r**
$\mathbf{a}_x, \mathbf{a}_y, \mathbf{a}_z$	Unit vectors of Cartesian coordinate system
A_n^m	Cosine coefficient of Legendre polynomial
B_n^m	Sine coefficient of Legendre polynomial
$\Delta B(t)$	Disturbance of magnetic flux density B_0 at time t
ΔB_0	Disturbance of static magnetic flux density
B	Vector of magnetic flux density
B_0	Scalar of static magnetic flux density

$\mathbf{B}_0$	Vector of static magnetic flux density
$\mathbf{B}_1$	Vector of magnetic flux density of RF pulse
$\mathbf{B}_{eff}$	Vector of effective magnetic flux density
$\mathbf{B}_r$	Vector of reaction magnetic flux density
$\mathbf{B}_{ex}$	Vector of excitation magnetic flux density
E	Dissipated energy
$\mathbf{E}$	Electric field
f	Larmor frequency
F	Force
$\mathbf{G}$	Vector of gradient of magnetic flux density
$\mathbf{H}$	Total magnetic field
$\mathbf{H}_r$	Vector of reaction magnetic field
$\mathbf{J}$	Vector of current density
$\mathbf{k}$	Reciprocal space vector
k	
m	Mass or meter
M	Mass

$\mathbf{M}$	Magnetization vector
$\mathbf{M}_{xy}$	Magnetization vector on x-y plane of Cartesian coordinate system
M_{xy}	Scalar magnetization on x-y plane of Cartesian coordinate system
$\mathbf{M}_z$	Magnetization vector on z-axis of Cartesian coordinate system
M_z	Scalar magnetization on z-axis of Cartesian coordinate system
N_p	Proton density
P_n^m	Associated Legendre polynomial
$\mathbf{r}$	Space vector
r	Radius of spherical coordinate system
Δr_t	Displacement of translation motion
$\Delta\mathbf{r}$	Difference between two space vectors
s	second
S	Area
ΔS	Area difference
Δt	Duration of RF pulse for magnetization flip
$\mathbf{T}_1$	Time constant of spin free induction decay
$\mathbf{T}_2$	Ideal time constant of spin phase-out

$\mathbf{T}_2^*$	Effective time constant of spin phase-out
$\mathbf{T}_E$	Spin echo time
$\mathbf{T}_R$	Repetition time of 90^0 RF pulses for spin echo sequences or ratio of forces
V_S	Voltage of signal of search-coil sensor
X	Displacement

Acronyms

DVA	Dynamic vibration absorber
FID	Free induction decay
FRF	Frequency response function
MR	Magnetic resonance
MRI	Magnetic resonance image
NMR	Nuclear magnetic resonance
OMT	Oxford Magnet Technology
OVC	Outer vacuum chamber
PE	Patient end of a cryogenic magnet
RF	Radio frequency
SE	Service end of a cryogenic magnet

1 Introduction

The magnetic resonance image (MRI) system is an effective imaging system for examining the human body in a non-invasive manner. Such an MRI system generally consists of imaging systems and a cryostat. A cryostat typically contains a super-conducting coil, a Helium Can and a cooling pump. For precision imaging a MRI system requires an extremely uniform static magnetic field. Any structural vibration may cause distortion and fluctuations in the magnetic field. Since the vibration level in existing products of Oxford Magnet Technology (OMT) is regarded as unsatisfactory a project was set up between the De Montfort University, the Sussex University and the Oxford Magnet Technology Ltd in the summer 1998.

The structural vibration had not been a leading problem in MRI before a system with high resolution was developed. The investigation of vibration problems of a cryostat as affecting the MR imaging was first seen in a report [46] in 1992 when the structure of the cryostat had been modified to meet commercial specifications. A serious experimental investigation of the vibration problem was merely started in 1996 by Siemens and OMT. Only very limited information of issues is available.

The phase-angle disturbance is believed to be caused by structural vibrations of the MRI scanner, which is subject to impulses from the cooling pump (known as Cold Head) [26,33,40,49~52]. For a cryogenic magnet, vibration sources are believed to be caused mainly by the cooling pump, which maintains cryogenic working environment of super-conducting media. The vibration could also be transmitted from the supporting ground, which passes ambient noises and vibration through. Figure 1-1 briefly illustrates the problem domain.

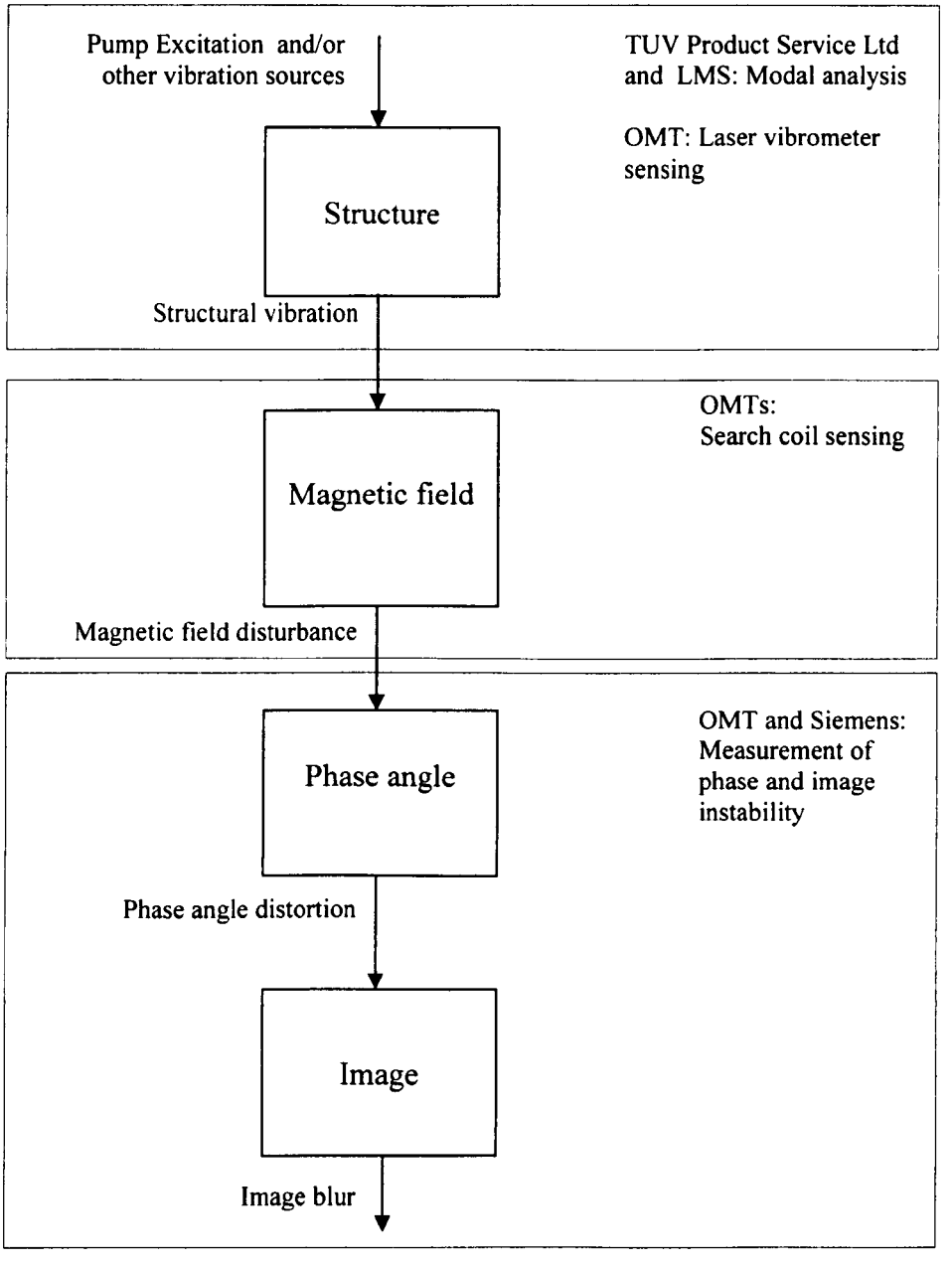

Figure 1-1 The problem domains and their relationships.

A reduction in the effect of structural vibrations on the magnetic field is critical for improving the performance of MRI systems. From 1996, Siemens and OMT have made great effort in reducing phase distortions caused by structural vibrations. They have been able to reduce the phase distortions to within 5^o from more than 20^o in most of their products. Traditionally, most of the improvements were obtained by strengthening structural rigidity, by changing positions of suspensions, by reducing vibration transmission or by isolating vibration sources. Those efforts were mainly based on engineering experience and experiments.

It is still demanding for further reduction of phase distortion in the existing high-resolution product. Some additional phase distortion has also been discovered in new types of MRI magnet. However, the further improvement of the phase distortion reduction has become more difficult using the traditional methods. The reasons for the difficulty are twofold. First the sources of the vibrations cannot be isolated completely and secondly lighter MRI magnets, demanded in modern commercial MRI markets, worsen the structural rigidity.

1.1 Problem Formulation

To date, there is no clear understanding of the relationship between the phase-angle distortions and the structural vibrations of the MRI system. So far most effort has gone into reducing the structural vibrations to reduce the distortions and improve the image quality. This research is focussed on finding the relationship between the phase-angle distortions and the structural vibration by developing a mathematical model from the first principles of a MRI system, electromagnetic field, and dynamic vibrations based on experiments carried out. Ideally the development should meet the following criteria:

- It should describe the distortion formations in mathematical models.

- It should allow to obtain quantitative results of the phase distortions with respect to different disturbances of magnetic field and structural vibrations in the existing products.
- It should direct the design and test of products with a reduced amount of distortion.
- It should develop a software package or tool for vibration analysis and phase-angle calculation.

1.2 Research Objectives

The fundamental aim of this research is to find out the mechanism of the MRI phase-angle distortion and structural vibration of the cryostats. This will allow existing products to be modified or products under development to be designed for a reduced amount of distortion and this with a minimum of cost. The following objectives are laid out to achieve the aim:

- Identify and understand better the nature of the existing magnetic field disturbances and phase-angle distortions in the cryostat and its relationship with the structural dynamic behaviours.
- Identify the transmittal mechanisms of the fluctuations from the mechanical structure to the magnetic field and then to the MRI phase-angle.
- Develop experiments to verify analytical results of the mechanisms with practical measurements.
- Find suitable solutions for the existing distortion problems to improve the performances of the products.
- Provide software for OMT to analyse measurements and to support the design of cryostat magnet with reduced phase angle distortion.

1.3 Basic Principle of Magnetic Resonance Imaging (MRI)

Magnetic Resonant Imaging (MRI) is one of the newest and most effective imaging tools developed for medical diagnoses. MRI does not use harmful x-rays, and produces no known harmful side effects. A patient is placed in the bore of a large magnet, a super-conducting solenoid, typically with a static uniform magnetic field of 1.0 to 1.5 Tesla. The human body contains plenty of hydrogen. Each of the hydrogen protons, spinning in the body can be looked upon as a tiny *bar magnet* with a "North" and "South" pole. When placed in a strong static magnetic field, the axes of these protons will tend to align along the direction of the magnetic field. When a short pulse of radio frequency, with so called Lamer frequency, is transmitted into the body, the energy of the transmitted signal will be absorbed by the protons and cause some of their magnetic (or spin) axes disturbed from their equilibrium to precess (or wobble) around the direction of the static magnetic field at the Lamer frequency. This is very much like a spinning top moving in the shape of a cone about the direction of gravity. This precession of tiny magnets induces an electric current in receiver coils placed outside the body. The induced current is the MR signal that can be transformed by a computer into an image. Figure 1-2 shows a cross section image of a human spine. Figure 1-3 shows an MRI cryogenic magnet awaiting shipment.

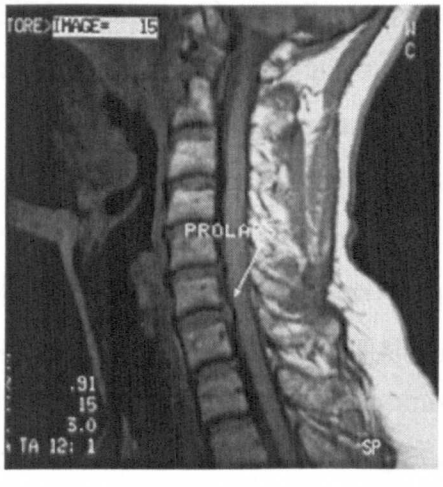

Figure 1-2 The magnetic resonance image of a human spine (courtesy to OMT).

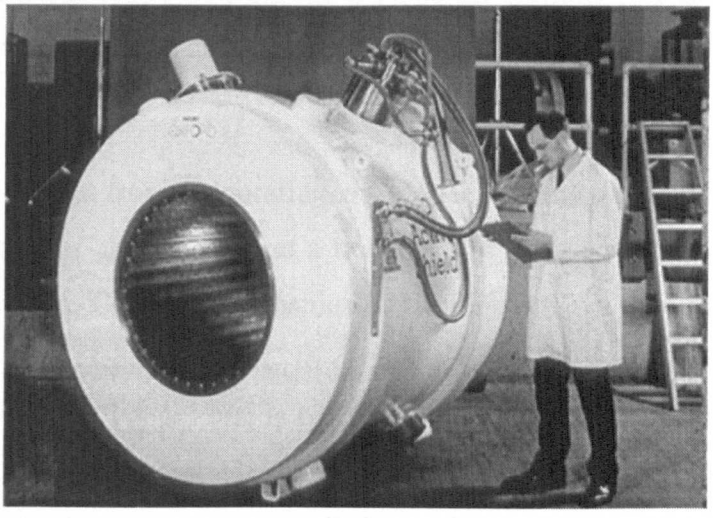

Figure 1-3 The Cryogenic magnet (courtesy to OMT).

1.4 Cryostat and MRI System Distortion

A super-conducting coil of magnet is contained in a cryostat. A cryostat, taking a typical example of OMT's Type OR70, mainly consists of five parts as shown in Figure 1-3 and 1-4: a super-conducting solenoid suspended in a helium vessel (He can), a 20K shield, a 80K shield, an outer vacuum chamber (OVC) and a cooling pump (Cold Head). Other parts of an MRI system are: a gradient system, a radio frequency (RF) system, a computer system and a console system for operation and evaluation. The super-conducting solenoid is made of niobium titanium, which must be kept below 7.5 Kelvin to retain the super-conducting properties. To maintain such low temperatures, the coils are almost completely immersed in liquid helium that has a boiling point of 4 Kelvin contained in the Helium Can made of steel. The Helium Can is in turn suspended in the OVC also made of stainless steel, as shown in Figure 1-4. The 20K and 80K shields (or cryo-shields) are made of pure aluminium to reduce the radiation between the Helium Can and the OVC.The shields encapsulate the Helium Can. There is a vacuum in the space between the Helium Can and OVC. The shields and the

Helium Can are suspended from steel rods and GRP rods respectively. These rods are the main heat conduction route from the OVC to the Helium Can, hence a trade off has to be made between strength and cross sectional area of the rods.

To prevent the helium from evaporating, a Cold Head is mounted on the OVC, in which a mass piston moves up and down at a frequency of 2 Hz compressing and vaporizing the cooling medium. Complex mechanical anti-vibration (AV) mounts and bellows are used between Cold Head and OVC to decrease vibration transmission from the Cold Head. There are many copper braids connected between the Cold Head and the shields both to conduct heat from the shield and to reduce the shield vibration. A Mounting of the Cold Head is shown in Appendix E. The vibrations that give rise to phase-angle distortion were regarded as mostly coming from the Cold Head.

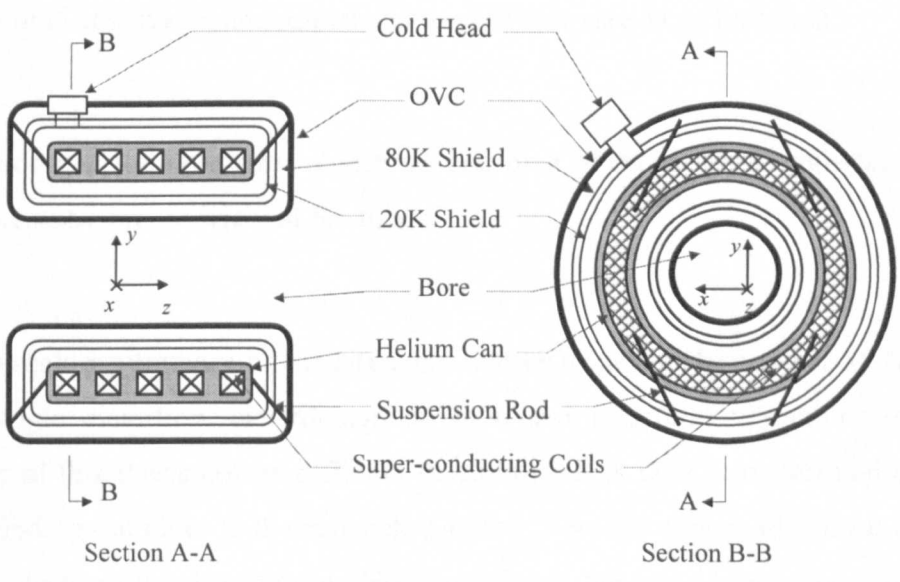

Figure 1-4 Cross sections of a cryostat.

As is illustrated in Figure 1-1, the magnetic resonance imaging system can be divided into four parts according to how the vibration transmits through the system. For the system, OMT and Siemens have made a series of experiments to measure structural vibration of cryostats [24-64], especially on Type OR71 [43], OR24 [61] and OR70 [24,25], and also Andrew Dewdney in OMT made significant progress in measuring and analysing the phase-angle and its related properties. Most of the research was focused on the measurements of the structural vibrations and phase distortions, whilst little research was related to the effects of eddy currents [42] and magnetic inhomogeneities [49].

1.5 Thesis Structure

This section outlines the presentation layout of the thesis. This thesis is organized in such a way as to generate a systematic and coherent theme from theoretical investigation of various related disciplines, methodologies, experiments, schemes and comparison between analytical and experimental results, presented in Chapter 2 – Chapter 10 to final conclusion and implementation of software MagDistortion.

Chapter 1 introduces the problems, objectives and plan of the research undertaken. It also gives a presentation overview of the thesis.

Chapter 2 presents a summary of the literature survey done on the subject of NMR, MRI, phase-angle distortion, electromagnetic field and structural vibration. As the subject matter of this thesis covers different disciplines, it is vital to understand all of them before finding out clues to the research. Chapter 2 covers almost all aspects of an MRI system regarding the distortion problem and forms the basic background for the

development of a method or methods for reducing MRI phase-angle distortion discussed in subsequent chapters.

Chapter 3 addresses a systematic approach to investigate the distortion problems based on the overall understanding of related subjects and previous work as described in Chapter 2. A logical relationship of different subjects regarding the distortion problem is presented using hierarchical schematics, which cover phase-angle distortion, magnetic field disturbance, magnetic inhomogeneity, eddy current and structural vibrations.

Chapter 4 presents the theory of structural vibrations of cryostats, of disturbances of the magnetic fields and the distortions of MR phase-angles. Three different modals of structural vibrations of a cryostat are considered and formulated: 1) translating vibration of super-conducting magnet, which makes the magnetic flux density of an inhomogeneous magnetic field changes at a fixed point of a non-inertial coordinate system; 2) rotational vibration of the magnet which turns the direction of the magnetic field; 3) Relative rotation between the magnets and the shields which produce the eddy-currents in the shields. The magnetic disturbances due to the motion of the magnet, the eddy-current and the directional change of the magnetic field are all formulated and analysed.

Chapter 5 develops the theoretical relationship between the magnetic field disturbance and the phase-angle distortion, concentrating on the three different natures of magnetic field disturbance mentioned above. The phase distortions according to structural vibrations and magnetic field disturbances are also evaluated using computer simulation and existing experimental results of former work.

Chapter 6 gives further analysis of the measurements carried out by OMT and LMS. The vibration spectra of the measurements of individual parts of a cryostat are investigated and the spectrum of the relative vibration between two of the individual

parts are derived. The relative vibration was obtained from the individual measurements of vibration, which is synchronized by means of cross-correlation.

Chapter 7 evaluates instruments, which have been extensively applied in measurements of structural vibrations and phase-angle distortions of MRI magnets. The reliability and sensitivity of the instruments are discussed. Improved measuring methods of the instruments are presented based on theoretical analysis and computer simulation.

Chapter 8 describes the set-up of the experiments carried out by the author. The feasibility and the effectiveness of the experiments are considered from the technical and economical points of view.

Chapter 9 analyses the experimental results to verify the mechanism of the phase-angle distortion problems as discussed in the previous chapters. The effect of magnetic gradient on the phase-angle distortions under structural vibrations is investigated quantitatively based on the results of the measurements and computer simulations. Vibration modals, which could impact the MRI phase-angle considerably are investigated from the experimental data.

Chapter 10 puts all the results together and gives a conclusion on the mechanism of the phase-angle distortion problems in the existing products at OMT. The main sources of the phase-angle distortions are indicated as some particular modals of vibration of the cryostat. Modifications of the cryostat structure of currents products and further investigations are also suggested.

Matlab programs are provided in Appendix H. The programs perform data transformation from experimental results to Matlab data formats, data synchronization

of individual measurements between two different parts of the cryostat, and the data analysis to obtain the vibration modals.

2 Literature Review and the State-of-the Art

The reasoning behind the Literature survey is to review the current knowledge on MRI principle, technology of the magnetic resonance (MR) measurement, vibrations of the cryostat, distortion of phase-angle and image, technology of measurement of an MRI system, eddy current calculation, technology of structural vibration reduction.

2.1 Magnetic Resonance Imaging

Magnetic resonance imaging (MRI) is an imaging technique used primarily in medical settings to produce high quality images of the inside of the human body. MRI is based on the principles of nuclear magnetic resonance (NMR). NMR as a physical phenomenon was first described by Bloch [74] and Purcell [75] in 1964, it was only a spectroscopic technique used by scientists to obtain microscopic chemical and physical information about molecules. NMR spectroscopy is still a very important analytical method in physics and chemistry. By the early fifties, researchers realised that NMR signals could be used to obtain spatial information, but a serious attempt to actually construct an NMR image did not take place until 1973 [76] after Lauterbur used their information and found that magnetic resonance could be used in making an image, using the backprojection technique used in computer tomography (CT). In 1975 Ernst proposed magnetic resonance imaging using phase and frequency encoding, the current MRI technique [8]. Lautebur's first experiments result in the imaging of lemons. In 1976 Rymod Damdian produce the image of a human body that took four hours to complete. From then on, progress in this technology has been rapid.

NMR is a phenomenon exhibited by hydrogen and certain atoms with odd numbers of neutrons, such as ^{13}C, ^{15}N, ^{19}F and ^{31}P. It is impossible to understand NMR fully without quantum mechanics. But there are still some books to describe the NMR phenomenon in a classical, which are helpful for us to understand the basic NMR principles [12,13,72,77].

2.1.1 Basic Principles of NMR

Atoms consist of a nucleus surrounded by one or more electrons. The nucleus is composed of positively charged protons and neutral particles called neutrons. These particles possess a remarkable characteristic known as ***spin*** or angular momentum. A particle with spin seems to rotate about its own axis, as shown in Figure 2-1. The nucleus of the hydrogen atom is the simplest in nature, consisting of just one proton and no neutron, which is the most common element found in the human body. Each proton with a spin is also magnetic, referred as magnetic dipole, a tiny current loop, hence has a magnetic moment. The remarkable inherent characteristic of the spin is that the spin does not change its magnitude and never stops. In the atomic nucleus, the spin of each couple of protons cancels. The nucleus as a whole will therefore have spin only when it contains an odd number of protons and/or an odd number of neutrons. Two thirds of the isotopes found in nature have an uneven number of protons or neutrons or both. Examples of these isotopes were given at the start of this section. But others, for instance one of the most common isotopes in human tissue, oxygen ^{16}O of 8 protons and 8 neutrons, are magnetically neutral, these isotopes cannot be used for magnetic resonance.

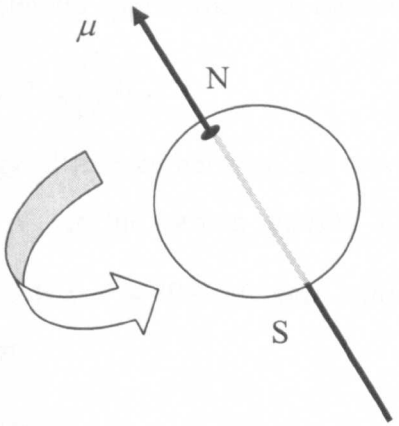

Figure 2-1 The proton viewed as a magnetic dipole, with a "north" and "south" poles.

For a proton, or any other nucleus, the ratio of its magnetic moment, μ, to its spin, I, is called its ***magnetogyric ratio***, γ, expressed as

$$\gamma = \frac{\mu}{I}. \tag{2.1}$$

For the hydrogen ^1H, the gyromagnetic ratio is

$$\gamma = 2.6752196 \times 10^8 \ \mathrm{T^{-1}s^{-1}}. \tag{2.2}$$

In a probe to be tested, the total of all hydrogen nuclei is known as a spin ensemble. Without an external magnetic field, the spins in the ensemble are randomly oriented. The probe appears to be non-magnetic to the outside. However, when the probe is positioned in a strong static magnetic field, the orientations of the magnetic moments or spins are no longer totally random and the external magnetization of the probe in the direction of the field lines can be measured after a certain period of time. In the quantum model the magnetic moments of the protons in a static magnetic field can have only two possible orientations: either parallel or antiparallel to the static magnetic field direction, which presents two different energy levels of the proton. The parallel spins

are slightly more than the anti-parallel spins, the difference of the proton densities, called spin excess, is excellently approximated at room temperature by the equation,

$$N_{parallel} - N_{antiparallel} = \frac{\Delta E}{2kT} N_p, \tag{2.3}$$

in which ΔE is the energy difference between the two energy levels, T represents the temperature in Kelvin, N_p is the proton density ($N_p = N_{parallel} + N_{antiparallel}$), and $k = 1.380658 \times 10^{-23}\ \mathrm{JK}^{-1}$. For $T = 293\,\mathrm{K}$ (room temperature), $B = 1\,\mathrm{Tesla}$, we can assume approximately that

$$\frac{N_{parallel}}{N_{antiparallel}} = 0.999993. \tag{2.4}$$

Clearly, the excess of spins is very small indeed. Therefore it will be seen that the NMR signal is very weak in practice and susceptible to a small external disturbance. From Equation (2.3) ΔE is found to be directly proportional to the flux density of the static magnetic field,

$$\Delta E = \hbar \gamma B_0 = \frac{h}{2\pi} \gamma B_0, \tag{2.5}$$

where $\hbar$ is a constant of nature called Planck's Constant, and B_0 is the magnetic flux density.

From Equation (2.5) and (2.3), it says that, at thermal equilibrium, the spin excess, and therefore the magnitude of the magnetization vector, $\mathbf{M}$, is directly proportional to the flux density of the static magnetic field and to the proton density, and inversely proportional to the absolute temperature.

But if an electromagnetic radiation at a specially tuned frequency, f, is applied to the ensemble of spins, there will be more protons jump from the lower to the higher energy state receiving energy from the radiation. This will only occur, however, if the energy of the photons comprising the radiation, hf, exactly equal the difference in energy between the two energy levels of the proton,

$$hf = \Delta E = \frac{h}{2\pi}\gamma B_0 \tag{2.6}$$

or

$$\omega_0 = 2\pi f = \gamma B_0, \tag{2.7}$$

where the frequency, f, is called Larmor frequency. The Larmor frequency of hydrogen proton is 63.866MHz in the magnetic field of 1.5Tesla. This equation is the condition of nuclear magnetic resonance.

When the radiation ceases the protons release radio signals, the free induction decay (FID), that are detected and processed by computer. The relative viscosity of the medium in which hydrogen atoms are suspended in alters the delay of releasing radio signals. This delay is characterised by the time constant T_1 which depends on the size of the tissue molecule and its type of surroundings. But the FID decays in a time constant T_2 much shorter then T_1 after a single RF radiation in practice, because of the spin-spin interaction. By means of different RF pulse sequence three different contrast images of the tissue can be obtained, i.e. a T_1-weighted image, T_2-weighted image and proton density image.

Explained in a classical model of spins and NMR, the tiny magnet of an isolated spin in the excess spins, with both a magnetic moment and an angular moment (spin), is exerted a torque by the external magnetic field, and therefore precesses around the magnetic field line (z axis) at the Larmor frequency, $\omega_0 = \gamma B_0$. The precession of magnetization can be described by the equation,

$$\frac{d\mathbf{M}}{dt} = \gamma \mathbf{M} \times \mathbf{B}_0, \tag{2.8}$$

where $\mathbf{M}$ and $\mathbf{B}_0$ are the magnetization vector and external magnetic field respectively, γ is the gyromagnetic ratio. Equation (2.8) is called Bloch's equation. Figure 2-2 shows the precession illustratively.

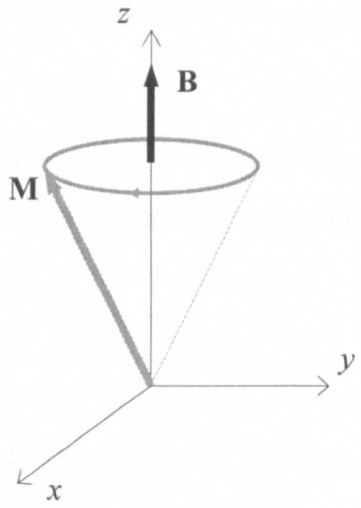

Figure 2-2 The motion of the magnetization in a static magnetic field.

In a new coordinate system $X'Y'Z'$ rotating at a constant angular velocity $\vec{\omega}$, Equation (2.8) is converted into

$$\frac{d\mathbf{M}}{dt} = \gamma\mathbf{M} \times \left(\mathbf{B}_0 + \frac{\vec{\omega}}{\gamma} \right) = \gamma\mathbf{M} \times \mathbf{B}_{eff}, \tag{2.9}$$

in which $\mathbf{B}_{eff}$ is effective magnetic field in the rotating coordinate system. If a magnetic field, $\mathbf{B}_1$, which rotates with the angular velocity of $\vec{\omega}_e$ in X-Y plane, is applied to previous static magnetic field $\mathbf{B}_0$, the effective field $\mathbf{B}_{eff}$ 'seen' from the coordinate system rotating at $\vec{\omega}_e$ is

$$\mathbf{B}_{eff} = \mathbf{B}_0 + \frac{\vec{\omega}_e}{\gamma} + \mathbf{B}_1. \tag{2.9}$$

As long as the excess spins relevant to the magnetization are of random phase orientation, their individual components cancel to zero in the transverse plane (x-y plane). Magnetization will be along the z-axis only, parallel to the external magnetic field. At the resonant condition, the magnetization is deflected from its state of

equilibrium by introducing energy of the electromagnetic radiation. At the same time, the spins are stimulated in a way which ensures that they are in phase.

The applied RF radiation is composed of two vectors of magnetic field counter rotating at the angular velocity of ω_e in X-Y plane. The resonant condition is

$$\vec{\omega}_e = -\gamma \mathbf{B}_0 . \tag{2.10}$$

Then in the rotating frame $X'Y'Z'$ the precession of $\mathbf{M}$ takes place around vector $\mathbf{B}_1$ in the equation,

$$\frac{d\mathbf{M}}{dt} = \gamma \mathbf{M} \times \mathbf{B}_{eff} , \tag{2.11}$$

in which $\mathbf{B}_{eff} = \mathbf{B}_1$, as shown in Figure 2-3. This resonant process was first discovered and solved by Bloch in 1946 [74].

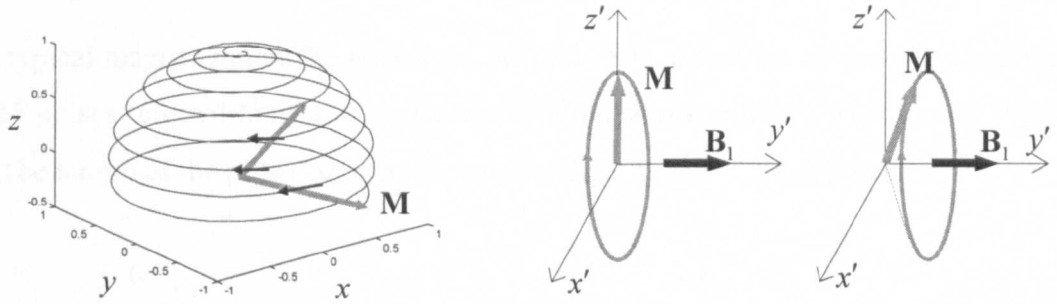

(a) (b) (c)

Figure 2-3 (a) The motion of the magnetization in the stationary coordinate system. (b) The precession of magnetization M around B_1, in which M was align with Z axis when the radio wave started. (c) The recession of magnetization M around B_1, in which M was flipped from Z axis when the radio wave started.

2.1.2 Relaxation and Spin Echo

A magnetization vector $\mathbf{M}$ can be decomposed into a component $\mathbf{M}_z$ along the z-axis and a component $\mathbf{M}_{xy}$ in the x-y plane as shown in Figure 2-4 (a). $\mathbf{M}_{xy}$ rotates around z-axis or $\mathbf{B}_0$ with Larmor frequency ω_e. The angle of $\mathbf{M}_{xy}$ to an axis, e.g. the x-axis, is called spin phase-angle or simply phase-angle, which along with the precession frequency ω_e are two most fundamental parameters in spatially locating image. In the discussions of spin echo and phase distortion, the phase-angle is defined in the rotating coordinate system $X'Y'Z'$.

By changing the duration, Δt, or magnetic flux density, $\mathbf{B}_1$ of the radiation (RF pulse) the magnetization angle to the Z axis, α, also called flip angle, can be controlled in the equation,

$$\alpha = \omega_1 \Delta t = \gamma B_1 \Delta t . \tag{2.12}$$

Two typical magnetization flip angles are 90° and 180°, which are achieved by applying the RF pulses referred to as a 90° pulse and 180° pulse respectively, as shown in Figure 2-4. The length of the pulse Δt is much smaller than T_1 and T_2 in application.

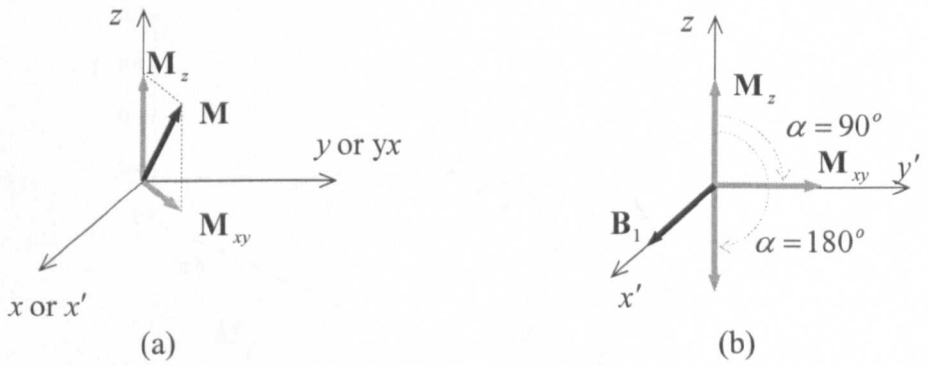

Figure 2-4 (a) (b) A 90° pulse flips the magnetization directly into the X'-Y' plane, while a 180° pulse inverts the magnetization vector and flips it exactly in to the opposite direction.

Once the magnetization is flipped to an angle of α, for instance 90°, from its equilibrium forming the spiral track as shown in Figure 2-3, it will start to recover to the equilibrium as soon as the external radiation is ceased, shaping another spiral track with the α decreasing (Figure 2-5). Vector $\mathbf{M}_{xy}$ still transversely rotates at the Larmor frequency in xy-plane emitting the signal (FID), but its decay is faster than the recovery of $\mathbf{M}_z$. This is because the individuals of the excess spins quickly fan out or lose their phase coherence due to the spin-spin interactions. These processes are called *spin relaxation*, described in Bloch's law of relaxation in a pair of differential functions. The solution of the equations is given in the functions,

$$M_z(t) = \left[M_z(0) - M_z(\infty)\right]e^{-t/T_1} + M_z(\infty), \text{ and} \tag{2.13}$$

$$M_{xy}(t) = M_{xy}(0)e^{-t/T_2}, \tag{2.14}$$

in which $M_z(0)$ and $M_z(\infty)$ are the lengths of $\mathbf{M}_z$ at the beginning and end of the relaxation, $M_{xy}(0)$ is the length of $\mathbf{M}_{xy}$ at the beginning of the relaxation. T_1 and T_2 are the time constants previously mentioned in this section and $T_1 >> T_2$ generally.

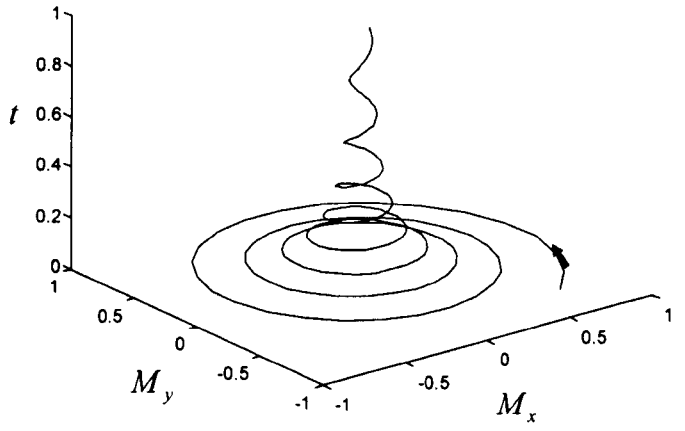

Figure 2-5 The free relaxation of transverse magnetization.

In practice, the magnetic field are not ideally homogeneous in a probe containing the excess spins. The spins in the higher field precesses faster than those in the lower field. The effective time constant T_2^* is shorter than T_2, because the inhomogeneities of the static magnetic field contribute to the dephasing of the spins. This effect of the static magnetic field inhomogeneities can be overcome by applying a particular technique, namely a *spin echo*. That is, after a time τ of relaxation a 180° pulse is applied to the probe. This "pulse" "turns" the individual spins around or reversed the order of the spin in the x-y plane. The spins rephase and a new MR signal generates which reaches its peak, after the full echo time T_E of 2τ, as shown in Figure 2-6.

In practical MRI or MR spectrum measurement, the FIDs are ignored and only the echoes are used. The production of even a single image requires a large number of successive spin echo pulse sequences. Each spin-echo pulse sequence is composed of a 90° pulse and one or more 180° pulses. The time interval between 90° pulses is referred to as the repetition time (T_R), as shown in Figure 2-7.

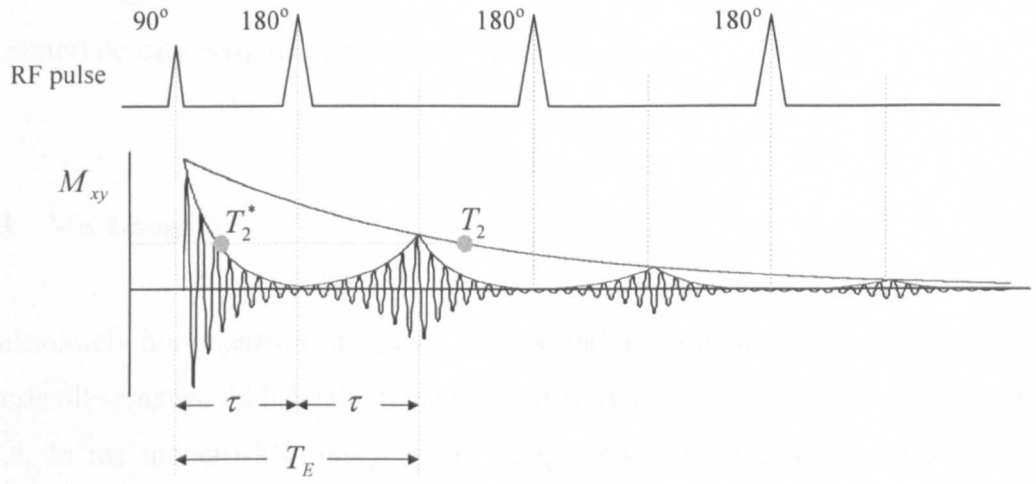

Figure 2-6 Transverse relaxation and echo time.

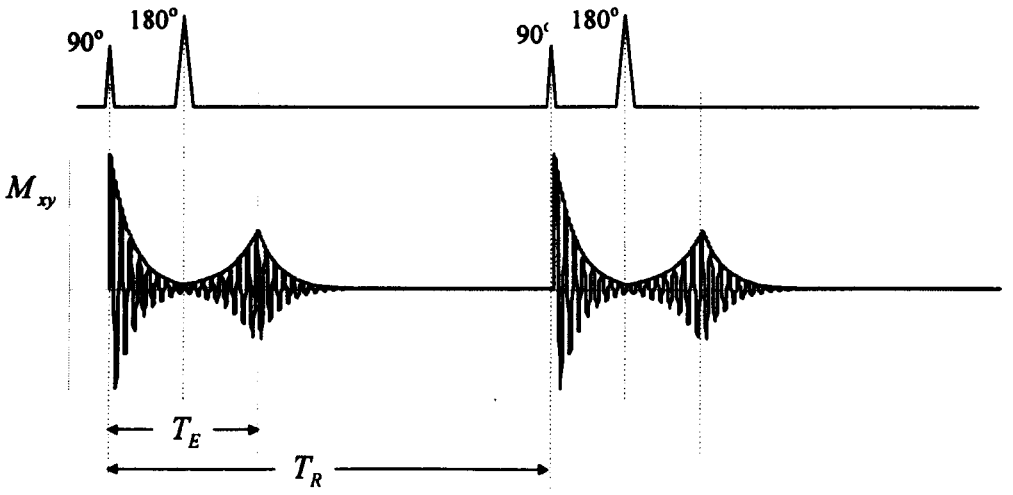

Figure 2-7 Repeated spin-echo sequences.

The data acquisition system of the MRI or MR spectrometer collects the spin-echo data once in a repetition time T_R, and the image or spectra (frequency, phase and magnitude) will be calculated from those data. By means of different spin-echo pulse sequences choosing different T_E and T_R along with the combination of RF, the information of different image contrasts become available, for instance the T_2-weighted, T_1-weighted and proton density weighted contrasts of images.

2.1.3 MR Imaging

An absolutely homogeneous magnetic field would not provide any spatial information, because all spins would have the same resonance frequency and emit an undifferentiable signal. In the modern MR imaging, the image is constructed using the technique of frequency and phase encoding. The imaging process is usually fulfilled in three steps respecting to spatial localisation of the MR signals.

First, a slice is selected, for instant a slice vertical to the z-axis. In an inhomogeneous magnetic field generated by a gradient along the z-axis called z-gradient, when a single frequency RF pulse is applied, only the spins within the corresponding resonance frequency location would respond or be excited. This location is a plane or a slice vertical to the z-axis. Actually this "slice" has a small thickness called slice thickness or slice width.

Second, columns of the selected slice are localised along the x-axis. For that propose, an x-gradient is turned on while the spin echo is read out. The excess spins will precess at a frequency determined by the magnetic field, which varies linearly along the gradient. This process is called the frequency encoding.

Third, rows of the selected slice are localised along the y-axis. A y-gradient is switched on briefly between the RF pulse and the spin-echo signal to cause the spins located in the stronger field to precess faster for a short period of time. The result is a predetermined, row-by-row phase shift between the spins, which is directly proportional to their locations. This process is called the phase encoding.

The rows and columns of the MR image are reconstructed with the help of the Fourier Transformation [2,10,78]. Since the original imaging paper in 1973 [76], various imaging methods have been proposed. A mathematical expression of reconstructing proton image which was presented in reference [2] is reviewed.

In a static magnetic field $\mathbf{B}_0$ with applied magnetic gradient $\mathbf{G}$ the local Larmor frequency is given by

$$\omega(\mathbf{r}) = \gamma B_0 + \mathbf{G} \cdot \mathbf{r}, \qquad (2.15)$$

where $\mathbf{G}$ is the magnetic gradient parallel to $\mathbf{B}_0$, $\mathbf{r}$ represents the spin coordinates. In the rotating coordinate system with frequency γB_0 or in another word by means of

quadrature detector with the reference frequency γB_0, the MR signal can be expressed as

$$S(t) = \iiint \rho(\mathbf{r}) e^{(i\gamma \mathbf{G}\cdot\mathbf{r}t)} d\mathbf{r}, \tag{2.16}$$

where $\rho(\mathbf{r})$ is the local spin (or proton) density, and $d\mathbf{r}$ represents the volume integration. In the formalism of $\mathbf{k}-space$, the image reconstruction is achievable in the pair of Fourier transform and its inverse,

$$S(t) = \iiint \rho(\mathbf{r}) e^{(i2\pi \mathbf{k}\cdot\mathbf{r})} d\mathbf{r}, \tag{2.17}$$

$$\rho(\mathbf{r}) = \iiint S(t) e^{(-i2\pi \mathbf{k}\cdot\mathbf{r})} d\mathbf{k}. \tag{2.18}$$

The reciprocal space vector, $\mathbf{k}$, is given by $\mathbf{k} = (2\pi)^{-1}\gamma \mathbf{G}t$.

Manipulating the magnetic gradient $\mathbf{G}$ in different ways in the imaging space, we can obtain different methods of the image constructions[8].

2.2 The Components of the MRI System

In experiments of measuring magnetic disturbances, both MR imaging system and MR spectrometer were used [30]. The former gives an image of a sample but complex to use, while the latter only produces MR signal which is easy to be analyzed in the research project. Understanding of their components will prevent one from omitting any possible major effects of the components causing the measured phase distortions.

2.2.1 Overview of MRI Systems

The typical MRI system consists of four subsystems: the magnet or cryogenic system, the gradient system, the RF system, and the computer system. Figure 2-8 illustrates those components [21,23,72,77].

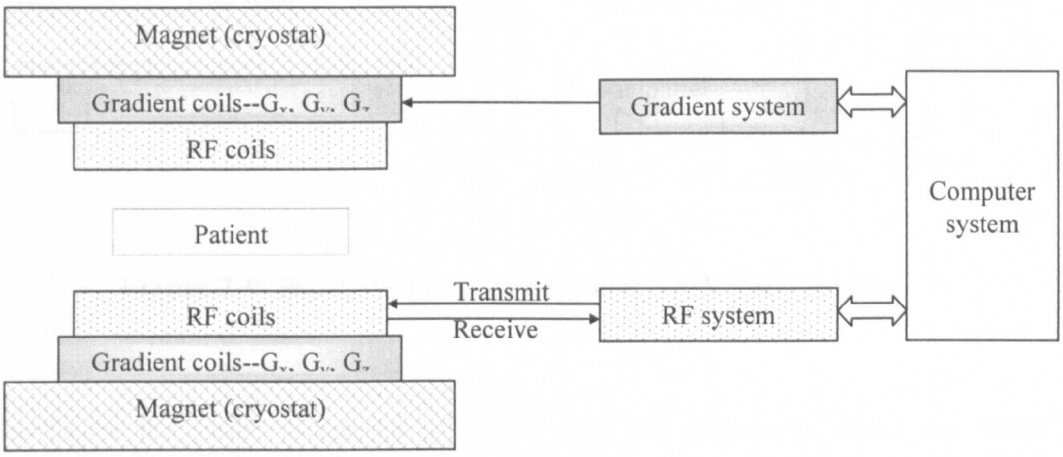

Figure 2-8 The components of the MRI system.

2.2.2 NMR Spectrometer

The NMR spectrometer is used to obtain the phase and spectrum of MR signals. The following figure illustrates a typical NMR spectrometer schematically [1,14,70,71].

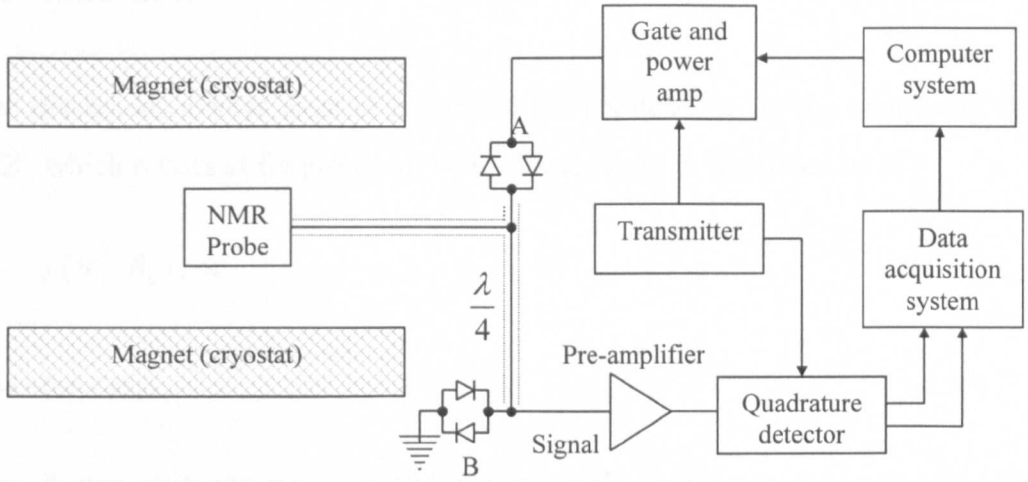

Figure 2-9 Block diagram of a typical NMR spectrometer.

In the figure the probe is consist of an RF coil and capacitors which are tuned to perform the electronic L-C resonance at the Larmor frequency. A sample to be tested is in the RF coil. The transmitter produces an RF signal at the Larmor frequency. This signal is amplified and switched to the probe through diodes A in a short period of time. Then an MR signal will be excited in the probe. This MR signal will be received by the quadrature detector in which the MR signal of high frequencies is converted into a low frequency signal by means of a heterodyne circuit. The quadrature detector also receives a reference signal from the transmitter to mix it with the MR signal. The signal of low frequency from the quadrature can be converted into digital signal and analyzed by the computer.

Most of the experiments carried out in OMT were based on such spectrometers.

2.3 Phase Distortion and its Measurement

2.3.1 Introduction

Phase distortions always exist in practical MRI applications. In the coordinate system $X'Y'Z'$ which rotates at frequency $\omega_e = \omega_0$, phase-angle ϕ is defined by [1]

$$\frac{d\phi}{dt} = -\gamma(B - B_0), \text{ or} \tag{2.19}$$

$$\frac{d\phi}{dt} = -(\omega - \omega_0), \tag{2.20}$$

where B represents the magnetic flux density in the probe tested, t is the time passed after the end of the 90^0 pulse. From the definition the phase-angle will be always constant if the magnetic field B is absolutely homogeneous and equal to B_0 anywhere in the probe. But that is impossible in practice, not only for the static magnetic inhomogeneities but also for any time-dependent magnetic variation [1] including the molecular diffusion motions in liquids. The latter motive effect, however, is generally irreversible, whilst the previous static effect can be cancelled by the spin echo as discussed in previous section.

The phase distortion is defined as [26]

$$\Delta\Phi = -\gamma \int_0^{T_E/2} \Delta B(t)dt + \gamma \int_{T_E/2}^{T_E} \Delta B(t)dt, \tag{2.21}$$

where T_E is the echo time equal to 2τ, and $\Delta B(t)$ is magnetic disturbance equal to $\left(B(t) - \omega_e/\gamma\right)$. Equation (2.21) also is the result of equation (2.18) in a full spin. If the magnetic disturbance is time-independent, the phase distortion will not exist according to equation (2.21).

The vector of transverse magnetization, $\mathbf{M}_{xy}$, can be written as the complex number $\mathrm{M}_{xy} = M_x + iM_y$ on x-y plane of the static coordinate system and as $\mathrm{M}_{x'y'} = M_{x'} + iM_{y'}$ in the frame rotating around z-axis with angular velocity of ω_e. As a result the motion

of the magnetization of transverse relaxation in the static and the rotating frames is described by the following equations respectively,

$$M_{xy}(t) = M_{xy}(0)e^{-t/T_2}e^{i(\omega t+\varphi)}, \text{ and} \tag{2.22}$$

$$M_{x'y'}(t) = M_{x'y'}(0)e^{-t/T_2}e^{i(\omega-\omega_e)t}. \tag{2.23}$$

To measure the phase-angle and the distortion, the detection of the real and imaginary components of equation (2.22) or (2.23) is used. That is usually feasible by means of a *quadrature detection system* [1, 14, 70]. Figure 2-10 shows the system schematically.

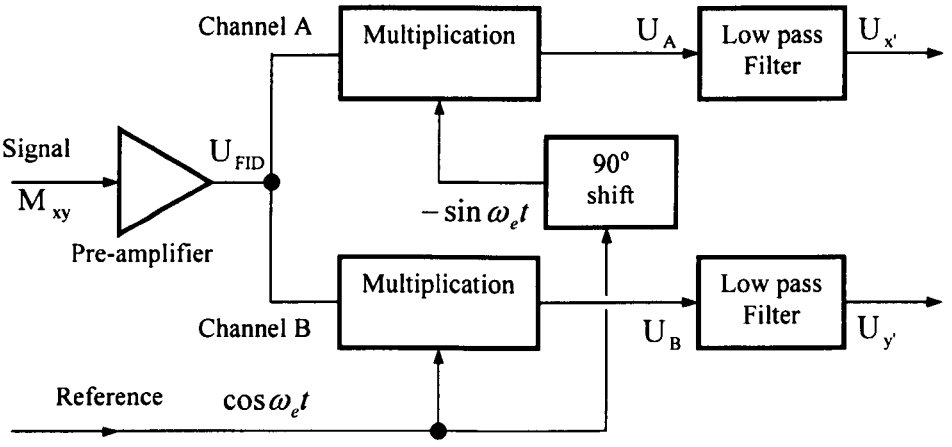

Figure 2-10 The quadrature detector.

In Figure 2-10 the angular velocity of the reference signal $\cos\omega_e t$ is also the main frequency component of the 90° and 180° pulses applied in the spin-echo pulse sequence, and

$$U_{FID}(t) = Ae^{-t/T_2}\cos(\omega t + \varphi), \tag{2.24}$$

$$U_A(t) = U_{FID}(t)\cos\omega_e t, \tag{2.25}$$

$$U_B(t) = -U_{FID}(t)\sin\omega_e t, \tag{2.26}$$

$$U_{x'}(t) = Ae^{-t/T_2}\cos(\omega - \omega_e)t, \tag{2.27}$$

$$U_{y'}(t) = Ae^{-t/T_2}\sin(\omega - \omega_e)t\,. \tag{2.28}$$

ω_e is generally tuned to satisfy the condition,

$$|\omega + \omega_e| >> |\omega - \omega_e|\,. \tag{2.29}$$

In the frame $X'Y'Z$ rotating around z-axis with angular velocity of ω_e, the phase-angle is measured to be

$$\phi = \tan^{-1}\frac{U_{y'}(t)}{U_{x'}(t)}. \tag{2.30}$$

Such a quadrature detector is usually built in an NMR spectrometer, as shown in Figure 2-9.

For a sinusoidal magnetic disturbance,

$$\Delta B(t) = \Delta B_0\cos(\Omega t + \Psi)\,, \tag{2.31}$$

the phase distortion is derived from Equation (2.21) as [40]

$$\Delta\Phi = \frac{\gamma\Delta B_0}{\Omega}\left(2\sin(\frac{T_E\Omega}{2} + \Psi) - \sin(T_E\Omega + \Psi) - \sin(\Psi)\right). \tag{2.32}$$

In practice, the peak-to-peak values of $\Delta\Phi$ are used to define the phase angle distortion, which possible maximum values expression by

$$\Delta\Phi_{pk-pk} = \frac{8\gamma\Delta B_0}{\Omega}. \tag{2.33}$$

For a $\Delta\Phi_{pk-pk}$ of 5° at 13Hz this gives a variation ΔB_0=3.3nT, which is 3.3×10^{-9} Tesla and is too weak to be measured in the general methods of magnetic measurement in the volume of an NMR probe (about $1cm^3$), especially with a strong background of 1.5 Tesla.

The Siemens's measurements are generally carried out with an echo time of 60ms. In OMT, both echo times of 40ms and 60ms are used. But it was found that the measurements with echo time of 40ms are more sensitive to all frequencies in the required range and automatically suppresses mains interference with 50Hz [40]. Figure 2-11 shows the sensitivities with different echo times, derived from equation (2.32) [27].

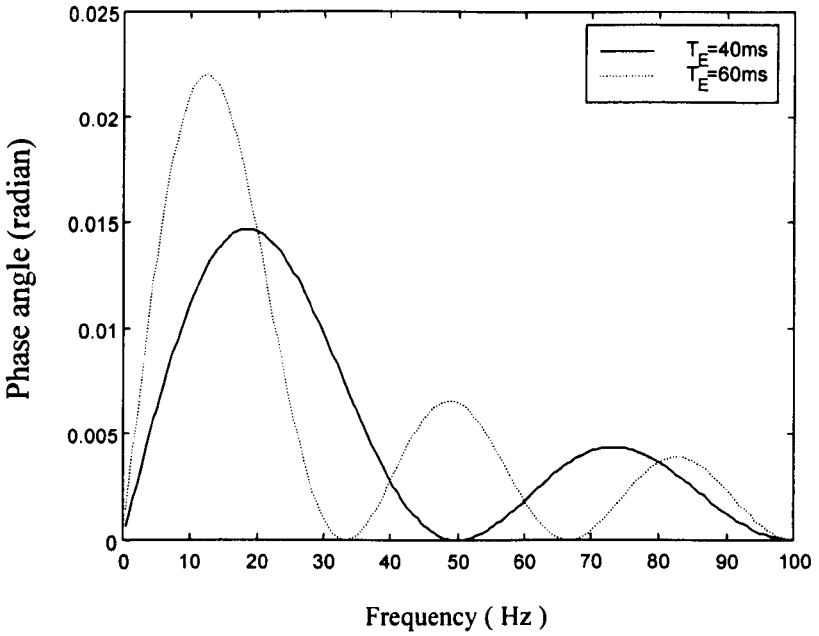

Figure 2-11 Frequency response of spin-echo measurements ($\Delta B = 2nT$).

A good agreement of the frequency response with the measured frequency response was reached in reference [33].

In the original OMT standard measurements, six data sets of 512 points each are required to build up a meaningful average figure, plus a check on the background noise with the fridge of the Cold Head switched off [40]. The six repetition rates are 191ms, 192ms, 251ms, 252ms, 301ms and 302ms, with the background taken using T_R=251ms. The echo times are 40ms and 60ms. The current scheme is to take six data sets with T_R=254ms and 255ms, ignore the highest and/or lowest, and average the remainder. The effect of background noise is taken off as [27]

$$\Delta\Phi = \sqrt{\Delta\Phi^2_{measured} - \Delta\Phi^2_{background}} \,. \tag{2.34}$$

It was shown that satisfactory images were obtained with phase distortion of 6°-8° within a 20cm radius area [30,31]. But the Siemens hopes that the phase variation should be less than 2° on 10cm radius, which is roughly equivalent to 4° on 20cm [40].

The phase distortion due to magnetic disturbance affects the MR imaging during phase encoding and makes the image blur. The similar effect was discussed in the susceptibility of the magnetic polarization of atoms and molecules in a magnetic field [2]. The influence of the local field variations is seen by adding the local precession frequency offset, $\gamma\Delta B_0(\mathbf{r})$. In the quadrature detector, the MR signal becomes

$$S(t) = \iiint \rho(\mathbf{r}) e^{[i\gamma(\mathbf{G}\cdot\mathbf{r}+\Delta B_0)]} d\mathbf{r} \,. \tag{2.35}$$

The Fourier pair of equation (2.17 and (2.18 becomes

$$S(\mathbf{k}) = \iiint \rho(\mathbf{r}) e^{i\gamma\Delta B_0(\mathbf{r})} e^{i2\pi\mathbf{k}\cdot\mathbf{r}} d\mathbf{r} \,, \tag{2.36}$$

$$\rho_I(\mathbf{r}) = \iiint S(t)e^{-i2\pi\mathbf{k}\cdot\mathbf{r}}d\mathbf{k}. \qquad (2.37)$$

Clearly $S(\mathbf{k})$ is not equal to the ideal reciprocal lattice explained in equation (2.16) and the reconstructed image, $\rho_I(\mathbf{r})$ is no longer a true representation of the original spin density, $\rho(\mathbf{r})$, explained in equation (2.18.

The measurements of image artifact intensity or "% ghosting" were used in the analysis of the MRI distortions [11, 46-59]. Since all the subsystems of an MRI system are required in this method, the distortions due to gradient system are inevitably included in the measurements. Some ambiguity in using the "% ghosting" analysis of an image was found [38]. Comparing to the "% ghosting", the NMR phase-angle measurement is found more accurate and simple, hence it is extensively applied in this research project.

2.3.2 The Phase Distortion in the Cryostat

Phase distortions were ascribed to the vibrations of Cold Head. That was first seen in an internal experimental memo of Siemens in 1992 [46]. A lot of such experimental investigations were carried out in Siemens and OMT from 1996 to 1999, and found that phase distortions due to Cold Head vibrations are evident [26-35,35,37-41,44-62,64-70]. The phase distortions investigated can be divided into following five categories:

- Spatial distributions of the phase distortions.
- Spectrum of the phase distortions.
- Relation with the Cold Head vibration.
- Effects of eddy current and magnetic homogeneities.
- Relations with the cryostat modals.

The phase distortion was measured and found that it increases according to the offset of the probe from the centre of the cryostat, as seen in appendix C [37]. Different products give different rates of rising curves of the phase distortions.

Because of the long repetition time (T_R from 191ms~301ms), the sampling rate of the acquisition system was less than 5Hz and most of the experimental data of the phase distortions were undersampled. Therefore the frequency information of the phase-angles had to extract from a pair of the data (for instance 251ms and 252ms) by hand using a Matlab script which simulates the under-sampling process [26]. The significant frequencies of the phase distortions obtained in this method in the existing products were tested to be within 50Hz [40]. The dominant frequencies varied in different types of products and they were different even in the same types of products.

All the frequencies of phase distortions were multiples of 2Hz which was driving frequency of the Cold Head. But it was difficult to ascribe the phase distortions to a small range of vibration frequencies of the Cold Head[27,29].

The Cold Head of Type OR24 cryostat led to image artifacts and instabilities, the field, gradient-like in x- and y-direction, was observed, a possible reason could be the movement of magnet coil relatively to the shim iron [49]. The image artifacts caused by the Cold Head were considerably less at the product K4/1 compared with the products K4/6, might be because of the much better magnetic homogeneity of K4/6 [50]. There was evidence to suggest that the cryo-shields actually assisted in reducing the phase distortion [39], while it was shown in other experiment report that the eddy currents generated in highly conductive cryo-shields by relative movement of the shields with respect to the magnet provided the most likely source of phase distortions[42].

Numerous tests of modal analysis and modal response were performed on Type OR71, OR24 and OR70 [24-25,43, 61,] to optimise product designs in reducing the phase

distortions. But none of them were correlated to the phase distortion with a clear understanding of the relationship between the vibrations of the system and the phase-angle. It was recommended that without the understanding of the relationship, the optimisation of the design was impossible [43]. In some reports of experiments, it was reported that magnet systems were prone to a low frequency, whole body side way's motion, which did exert some influence on the phase-angle instability [41].

2.3.3 Surface Harmonic and Magnetic Inhomogeneity

In OMT the magnetic inhomogeneity is defined as the peak to peak variation of the field on the surface of a predetermined sphere [67]. The field values are determined at discrete points on the surface. If the peak to peak variation of the field is inside specification, the magnet is deemed to be inside specification, if the peak to peak is outside the stipulated specification, the magnet needs to be shimmed further. The field distribution inside the sphere can be calculated in terms of the surface harmonic.

The surface harmonic is derived from the general solution of Laplace's equation expressed in spherical polar coordinates [7]. In terms of the distance from the origin r, the colatitude angle θ measured from the z-axis, and the longitude angle ϕ measured about the z-axis from the xy-plane, Laplace's equation takes the form

$$\frac{\partial}{\partial r}\left(r^2\frac{\partial V}{\partial r}\right)+\frac{1}{\sin\theta}\frac{\partial}{\partial\theta}\left(\sin\theta\frac{\partial V}{\partial\theta}\right)+\frac{1}{\sin^2\theta}\frac{\partial^2 V}{\partial\phi^2}=0. \qquad (2.38)$$

Generally the solutions of the equation can be found in the form

$$V = R\Theta\Phi = RS, \qquad (2.39)$$

where the function $S = \Theta\Phi$ is called a surface harmonic which represent the solutions on the sphere of a predetermined radius r. In OMT, the z component of the magnetic field B_z is expressed as the potential of V in the form

$$B_z(r,\theta,\phi) = A_0^0 + \sum_{n=1}^{\infty}\left(\frac{r}{R_0}\right)^n \sum_{m=0}^{n} P_n^m(\mu)\left(A_n^m \cos m\phi + B_n^m \sin m\phi\right), \qquad (2.40)$$

That is a constant main field, A_0^0, plus error terms. In the expression, R_0 is the radius of the sphere where the magnetic field is measured, $\mu = \cos\theta$, $P_n^m(\mu)$ denotes the associated Legendre polynomial and A_n^m, B_n^m are arbitrary constants to be determined by the discrete values of magnetic field measured on the sphere [65]. A table and graph of Legendre polynomials are given in appendix D.

A reverse problem of surface harmonics is to determine those coefficients, A_n^m and B_n^m from a set of measurements of magnetic field in a given sphere. Given a colatitude angle θ on a sphere with radius r, a circle will be produced in a x-y plane. By equally dividing this circle in the longitude angles ϕ, there are discrete samples of points on the sphere. Assuming N_z as the number of x-y planes specified by equal-angles θ_i and N_ϕ as the number of samples in each of the x-y planes specified by equal-angles ϕ_j, the coefficients are calculated as

$$A_n^m = \frac{(2n+1)(n-m)!}{(N_\phi - 1)(n+m)!}\sum_{i=1}^{N_z} \omega_i P_n^m \cos\theta_i \sum_{j=1}^{N_\phi} B_z(\theta_i,\phi_j)\cos(m\phi_j),$$

$$B_n^m = \frac{(2n+1)(n-m)!}{(N_\phi - 1)(n+m)!}\sum_{i=1}^{N_z} \omega_i P_n^m \cos\theta_i \sum_{j=1}^{N_\phi} B_z(\theta_i,\phi_j)\sin(m\phi_j),$$

where ω_i is one of weights. Samples of magnetic field $B_z(\theta_i,\phi_j)$ can be measured with MR Probe-Array on a specified sphere, their positions are illustrated in Figure 2-12.

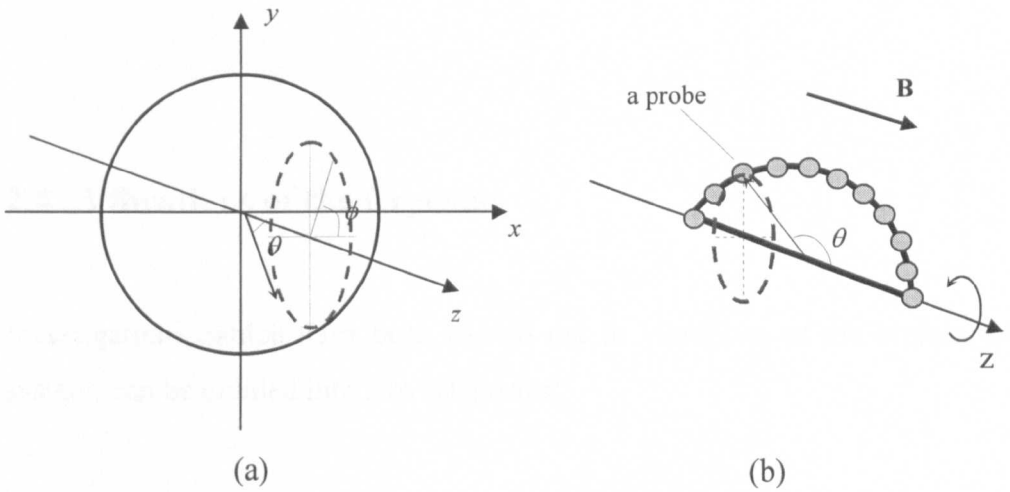

Figure 2-12 (a) Positions of samples on a sphere with spherical coordinates. (b) MR probe array in a magnetic field camera

A real MR Probe-Array Type MFC-3045 is displayed in Figure 2-13

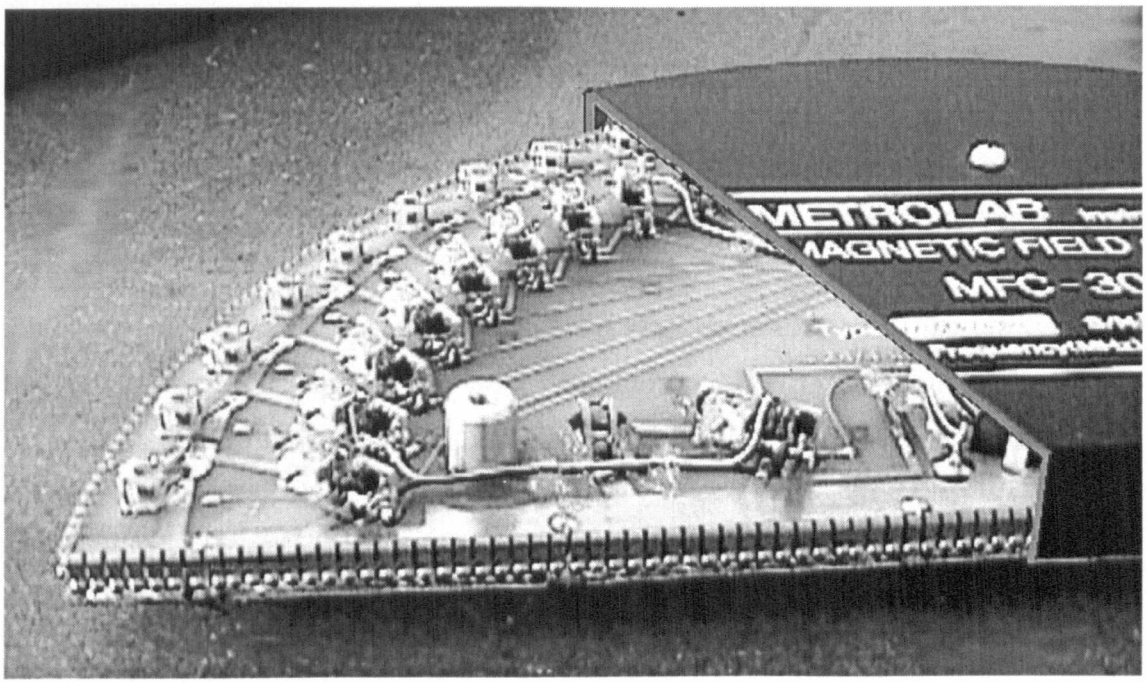

Figure 2-13 Partial view of a Half Moon type Probe-Array with a part of cover removed, showing probes.

2.4 Vibrations of the Cryostat

Investigations, which have been carried out in vibrations of the cryostat of the MRI system, can be divided into five categories:

- the vibrations and control of the Cold Head [27,35,45-46,49-60,62];
- the structural dynamic tests and analysis [24-25,43-44 ,61];
- the vibrations in the transportation [43], [63];
- the vibrations of the floor and their transmissions [29,48];
- fatigues of the structural components due to the vibrations.

Among them the investigations of the first and the second closely correlate with the phase distortions.

The vibration of the Cold Head was found to be the main source of the structural vibrations of the cryostat and phase distortions. The Cold Head is mounted in the cryostat as shown in Figure 1-3 and in appendix E. There are two main paths for vibration, via the braids and via the OVC and suspension elements. The top flange of the AV mount is the input to the braid path and the OVC is the input to the others. Figure 2-14 gives a schematic vibration model of the Cold Head and its AV mount [49].

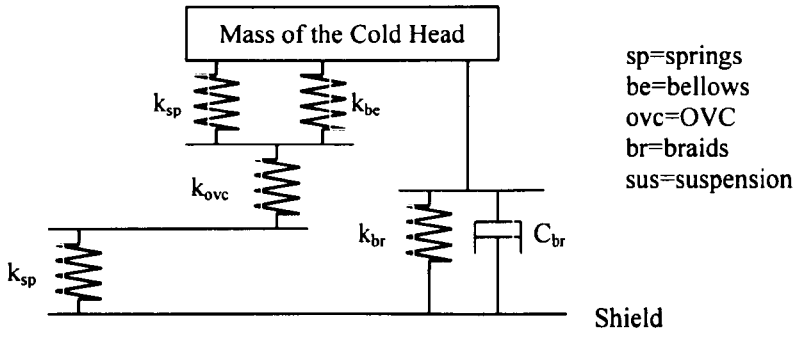

Figure 2-14 Vibration model of the Cold Head.

There are many types of cryostats, in which Type OR24, OR71 and OR70 were more completely investigated in the structural dynamics. Different types possess different modals. Within 50Hz all of the mode shapes can be regarded as of rigid body vibrations [44-45,57-58]. In Type OR71 and OR70, the lower frequencies tend to be matched to both the Helium Can and the shields indicating a bulk movement of them [24,42]. The similar low frequency whole body resonance was observed in Type OR58, OR26 and OR24 [41]. Completely different dynamics of a cryostat was found between two experiments with and without the magnetic field, such as significant frequency shifts and enormous damping increases when magnet is energised [24].

2.5 Eddy Current

The eddy current exists in the shields of the cryostat, because of the relative motion between the shields and magnet measured. The eddy current affects dynamics of the cryostat significantly, increasing the natural frequencies and the damping [24]. The eddy currents were also regarded as a main source of phase distortions [42,44]. A primary calculation of the eddy current was proposed excluding the effect of the inductance of the shield [42]. But that may be too cursory to give an exact result.

A general problem of the distribution of eddy currents in a slab of conducting saturable material is expressed in the following Maxwell's equations [6,719],

$$\nabla \times \mathbf{E} + \frac{\partial}{\partial t}(\mathbf{B}_r + \mathbf{B}_{ex}) = 0, \tag{2.41}$$

$$\nabla \times \mathbf{H} = \mathbf{J}, \tag{2.42}$$

$$\mathbf{B} = \mu(|\mathbf{H}|)\mathbf{H}, \tag{2.43}$$

$$\nabla \cdot \mathbf{B} = 0, \tag{2.44}$$

$$\nabla \times \mathbf{J} = 0, \tag{2.45}$$

$$\mathbf{B} = \mathbf{B}_{ex} + \mathbf{B}_r. \tag{2.46}$$

The notations are given as

$\mathbf{B}$	total magnetic flux density in units of Tesla,
$\mathbf{B}_r$	reaction magnetic flux density in units of Tesla,
$\mathbf{B}_{ex}$	excitation magnetic flux density in units of Tesla,
$\mathbf{H}$	total magnetic field strength in units of A/m,
$\mathbf{E}$	induced electric field in units of V/m,
$\mathbf{J}$	vector of the current density in units of A/m^2,
μ	magnetic permeability in units of N/A^2.

To try to obtain a general solution for such a complicated problem appears quite unrealistic. The eddy current calculation has become a special subject and complex to apply in engineering. It needs careful consideration of choosing the boundary conditions, the formulations and numerical methods [19-21]. Therefore it is recommended here to use substitutive methods in the estimation of the eddy current

effects. The combination of the experimental and analytical methods may be one to be used in the research.

2.6 Vibration Isolation and Control

In many practical situations, it is possible to reduce but not eliminate the dynamic forces that cause vibrations. Several methods can be used to control vibrations. Among them the following are noteworthy [3,4,9,15]:

- by controlling the natural frequencies of the system and avoiding resonance under external excitations;
- by preventing excessive response of the system, even at resonance by introducing a damping or energy-dissipating mechanism;
- by reducing the transmission of the excitation forces from one part of the machine to another, by use of vibration isolators;
- by reducing the response of the system, by the addition of an auxiliary mass neutraliser or vibration absorber.

Before attempting to reduce the vibration levels in a machine or structure by increasing its damping, every effort should be made to reduce the vibration excitation at its source [18].

2.6.1 Control of Natural Frequencies

It is well known that whenever the frequency of excitation coincides with one of the natural frequencies of the system, resonance occurs. The resonance conditions must be avoided in any system, since the amplitude of vibration will reach its maximum value at

resonance. The natural frequency of a system can be changed either by varying the mass or the stiffness. Obviously this method is restricted by the functional requirements of the systems.

2.6.2 Using Damping Materials

In many cases, a system or machine may be required to undergo a range of vibration frequencies. It may not be possible to avoid resonance under all operating conditions. In such cases, damping materials, such as cast iron or laminated materials, can be used to reduce the system vibrations. The equation of motion of a single degree of freedom system with internal damping, under harmonic excitation can be expressed as

$$m\ddot{x} + k(1 + i\eta)x = F_0 e^{i\omega t}, \tag{47}$$

where η is called the loss factor. The loss factor is defined as $\eta = \frac{E}{E_s}$, where E represents the Energy dissipated in one cycle of harmonic displacement per radian, and E_s is the maximum strain energy in the cycle.

The amplitude of the response of the system at resonance is given by $\frac{F_0}{k\eta}$.

2.6.3 Passive vibration isolation

Vibratory forces generated by machines and other sources are often unavoidable, their effects on a dynamical system can be minimised by proper isolator design. An isolation system attempts either to protect a delicate object from excessive vibration transmitted to it from its supporting structure or to prevent vibratory forces generated by machines from being transmitted to its surroundings. Figure 2-15 (a) and (b) show these two cases

respectively. The basic problem is the same for these two cases, that of reducing the transmitted force [3,15].

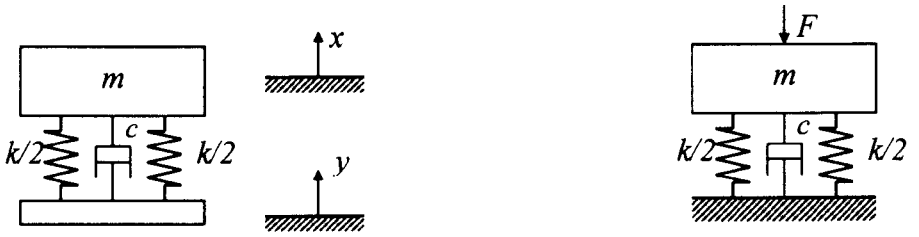

(a) (b)

Figure 2-15 (a) Motion transmitted from the support structure. (b) Disturbing force transmitted by the machine to the supporting structure.

In Figure 2-15(b), The force transmitted is expressed in the equation,

$$F_T = \sqrt{(kX)^2 + (c\omega X)^2} = kX\sqrt{1+\left(\frac{2\xi\omega}{\omega_n}\right)^2}, \tag{2.48}$$

where ω_n and ξ are the natural frequency and damping ratio defined as

$$\omega_n = \sqrt{\frac{k}{m}}, \text{ and} \tag{2.49}$$

$$\xi = \frac{c}{2\sqrt{km}}. \tag{2.50}$$

The transmissibility T_R, defined as the ratio of the transmitted force to that of the disturbing,

$$T_R = \left|\frac{F_t}{F_0}\right| = \sqrt{\frac{1+(2\xi\omega/\omega_n)^2}{\left[1-(\omega/\omega_n)^2\right]^2+[2\xi\omega/\omega_n]^2}}. \tag{2.51}$$

The ratio of the system displacement to that of the support structure, as shown in Figure 2-13(b), is the same as the transmissibility, that is

$$T_R = \left|\frac{F_t}{F_0}\right| = \left|\frac{X}{Y}\right|. \tag{2.52}$$

The transmissibility illustrates in Figure 2-16.

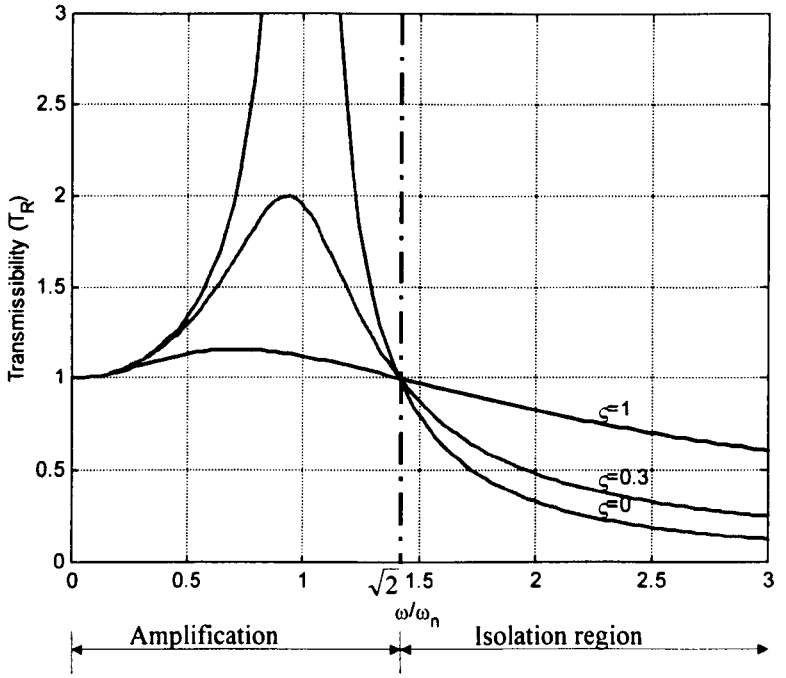

Figure 2-16 The transmissibility against frequency ratio.

The criteria for isolation must be obviously that the transmissiblility be as small as possible or $T_R \to 0$. Inspection of the graphs of Figure 2-16 shows that this requirement

is met only if the natural frequency of the system, ω_n, is much less than the frequency of the disturbing force, ω. For a given mass m this means that the stiffness k be small so that the system be very flexible. Conversely, for a given stiffness k it means that the mass m must be made large.

2.6.4 Active Vibration Isolation

A vibration isolation system is called active if it uses external power to perform its function. The external force is adjusted according to the feedback of the vibration of the objective system to eliminate the vibration. It consists of a sensor, controller (or signal processor), and an actuator. A typical schematic and a flow chart of an active isolation system are shown in Figure 2-17.

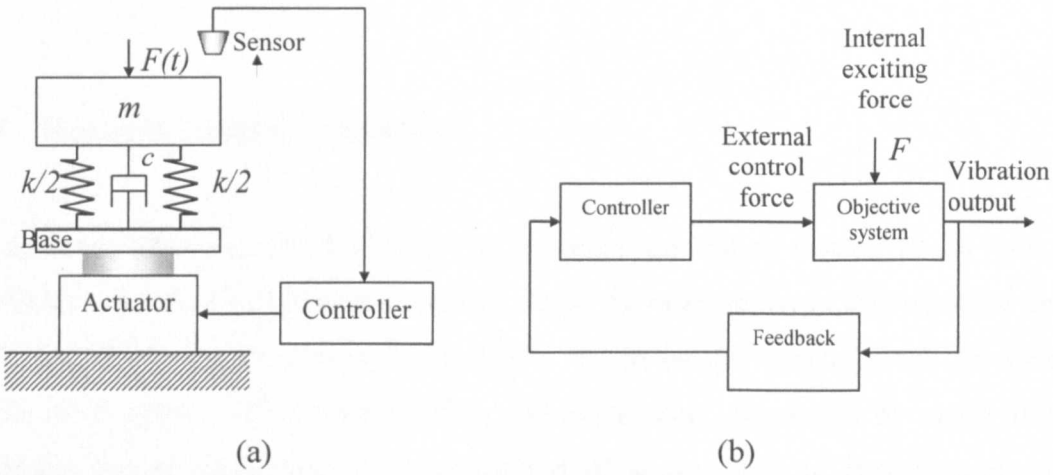

Figure 2-17 (a) An active vibration isolation system. (b) A flow chart of an active vibration control system.

This system tries to maintain zero vibration amplitude of the vibrating mass. As the force $F(t)$ applied to the system, the system fluctuates up and down. This excitation of the vibrating body is sensed by the sensor, which produces a signal proportional to the

excitation. The signal is processed in the controller and converted into a control signal of the actuator. The actuator develops a motion or force proportional to the signal. The force will control the base displacement such that the vibration of the system is minimised.

In Figure 2-17(a), the actuator may be a mechanical system such as a rack-and-pinion or ball screw mechanism, fluidic system or piezoelectric and electromagnetic force generating systems. The controller may be a mechanical system or a microprocessor system.

In Figure 2-17(b), the dynamics of the objective system may be described with linear differential functions or neural networks. The controller may be a PID or LQG controller, self-adaptive control algorithm or neural networks. Numerous modelling and controlling methods have been developed and applied to various vibration control systems.

2.6.5 Dynamic Vibration Absorbers

The dynamic vibration absorber (DVA) is a device, generating inertia, which reduces the vibration level of a protected structure. There are other terms in the literature for a DVA, e.g. 'anti-vibrator', 'dynamic damper', 'vibration absorber', 'shock absorber', etc.. In most cases a DVA consists of an additional mass, connected by means of an elastic and a damping element to the structure needing protection or directly to the out-of-balance machine, the source of vibrations. Figure 2-18 shows a typical DVA schematically.

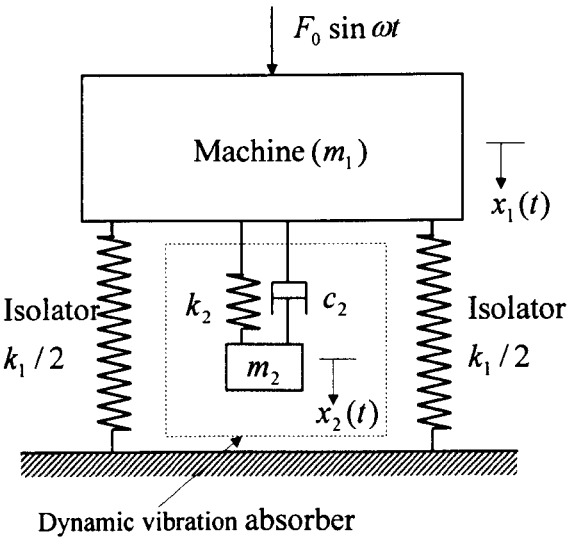

Figure 2-18 Design scheme for a system with a damped DVA

The magnitude of the machine vibration can be expressed as

$$\frac{X_1}{\delta_{st}} = \left[\frac{(2\xi q)^2 + (q^2 - p^2)^2}{(2\xi q)^2 (q^2 + \mu q^2 - 1)^2 + \{\mu q^2 p^2 - (q^2 - 1)(q^2 - q^2)\}^2} \right]^{1/2}, \tag{2.53}$$

in which the notes are defined as

X_1	Steady-state amplitude of the main mass in units of meter.
$\mu = m_2/m_1$	Mass ratio.
$\delta_{st} = F_0/k_1$	Static deflection of the system in units of meter.
$\omega_a = \sqrt{k_2/m_2}$	Natural frequency of the absorber in units of radian.
$\omega_n = \sqrt{k_1/m_1}$	Natural frequency of the main mass in units of radian.
$p = \omega_a/\omega_n$	Ratio of natural frequencies.
$q = \omega/\omega_n$	Forced frequency ratio.

$\xi = \dfrac{c_2}{2m_2\omega_n}$ Damping ratio.

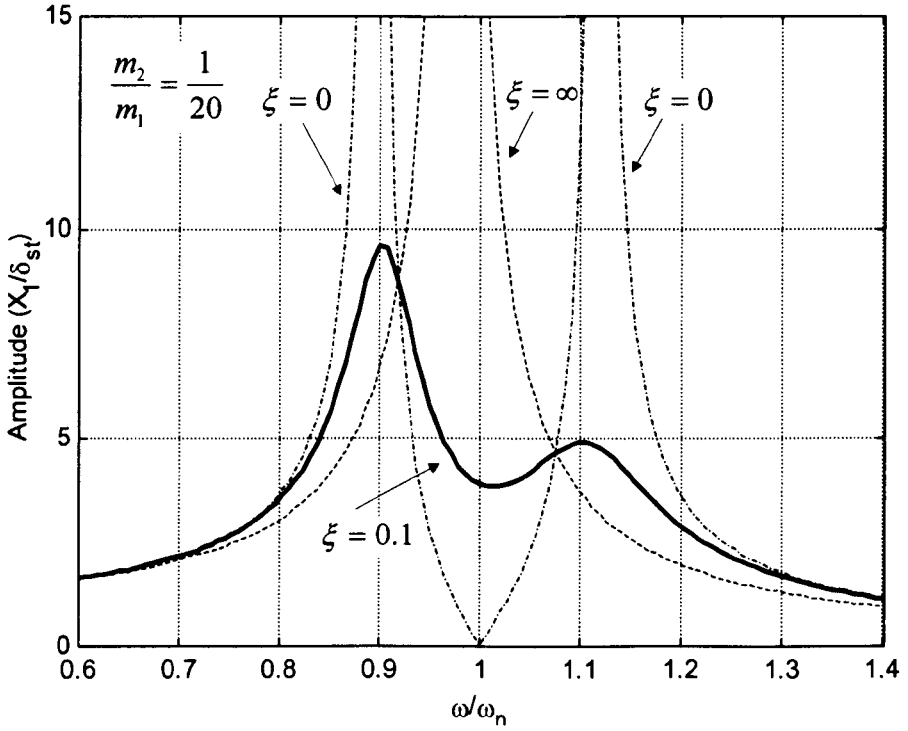

Figure 2-19 Effect of damped vibration absorber on the response of the machine.

Equation (2.53) is illustrated in Figure 2-19 and shows that the dynamic vibration absorber, while almost eliminating vibration at the known impressed frequency ω_n, introduces two resonant frequencies at which the amplitude of the machine limited by the damper. By optimally tuning mass m_2 and damping ratio ξ more effective result can be obtained. In various cases, other methods of DVA such as DVA with non-linear stiffness or multi-mass vibration absorbers, are applicable [17].

3 Systematic Approach to Investigate MRI Phase Distortion Problem

In an MRI system, the cryostat is the most fundamental and expensive component, and needs an extremely static uniform magnetic field for precision imaging. Any structural vibration may cause distortion in the magnetic field and produce image blur according to the previous investigation. The problems exist in the MRI cryostats since vibration transmissions from the Cold Head are inevitable in practice. The improvement of the products will be restrained in the absence of a clear understanding of the problem. The vibration problem of the MRI system is relevant to many different sciences and technologies, therefore an approach of the investigation must be sorted out to avoid 'shooting in dark' before starting any costly researches. In this section, we discuss a systematical approach to find out which and how the structural vibrations influence the phase angle on a systematical point of view. In the succeeding sections the specific topics proposed here will be discussed in detail.

3.1 A Brief Review

The basic structure of the cryostat was presented in Figure 1-4 in section 1.4. Parts of the disassembled components are schematically illustrated in Figure 3-1.

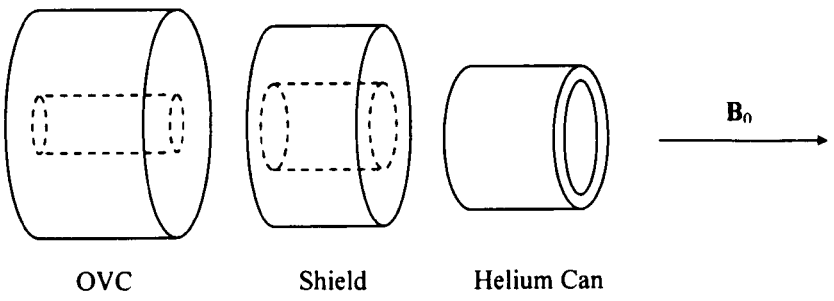

Figure 3-1 Components of the cryostat.

In the figure each component consists of two coaxial cylinders and end panels, and the inner cylinder of each component is depicted in dashed lines.

A magnetic flux density of about 1.0 Tesla or even more than 2.0 Tesla for higher resolutions is used in MRI imaging. The field is produced along the axial direction of the magnet by the super-conducting coils in the Helium Can. A criterion of evaluating the product quality in effects on the imaging blur is to measure the phase angle of the magnetization precession in the magnetic resonance. The phase distortion is zero in an absolutely static magnetic field [1]. The more the magnetic field fluctuates, the more the phase distortion is produced.

The precession of magnetization is governed by Bloch's equation,

$$\frac{d\mathbf{M}}{dt} = \gamma \mathbf{M} \times \mathbf{B}, \qquad (3.1)$$

in which the top of vector **M** rotates in the Larmer frequency of ω ($\omega = \gamma|\mathbf{B}|$) about vector **B** forming the track of a cone. Distortions of the phase angle can be measured by means of an NMR spectrometer, if the magnetic field, **B** , or the angular velocity of the precession, ω, is changing during the measurement [14].

3.2 System analysis

An MRI system can be divided into three subsystems according to inputs and responses. The first is the magnetic resonance system, which is mainly governed by Bloch's equation. The second is the electromagnetic system in which the field of the super-conducting magnet is included, this system is mainly dominated by the Maxwell's

equations. The last is the system of the mechanical structure, its vibration properties can be characterised by the theory of vibration. These subsystems and their relations with each other are illustrated in Figure 3-2.

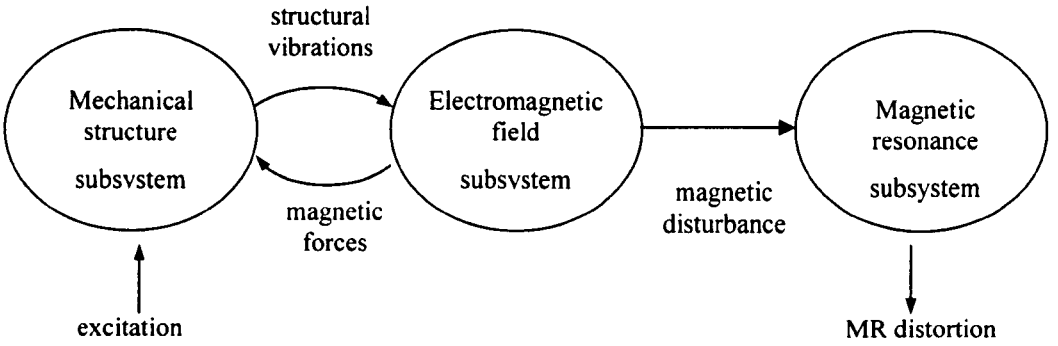

Figure 3-2 Consistence of MR system.

The problem of the system is the phase distortions due to the structural vibrations. The goal of the problem system is to find out the source of the vibration and its relationship with the phase distortion, and consequently to reduce the phase distortion at least cost.

From the principles of structural vibration damping, before attempting to reduce the vibration levels in a structure by increasing its damping, every effort should be made to reduce the vibration excitation at its source [18]. But in many cases, the source of vibrations is inevitable. In an MRI system even a structural vibration with amplitude of 5 μm causes a significant phase distortion. Therefore, optimisation of the structure is necessary by analysing the vibration modals and frequency response functions (FRF) of the mechanical system. There are infinite numbers of vibration modals in an MRI system, but only few of them may affect the phase angle of the precession of magnetization. It is obvious that system analysis of the vibrations are essential to reduce the cost in the product modifications and improvements.

From Bloch's equation (3.1), the precession of magnetization is only affected by magnetic field **B**. Since **B** is a vector, both directional and scalar changes of **B** will cause the angular velocity of the precession to fluctuate, thus distorting the phase angle of the precession. Different structural vibrations will be aroused by an excitation through different transmissions and in different vibration modals. For example the vibration of the Cold Head can be transmitted to the shields through the OVC and suspension rods or through the brass braids, as shown in appendix D [45]. These vibrations will affect the magnetic field in different ways. The relationships among phase distortions, magnetic disturbances and structural vibrations are illustrated in Figure 3-3.

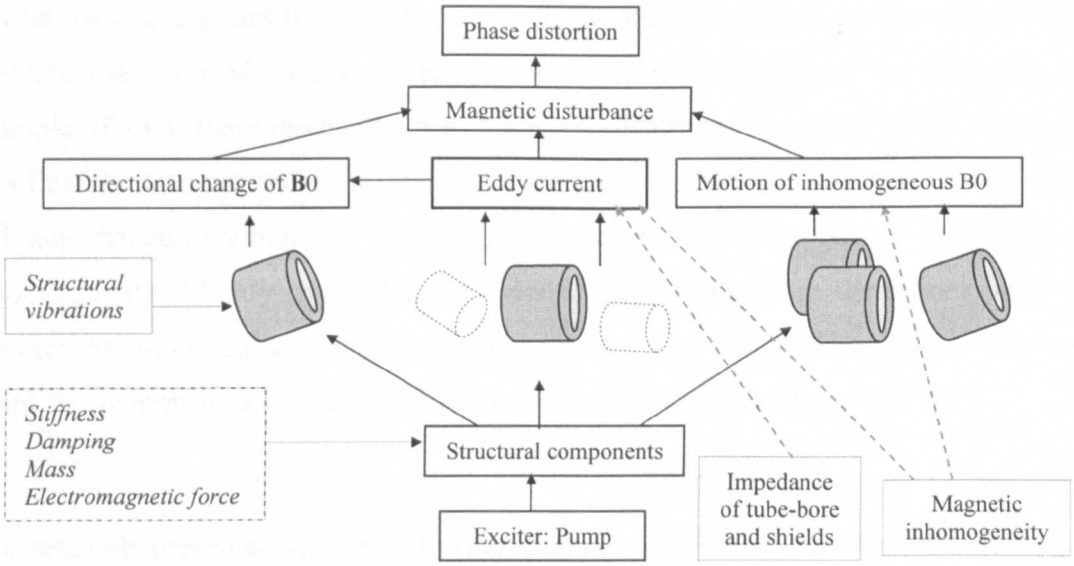

Figure 3-3 Schematic of system analysis.

It is shown in above figure that the phase distortion is aroused by the magnetic disturbances, which are ascribed to the directional change of magnetic field, the eddy current and the motion of inhomogeneous magnetic field. The reason to ascribe magnetic disturbances to these three aspects comes from the following considerations.

Firstly, the directional change of the magnetic field affects phase angle in very different ways from the scalar change of the magnetic field, it will be discussed in a subsequent section. Secondly, they are aroused by different structural vibrations in very different ways. For instance, a rotational vibration of the Helium Can (gray color in Figure 3-3) is able to cause directional change of magnetic field whilst only relative motions or mainly relative rotation between the Helium Can and shields can produce eddy currents in the shields. And motions of the Helium Can are able to cause magnetic fluctuations, only if the magnetic field is sufficiently inhomogeneous. The effects of eddy currents and magnetic inhomogeneity on the phase distortions also depend on non-structural factors, such as the electronic impedance of the shields and the magnetic gradient respectively.

Figure 3-3 gives a clear indication to find out the formation of the phase distortions. It can be used to instruct the investigations of the phase distortion problem and to pre-evaluate the costs of various investigations and modifications of the products. For example, if all of these three aspects of magnetic disturbances produce phase distortions significantly, a compromise must be made between modifications of structural vibration and non-structural vibration. The latter are the electronic impedance and magnetic inhomogeneity. If only parts of them produce significant phase distortions, only the relevant vibrations and structures need to be investigated and modified further. That will simplify the improvements of the products and reduce costs in the production.

The research presented in the following chapters is derived based on the results of systematical approach given in this chapter.

4 Theoretical Development

4.1 Cryostat Structural Vibrations

In this section basic structural vibrations of the cryostat will be discussed for the purpose of deducing fundamental relationships between structural vibration and magnetic disturbance in following sections. There are different types of cryostats, such as Type OR24, OR42, OR70 and OR71 etc.. The common feature is that each one consists of a Helium Can, an OVC and one or two shields, as shown in Figure 3-1. Here only rigid motions of the Helium Can and rigid relative rotations between the Helium Can and other components, such as the shields or OVC, will be discussed with regard to their effects on the magnetic disturbances.

4.1.1 Vibration of Rigid Body

Consider a hollow cylinder, which represents a cylindrical bore of a component of the cryostat, as shown in Figure 4-1.

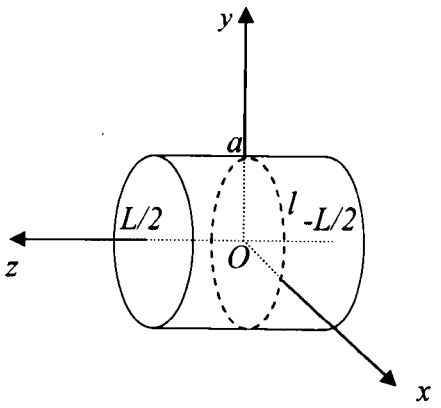

Figure 4-1 The cylindrical bore of cryostat.

its forced vibration function can be described in the equation,

$$\mathbf{M}\ddot{\mathbf{X}} + \mathbf{C}\dot{\mathbf{X}} + \mathbf{K}\mathbf{X} = \mathbf{F}, \qquad (4.1)$$

where $\mathbf{M}$, $\mathbf{C}$ and $\mathbf{K}$ are 6 by 6 matrices of mass, damping and stiffness respectively. $\mathbf{X}$ and $\mathbf{F}$ are column vectors denoting the rigid body motion of the cylinder in the space and the exciting force from the suspensions or connection with the pump, respectively. They are shown as follows:

$$\mathbf{X} = [x_1 \quad x_2 \quad x_3 \quad x_4 \quad x_5 \quad x_6]^T, \ \mathbf{F} = [f_1 \quad f_2 \quad f_3 \quad f_4 \quad f_5 \quad f_6]^T,$$

where x_1, x_2, x_3 represent the origin of reference with respect to the rigid body, and x_4, x_5, x_6 represent the rotation of the rigid body.

Since the pump excites the structure periodically, denoting Ω as its basic frequency, the Fourier extensions of its components are given by

$$f_i = \sum_{n=1}^{\infty} a_{in}^{'} \cos\left(n\Omega t + \Psi_{in}^{'}\right). \qquad (4.2)$$

To solve equation (4.1), the vibration modals and pump exciting spectrum are needed. The solution of equation (4.1) should be in the form as

$$x_i = \sum_{n=1}^{\infty} a_{in} \cos(n\Omega t + \Psi_{iin}), \qquad (4.3)$$

from which the motion of a point fixed in reference of the rigid body can be calculated by the equation,

$$\mathbf{r}(t) = \mathbf{c}_1(t) + \mathbf{A}_1(t)\mathbf{r}_1, \qquad (4.4)$$

where $\mathbf{c}_1(t)$ represents the motion of the body-reference origin, specified by x_1, x_2, x_3, and $\mathbf{A}_1(t)$ is the rotation matrix of the body reference specified by x_4, x_5, x_6. In fact the shield and Helium Can are suspended on OVC, therefore their motions are coupled with that of OVC.

It is impossible to obtain all vibration modals of the cryostat by experiment. It is also complicated and difficult to deduce the relationship between the all of the structural vibrations and the magnetic disturbances even if the general solution of the vibration given by equation (4.4) can be found. In fact, only some basic vibration modals are strong and exited by the pump, the relations between those modals and magnetic disturbances need to be examined

4.1.2 Motions of the Helium Can

The analysis starts from two DOF vibrations of the cylindrical Helium Can. That is, the axis of the Helium Can only translates along the x-axis in the x-z plane and/or rotates about the y-axis in the x-z plane in sinusoid, as shown in Figure 4-2.

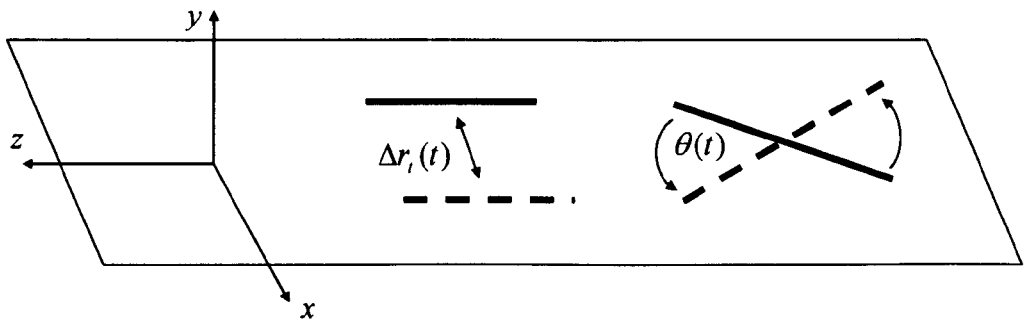

(a) (b)

Figure 4-2 The vibration of the Helium Can.

These vibrations can be described respectively by the equations,

$$\Delta r_t(t) = \Delta r_t \cos(\Omega_t t + \Psi_t) \text{ and} \qquad (4.5)$$

$$\theta(t) = \theta_r \sin(\Omega_r t + \Psi_r). \qquad (4.6)$$

Considering the fact that the rotational angle of θ_r is very small, the basic motion of a point in the bore of the Helium Can is regarded as sinusoidal vibration given by the equation,

$$\Delta\mathbf{r}(t) = \Delta r \cos(\Omega_1 t + \Psi_1)\mathbf{u}, \qquad (4.7)$$

where **u** is a static unit vector in the x-z plane, Δr, Ω_1 and Ψ_1 are amplitude, frequency and phase of the vibration respectively. Δr is variable in the space.

4.1.3 Relative Rotation between Helium Can and Shield

The relative rotation between the Helium Can and shield is assumed to be a sinusoidal vibration of their axes in a plane, as shown in Figure 4-3. Since the magnetic field in the bore is symmetric to its axis, the magnetic flux changes in the bore of the shield is regarded mostly due to the relative vibration, hence the other relative motions will not be discussed at the moment.

Figure 4-3 illustrates this rotation, in which the bore-tube of the shield is depicted in dashed lines. In the bore a surface current will occur and produce electromagnetic field, which may be one of the sources of the magnetic field distortions.

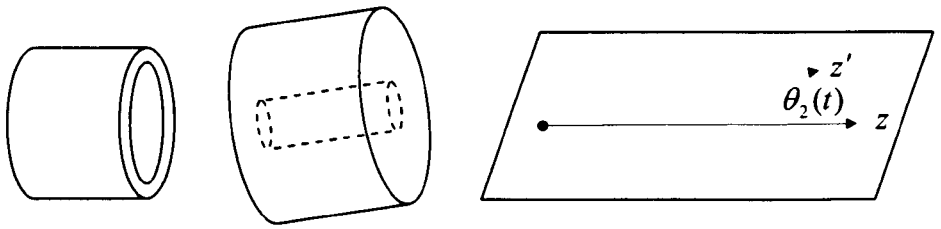

Helium Can Shield

Figure 4-3 The relative rotations between the shield and Helium Can.

These relative rotations can be described in the form as

$$\theta(t) = \theta_2 \sin(\Omega_2 t + \Psi_2), \qquad (4.8)$$

where θ_2, Ω_2 and Ψ_2 represent the amplitude, frequency and phase of the relative vibration, respectively.

4.2 Theoretical Description of Magnetic Disturbance

The magnetic field at a point in the field may change either in its direction or in its magnitude if mechanically excited. From Bloch's equation both directional and scalar change of the magnetic field will affect precession of the magnetization, hence cause the phase distortions.

In this section the disturbances of magnetic field of the cryostat are investigated from three aspects of magnetic variations. They are the motion of the inhomogeneous magnetic field, directional change of the magnetic field, and eddy current in the conductors of the cryostat respectively. The relationship between the magnetic disturbance and structural vibration will be discussed. And also some important characteristics of the magnetic disturbances will be revealed.

4.2.1 Disturbance due to Magnet Motion

The manufacturers of the MRI magnets go to great lengths to provide a homogeneous magnetic field in the region of the sample space, incorporating first-, second-, and higher-order shim for fine correction. However it is inevitable that some variation in magnetic field across the sample will still occur, although typically this leads to a broadening of no more than a few Hz in the proton NMR spectrum or less than 20nT of magnetic field variation. In intuition, it is obvious that the motion of the magnet will cause the magnetic field to change if the field is measured at a fixed point of laboratory coordinates. To express this magnetic disturbance mathematically, a proper definition of static magnetic inhomogeneity is required.

In OMT the definition of magnetic inhomogeneity is the peak to peak variation of the field about the central frequency [67]. But it is difficult to describe local magnetic inhomogeneities in the field by this definition. Here the gradient of magnetic field density is used to define the magnetic inhomogeneity, or local magnetic inhomogeneity.

The magnetic field is denoted by vector $\mathbf{B}(\mathbf{r}')$ in the position pointed by space vector $\mathbf{r}'$ in the body reference of the magnet. In the vicinity of the tip of vector $\mathbf{r}'$, the magnetic field can be described by the equation,

$$B(\mathbf{r}'+\Delta\mathbf{r}) = B(\mathbf{r}') + \Delta\mathbf{r}'\cdot\mathbf{G}(\mathbf{r}'), \tag{4.9}$$

where $\mathbf{G}(\mathbf{r}')$ is the gradient of the magnetic field at the position pointed by vector $\mathbf{r}'$, and $\Delta\mathbf{r}'$ is an offset vector from $\mathbf{r}'$. In the following discussion, $\mathbf{G}(\mathbf{r}')$ is supposed to be constant in the vicinity of the position pointed by $\mathbf{r}'$. The gradient, $\mathbf{G}(\mathbf{r}')$, is the rate of magnetic variation at the given position in the space, hence it reflects the magnetic inhomogeneity at this position.

Neglecting the directional change of the magnetic field in a position, we write the magnetic flux density due to its inhomogeneity and motion as follows,

$$B(\mathbf{r},t) = B_0(\mathbf{r}) + \Delta\mathbf{r}(t)\cdot\mathbf{G}(\mathbf{r}), \tag{4.10}$$

where $\Delta\mathbf{r}(t)$ represents displacement of a position in the magnet in the laboratory frame, $B_0(\mathbf{r})$ is the magnetic flux density when the magnet is in the equilibrium and $\mathbf{G}(\mathbf{r})$ is the gradient of the magnitude of the magnetic flux density in vicinity $\Delta\mathbf{r}$ of $\mathbf{r}$. Then the maximum disturbance of the magnetic flux density is expressed as

$$\Delta B_{\max}(\mathbf{r}) = \Delta\mathbf{r}_m(\mathbf{r})\cdot\mathbf{G}(\mathbf{r}) \tag{4.11}$$

where $\Delta\mathbf{r}_m(\mathbf{r})$ is the displacement between positions in the track of a vibrating point , which maximises the dot product of the displacement and gradient.

From equation (4.11), it is revealed that the magnitude of the disturbance of the magnetic field depends both on the magnetic gradient and motion of the magnetic field. Therefore, any motion of the magnet can cause the magnetic disturbance, if a magnetic gradient exists in the direction of motion. On contrary, there is no magnetic disturbance when the magnetic gradient is zero in the direction of motion, even if the vibration displacement is significant in the direction.

From previous discussion, possible modification of the structure is also implied. That is, if the effect of static inhomogeneous magnetic field cannot be neglected, then the static magnetic gradient and vibration of the magnet must be investigated. Then, either to have the magnetic gradient decreased or to modify the mode shape of the vibration of the magnet is necessary to reduce the magnetic disturbance.

4.2.2 Disturbance due to Eddy Current

Only the eddy current in the inner cylindrical bore of a shield is discussed in this subsection, because the others are far away from the probe and much weaker compared to the previous one. The eddy current is regarded as mainly caused by the relative rotation between the conductive bore-tubes and the homogeneous magnetic field.

Consider the relative rotation between the cylindrical shield and magnet indicated in Figure 4-3 and equation (4.8), the external magnetic field, $\mathbf{B}_0$, is assumed homogeneous and constant, sine eddy-current due to the magnetic flux change of magnetic inhomogeneity is negligible compared to that due to change of $\mathbf{B}_0$ itself. Looked from the reference frame of the shield, the magnetic field vibrates rotationally that can be expressed by the equations,

$$\mathbf{B}(t) = B_0 \sin\theta(t)\mathbf{a}_x + B_0 \cos\theta(t)\mathbf{a}_z \qquad (4.12)$$

and

$$\theta(t) = \theta_2 \sin(\Omega_2 t + \Psi_2), \tag{4.13}$$

where θ_2, Ω_2 and Ψ_2 represent the amplitude, frequency and phase of the rotational angular vibration respectively. In equation (4.12) the flux density, $\mathbf{B}(t)$, consists of two components as shown in Figure 4-4.

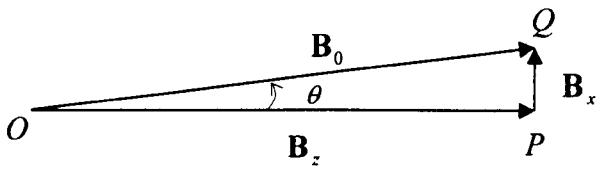

Figure 4-4 Magnetic Variation of horizontal component.

Since the rotation angle θ is very small, for instance usually $\theta \leq 1.5\times10^{-5}$ (rad), the components of $\mathbf{B}_0$ can be written approximately in Taylor expansion,

$$B_z = B_0 - \frac{1}{2}B_0\theta_2^2 + \frac{1}{4}B_0\theta_2^2\cos(2\Omega_2 t + 2\Psi_2) \tag{4.14}$$

and

$$B_x = B_0\theta_2 \sin(\Omega_2 t + \Psi_2). \tag{4.15}$$

The time-dependant components of B_x and B_z on the right-hand sides of these two equations are respectively described by the equations,

$$\Delta B_z = \frac{1}{4}B_0\theta_2^2\cos(2\Omega_2 t + 2\Psi_2) \tag{4.16}$$

and

$$\Delta B_x = B_0\theta_2 \sin(\Omega_2 t + \Psi_2). \tag{4.17}$$

From the equations it shows that the magnitude of magnetic field changes much greater in the x-axis than that in the z-axis.

According to Faraday's Law of induced electric potential,

$$\varepsilon = \oint_l \mathbf{E} \cdot d\mathbf{l} = -\frac{d\phi}{dt} = -\frac{d}{dt}\int_S \mathbf{B} \cdot d\mathbf{s}\,, \tag{4.18}$$

electric fields will be produced about x-axis and z-axis due to the variations of B_x and B_z respectively. If the shield is an electric insulator, there will no eddy current in the shield. But if the shield is a conductor, eddy currents will be induced in the shield. According to the Lenz's Law [5], *the current flows in the closed loop in such a direction as to oppose the change in the linking magnetic flux*, as show in the dashed lines in Figure 4-5.

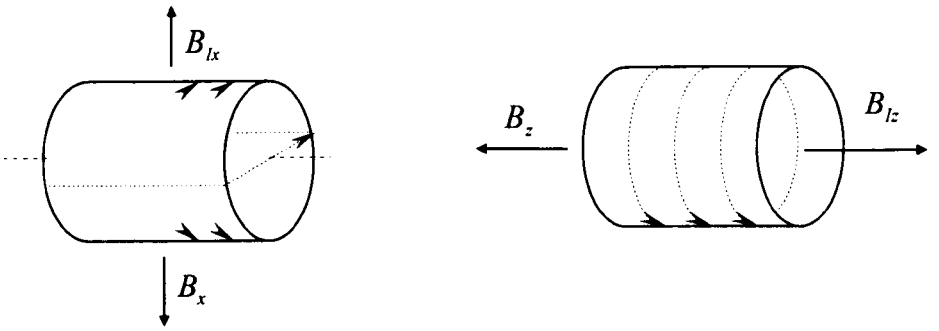

Figure 4-5 Eddy current distribution in the cylindrical shields due to B_x and B_z.

The eddy currents in turn produce the magnetic field $\mathbf{B}_{lx}$ and $\mathbf{B}_{lz}$. We call the sum of $\mathbf{B}_{lx}$ and $\mathbf{B}_{lz}$ the induced magnetic fields, and $\mathbf{B}(t)$ the external magnetic field. In fact, the eddy current is induced by the vector sum of both the external magnetic field and the induced magnetic field, and their relationships must be obeyed by Maxwell equations [5,16]. The results can be calculated by applying specific algorithm. But that is what we are going to avoid, because of the complexity of calculation.

In practice the change of the self-linking magnetic flux or the change of the magnetic flux induced by the eddy current must be always less than the change of the external magnetic flux in their magnitudes. The maximum value of the induced magnetic field will be reached if the shield is super-conductive. In this condition the external magnetic flux change is opposed by the eddy current and the total flux change is exactly cancelled. That means the total magnetic flux is constant in the reference frame of the magnet. But the magnetic field induced by the eddy current may not perfectly oppose the change of the external magnetic field in every point in the space. The induced field is an integration of the differential magnetic flux density governed by the Biot-Savart Law,

$$d\mathbf{B}_I = \frac{\mu_0}{2\pi}\frac{d\mathbf{I}\times\mathbf{r}}{r^3}. \tag{4.19}$$

In this equation, $d\mathbf{I}$ and $\mathbf{r}$ represent the differential eddy current and the displacement pointing to the position of $d\mathbf{B}_I$ from the position of $d\mathbf{I}$, as shown in Figure 4-6. The integration is expressed in the equation,

$$\mathbf{B}_I(\mathbf{r}) = \iint_S \frac{\mu_0}{2\pi}\frac{d\mathbf{I}\times\mathbf{r}}{r^3}, \tag{4.20}$$

where area S represents the surface of the shield and $\mathbf{B}_I$ is the induced magnetic flux density at position pointed by $\mathbf{r}$ in the space. Now the upper limit of the induced magnetic flux density inside the cylinder of the shield can be decided from following deduction.

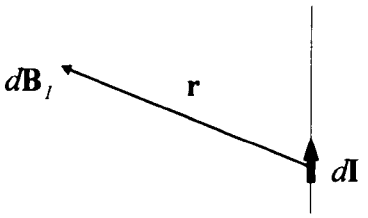

Figure 4-6 The magnetic flux density produced by a differential current.

The magnetic flux from the eddy current is defined by the integration of the production of the differential area of shield surface area S and the normal component of the magnetic flux density on the differential area, as expressed in the equation,

$$\phi_I = \iint_S \mathbf{B}_I \cdot d\mathbf{s} . \tag{4.21}$$

Generally the magnitude of the magnetic flux density is always less if its distance from the current source is longer. Therefore the magnitude of $\mathbf{B}_I$ will increase from the axis to the inner surface of the shield. If the lengths of the shield and the magnet are infinite, it is known that B_{Ix} is homogeneous in the line parallel to the axial of the cylinder, and B_{Iz} is homogeneous everywhere inside the cylinder [73], hence the radial and axial components of the induced magnetic field are given respectively by

$$B_{Ix} < B_x = B_0 \sin\theta(t) \tag{4.22}$$

and

$$B_{Iz} < B_z = B_0 \cos\theta(t) . \tag{4.23}$$

It can be inferred that if the length of the shield is much longer than its radius, these two equalities generally are still true, especially near the z-axis of the shield. These equalities will further discuss in next section.

4.2.3 Directional Change of Magnetic Field

The directional change of the magnetic field can be caused either by the rotational vibration of the magnet or by the eddy current in the shield.

Neglecting all the scalar changes of the magnetic field, a pure sinusoidal directional vibration of the magnetic field is expressed in the equations,

$$\mathbf{B}(t) = B_0 \sin\theta(t)\mathbf{a}_x + B_0 \cos\theta(t)\mathbf{a}_z \tag{4.24}$$

and

$$\theta(t) = \theta_0 \sin(\Omega t)\,. \tag{4.25}$$

In next chapter, the phase distortion due to a directional change of the magnetic field will be discussed based on these expressions.

4.3 Theoretical Description of Phase Distortion

The theoretical description of the phase distortion was discussed in the modular variation of the magnetic field before [26]. In this section a further description is given to the effect of the magnetic modular variation on the phase angle. From Bloch's equation, the phase angle of the magnetization is also affected by the directional change of the magnetic field, thereby the effect of the directional variation is investigated theoretically in this section.

4.3.1 Effect of Modular Change of Magnetic Field

Rewriting the definition of the phase distortion in general magnetic disturbance as

$$\Delta\Phi = -\gamma \int_0^{T_E/2} \Delta B(t)dt + \gamma \int_{T_E/2}^{T_E} \Delta B(t)dt . \qquad (4.26)$$

It can be seen that the first integration is the area between the field disturbance, $\Delta B(t)$, and the horizontal axis during the first half of echo time T_E, and the second integration is that during the second half of echo time T_E. The phase distortion is the net area subtracting the first area from the second. Considering two sinusoidal variations of magnetic field with same magnitude but different frequencies, their effects are obviously different. The phase distortion due to the magnetic disturbance with the higher frequency is less than that due to the magnetic disturbance with the lower frequency. That is because the magnetic disturbance of higher frequency makes less net area both during the first and second half of echo time T_E comparing to that of lower frequency, hence produces less difference of subtracting these two areas. The magnetic disturbances with two different frequencies are shown in Figure 4-7, where the areas which make the phase distortions are illustrated with gray colour.

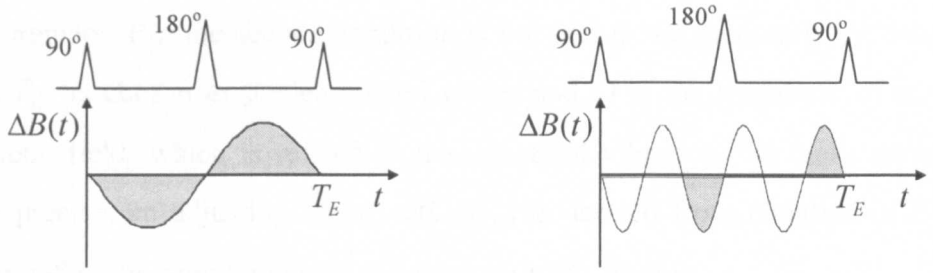

(a) Ω (b) 3 Ω

Figure 4-7 Phase angle distortions due to sinusoidal magnetic disturbances with different frequencies.

Theoretically the phase distortion due to a sinusoidal magnetic disturbances can be described by the equation,

$$\Delta\Phi = \frac{\gamma\Delta B_0}{\Omega}\left(2\sin(\frac{T_E\Omega}{2}+\Psi)-\sin(T_E\Omega+\Psi)-\sin(\Psi)\right). \tag{4.27}$$

The maximum possible value of peak to peak phase variation was expressed in the equation,

$$\Delta\Phi_{pk-pk} = \frac{8\gamma\Delta B_0}{\Omega}. \tag{4.28}$$

A further investigation shows that this phase variation is measured only if the following two conditions are simultaneously satisfied:

$$\Psi = \pm\frac{\pi}{2} + 2\pi k,\ k = 0,1,2,\cdots, \tag{4.29}$$

and

$$\Omega = \frac{2\pi n}{T_E},\ n = 1,2,3,\cdots. \tag{4.30}$$

The first condition usually is satisfied, because of the random of Ψ in each of the measurement. But the second condition is not met in the measurement, since the echo time, T_E, is chosen as predetermined values and Ω is the frequency of the sinusoidal magnetic field, which is related to the structural vibration. To make equation (4.28) more precise, an adjusting factor, $\alpha(\Omega/\Omega_E)$ is derived from equation (4.27) and it is multiplied to the right-hand side of equation (4.28). That is

$$\Delta\Phi_{pk-pk} = \frac{8\gamma\Delta B_0}{\Omega}\cdot\alpha\left(\frac{\Omega}{\Omega_E}\right), \tag{4.31}$$

where $\Omega_E = 2\pi/T_E$, and $\alpha(\Omega/\Omega_E)$ is determined by

$$\alpha\left(\frac{\Omega}{\Omega_E}\right) = \max_{\Psi}\left[\frac{1}{2}\sin\left(\pi\frac{\Omega}{\Omega_E}+\Psi\right)-\frac{1}{4}\sin\left(2\pi\frac{\Omega}{\Omega_E}+\Psi\right)-\frac{1}{4}\sin(\Psi)\right].$$

This equation is illustrated in Figure 4-8, which shows that the adjusting factor varies in a similar sinusoidal wave with respect to the ratio of Ω/Ω_E.

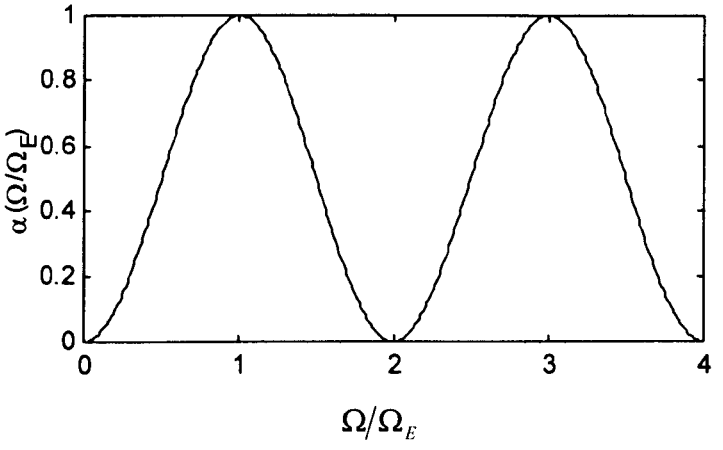

Figure 4-8 The adjusting factor.

It is obvious that the value of $\alpha(\Omega/\Omega_E)$ is within zero and one. Thus for a given echo time, T_E, equation (4.28) should be written by the inequality,

$$\Delta\Phi_{pk-pk} \leq \frac{8\gamma\Delta B_0}{\Omega}. \tag{4.32}$$

The right hand side of previous inequality can still be used as the maximum estimation of peak to peak value of the phase distortion, which is possible to be measured.

According to equation (4.31) the phase distortion is proportional to the magnitude of the magnetic disturbance, but its sensitivity to the frequency is modulated reversely by the frequency of the magnetic disturbance and proportionally by the adjusting factor, $\alpha(\Omega/\Omega_E)$. The frequency sensitivity of the phase distortion is defined as

$$S_{\Delta\Phi} = 2\alpha\left(\frac{\Omega}{\Omega_E}\right)\frac{1}{\Omega}, \tag{4.33}$$

which is illustrated in Figure 2-11. The following important properties of phase distortions are illustrated from these two figures:

- The phase distortion are most sensitive to the frequencies of magnetic disturbances near the half of Ω_E,
- To the frequencies higher than Ω_E the sensitivities are less than a quarter of the maximum value.
- At the frequencies of multiples of Ω_E the phase distortions vanish completely.

In the MR phase distortion measurement, more sensitive measurement is required to evaluate the magnetic disturbances in the wider frequency band, while in MR imaging applications the most sensitive frequency to the magnetic disturbance must be avoided if possible.

4.3.2 Spin Phase Angle in a Small Sample or Probe

In the experiment of measuring magnetic field disturbance with NMR spectrometer, a small sample or probe is used to produce MR signals. To analyse the measured MR signals theoretically, the relationship of the spin phase distortion between a point and the whole sample consisting of many points are needed.

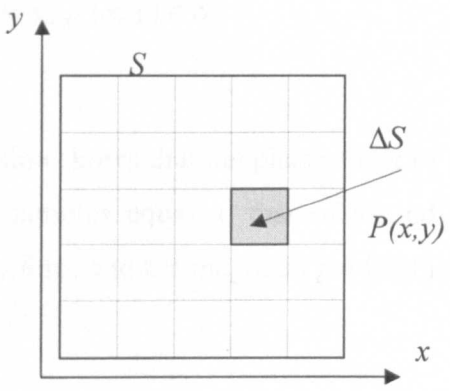

Figure 4-9 The cross section of a sample in the NMR probe.

Denote S as the area of a cross section of the sample and ΔS as the vicinity of a point in this area, as shown in Figure 4-9.

Then from equation (4.26) and the principles of spin echo, the deflected spin phase angles in the whole cross section of the sample are summarised into

$$\Delta\Phi_S = \tan^{-1}\left(\frac{\int_S \rho(x,y)\sin(\Delta\Phi(x,y))dxdy}{\int_S \rho(x,y)\cos(\Delta\Phi(x,y))dxdy}\right) \tag{4.34}$$

or

$$\Delta\Phi s = \tan^{-1}\left(\frac{\int_S \rho(x,y)\sin(\gamma\Delta\mathbf{r}\cdot\mathbf{G}(x,y)\xi)dxdy}{\int_S \rho(x,y)\cos(\gamma\Delta\mathbf{r}\cdot\mathbf{G}(x,y)\xi)dxdy}\right) \tag{4.35}$$

specially for the magnetic disturbance caused by the motion of the static inhomogeneous magnetic field.

If $\mathbf{G}(x,y)$ is constant and the density of the sample, $\rho(x,y)$ is homogeneous in area S, then

$$\Delta\Phi s = \Delta\Phi(x,y),\ \ (x,y)\in S. \tag{4.36}$$

This expression shows that the phase angle of summing all magnetization vectors of the spin in the samples equal to that of its individual vector of the spin, if the sample density is uniform and the magnetic gradient is constant in the sample.

4.3.3 Effect of Directional Change of Magnetic Field (the Adiabatic theorem)

The Adiabatic theorem states that *if the change of direction of the magnetic field is sufficiently slow, the axis Of the precession cone of the magnetization vector follows the direction of the field, and the angle of the cone does not change* [1].

In the above explanation, a "sufficiently slow" change of direction of the magnetic field means that the angular velocity of vector **B** is much smaller than the angular velocity $\gamma\mathbf{B}$ of the precession of spin. Figure 4-10 shows the adiabatic change of magnetic field illustratively.

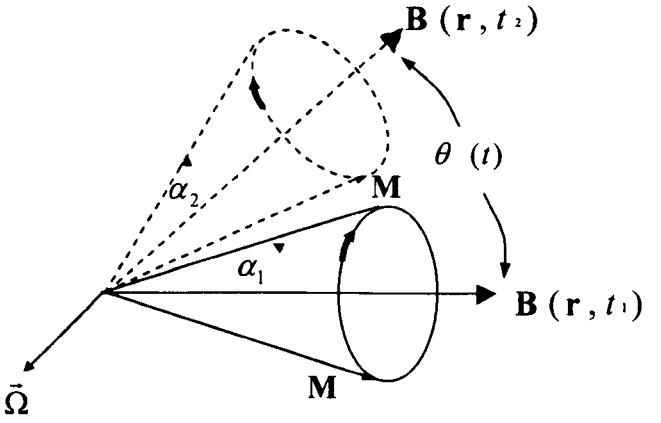

Figure 4-10 Adiabatic change of the magnetic field, $\alpha_1 = \alpha_2$.

In this figure $\theta(t)$ and $\vec{\Omega}$ represent the rotational angle and angular velocity of the magnetic field respectively, α_1 and α_2 are the precession angles at time t_1 and t_2, and $\mathbf{M}$ is the precessing vector of the magnetization. If $\theta(t)$ is given by equation (4.6), the angular velocity of the magnetic field can be expressed by the equation,

$$\vec{\Omega} = \frac{1}{|\mathbf{B}|^2}\frac{d\mathbf{B}}{dt} \times \mathbf{B} = \theta_r \Omega_r \cos(\Omega_r t + \Psi_r). \qquad (4.37)$$

Considering all the vibration frequencies measured by OMT and LMS smaller than 200Hz [25], which is much smaller than the typical Larmor frequency of about 63.86MHz, the possible angular velocities of the magnetic field are much smaller than the angular velocity of the spin precession. Therefore the directional change of magnetic field existing in the cryostat is the adiabadic change, that means the Larmor frequency of the magnetization does not change during the directional change.

5 Evaluation of Relationship between Phase Distortion and Magnetic Disturbance

In the previous sections, the theoretical descriptions of three magnetic disturbances were discussed. They are the directional change of the magnetic field, eddy current and the static magnetic inhomogeneity. In addition, the descriptions of the phase distortions were given. The fundamental relationship between the phase distortion and the magnetic disturbance was investigated. In this section, a further discussion of the relationship is presented and some quantitative evaluations are carried out to determine which of three magnetic disturbances will significantly affect the phase angle stability.

5.1 Effects of Directional Change in Magnetic Field

In section 4.3.3, the phase distortions due to the directional change in the magnetic field were discussed based on Adiabatic theorem. The theorem is the approximation with an error determined by the ratio of magnetic disturbance frequency to the Larmor frequency. But the vibration amplitude in the magnetic disturbance problems is within several nano-Tesla, or the phase angle distortion within 15 degree. Therefore the evaluation of the phase distortion from different aspect or with more precise method is required.

5.1.1 Theoretical Analysis

The precession of the MR magnetization is described by Bloch's equation as

$$\frac{d\mathbf{M}}{dt} = \mathbf{M} \times \gamma \mathbf{B}, \tag{5.1}$$

in which $\mathbf{M}$ is the vector of the magnetization, $\mathbf{B}$ is the magnetic flux density of the cryogenic magnet and γ is the gyromagnetic constant $\left(\gamma = 2.675 \times 10^8 T^{-1} s^{-1}\right)$. Consider the momentary rate of change of $\mathbf{B}$ written in the general form

$$\frac{d}{dt}\mathbf{B} = \vec{\Omega}_v \times \mathbf{B} + \Omega_1 \mathbf{B}, \tag{5.2}$$

in which the rate of change of $\mathbf{B}$ is represented as the sum of two components, perpendicular and parallel to $\mathbf{B}$ [1]. The quantities $\vec{\Omega}_v$ and Ω_1 with dimensions of s^{-1} can be interpreted as follows: $\vec{\Omega}_v$ determines the angular velocity with which vector $\mathbf{B}$ changes its direction, and Ω_1 determines the speed of change in the magnitude of $\mathbf{B}$. Consider a coordinate system $X'Y'Z'$ in which the axis Z' is in direction of vector $\mathbf{B}$. From the theory of kinematics [79], the motion of the magnetization in this rotating frame of reference can be written as

$$\frac{d\mathbf{M}}{dt} = \mathbf{M} \times \left(\gamma \mathbf{B} + \vec{\Omega}_v\right). \tag{5.3}$$

Let the coordinate system $X'Y'Z'$ rotates about y-axis of the laboratory coordinate system and the magnitude, B, of vector $\mathbf{B}$ is constant. Than in the coordinate system $X'Y'Z'$, Equation (5.3) can be decomposed into three scalar ones:

$$\frac{dM_{x'}}{dt} = \gamma M_{y'} B - M_{z'} \Omega_v, \tag{5.4}$$

$$\frac{dM_{y'}}{dt} = \gamma M_{x'} B, \tag{5.5}$$

$$\frac{dM_{z'}}{dt} = M_{x'} \Omega_v. \tag{5.6}$$

The Adiabatic theorem is obtained by omitting the term, $M_z \cdot \Omega_v$, in Equation (5.4), when $\Omega_v << \gamma B$. Consider that the axis of the magnet vibrates rotationally in equation (5.7), as illustrated in Figure 5-1.

$$\theta(t) = \theta_0 \sin(\Omega t). \tag{5.7}$$

The maximum angular velocity of the frame is

$$\left|\vec{\Omega}_v\right|_{\max} = \theta_0 \Omega, \tag{5.8}$$

which is only 6.28×10^{-4} rad/s if the rotational angle, θ_0, is equal to 1×10^{-5} rad and the rotational velocity, Ω, is 10Hz. On the other hand, the angular velocity of the Larmor frequency is about 4.01×10^{8} rad/s for a magnetic field, **B**, of 1.5 Tesla, that is 6.4×10^{11} times of the angular velocity of the magnet vibration. This means that the magnetization precesses 6.4×10^{11} times about the vector, **B**, in a period of the magnet vibration. Therefore the angular velocity of the precession can be regarded as constant in the rotating frame as if the magnetic field is statically slanted from its original position.

In theoretical analysis, if the axis of the precession cone is slant in a constant angle of, for instance, θ, the angular velocity of vector $M_x(t)$ fluctuates around the value of the angular velocity of the Larmor frequency. Obviously the fluctuating frequency of the angular velocity of vector $M_x(t)$ is the same as the precession. Then the peaks of the velocity are constants. The maximum and minimum peaks of the angular velocity of component $M_x(t)$ are given by

$$\omega_{x\max} = \frac{\omega}{\cos\theta} \tag{5.9}$$

and

$$\omega_{x\min} = \omega\cos\theta. \tag{5.10}$$

If the receiving coil is put along the x-axis and only the variation of component $M_x(t)$ induces signal in the coil, the phase distortions will be given by

$$\Delta\Phi_{pk-pk} \leq 8\theta_0^2, \tag{5.11}$$

according to equation (4.32). The value of the right side of equation (5.11) is only 4.59×10^{-8} degrees, if $\theta_0 = 1\times10^{-5}$ rad.

5.1.2 Computer Simulation

In the MR spectrometer application, the MR signal is induced by the transverse component, $\mathbf{M}_{xy}$, of the magnetization, $\mathbf{M}$, in the RF coil, as shown in Figure 5-1.

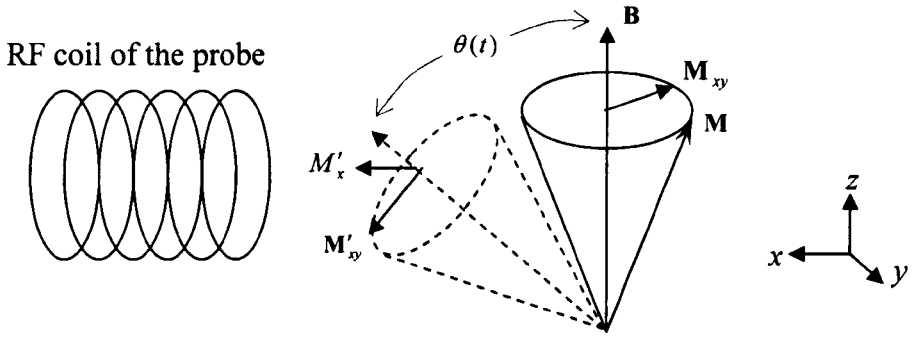

Figure 5-1 Experimentation of MR signal.

From the Bloch's equation $\mathbf{M}_{xy}$ rotates about the vector of the magnetic field if the field is static. Its x-axis component can be expressed as the equation

$$M_x(t) = M_{xy}\sin(\omega_e t), \tag{5.12}$$

where ω_e is the Larmor frequency. Assume that the coil surrounding the sample is parallel to the x-axis. The x component of $\mathbf{M}_{xy}$ penetrates the coil at right angles to its cross-section, thereby inducing an electromotive force.

The directional change of the precession axis is illustrated in Figure 5-1. This process can be simulated numerically from Bloch's equation, and its effect on the MR signal, hence on the phase distortion can be evaluated. The induced MR signal is simulated and illustrated in Figure 5-2 and Figure 5-3. These two simulations are carried out in relative lower frequency of the magnetization precession comparing to the practical value. This is because an acceptable precision can not be acquired with the very high ratio of the precession frequency to the frequency of the magnetic disturbance in the computer currently used by the author.

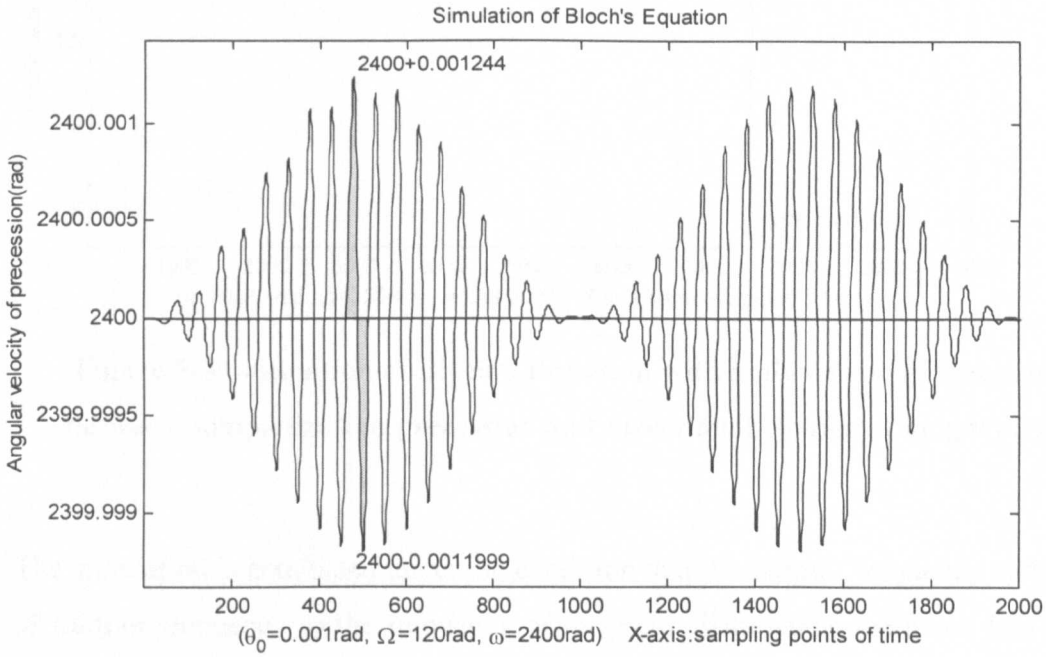

Figure 5-2 Simulation of the precession in the angular velocity, of $M_x(t)$, vs time.

From the graphs of simulations, it is shown that the momentary angular velocity of the vector $M_x(t)$ fluctuates around the value of the Larmor frequency of precession at the same Larmor frequency. And the magnitudes of the peaks of the angular velocity vary periodically in phase of the angular variation of the axis of the precession cone or in phase of the structural vibration.

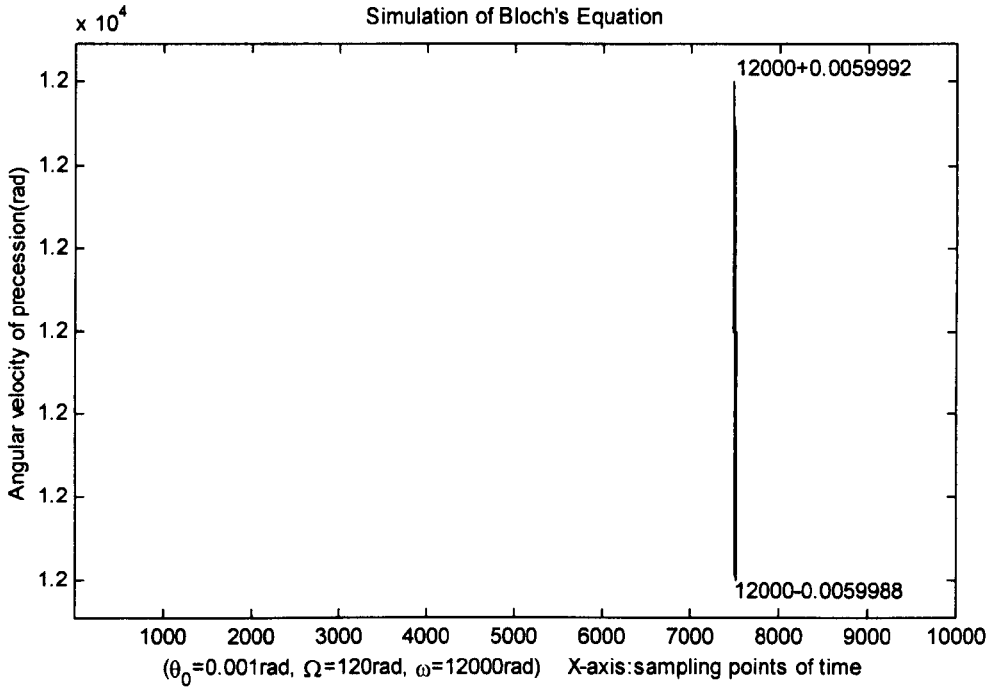

Figure 5-3 Simulation of Bloch's Equation with higher ratio of frequencies between magnetization precession and directional change of magnetic field.

The simulation is conducted under the condition that the Larmor frequency and the ratio of Larmor frequency to the frequency of magnetic disturbance are much less than the practical value. The Larmor frequency and the magnetic disturbance frequency are given to be 2400 rad/s and 120rad/s respectively in the simulation. The results are shown in Figure 5-2. The simulation with the higher Larmor frequency of 12000 rad/s and the higher ratio of frequency, are shown in Figure 5-3.

The maximum and minimum values of the velocity fluctuation indicated as ± 0.0012 and ± 0.0060 respectively in Figure 5-2and 5-3, that results match theoretical results of Equation (5.9) and (5.10).

Through further investigations of the simulation, it has been confirmed that the precession of magnetization is almost not affected by the directional change of magnetic field, except for a slant of the axis of the precession cone according to the direction change of the magnetic field. That is true even if in the simulation with a lower ratio of frequencies of the spin precession and structural vibration, for instance the ratio is only 10. The higher the ratio of frequencies of precession to that of the directional change of magnetic field, the less independent the precession of magnetization. This result also confirms the Adiabatic theorem with computer simulation. In the simulation, the maximum vibration angle of 0.001 radians is used, which is much bigger than the practical value (about $\theta_0 = 1 \times 10^{-5}$ degrees).

According to previous investigations, the distortion of the phase angle due to a small directional change of magnetic field can be neglected, because the value of it is always less than the gyromagnetic ratio multiplied by the shaded area in Figure 5-2 and 5-3. For a given maximum rotational angle of $\theta_0 = 1 \times 10^{-5}$ radians, which is about the angular displacement produced by the magnet vibration displacement of 5 μm, the possible phase distortion is only 5.53×10^{-8} degrees.

This analytical result is matched from the experimental data of spin phase variations in products of Type OR24, OR26 and OR42, as shown in Appendix C, in which the phase distortions explicitly increase with respect to the increase of the probe offset from the centre. Otherwise, if the directional change of magnetic field affects the phase angle significantly, the distortion of the phase angle must be almost constant across the imaging volume. Obviously that contradicts to the experimental results illustrated in

appendix C, in which the peak phase variation vanishes at the centre whilst approximately proportional to the distance from the centre.

5.2 Evaluation of the Eddy Current Effect

In this section, the phase distortion due to the eddy current is evaluated from theoretical and experimental analysis.

5.2.1 Theoretical analysis

According to the theoretical description of the magnetic disturbance discussed in section 4.2, the magnetic fields produced by the eddy currents yields to

$$B_{Ix} \leq B_0 \sin\theta_0 \tag{5.13}$$

and

$$B_{Iz} \leq B_0 \cos\theta_0, \tag{5.14}$$

where B_{Ix} and B_{Iz} represent the components of the induced magnetic field in x-axis and z-axis of the body reference respectively, B_0 and θ_0 are the magnitudes of the magnetic field and the rotating vibration of the field. The possible maximum disturbance of magnitude of the magnetic field is given by (detailed in appendix A)

$$\Delta B_I = B_0\theta_0^2. \tag{5.15}$$

Assuming $\theta_0 = 1\times10^{-5}$ rad, $B_0 = 1.5$ Tesla and the vibration frequency 20Hz, the maximum estimated value of the magnetic disturbance and phase angle distortion due to the induced currents are as follows:

$$\Delta B_{\max} = 1.5 \times 10^{-10} \text{ Tesla,} \tag{5.16}$$

$$\Delta \Phi_{pk-pk} \leq \frac{8\gamma \Delta B}{\Omega} = 0.146 \text{ degrees.} \tag{5.17}$$

More evaluation is illustrated in Figure 5-4, where the relationship between the displacement and rotational angle of the structural vibration is defined as

$$\text{rotational angle} = \operatorname{actan}\left(\frac{\text{relative displacement between two ends of the bore - tube}}{\text{length between pit 1 and 4 of bore - tube (1.2 meter)}}\right).$$

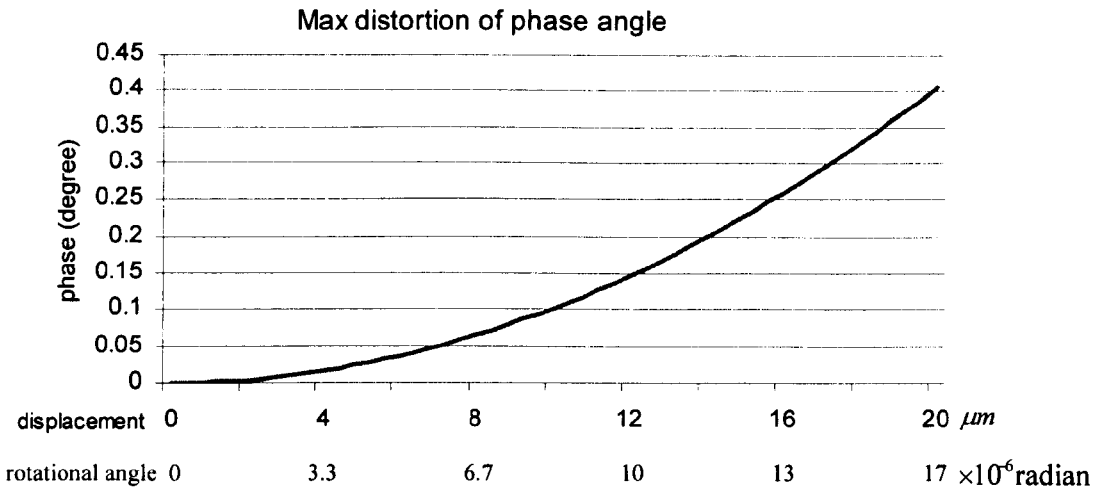

Figure 5-4 Maximum distortions of the phase angles due to the eddy currents respect to rotational vibration under the frequency of 20Hz.

In practice, the rotational angle of cryostat vibration is much less than 1.0×10^{-5} (rad). Therefore, it is concluded that the effect of eddy current on the phase angle is much less than the distortion evaluated here.

This result is supported by the experimental result of phase angle variation across the imaging area, shown in appendix C, in which the magnitude of magnetic disturbance almost vanishes at the centre but increases proportionally to the offset from the centre. Nevertheless it is impossible in practice. Considering the Lenz's Law and Biot-Savart Law, the magnetic field produced by eddy currents of shields with a radius of 50cm can not be eliminated at the centre of bore-tubes and posses a great magnitude at the offset of 20cm from the centre. A further discussion of experimental data will be presented in the following subsection.

5.2.2 Analysis of Experimental Phase Variation across Imaging Volume

In this subsection, it is assumed that the phase variations illustrated in appendix C is caused by eddy currents in the shield of Type OR24, OR26 and OR42. Analysing these data of phase variations, it is found that the phase variation almost vanishes at the centre, whilst a big variation is achieved at 20cm offset. Because the phase variation is proportional to the magnitude of induced magnetic field, the induced magnetic field is almost vanished at the centre whilst it is significantly big at 20cm offset. The eddy currents in the shield of 0.5 m radius does not seem to produce such a big difference of the magnetic amplitude (ratio of magnetic fields) between the 20cm offset and the centre of the shield. Through the following discussions, it will be found that the experimental data contradict with the consequence deduced from analysis of several typical eddy current distributions.

According to Biot-Savart Law [5], the magnetic flux density due to a current element $d\mathbf{I}$ is given by

$$d\mathbf{B} = \frac{\mu_0}{2\pi} \frac{d\mathbf{I} \times \mathbf{R}}{R^3}, \tag{5.18}$$

where the vector notations are shown in Figure 5-5(a).

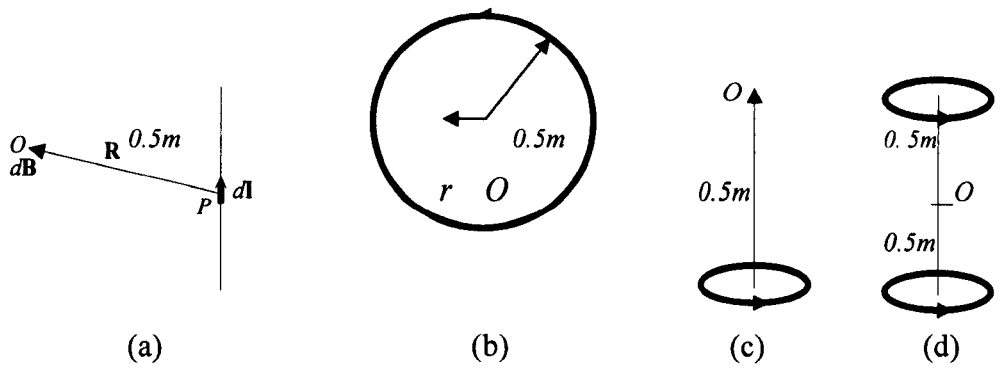

Figure 5-5 Different eddy current distributions. The field (a) from an elemental current source, (b) inside an circular current loop; (c) along the axis of a circular current loop; (d) along the axis of two coaxial current loops.

Three other kinds of eddy current distributions are illustrated in Figure 5-5(b), (c) and (d). In each of them the distance between the centre, O, and the current source is chosen as 0.5m to approach to the practical situation. The radii of eddy current loops are chosen as 20cm, while it can be any size. A normalised magnetic field is defined as

$$B_n(r) = \frac{B(r)}{B(O)}, \tag{5.19}$$

where r is the distance from the centre O to the point in the field evaluated. The normalised magnetic distributions are illustrated in Figure 5-6 and 5-7 with respect to the eddy current distributions given in Figure 5-5.

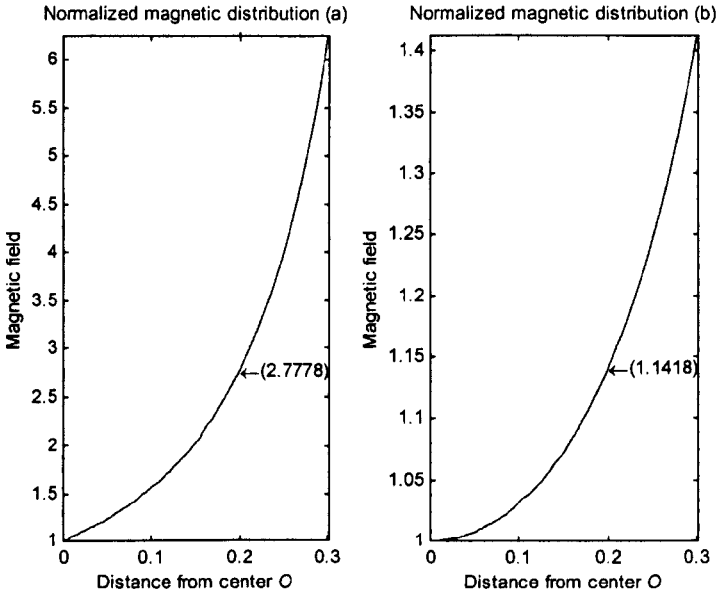

Figure 5-6 Normalised magnetic distribution, (a) between the centre and the elemental current source; (b) inside the circular loop of current.

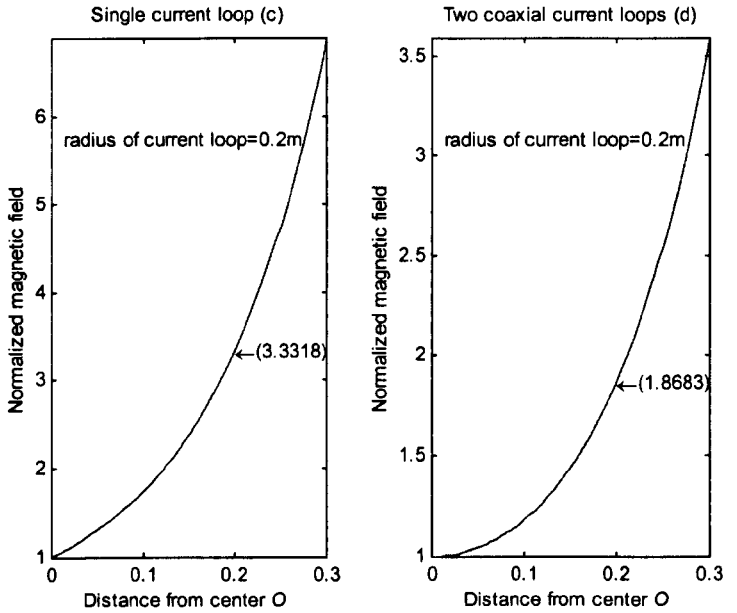

Figure 5-7 Normalised magnetic field distributions, (c) between the centre, *O*, and the centre of the current loop; (d) between the centres of current loops and *O*.

The normalised magnetic fields at distance of 20cm are 2.7778 and 3.3318 in Figure 5-6(a) and 5-7(c) respectively, but they are only 1.1418 and 1.8683 in Figure 5-6(b) and 5-7(d) respectively. Since the magnetic field of two coaxial current loops produce a magnetic field vertical to the main magnetic field, it increases the magnitude of the main magnetic field in order of B_{Ix}^2/B_0 (appendix A), thus the square of 1.8683 must be used to compare with the experimental normalised values. The value is 3.475.

The normalised magnetic field deduced from experimental data of appendix C are given in Table 5-1.

Table 5-1 The normalised magnetic fields from experiments

Type	Offset	Center			20cm offset			Normalized field
		fridge off	fridge on	Δ_0	fridge off	fridge on	Δ_1	Δ_1/Δ_0
OR24	x-offset	0.40	0.90	0.81	0.75	4.50	4.44	5.58
#5	y-offset	0.40	0.90	0.81	0.40	3.50	3.48	4.34
OR26	x-offset	0.32	0.59	0.50	0.39	1.27	1.21	2.56
#2	y-offset	0.32	0.59	0.50	0.70	2.40	2.30	4.84
OR42	x-offset	0.60	0.75	0.45	0.85	4.50	4.42	10.00
#1053	y-offset	0.60	0.75	0.45	0.85	2.50	2.35	5.56
OR42	x-offset	0.60	0.65	0.25	0.85	4.75	4.67	19.00
#1052	y-offset	0.60	0.65	0.25	0.85	4.25	4.16	17.00

In this table Δ represents the phase angle with the background noise taken off, as it is expressed in equation (2.34). It is obvious that the normalised experimental magnetic fields in Table 5-1 are stronger than the normalised analytical magnetic fields in Figure 5-6 and 5-7 except in y offset of Type OR24 and x offset of TypeOR26.

It has been stated in section 5.2.1 that the eddy currents in a shield are mostly distributed as that shown in Figure 5-5(b) and (d).

Now consider the contrary to the previous eddy current distribution. If vectors of eddy currents in a shield were to be symmetric in amplitude and shape to the axis of the shield, but inverse in the direction, as shown in Figure 5-8(a), the induced magnetic field would vanish at the centre of the shield in this situation. Hence the relevant normalised magnetic field would be infinite at the centre. But this kind of eddy currents is impossible to exist unless the bore-tube vibrates in mode shapes of continuous structural vibrations, as shown in Figure 5-8(b). Continuous structural vibrations were with higher frequencies comparing to rigid body vibrations, hence they could not be the main sources of the phase distortions [24,25], and were excluded in discussions.

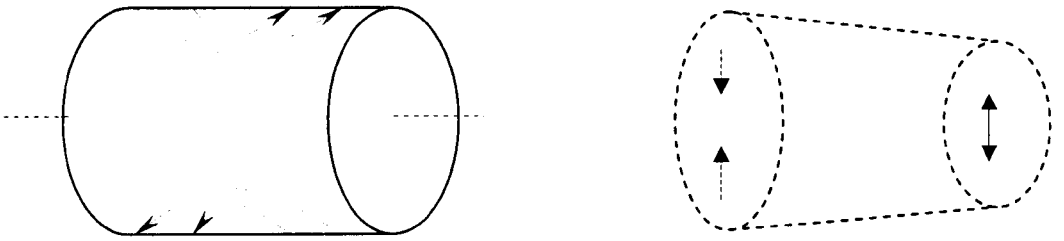

Figure 5-8 Eddy currents in shields.

A practical magnetic field and induced current is more complex than that discussed previously, but considering the individual model of structural vibrations, analyses given above are reasonable.

There are still some unrecognised measurements, for example, the phase distortions ranging from 0.25 to 0.81, shown in Table 5-1, existed at centres of the bore-tubes, in which the magnetic fields should be homogeneous. What did cause these phase distortions if they were not from the motions of inhomogeneous magnetic fields?

Explanations to these phase distortions are desired, and the reason of the distortions is to be found in the future. Nevertheless the distortions can be ascribed to eddy currents by the moment. It seems reasonable, since the phase distortions are only within 1.0 degree.

5.2.3 Numerical calculations of eddy currents

The effect of the eddy current on the distortion of phase angle can be estimated more precisely by numerically solving the formulas given in appendix B. This process will be fulfilled in the future, since it belongs to another special area of research.

5.2.4 Search coil experiment for evaluating eddy current effects

In this subsection, a basic method deduced, in which the magnetic fields produced by the eddy currents can be separated from the signals measured by search coils. Hence an experimental evaluation of magnetic disturbance due to eddy currents is available from the search coil experiment.

The axes of shields are assumed to vibrate relative to the magnet rotationally in a vertical plane, and a search coil is put transverse to the plane, as shown in Figure 5-9.

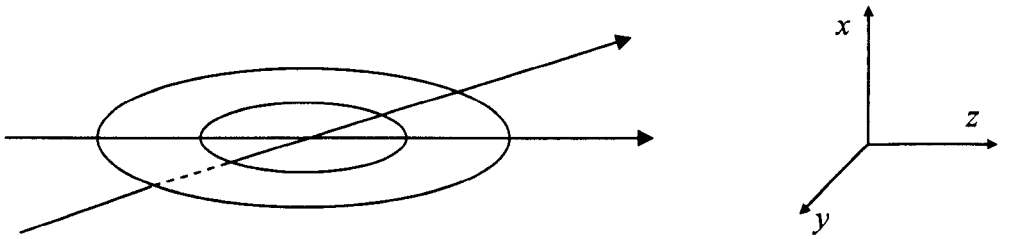

Figure 5-9 the orientation of a search coil in the bore-tube.

In Figure 5-9, the arrow lines represent the axes of the bore-tube or magnet vibrating in the x-z-plane about the y-axis, while the search coil is put in bore-tube horizontally.

Assume the surface current density of shield, $\mathbf{J}(R,z,\theta,t)$, is a vector, which magnitude is sinusoidal and in phase everywhere on the surface of the shield. That is

$$\mathbf{J} = \mathbf{J}_0(r,\theta)\sin(\Omega t + \Psi). \tag{5.20}$$

By the Biot-Savart Law, the magnetic field induced by the shield current (which is an induced current by shield vibration relative to the magnet) is

$$\mathbf{B}_S(r,z,\phi) = \frac{\mu_0}{2\pi}\oint_S \frac{\mathbf{J}\times\mathbf{R}}{R^3} ds, \tag{5.21}$$

where $\mathbf{R}$ is a vector from position (r,z,θ) to the surface of the shield. Denote V_S as the signal of the search coil induced by magnetic field $\mathbf{B}_S$, then

$$V_S(t) = kB_S\Omega\cos(\Omega t + \Psi), \tag{5.22}$$

if the induced magnetic field $\mathbf{B}_S$ is sinusoidal with frequency of Ω. In Equation (5.22), k is a coefficient of the search coil to be calibrated and B_S is an average of magnetic flux density of $\mathbf{B}_S$ linked to the search coil.

But V_S is not the real signal measured in the search coil, which has been contaminated by the rotational vibration of the magnet, as given by

$$\theta(t) = \theta_r \sin(\Omega_r t), \tag{5.23}$$

and the contaminating signal can be described at the centre of the bore-tube as

$$V_V(t) = kB_0\Omega_r\theta_r \cos(\Omega_r t), \tag{5.24}$$

where θ_r can be measured in an experiment. Therefore, the real signal in the search coil is the sum of Equation (5.21) and (5.24), that is

$$V(t) = V_S(t) + V_V(t). \tag{5.25}$$

Finally, it is evident to separate $V_S(t)$ from $V(t)$.

In practice, the magnet and shields vibrate in more complex shape than we discussed above. However, the signal caused by eddy currents can still be separated from the mixed signal in the search coil, by measuring the vibration shape of the magnet and applying specific mathematical method based on the previous expressions.

5.3 Evaluation of Effect for Magnetic Inhomogeneity

From the previous investigation, the directional change of the magnetic field and the eddy current would not affect the phase angle significantly. Naturally, the attention is turned to the magnetic inhomogeneity. In a shimmed product, the magnetic inhomogeneity was measured to be 5ppm by OMT's standard [67]. The value of 5ppm would analytically lead to the phase angle distortion of less than 0.6, in the vibration

magnitude of 10 μm at the frequency of 13Hz. But the phase distortion was about 6.0 degrees in practice. That seems to give rise to a kind of absurdity.

In this section, the quantitative relationship between the phase distortion and magnetic gradient is discussed. And then a reasonable explanation is proposed to break the absurdity. Finally, the phase distortion across the imaging volume is explained as due to the magnetic inhomogeneity.

5.3.1 Analytical evaluation

From section 5.2 and 4.2, the magnetic disturbance and phase angle distortion can be described by the following equations, respectively

$$\Delta B(\mathbf{r}) = \Delta \mathbf{r}(\mathbf{r}) \cdot \mathbf{G}(\mathbf{r}) \tag{5.26}$$

and

$$\Delta \Phi_{pk-pk} = \frac{8\gamma \Delta B(\mathbf{r})}{\Omega}. \tag{5.27}$$

The phase distortions according to different displacements of $\Delta \mathbf{r}$ and different magnetic gradient of $\mathbf{G}$ are illustrated in Figure 5-10, based on the magnetic disturbance frequency of 13Hz. From the graphs, it is shown that the phase distortion is about 6 degrees, if the magnetic gradient is 1mT/m, and the displacement 5 μm

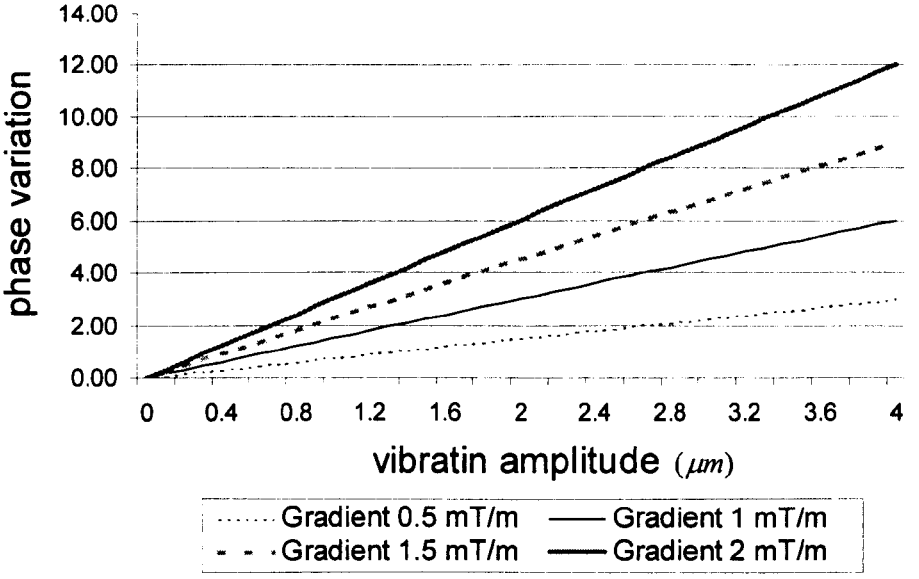

(a)

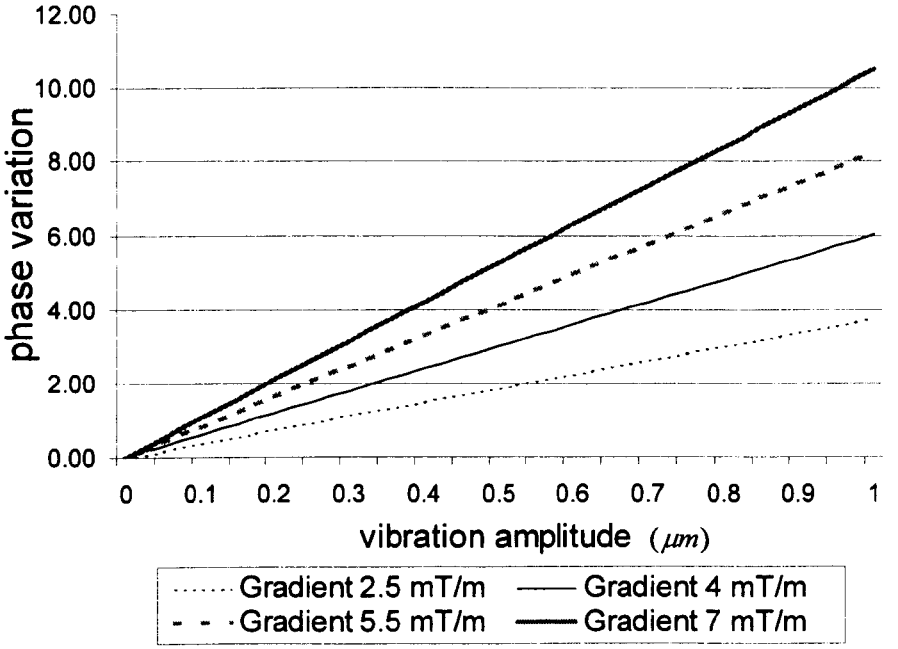

(b)

Figure 5-10 The phase distortions due to different magnetic inhomogenities and displacements under the vibration frequency of 13Hz.

Definition of homogeneity as adopted by OMT is based upon the field values determined at discrete points on the surface of a sphere. And the inhomogeneity is determined by the peak to peak value of the field measured at the discrete points. It does not give the magnetic gradient expressively, therefore can not be used to calculate the phase distortion directly.

From the expansion of the magnetic modular in Legendre Polynomials as given in section 2.3.3, the magnetic gradient along the spherical radius can be expressed as

$$G_r(r,\theta) = \sum_{n=0}^{\infty} \frac{nr^{n-1}}{R_0^n} P_n^0(\mu) A_n^0, \tag{5.28}$$

for an axially symmetric magnetic field. Along the radius of the bore-tube, the first eight Legendre's coefficients are P_n^0=1, -1/2, 3/8, -5/16, 35/128, for n=0, 2, 4, 6, 8, and $P_n^0 = 0$, for n=1,3,5,7. The gradient can be expressed in the polynomial,

$$G_x(r) = a_2 \frac{r}{R_0^2} + a_4 \frac{r^3}{R_0^4} + a_6 \frac{r^5}{R_0^6} + a_8 \frac{r^7}{R_0^8} + \ldots. \tag{5.29}$$

A set of coefficients, A_n^0, of a product has been obtained and used to calculate the gradient, as shown in Figure 5-11. It shows that the magnetic gradient is zero at the centre and almost linearly increases from the centre to the 20cm offset. It demonstrate a stronger non-linearity approaching to the edge of the bore-tube. The gradient reaches 1000ppm per meter at 20cm offset, this is equivalent to the gradient of 1.5mT/m for a main field of 1.5 Tesla. The magnetic inhomogeneity, however, still has to be used to estimate the phase distortion, since with only one set of the data it is not convincible to determine the properties of the magnetic gradient.

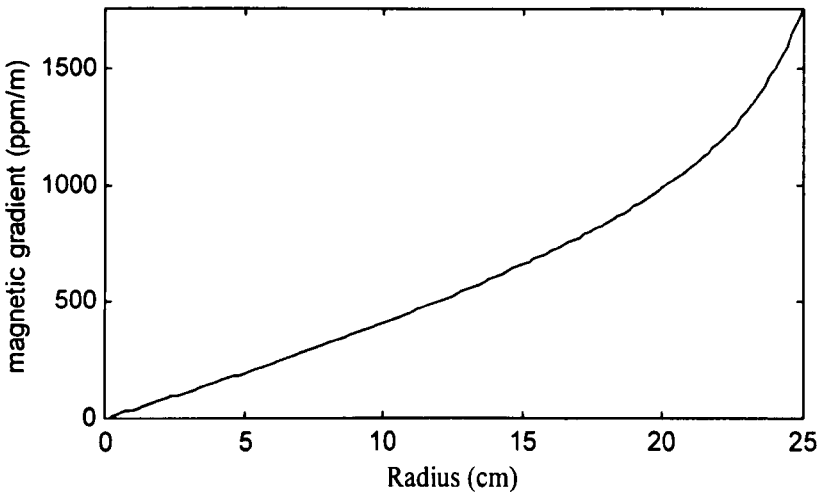

Figure 5-11 The magnetic gradient along the radius of the bore-tube at the centre.

All cryostats are shimmed to meet the standard specification of magnetic inhomogeneity before shipped to customers. For Type OR70, the magnetic inhomogeneity achieves about 5ppm on the sphere with 25cm radius after shimmed, while it is more than 500ppm without shimming. The peak-to-peak value of 500ppm means that the magnetic gradient of at least 1.5mT/m exists in the sphere, and it is enough to cause the phase distortion of 6 degrees by magnet displacement of several micro meters. An unusual phenomenon is that the phase distortion measurement shows no significant difference between the products with and without shimming. The reasonable explanation may be that the Helium Can vibrates relative to the gradient coil in which the magnetic shims are mounted, and the original performance of shimming is distorted by the relative vibrations.

To give a convincing explanation of the phenomenon, more investigation of the magnetic inhomogeneity is required and planned in the next stage of programme.

5.3.2 Analysis of Experimental Data of Phase Variation across Imaging Volume

From section 5.2.2 it appears that the eddy current is not to be the main source of the measured phase variations illustrated in appendix C. Thus the phase distortions are ascribed to the motions of inhomogeneous magnetic field. Here some possible distributions of magnetic gradient across imaging volume are deduced from the experimental data illustrated in appendix C and evaluated.

From graphs illustrated in appendix C, the relationship between the phase distortion and distance in each of the products can be approximated to be linear. Because the phase distortion is proportional to magnetic gradient, the relationship between magnetic gradient and the distance can be given by the equation,

$$G(r) = ar, \tag{5.30}$$

where r is the radius at the centre of a bore-tube. Thus the magnetic distribution can be described by

$$B(r) = \frac{1}{2}ar^2 + c. \tag{5.31}$$

As it has been mentioned, the magnetic gradient vanishes at the centre, therefore the constant c is zero. From last two equations, the magnetic gradient can be calculated if the difference of magnetic flux densities between the centre and 20cm offset is given or measured, and a phase distortion is able to be evaluated if the vibration amplitude and shape of a magnet is given. For example, assuming that the magnetic inhomogeneity is 100ppm (for $B_0 = 1.5$ Tesla) between the centre and the 20cm offset. Then coefficient a is calculated to be 7.5mT/m^2, the magnetic gradient at 20cm offset will be 1.50mT/m and the relevant phase distortion will be 4.5 degrees under the vibration with 2 μm amplitude and 13Hz frequency. The phase distortion reaches 9.0 degrees if the magnetic inhomogeneity is 200ppm.

The last two equations appear to be reasonable compared to the graphs shown in Figure 5-11 and 5-12. The graphs are obtained by substituting the data given in Table D-1 in Appendix D into the expansion of Legendre polynomials.

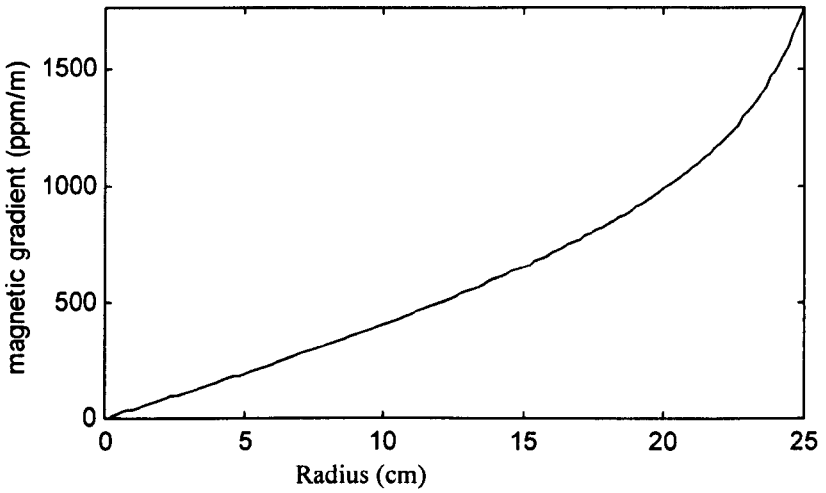

Figure 5-12 The magnetic field distribution along the radius of the central cross section of the bore-tube.

6 Spectral Analysis of Cryostat Vibrations

A huge amount of vibration data has been acquired for the investigation of the cryostat vibration problem by OMT [28-46]. It can be categorized into three groups:

- The vibrations of cryostat components, such as OVC, shields, Helium Can and Cold Head, with accelerometers or a laser vibrometer.
- The magnetic flux change in the bore-tube with a search coil.
- The phase angle with a probe and spectrometer.

Vibration velocities were measured by the laser vibrometer at the ends of the 20K shield, 80K shield and the Helium Can. The Cold Head vibration was measured in the direction of the piston motion with an accelerometer. There was only one search coil and laser vibrometer during the experiments. To obtain the rotational vibration of a vessel or the relative vibration between two vessels, for example between Helium Can and 20K shield, simultaneous tests are required. The cross-correlation method is effectively applied to match the measurements to the pace of a reference. The signal of the Cold Head acceleration is acquired as a reference signal for the correlation of all other signals. This is because the cold head is the main source of the vibrations with a precise periodicity and the cold head vibration is measured all the time, while other vibration signals are measured in sequence with single laser vibrometer. To obtain cross-correlation between two signals, each of these two signals is cross-correlated with the reference signal and than the phase delay between these two signals can be calculated as if the two signals were to be measured at the same time.

The initial result of the analysis is illustrated in Figure 6-1 to 6-6. The vibration velocities of cryostat components, such as Helium Can, 20K shield, 80K shield, were tested with one Laser Vibrometer respectively. To obtain signal of the rotation of each component and the relative vibration between two of the components shown in the

figures, the original data are pretreated to have them synchronized with each other by the cross-correlation to the reference signal.

6.1 Vibrations of Cold Head and OVC

The spectra of the Cold Head vibration are concentrated around 56Hz, which is regarded as the resonant frequency of the Cold Head itself. The spikes in the time domain are clearly observed after each interval of half seconds, which is due to the motion of the piston. The frequency of 2Hz is regarded as the basic component of the Cold Head vibration.

The spectrum of the OVC is very similar with that of the Cold Head except for their reduced amplitudes. The spike in the Cold Head vibration has absent in this spectrum but a transient vibration with high amplitudes follows the spike.

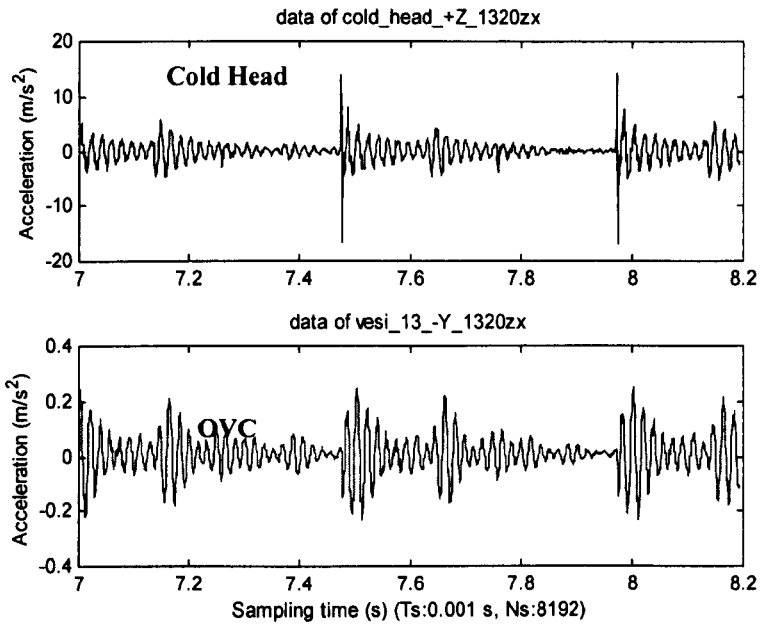

Figure 6-1 The records of the Cold Head and OVC vibrations.

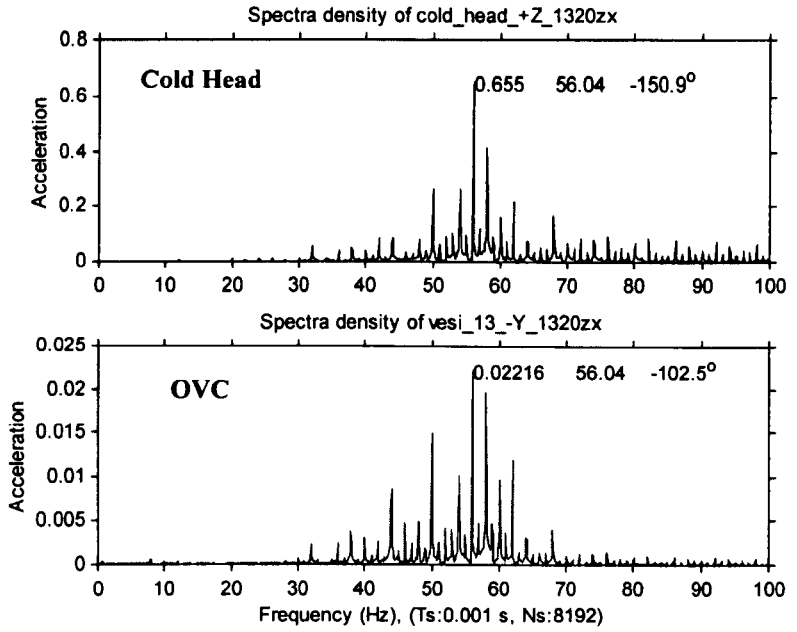

Figure 6-2 The spectra of the Cold Head and OVC vibrations.

6.2 Relative Vibrations at Low Frequencies

Relative vibration is defined as the vibration of the Helium Can relative to the shield. Figure 6-3 shows that the vibration amplitudes of the Helium Can and 20K shield are dominant at 8Hz within the range of zero to 25Hz, while the amplitudes of the relative vibrations at 8Hz become much less than that at the frequencies of 13Hz, 20Hz and

24Hz in Figure 6-4. That means the Helium Can and 20K shield vibrate in phase at the frequency of 8Hz. The property of the spectrum at relative low frequencies is important, since the phase angle is more sensitive to the low frequencies.

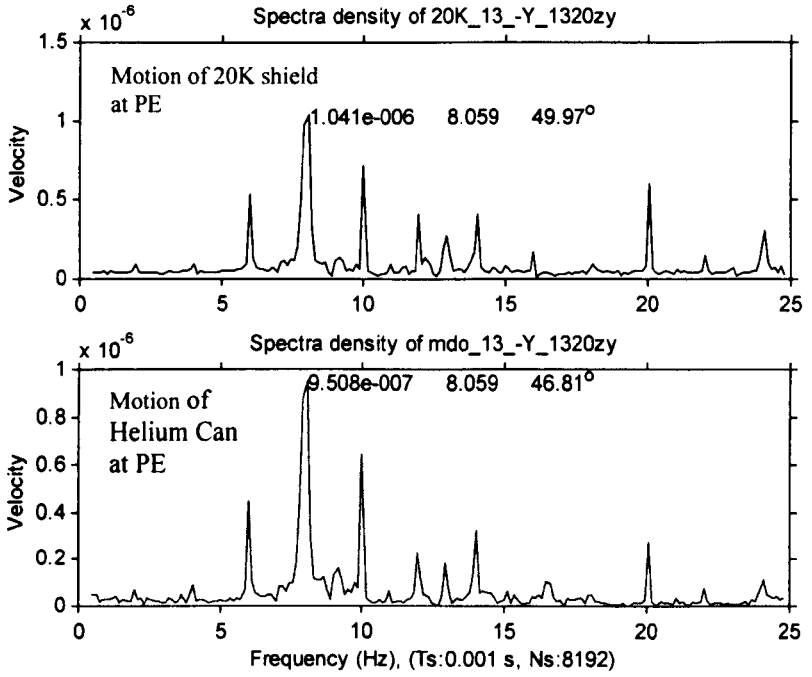

Figure 6-3 The spectra of the 20K shield and Helium Can vibrations within 25Hz.

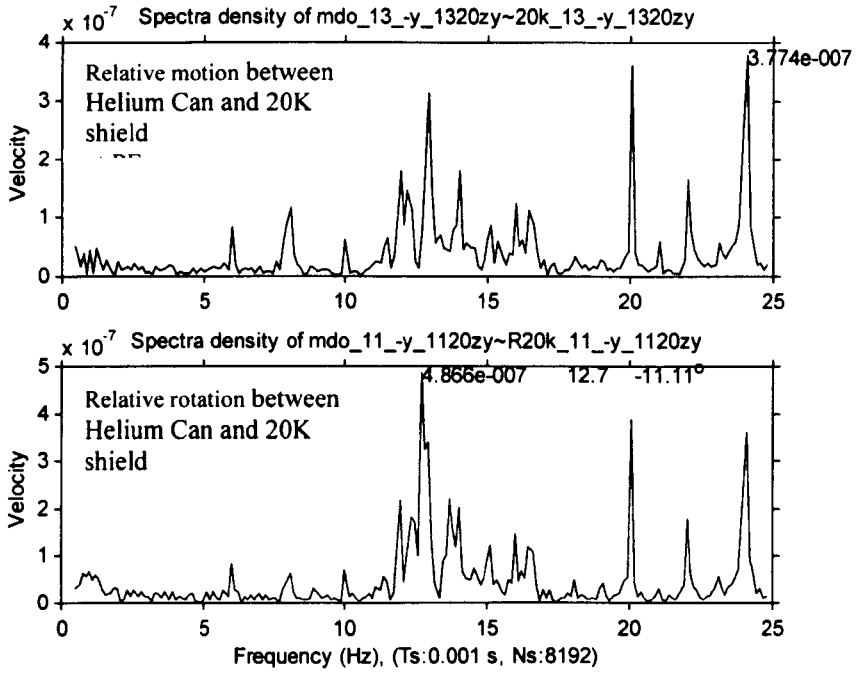

Figure 6-4 The spectra of relative vibration between the 20K shield and Helium Can within 25Hz.

6.3 Vibration at High Frequencies

Figure 6-5 shows that the vibration amplitudes of the Helium Can and 20K shield are much bigger at discrete frequencies near the dominant frequency of 58Hz, while the amplitudes of the relative vibrations do not give significant changes in the spectra as shown in Figure 6-6, that means the Helium Can and 20K shield vibrate out of phase at the high frequencies. The vibrations at the high frequencies should not be ignored respecting to their high amplitude, even if the phase angle is less sensitive to the higher frequency.

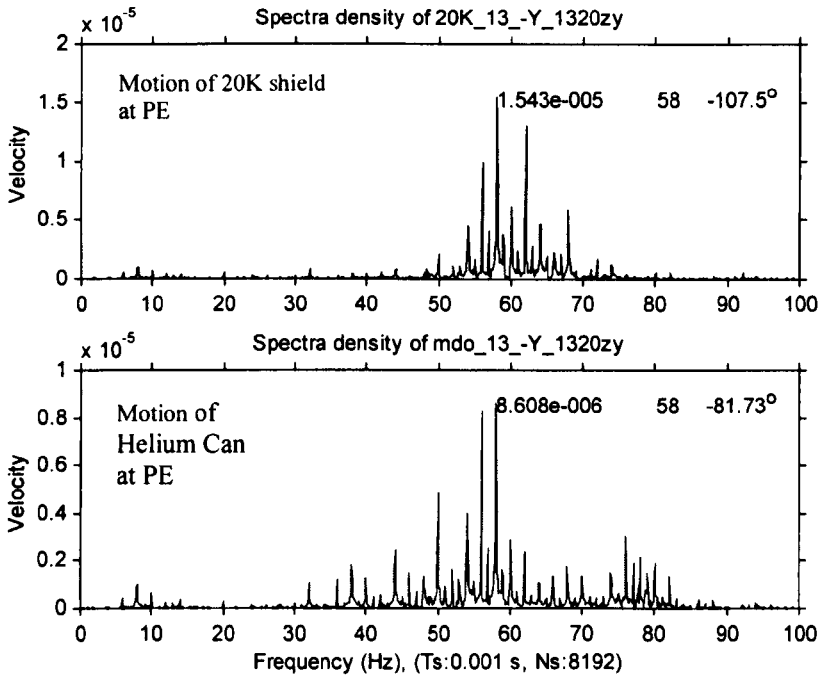

Figure 6-5 The spectra of the 20K shield and Helium Can vibrations within 100Hz.

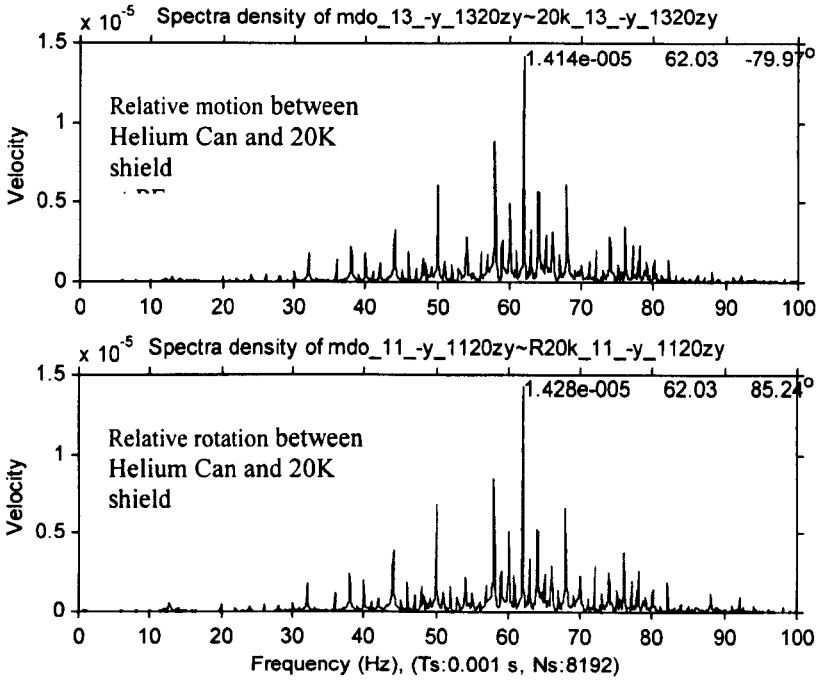

Figure 6-6 The spectra of relative vibration between the 20K shield and Helium Can within 100Hz.

7 Instrumentation

In the measurement of the magnetic field instability, two kinds of instrument are used, a search coil sensor to pick up any disturbance of magnetic field directly and an NMR spectrometer to measure the phase-angle distortion. The search coil sensor, which is composed of two orthogonal annulus of electromagnetic coils, is sensitive to the change of magnetic flux. It was expected to acquire the magnetic field disturbances generated by eddy currents in the cryostat. A huge amount of experiments were carried out by LMS and OMT to directly read magnetic field variation using the search coil sensor, and many results were given based on those data. But its usability needs to be evaluated, because there are two different changes of magnetic field, which affect the reading of the search coil sensor, the modular variation and the directional vibration of the magnetic field. Since only the modular variation of the magnetic field affects the phase-angle considerably, the search coil sensor is not applicable if the directional change of the magnetic field acts as a main role in the sensor. In this chapter an overall analysis of the reliability and accuracy of the search coil sensor is presented mathematically.

Another instrument is the NMR spectrometer, which has been the most effective instrument so far in testing MR phase-angle distortions. It is also used to pick up dominant spectra of magnetic field variation at OMT. But its accuracy is limited both by the alias frequencies due to under-sampling and by the short sampling number of OMT's standard. In the second part of this chapter its accuracy and reliability are analyzed and a more accurate and reliable method is developed.

7.1 Reliability and Sensitivity of Search-coil Sensor

7.1.1 Search-coil Constitution and Applications

The search-coil sensor consists of two orthogonal annuli of electromagnetic coils, which are connected serially with one end of each coil, as show in Figure 7-1(a). These coils are put in a wooden box and fixed to the box firmly. They have same area if their wires expand in circles of single coil respectively. Same effect has been discussed in the single annulus and double annuli of electromagnetic coils in the following subsections. Figure 7-1(b) depicts an equivalent single electromagnetic coil.

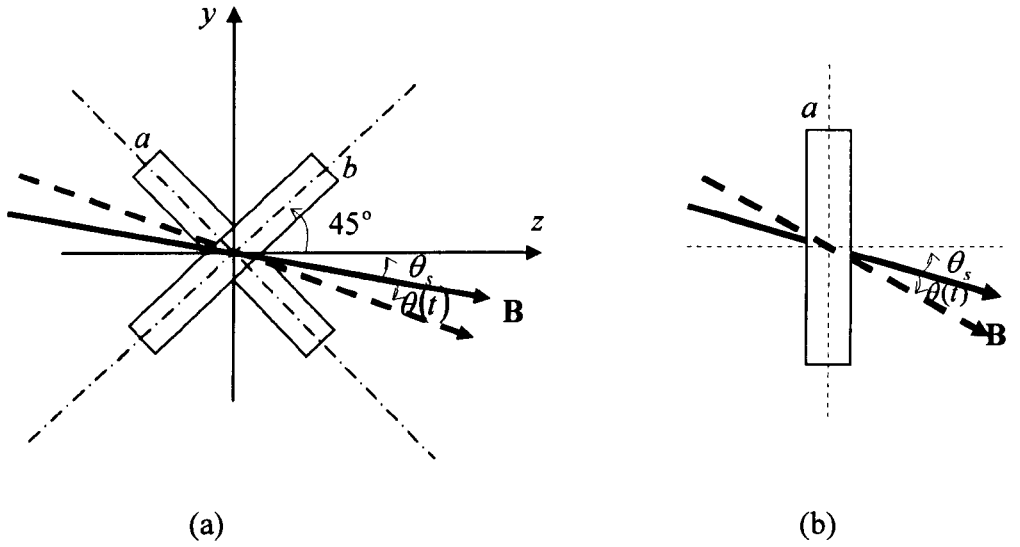

(a) (b)

Figure 7-1 (a) The orientation of the search-coil sensor. (b) The single coil sensor.

The search-coil sensor is frequently used to measure the magnetic field variation in x-, y- and z-axis. The idea of its application is that the sensor is along the direction of magnetic field (the z-axis) and when the magnetic field, especially the magnitude of the field is being disturbed, the change of the magnetic flux can be sensed by the coils. But one question is come out that the search-coil sensor may be more sensitive to the directional change of the magnetic field than to the modular change. According to the

theoretical analysis and computer simulation of Chapter 5, the directional change of magnetic field produces negligible amount of phase-angle distortions. In the following two sections the sensitivities of the search-coil sensor are derived and evaluated with respect to the orientation of the sensor.

7.1.2 Search-coil Parallel with the Bore-tube Axis

Ideally the direction of magnetic field coincides with the z-axis in a static state. But orientation error θ_s is always unavoidable in practice. In figure 7-1, the solid line of magnetic field indicates the static or equilibrium position of the directional vibration of the magnetic field. The modular and directional changes of the magnetic field are respectively expressed by the equations,

$$\theta(t) = \theta_0 \sin(\Omega t + \Psi) \tag{7.1}$$

and

$$|\mathbf{B}(t)| = B_0 + \beta \sin(\Omega t) . \tag{7.2}$$

Assuming that the area is equal to A, a homogeneous magnetic field B illustrated in figure 7-1(a) will respectively yield magnetic fluxes in two annuluses as

$$\varphi_a = B(t) A \cos(\theta_1) \tag{7.3}$$

and

$$\varphi_b = B(t) A \sin(\theta_1) \tag{7.4}$$

where

$$\theta_1 = \frac{\pi}{4} + \theta_s + \theta(t) . \tag{7.5}$$

Therefore the sum of the fluxes is

$$\varphi = B(t)A\sqrt{2}\sin\left(\theta_1 + \frac{\pi}{4}\right) \tag{7.6}$$

and the induced voltage is given by the equation

$$V = -A\sqrt{2}\left[\frac{\partial B(t)}{\partial t}\sin\left(\theta_1 + \frac{\pi}{4}\right) + \frac{\partial \theta(t)}{\partial t}B(t)\cos\left(\theta_1 + \frac{\pi}{4}\right)\right]. \tag{7.7}$$

Since the rotation angle is very small ($\theta_0 < 1\times10^{-5}$ radians), the induced voltage can be approximated by

$$V \approx -A\sqrt{2}\Omega\cos(\Omega t)[\beta\cos(\theta_s + \theta(t)) - \beta_1 - \beta_2\sin(\Omega t)]$$

$$V \approx -A\sqrt{2}\Omega\cos(\Omega t)[\beta_0 - \beta_1 - \beta_2\sin(\Omega t)], \tag{7.8}$$

where $\beta_0 = \beta$, $\beta_1 = B_0\theta_0\theta_s$ and $\beta_2 = B_0\theta_0^2$.

In equation (7.8), the second term of the right hand side is related to the orientation error angle, which is unpredictable in practice. Both of the last two terms are related to the angular amplitude of vibration of the magnetic field direction, which will not be sensed by the MR probe. Whilst the first term reflects the modular change of the magnetic field, which can be picked up by the MR spectrometer in the phase distortion. In practical measurement, the phase distortion at X-20cm offset is at least three times of that at the centre in OR70#28. Such a difference must be detected by the search-coil if β is the dominant term in equation (7.8). But in fact no such a difference has been tested with the search-coil. In other hand, according practical parameters, $B_0 = 1.5$ Tesla, $\beta = 3\times10^{-8}$ Tesla, $\theta_0 = 1\times10^{-5}$ radians and $\theta_s = 0.026$ radians (or 1.5 degrees), we have $\beta_1 = 3.93\times10^{-7}$ Tesla, $\beta_2 = 1.5\times10^{-10}$ Tesla. Hence

$$\beta_1 >> \beta_0 >> \beta_2. \tag{7.9}$$

To obtain an accuracy of 3dB in the measurement of the modular change of magnetic field with the search coil sensor, the following relation must be kept,

$\beta_0 = 2\beta_1$.

Introducing previous parameters in this equation, the allowed range of the orientation error, θ_s, is less than 0.086 degrees. But it is impossible in practice to make such an accuracy of the orientation angle at the moment.

Figure 7-2 illustrates the influence of search coil orientation on the search coil readings. It can be seen that the search coil sensor is too sensitive to the orientation error, θ_s, in the measurement of the axial magnetic field disturbance. The search coil reading exactly reflects the modular change of magnetic field, only if $\theta_s = 0$. The search coil signal induced by the modular change of magnetic field is much less than the signal produced by the directional change of magnetic field when $\theta_s > 0$. The reading is as much as ten times of the signal due to the modular change when $\theta_s = 1.5$ degrees.

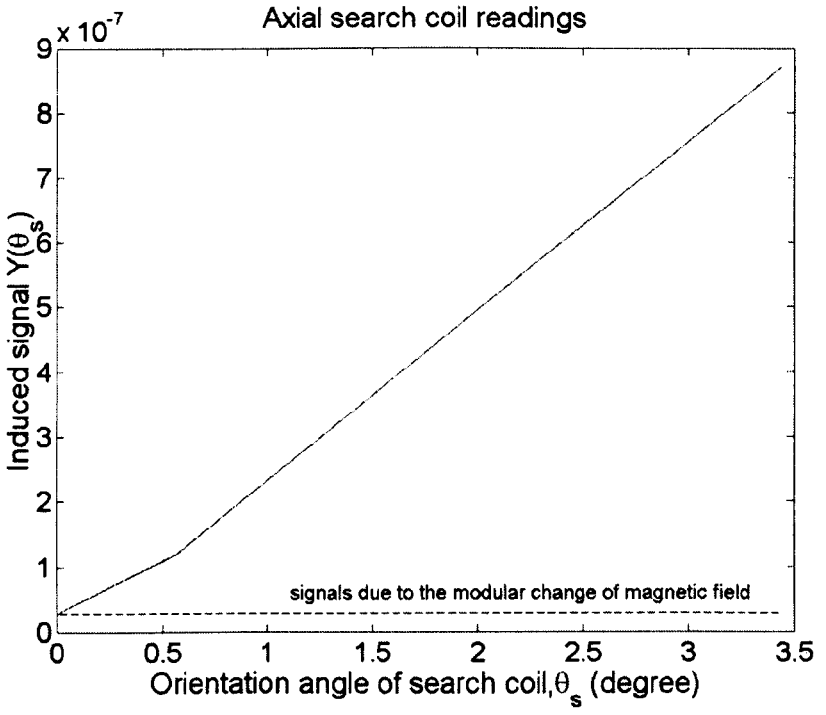

Figure 7-2 Measurement of magnetic field along the bore-tube of cryostat with a search coil sensor.

Equation (7.9) suggests a meaningful prediction, i.e. most of the search-coil readings are not from the modular change of magnetic field β but from the directional change of magnetic field, and the magnitudes of the search coil readings are significantly affected by the orientation error of the search coil sensor.

7.1.3 Search-coil Perpendicular to the Bore-tube Axis

Many times, the search coil sensor was used to measure the change of the magnetic field perpendicular to the bore-tube axis, for instance along y-axis. The search coil reading in this case can be obtained by adding 90 degrees to the angle of θ_1 in equation (7.7), as given by the following equation,

$$V = -A\sqrt{2}\left[\frac{\partial B(t)}{\partial t}\sin\left(\theta_1 + \frac{\pi}{2} + \frac{\pi}{4}\right) + \frac{\partial \theta(t)}{\partial t}B(t)\cos\left(\theta_1 + \frac{\pi}{2} + \frac{\pi}{4}\right)\right]. \tag{7.10}$$

Similar to equation (7.8), the following approximation can be deduced from the previous equation,

$$V \approx A\sqrt{2}\Omega\cos(\Omega t)[\beta_0 + \beta_1\sin(\Omega t) + \beta_2], \tag{7.11}$$

where $\beta_0 = \beta\theta_s$, $\beta_1 = \beta\theta_0$ and $\beta_2 = \theta_0 B_0$. (7.12)

By giving $B_0 = 1.5$ Tesla, $\beta = 3\times10^{-8}$ Tesla, $\theta_0 = 1\times10^{-5}$ radians and $\theta_s = 0.026$ radians (or 1.5 degrees), we have $\beta_0 = 7.8\times10^{-10}$, $\beta_1 = 3\times10^{-13}$ Tesla, $\beta_2 = 1.5\times10^{-5}$ Tesla. Hence

$$\beta_2 >> \beta_0 \text{ and } \beta_2 >> \beta_1. \tag{7.13}$$

Equation (7.11)-(7.13) indicate that the search-coil reading in vertical direction to the bore-tube axis mainly reflects the directional change of the magnetic field, which can be caused by either the directional change of the Helium Can or the eddy current. The directional change of the Helium Can must be same in the bore-tube, whilst the nearer to the shield the eddy current is, the stronger is the effect of the eddy current.

The relationship between the induced signal and orientation angle is illustrated in figure 7-3. It is shown that the measurement is very robust to the change of the orientation angle, when the search coil sensor is used to test the magnetic field perpendicular to the bore-tube.

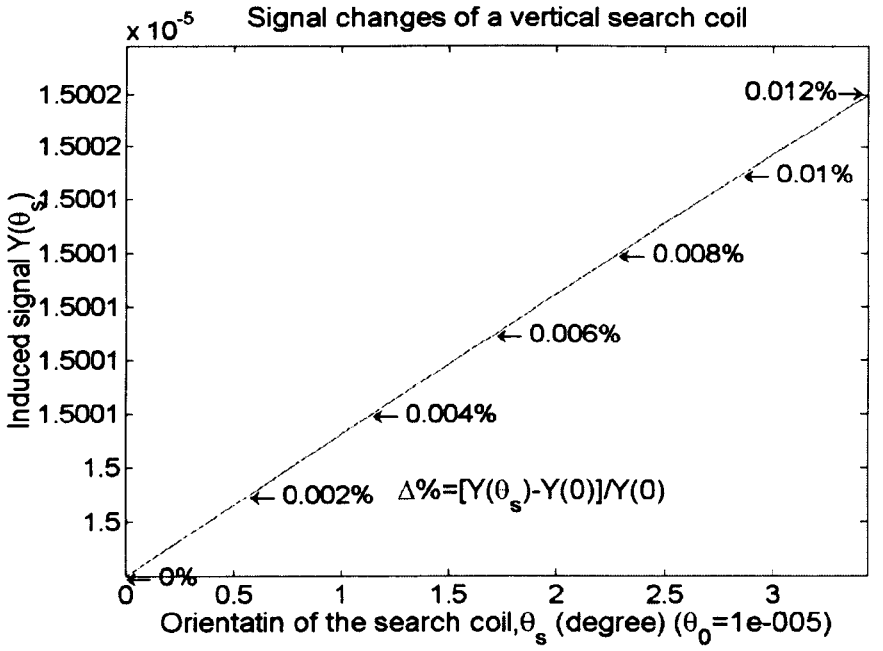

Figure 7-3 Measurement of magnetic field perpendicular to the bore-tube of cryostat with a search coil sensor.

7.2 Reliability and Sensitivity of MR Probe

The sensitivity of the MR probe to the amplitude of the magnetic disturbance has been discussed in section 3.4. Extracting magnetic field frequencies from the alias spectrum of the MR phase distortion is applied many times in practice. But a further analytical investigation indicates that some of the frequencies of the magnetic field can not be recovered from the spectrum of under-sampled phase-angles, since the OMT's standard of phase-angle measurement needs to be improved to obtain a higher accuracy of the measurement of magnetic field spectrum.

7.2.1 Undersampling and OMT Standard of Measurement

Undersamping with MR probe in the measurements of the vibration frequencies were discussed using computer simulation [40]. Here further results are given both in mathematical analysis and computer simulation.

From equation (2.31) and (2.32), the phase-angle started at anytime t with echo-time T_E is given by the equation,

$$\Delta\Phi(t)=\frac{2\gamma\Delta B_0}{\Omega}\left(1-\cos\frac{T_E\Omega}{2}\right)\sin\left(\Omega t+\frac{T_E\Omega}{2}+\Psi\right). \qquad (7.14)$$

This equation indicates that phase-angles tested with MR probe changes in sine wave at the frequency of the magnetic field disturbance, Ω. Actually the phase-angle, $\Delta\Phi(t)$, can only be measured in the interval of repetition-time T_R. Since time T_R is usually longer than the period of the magnetic field vibration, the measurement is undersampled. Applied two repetition rates of T_{R1} and T_{R2}, which are very close with each other, for instance 191ms and 192ms, the original spectrum can be recovered from

its two alias spectra in most range of frequencies. The relationship between the real frequency and its alias frequencies are discussed below.

For a given sine wave of equation (7.14), denoting f_1 and f_2 as the alias frequencies measured with repetition rates of T_{R1} and T_{R2} respectively, the real frequency can be calculated by the following equations.

$$\Omega = 2\pi \frac{f_2 + f_1}{T_{R2} - T_{R1}} \tag{7.16}$$

if

$$\frac{2m\pi}{T_{R1}} < \Omega < \frac{2m\pi}{T_{R2}}, \text{ m=2,3,4, ... ;} \tag{7.17}$$

$$\Omega = 2\pi \frac{1 - f_2 - f_1}{T_{R2} - T_{R1}} \tag{7.18}$$

if

$$\frac{(2m+1)\pi}{T_{R1}} < \Omega < \frac{(2m+1)\pi}{T_{R2}}, \text{ m=2,3,4, ...;} \tag{7.19}$$

$$\Omega = 2\pi \frac{|f_2 - f_1|}{T_{R2} - T_{R1}} \tag{7.20}$$

if Ω does not fall into above two ranges indicated by equation (7.17) and (7.19).

The alias frequencies, f_1 and f_2, when normalized by the Nyquist frequency, vary between 0 and 0.5. There are three different ranges of frequencies, where equation (7.16), (7.18) and (7.20) are valid respectively. Since the repetition rates of T_{R1} and T_{R2} are very close with each other, equation (7.20) is valid in most of the frequency range. An example of frequency recovery is shown in figure 7-4 where the real signal is a sum of sine waves at 20.9, 30.0 and 60.0 Hertz as given by the equation

$$\Delta\Phi(t) = \sin(2\pi \times 20.9 \times t) + \sin(2\pi \times 30 \times t) + \sin(2\pi \times 60 \times t). \qquad (7.21)$$

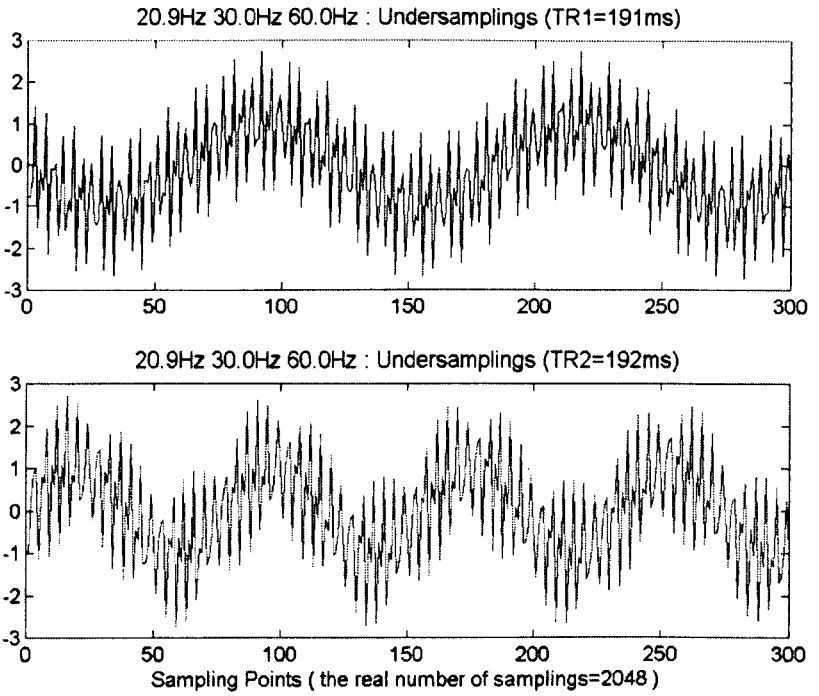

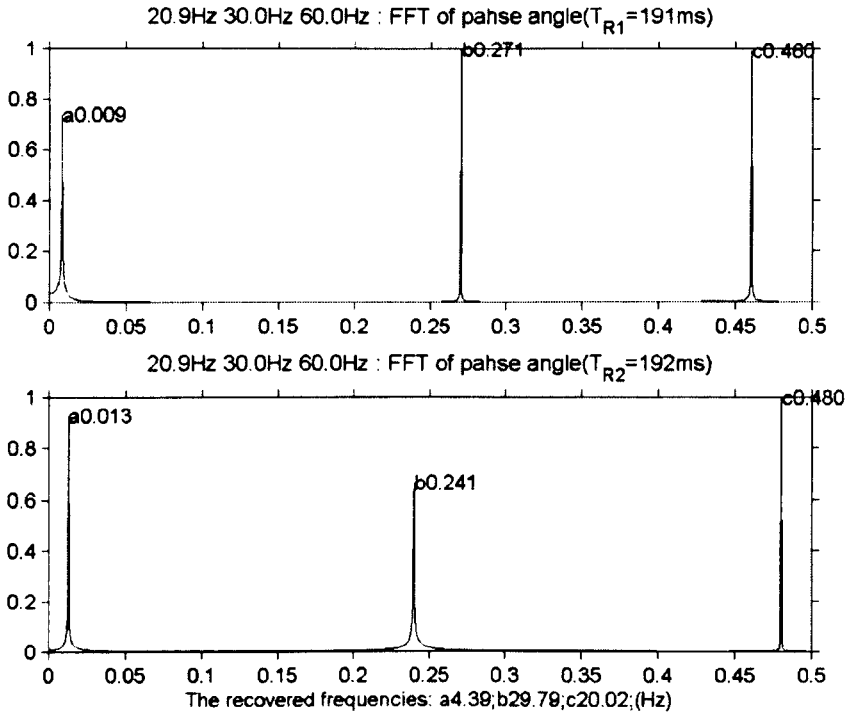

Figure 7-4 Undersampled signal, spectrum and frequency recovery.

In this figure, the recovered frequencies are all calculated with equation (7.20). From the FFT of the under-sampled data, the alias frequencies are 0.009, 0.271, 0.460 for the sampling period of 191ms (TR1), and 0.013, 0.241, 0.48 for the sampling period of 192ms (TR2). From these three pairs of alias frequencies, three recovered frequencies, 4.39Hz, 29.79Hz and 20.02Hz are derived by equation (7.20). But two of them do to reflect the correct frequencies. That is because the real frequencies 20.9Hz and 60Hz happen to fall into the bandwidths determined by equation (7.17) and (7.19) respectively. According to equation (7.17) and (7.19) these bandwidths are near 0 and 0.5 in alias spectrum as shown in figure 7-4 and they are very narrow with tow close sampling periods T_{R1} and T_{R2} . Most of the frequencies fall into the bandwidth determined by equation (7.20) and can be recovered correctly. The following figure illustrates the recovered frequencies against the real frequencies in an OMT standard with sampling periods 191ms and 192ms and with a sampling number of 256. These sampling periods limit the Nyquist's frequency to lower than 2.7Hz, which is far less than the demanded bandwidth of 50Hz in practical measurements.

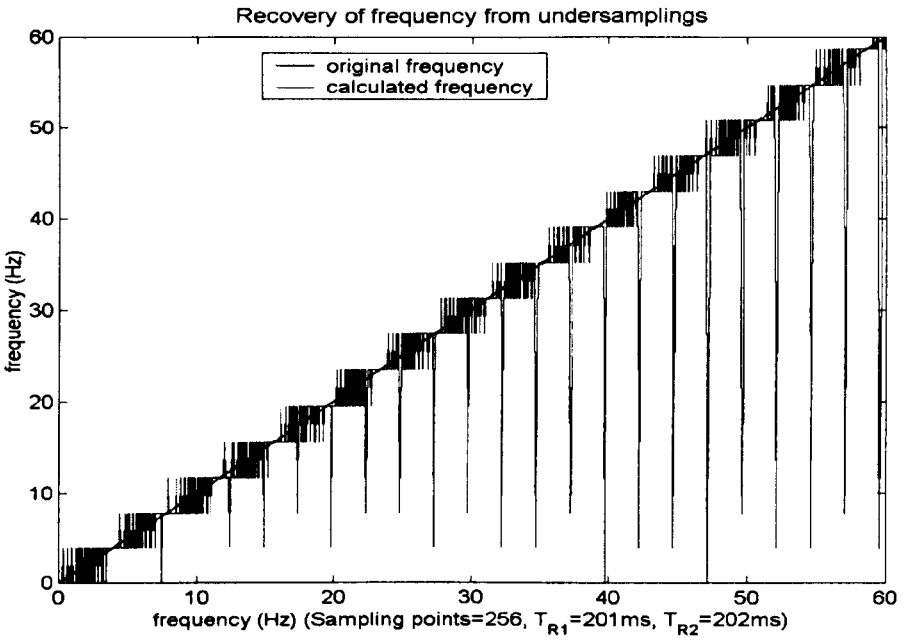

Figure 7-5 Computer simulation of spectrum recovery of magnetic field from under-sampled of MR phase-angles on OMT's standard.

The spikes in figure 7-5 are produced due to the use of equation (7.20) instead of equation (7.16) or (7.18) in their respective bandwidths. Obviously spikes fall into the bandwidths determined by equation (7.17) or (7.19). It shows in the figure that an error of about 4Hz exists almost in the whole range of frequency, even though the recovered frequencies fall into the bandwidths determined by equations (7.20). Such a large error is not acceptable in practice.

7.2.2 Improvement of Measurement of Magnetic Field Spectrum

Figure 7-5 shows that it is not accurate and reliable to recover the original spectrum from the alias spectra. According to the theoretical analysis of equation (7.16)-(7.20), the spikes in the recovered frequencies are inevitable unless the original frequency is known. But these relatively small errors are not inheritance of these formulas. These

errors can be suppressed with a longer acquisition time. The new results of simulation are illustrated in the following figure.

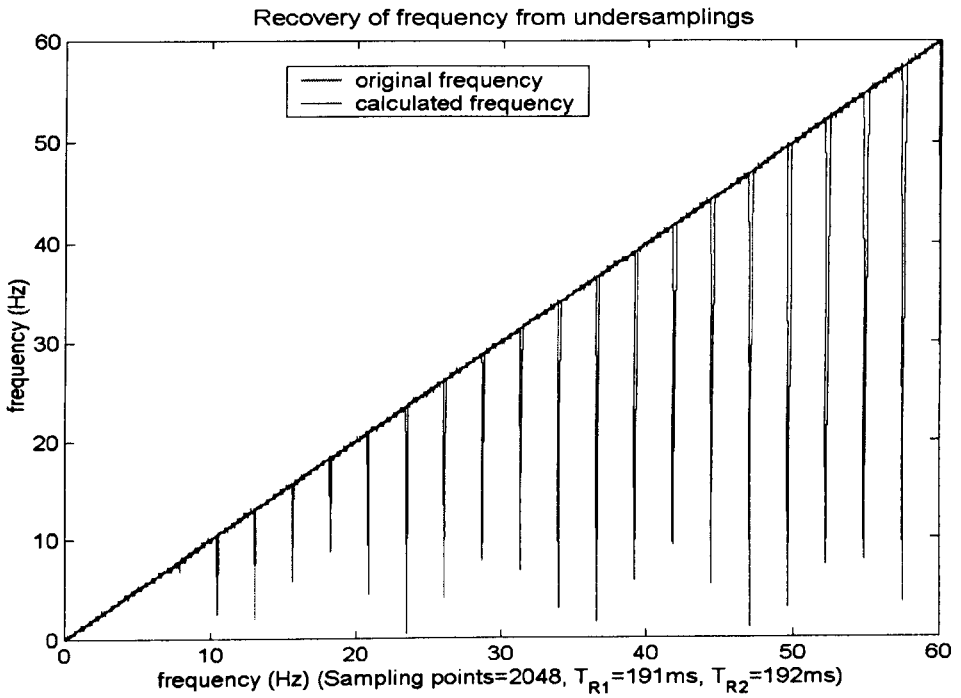

Figure 7-6 Computer simulation of spectrum recovery of magnetic field from under-sampled MR phase-angles.

In figure 7-6 much finer traces of recovered frequencies are obtained with a longer acquisition time in most of the bandwidth than in figure 7-5, except for the spikes. But in other hand, although the spikes are unavoidable, they can be shifted to other frequencies by choosing different repetition rates, for instance $T_{R1} = 197ms$ and $T_{R2} = 198ms$. A figure corresponding to Figure 7-6 but with repetition times of 197ms and 198ms is illustrated in Figure 7-7. The frequencies covered by the spikes according to these two pairs of repetition rates are displayed in Table 3-1, where unshaded data

represent frequencies with repetition times of 191ms and 192 ms, and shaded data represent frequencies with repetition times of 198ms and 198ms. It is indicated in the table that all the spikes are not overlapped with each other. Using this table we can find those frequencies which fall into the frequency ranges of the spikes. For instance, if a same frequency is recovered twice respectively using these two different repetition times, the frequency is usually a real spectrum concealed by under-sampling. But it is not always true. For example, if any two real spectra fall into spikes and appeared as the same recovered frequency, it seems that a same frequency is recovered twice. Obviously this frequency is not a real spectrum and is unpredictable. Fortunately those spikes occupy minor range of frequencies. Therefore the probability of misleading spectrum will be very small. This shortage of frequency recovery can also be improved by choosing more than tow pairs of repetition times.

Table 7-1 Frequency ranges of the spikes produced with repetition rates of (191ms, 192ms) and (197ms, 198ms) (Data are calculated with Matlab program umdersamp.m)

Frequency lower limit (Hz)	Frequency upper limit (Hz)	Frequency Lower limit (Hz)	Frequency upper limit (Hz)	Frequency lower limit (Hz)	Frequency upper limit (Hz)
5.051	5.076	23.438	23.560	42.929	43.147
5.208	5.236	25.253	25.381	44.271	44.503
7.576	7.614	26.042	26.178	45.455	45.685
7.813	7.853	27.778	27.919	46.875	47.120
10.101	10.152	28.646	28.796	47.980	48.223
10.417	10.471	30.303	30.457	49.479	49.738
12.626	12.690	31.250	31.414	50.505	50.761
13.021	13.089	32.828	32.995	52.083	52.356
15.152	15.228	33.854	34.031	53.030	53.299
15.625	15.707	35.354	35.533	54.688	54.974
17.677	17.766	36.458	36.649	55.556	55.838
18.229	18.325	37.879	38.071	57.292	57.592
20.202	20.305	39.063	39.267	58.081	58.376
20.833	20.942	40.404	40.609	59.896	60.209
22.727	22.843	41.667	41.885		

When applied equations (7.17)-(7.19) to the calculations of frequency recovery, lines in figure 7-6 will become finer as shown in figure 7-7.

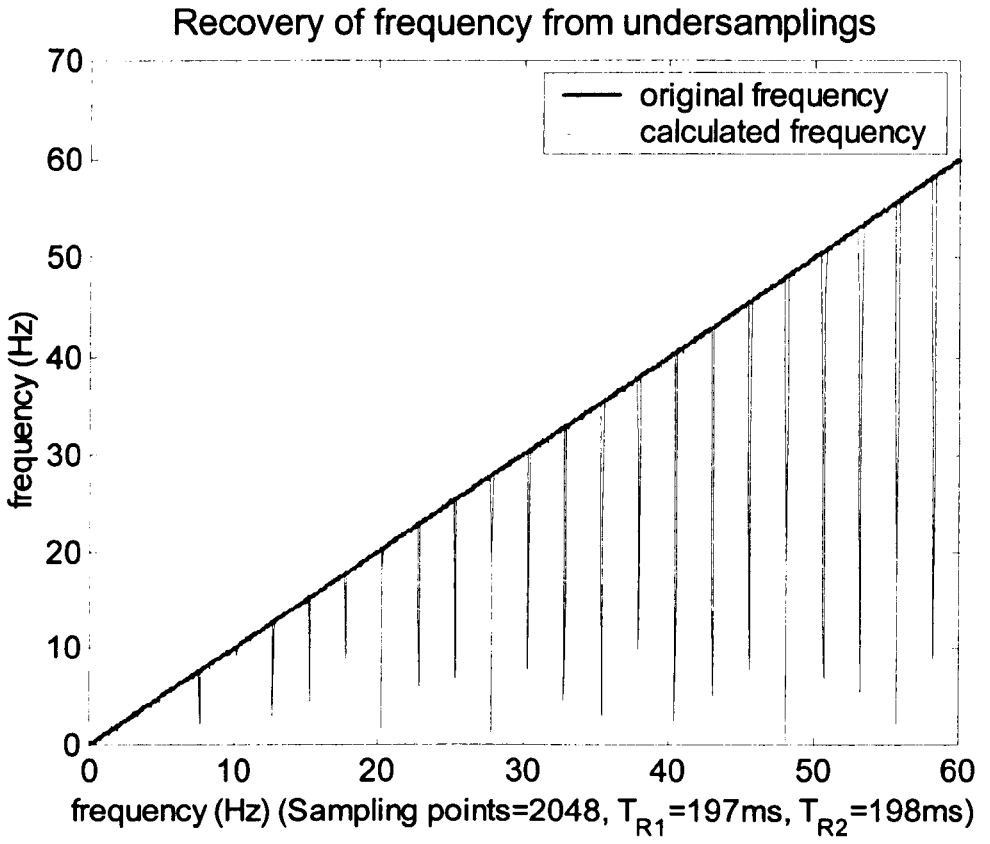

Figure 7-7 Computer simulation of spectrum recovery of magnetic field from undersamped MR phase-angles.

7.3 A New Method to Measure Magnetic gradient Using NMR Probe

7.3.1 Introduction

From the theoretical analysis in Chapter 5, the magnetic gradient of an MRI magnet is one of the possible sources of MR phase-angle distortion. Normally the magnetic field

is mapped with an experimental instrument like MFC-3045 as described previously in Section 2.3.3. Since there is a limited number of probes in the instrument, for instance only 24 probe in MFC-3045, the magnetic field between the probes is estimated by means of mathematical surface harmonics, ignoring the high order harmonics which contribute to a local magnetic gradient more than lower harmonics. Therefore the mapped field is smoother and produces less contribution to the MR phase distortion compared to the real one. In this section, for a given magnetic gradient, an analytical relationship between structural vibration and phase-angle distortion is derived. And than an experiment is developed based on the analysis to determine whether the magnetic gradient has considerable effect on the MR phase distortion or not. This experiment is realized by applying a small vibration to the MR probe, while the phase-angle is measured.

7.3.2 Magnetic gradient and phase-angle distortion

Magnetic field disturbance caused by motions of a magnet and the magnetic gradient was discussed in Chapter 5. The same relation exists for a relative vibration between an MR probe and magnetic field when the MR probe instead of the magnet is vibrated. That is

$$\Delta B(\mathbf{r},t) = \Delta\mathbf{r}(\mathbf{r},t)\cdot\mathbf{G}(\mathbf{r}), \tag{7.22}$$

where $\mathbf{G}(\mathbf{r})$ represents the magnetic gradient at a position pointed by vector $\mathbf{r}$ with displacement of $\Delta\mathbf{r}(\mathbf{r},t)$. As it was discussed in Chapter 6, this magnetic disturbance produces phase distortion in an echo-time of T_E according to equation (4.26). In practice $|\Delta\mathbf{r}(\mathbf{r},t)|$ is usually within the order of microns, in which the magnetic gradient, $\mathbf{G}(\mathbf{r})$, can be seen as a constant. Given displacements of $\Delta\mathbf{r}(\mathbf{r},t)$ along the vector of $\mathbf{G}(\mathbf{r})$, equation (4.26) is converted to the form,

$$\Delta\Phi(\mathbf{r}) = G(\mathbf{r})\gamma\left(-\int_{0}^{T_E/2}\Delta r(\mathbf{r},t)dt + \int_{T_E/2}^{T_E}\Delta r(\mathbf{r},t)dt \right). \tag{7.23}$$

The integration in the parentheses in equation (7.23) can be calculated as long as $\Delta r(\mathbf{r},t)$ is tested. But the magnetic gradient is still difficult to be drawn from equation (7.23), because the measurement of the phase distortion, $\Delta\Phi(\mathbf{r})$, and the measurement of the displacements, $\Delta r(\mathbf{r},t)$ are not synchronized exactly in time in practice, this means $\Delta\Phi(\mathbf{r})$ and $G(\mathbf{r})$ are not strictly correlated. In the practical experiment, the measurement of the phase-angle is repeated continuously many times with a repetition time period T_R, where echo-time T_E is encapsulated. The phase distortion is determined by the peak-to-peak value of the phase-angles tested. Equation (7.23) represents only one of the measurements. It is now modified to express the serial measurements of the phase distortions,

$$\Delta\Phi(\mathbf{r},n) = \gamma G(\mathbf{r})\Delta S(\mathbf{r},n), \tag{7.24}$$

where $n = 0,1,2,\cdots N$, and

$$\Delta S(\mathbf{r},n) = -\int_{nT_R}^{T_E/2+nT_R}\Delta r(\mathbf{r},t)dt + \int_{T_E/2+nT_R}^{T_E+nT_R}\Delta r(\mathbf{r},t)dt. \tag{7.25}$$

As mentioned in equation (2.33), the phase distortion is defined by the peak-to- peak value of $\Delta\Phi(\mathbf{r},n)$ as given in the form:

$$\Delta\Phi_{pk-pk}(\mathbf{r}) = \max_{n}\Delta\Phi(\mathbf{r},n) - \min_{n}\Delta\Phi(\mathbf{r},n). \tag{7.26}$$

In the same way we define

$$\Delta S_{pk-pk}(\mathbf{r}) = \max_{n} \Delta S(\mathbf{r}, n) - \min_{n} \Delta S(\mathbf{r}, n). \tag{7.27}$$

From equation (7.25) to (7.27), the magnetic gradient can be calculated by the following equation,

$$G(\mathbf{r}) = \frac{1}{\gamma} \frac{\Delta \Phi_{pk-pk}(\mathbf{r})}{\Delta S_{pk-pk}(\mathbf{r})}. \tag{7.28}$$

In Equation (7.23), a sinusoidal vibration of $\Delta r(\mathbf{r}, t)$ is obviously the simplest excitation. By giving the vibration function with frequency Ω,

$$\Delta r(\mathbf{r}, t) = \Delta r_0(\mathbf{r}) \sin(\Omega t + \Psi), \tag{7.29}$$

equations (7.26) and (7.27) are modified into the following equations respectively,

$$\Delta S_{pk-pk}(\mathbf{r}) = \frac{8\Delta r_0(\mathbf{r})}{\Omega} \alpha(\vartheta) \tag{7.30}$$

and

$$\Delta \Phi_{pk-pk}(\mathbf{r}) = \gamma G(\mathbf{r}) \Delta S_{pk-pk}(\mathbf{r}). \tag{7.31}$$

Comparing equation (7.30) with equation (4.31), they have the same sensitivity to the vibration frequencies.

Practical applications of this theoretical result in measurements of magnetic gradient are presented in the following Chapters.

8 Experiment Set-up

8.1 Introduction

Experiment is essential for validating an analytical result or to give a quantitative estimation. But in practice, there are many restrictions on carrying out experiments and the precision of an experiment depends on how it is built. Since the cryostat under the investigation is very expensive, any structural modifications may cost a lot. The extremely low temperature, the extremely high vacuum and the strong magnetic field of the cryostat increase the complexity of any structural modifications for the experiments. In the investigation of phase angle distortion, the vibration modal of Helium Can, the vibration modal of shields, the magnetic gradient and the phase angle distortion are three most important parameters according to the previous discussions. Although a huge amount of experimental data has been measured by OMT and LMS, their usability is limited due to lack of a theoretical support.

This chapter presents the set-up of two major experiments to obtain experimental data, which will be analyzed in the following chapter. One experiment is to measure structural vibrations and phase angle distortions to find the vibration modals and their contribution to the phase angle distortions. Another one is to measure phase angle distortions due to pure magnetic gradients under relative vibration between the magnetic field and the MR probe, excluding the effect of eddy-currents of the cryostat on the phase angle distortions. Since there have already been some experimental equipment and a modified cryostat of Type OR70 for experimental purposes, these devices were used extensively to minimize the costs and complexities of the experiments. Carefully designed formats of data file and file name convention are also discussed in this chapter.

8.2 Swept Sine Excitation and Fridge Excitation

A series of experiments have been carried out by the author to measure the structural vibration and frequency responses of MR phase distortion by applying swept sine forces on the Cold Head of cryostat Type OR70#80 with a magnetic field of 1.5 Tesla. The frequencies range from 2Hz to 70Hz. The amplitudes of the applied signals generated by a function generator were kept constant in all frequencies. The measurement process and instrumentation are illustrated in Figure 8-1, 8-2 and 8-3.

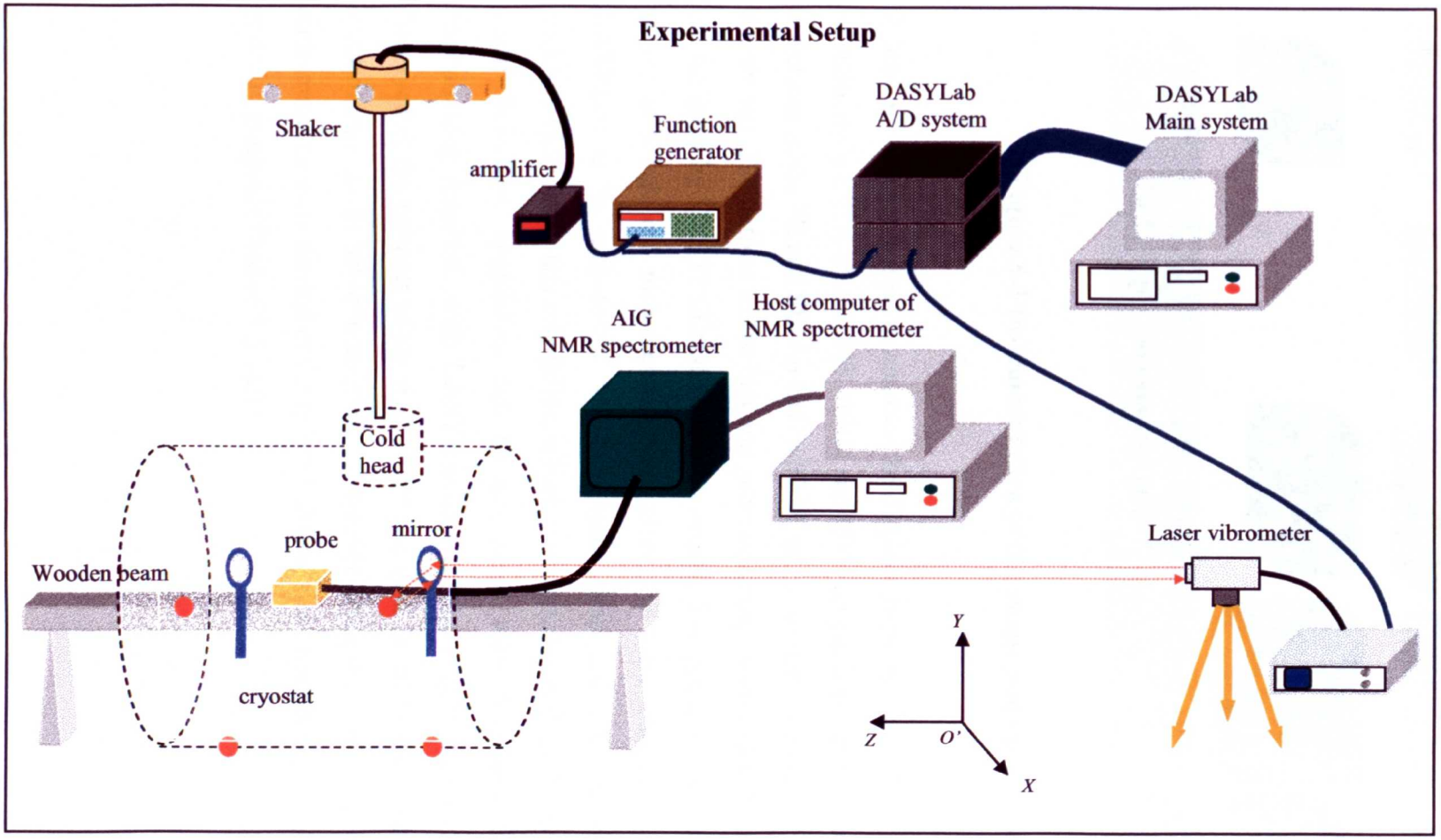

Figure 8-1 experimental setup for vibration modal tests.

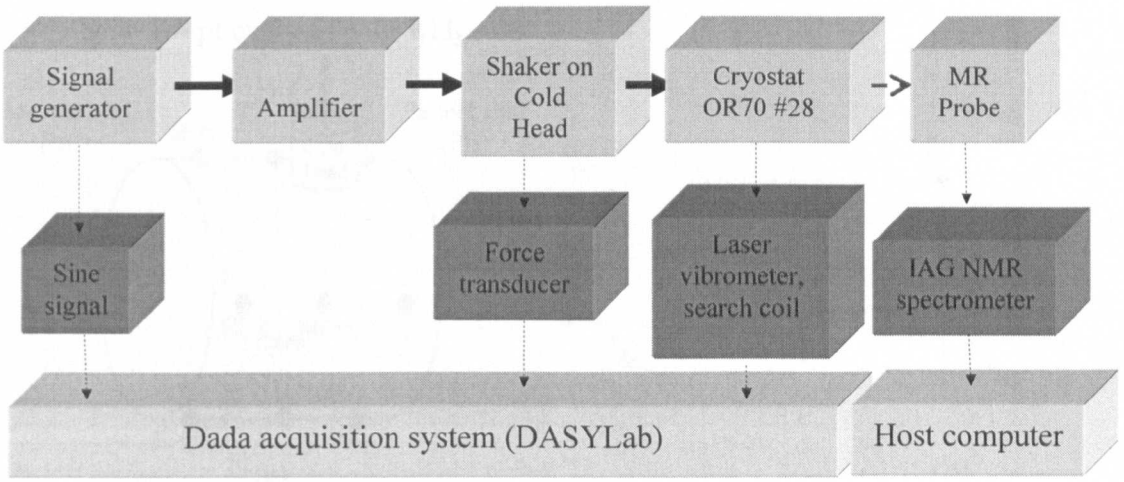

Figure 8-2 Instrumentation of the swept sine experiment

A laser vibrometer is used to measure the displacements and velocities of the vibrations of Helium Can, 20K shield, 80K shield and OVC respectively in vertical and horizontal directions at the PE and SE. An IAG's NMR spectrometer is applied to test phase angle distortions. The outputs of the function generator, force transducer and laser vibrometer are sampled by DASYLab system synchronously. The phase angle was independently tested, although it's measurement was under the same excitation of Cold Head. DASYLab is an easy-to-use Windows-based graphical data acquisition software package with which data acquisition is built more quickly and easily. By using an icon-based flowchart, application can be developed with point-and-click ease – no programming required. With DASYLab data can be acquired up to 1 MHz and be displayed at throughputs of up to 250 kHz and than saved to hard disk. The IAG MR spectrometer can be set to measure any frequency between 10MHz and 64MHz. But the measurements were carried out only at 63.8MHz, since the undergone cryostats were in their full magnetic field of 1.5 Tesla.

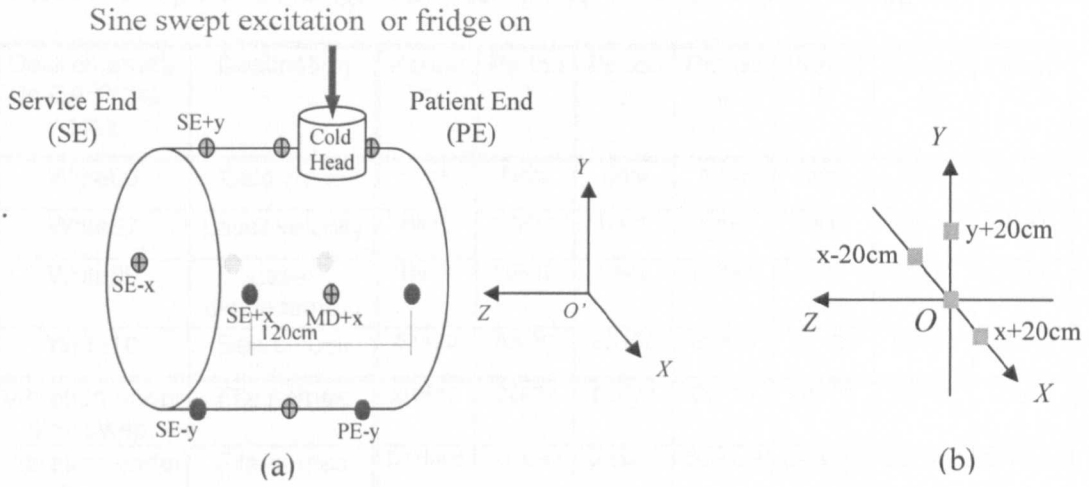

Figure 8-3 (a) Locations of optical holes on the bore-tube of a cryostat for vibration measurements of the shields and Helium Can using a laser vibrometer. (b) Locations of MR probe in the bore-tube.

In this figure (a), those solid circles indicate locations of optical holes. Since only rigid-body vibrations are under consideration in our discussions, measurements were only performed at the four locations, SE+x, SE-y, PE+x and PE+y. Vibrations of Helium Can, 20K shield, 80Kshield and OVC were tested at these four position with only one laser vibrometer respectively. They can be synchronized using technique of cross-correlation, although the data tested with the DASYLab were not synchronous to phase angles tested with the NMR spectrometer. The force of shaker excitation was chosen as a reference to make cross-correlation with other signals, because it is the main source of vibration of a cryostat and its position is just on the top of Cold Head. In measurements of phase distortion, the MR probe was placed at the centre, x-20cm offset, x+20cm offset, y-20cm offset and y+20cm offset in the bore-tube as illustrated in Figure 8-3 (b).

Data definitions, file name convention, cable labels, cable connections, A/D channels and data channels in DASYLab schematic program etc. were defined and built for efficiency, as shown partly in Table 8-1. DASYLab's acquisition rate was 500Hz.

Table 8-1 A part of configuration for set-up of frequency sweeping experiment.

Data channels in DASYLab files	Description	Period 1	Period 2	Period 3	Period 4	Period 5	Period 6	Period 7
Write06	Cold Head	force	force	force	force	force	force	Force
Write07	Laser velocity	He13	20K13	He43	20K43	He11	20K11	He41
Write09	Laser displacement	He13	20K13	He43	20K43	He11	20K11	He41
Write10	Search coil	SX+20	AX-20	SX+00	SY+00	SY+20	SZ+00	SZ+00
Vibration under sine swept	File names	D1F??	D2F??	D3F??	D4F??	D5F??	D6F??	D7F??
Vibration under fridge	File names	D1Head	D2Head	D3Head	D4Head	D5Head	D6Head	D7Head
Phase angles under sine	File names	P1F??	P2F??	P3F??	P4F??	P5F??	P6F??	P7F??
Phase angles under fridge	File names	P1Head	P2Head	P3Head	P4Head	P5Head	P6Head	P7Head

In this table, "He13" indicates position at PE+x on the Helium Can, "20K11" at SE+x on the 20K shield, "He43" at PE-y on the Helium Can and etc. Question marks in the file names were replaced by excitation frequencies when the data were saved in the file.

File name conventions are defined as follows:

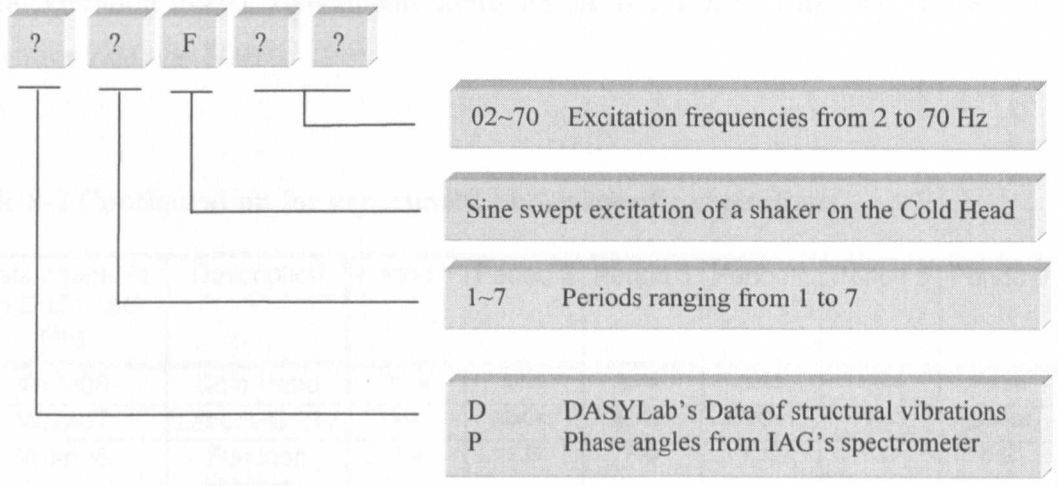

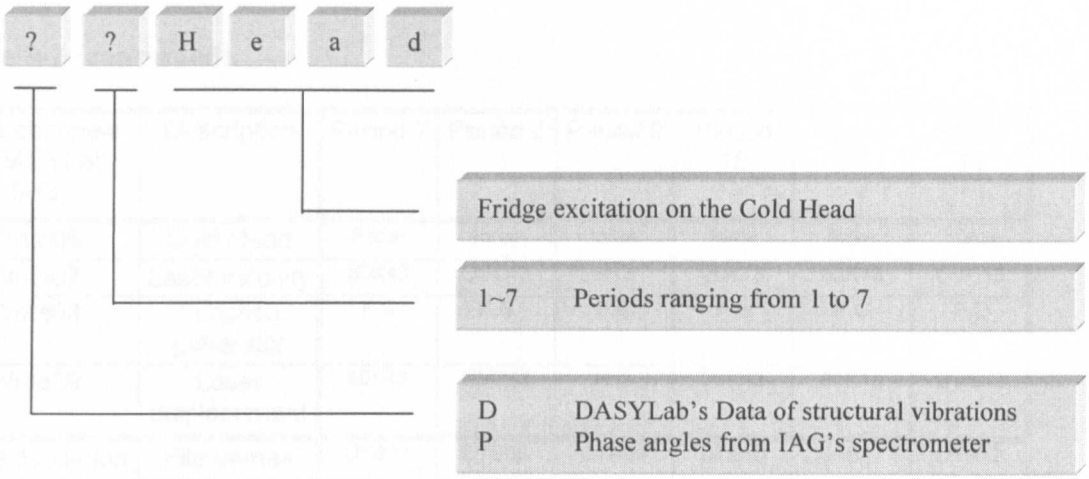

8.3 Experiment under Specific Excitations

By realizing some resonant frequencies from the previous experiments, further experiments of structural vibrations were set-up focusing excitations on 8, 14 and 39 Hz. And also pulse excitations were applied to the Cold Head to obtain the dominant natural vibration modal. Experiment configuration is given in Table 8-2. DASYLab's acquisition rate was 500Hz.

Table 8-2 Configuration for experiment under specific excitations

Data channels in DASYLab files	Description	Period 1	Period 2	Period 3	Period 4	Period 5	Period 6
Write06	Cold Head	force	force	force	force	force	Force
Write07	Laser velocity	He41	20K41	80K41	OVC41	He43	20K43
Write08	Function generator	F.G	F.G	F.G	F.G	F.G	F.G
Write09	Laser displacement	He41	20K41	80K41	OVC41	He43	20K43
Pulse excitation	File names	DTB01	DTB02	DTB03	DTB04	DTB05	DTB06
Sine excitation	File names	DTB01F??	DTB02F??	DTB03F??	DTB04F??	DTB05F??	DTB06F??
Fridge excitation	File names	DTB01H	DTB02H	DTB03H	DTB04H	DTB05H	DTB06H

Table 8-2 (continued)

Data channels in DASYLab files	Description	Period 7	Period 8	Period 9	Period 10	Period 11	Period 12
Write06	Cold Head	Force	force	force	force	force	Force
Write07	Laser velocity	80K43	OVC43	H13	20K13	80K13	OVC13
Write08	Function generator	F.G	F.G	F.G	F.G	F.G	F.G
Write09	Laser displacement	80K43	OVC43	H13	20K13	80K13	OVC13
Pulse excitation	File names	DTB07	DTB08	DTB09	DTB10	DTB11	DTB12
Sine excitation	File names	DTB07F??	DTB08F??	DTB09F??	DTB10F??	DTB11F??	DTB12F??
Fridge excitation	File names	DTB07H	DTB08H	DTB09H	DTB10H	DTB11H	DTB12H

Table 8-2 (continued)

Data channels in DASYLab files	Description	Period 13	Period 14	Period 15	Period 16	Period 17
Write06	Cold Head	force	force	force	force	force
Write07	Laser velocity	He11	20K11	80K11	OVC11	OVCZ
Write08	Function generator	F.G	F.G	F.G	F.G	F.G
Write09	Laser displacement	He11	20K11	80K11	OVC11	OVCZ
Pulse excitation	File names	DTB13	DTB14	DTB15	DTB16	DTB17
Sine excitation	File names	DTB13F??	DTB14F??	DTB15F??	DTB16F??	DTB17F??
Fridge excitation	File names	DTB13H	DTB14H	DTB15H	DTB16H	DTB17H

In this table, file name definitions are similar with that in Table 8-1 except that all file names are prefixed with "DTB" meaning DASYLab' data of Transient response in full magnetic field (B). From Table 8-2, it can be seen that all of the main parts, Helium Can 20K shield, 80K shield and OVC are tested. Pulse excitation was conducted as shown in the following figure.

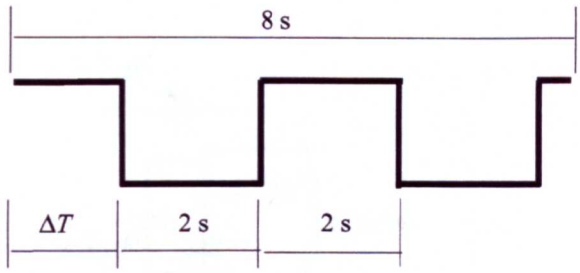

Figure 8-4 Shape of pulse excited by shaker on the Cold Head.

In this figure ΔT is undetermined and varies in different periods of measurement.

8.4 Experiment for MR probe vibration

The experiment was carried out by exciting an NMR probe in a magnetic field of 1.5 Tesla with a shaker, as shown in Figure 8-5.

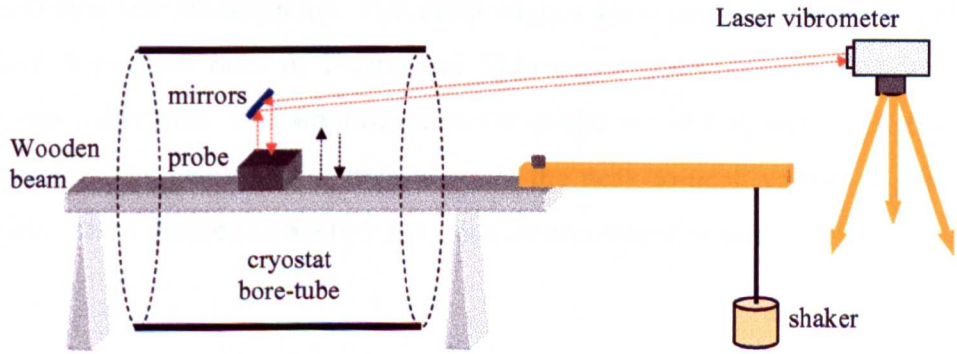

Figure 8-5 Schematics of MR probe vibration.

The NMR probe was a sample of doped water with an r.f. coil wound around the outside of the container. This inductor was formed into a tuned circuit by inclusion of capacitors, as shown in Figure 8-6.

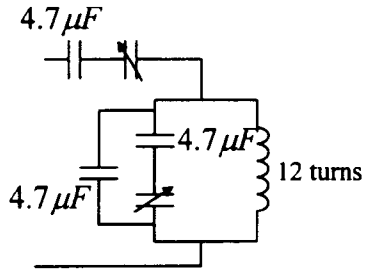

Figure 8-6 63.8MHz probe circuit.

The probe was encapsulated in a box, which is tightly fixed on a wooden beam. A vertical sinusoidal excitation was applied to the wooden beam with a shaker, while the displacement of the case vibration was tested with a laser vibrometer. To restrict a relative vibration between the coil and case, the coil and sample were firmly stuck to the case with a resin filled in. The exciting frequencies were from 8 to 10Hz, at which are the most suspicious frequencies producing phase distortion according to previous experiments and investigation. The phase angles were being tested during the probe is excited. Repetition rates of 191ms and 192ms were selected, with 256 samplings for each repetition rate. The amplitudes of the probe vibrations were tested with a laser vibrometer. The phase angles measured are the peak-to-peak values of phase angle as they have been defined in Section 4.3, plus measurement noises.

Such a measurement of phase angles was repeated with four different vibration amplitudes at three different positions respectively. File name convention is given following Table 8-4. DASYLab's acquisition rate was 1000Hz. In this table, notation F, D and B represent the locations of the probe at center, 10cm offset and 20cm offset respectively.

Table 8-4 (continued)

Data channels in DASYLab files	Description	Period B Y+20cm	Period D Y+10cm	Period F Y+0cm
Write00	Function generator	F.G	F.G	F.G
Write01	Laser displacement	Laser dis.	Laser dis.	Laser dis.
Write02	Laser velocity	Laser vel.	Laser vel.	Laser vel.
DASYLab data	File names	DG??B??	DG??D??	DG??F??
IAG' spectrometer	Phase angle File names	PG??B??	PG??D??	PG??F??

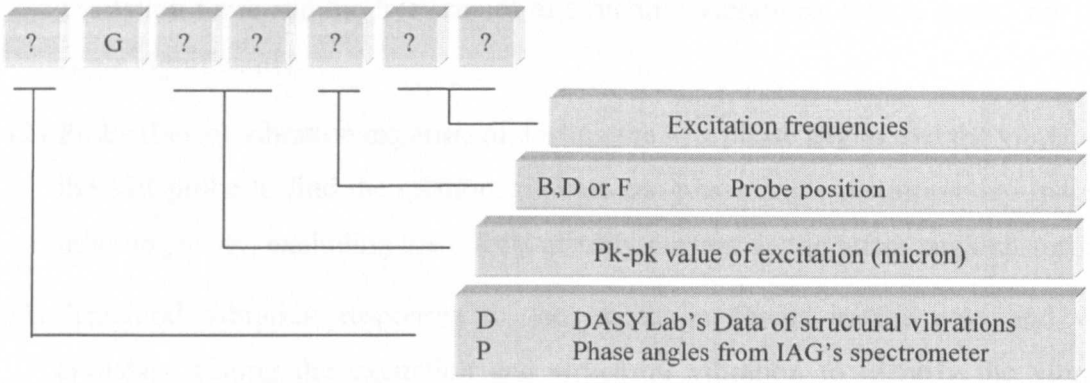

8.5 Summary and discussions

Experiments are set up to measurement structural vibrations and phase angle distortions of cryostat Type OR70#8 under various excitations of the Cold Head of the cryostat. A very good repetition has been presented in each of the experiments. The main equipment used in the measurements is a laser vibrometer and an NMR probe. Although a search coil sensor and many accelerometers are applied in the experiments due to OMT's request, they are not presented here because of their poor reliability and their redundancy.

9 Experimental Data Analysis

According to the theoretical analysis and preliminary measurements discussed in previous chapters, the magnetic field inhomogeneity and eddy current are the two most libels sources of phase angle distortions. To verify the theoretical conclusion of phase angle distortion problems quantitatively, the following experiments have been carried out with OR70#28 based on the experimental set-up presented in Chapter 8:

(1) Swept sine experiment in the cold cryostats, testing the MR phase angles, the excitation force and the frequencies of structural vibrations, which impact the phase angle significantly.

(2) Probe (beam) vibration experiment, testing the MR phase angles and the vibration of the MR probe to find the relationship between phase angle distortion and magnetic inhomogeneity, excluding the effects of eddy-current on the phase angle distortions.

(3) Structural vibration responses to the excitation forces in the cold and warm cryostats, testing the excitation and structural vibration to identify the vibration modals and to find the properties of vibration transmission from the cold-head to other parts of the cryostat.

Between the evaluations of magnetic inhomogenity and eddy-current, most efforts of the experiments are focused on the evaluation of magnetic inhomogeneity. This is because the evaluation of eddy current is more difficult and less accurate both in analyses and experiments compared to that of the magnetic inhomogeneity. The magnetic gradients are also derived from the experimental data of the magnetic map to compare them with the gradient derived from probe vibration experiments. Most of analyses were carried out using MATLAB programs, written by the author, the source code for these programs are provided in Appendix H.

9.1 Frequency Response of Phase Distortion

Phase distortions under swept sine excitations of the cold head have been measured to generate frequency response functions (FRF) experimentally. The MR probe is put at the centre, X-20cm offset, X+20cm offset and Y+20cm offset in the bore-tube. The original data of phase distortions are presented in Appendix G. The frequency response of the phase distortion to the cold head force is illustrated in Figure 9-1, Figure 9-2 and Figure 9-3. The FRF is normalized by the force of the shaker (Figure 9-11). It is indicated both in the FRF and the original data that the phase distortion is particularly susceptible to the cold head forces at the frequencies of 8Hz, 19 Hz and 39Hz.

The phase distortions at offset along x-axis are dominated at the frequencies of 8Hz and 37~39Hz, as shown in Figure 9-1, while along y-axis it is at the frequencies of 19~22H, as illustrated in Figure 9-3. A relatively strong response of the phase distortion is also at 59Hz in Figure 9-2, although the magnitude of the FRF is much less than that shown in Figure 9-1.

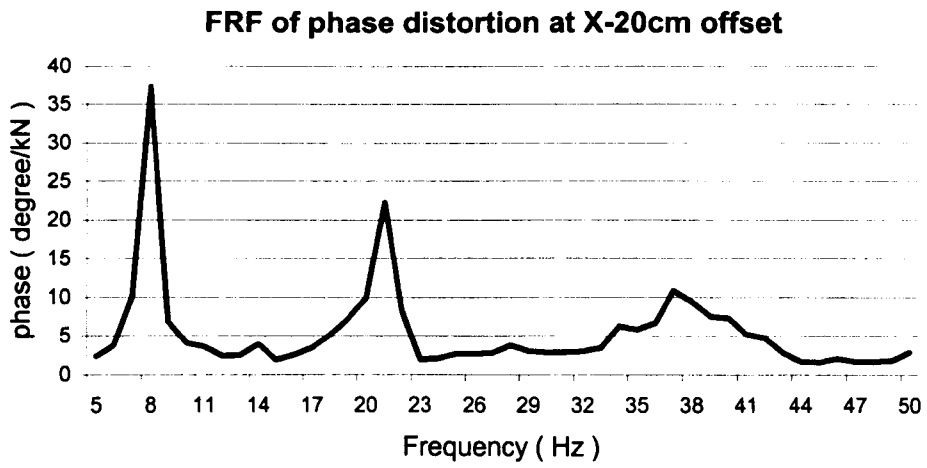

Figure 9-1 The frequency response of the phase distortion measured at offset x-20cm against to the cold head force.

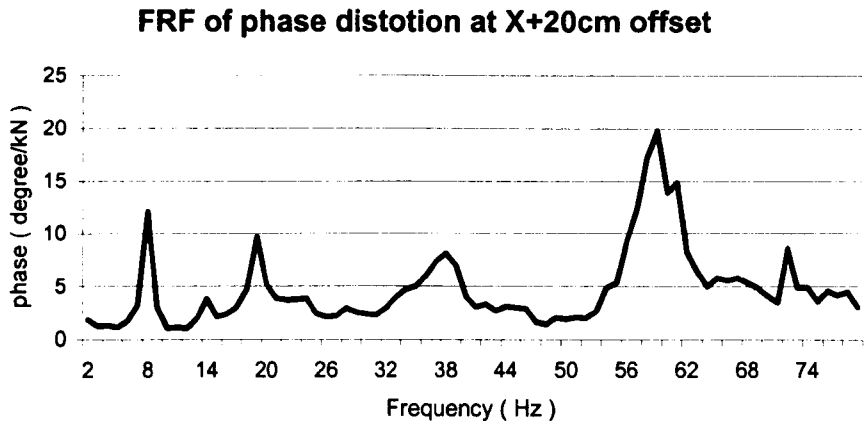

Figure 9-2 The frequency response of the phase distortion to the force on the cold head.

Comparing Figure 9-1 and Figure 9-2, the frequency responses of phase distortions are not symmetric at the two probe locations on x-axis. The phase distortions under 30Hz are approximately twice as much in the location of X-20cm as they are in the same frequency range in the location of X+20cm. It implies that the disturbances of magnetic

field are considerably different in these two symmetric locations. According to the theoretical analysis of eddy-current discussed in Chapter 4, the eddy-current is mainly generated by a lump change of magnetic flux (directional change of 1.5 Tesla magnetic field) rather than by the tiny magnetic inhomogeneity (the gradient is less than 3000ppm/m of 1.5 Tesla magnetic field). Since the structural vibrations under 200Hz are a vibration of a rigid body according to the LMS's measurements [24, 25], the vibrations under 30Hz must be symmetric, and would generate a symmetric eddy-current and magnetic disturbances at symmetric locations inside the bore-tube. But obviously this expectation of symmetry has not been observed in this experiment.

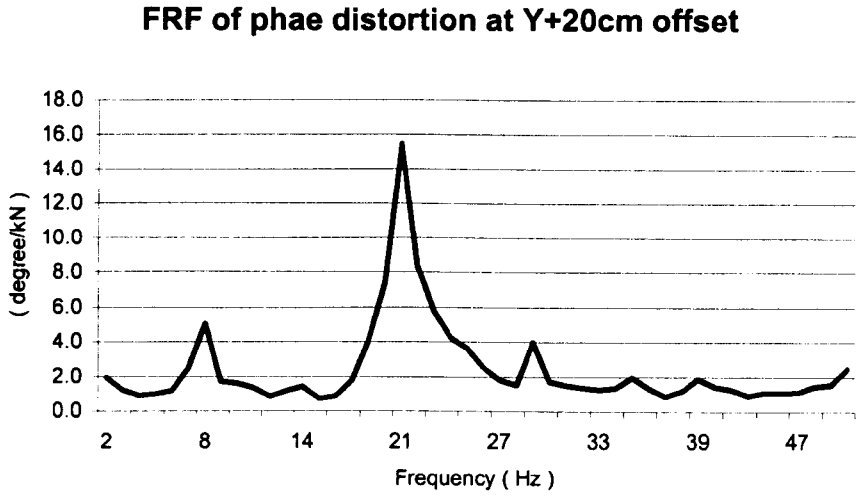

Figure 9-3 The frequency response of the phase distortion to the force on the cold head.

What would be the main source of the phase distortion if it is not the eddy-current? It most likely is the magnetic disturbance directly from the moving inhomogeneous magnetic field according to the theoretical results. Why are the phase distortions particularly high at 8 Hz, 20 Hz, 39 Hz and 59 Hz? These questions will be discussed in the following clauses using particularly designed experiments and previous measurements.

9.2 Probe (Beam) Vibration Experiment and Magnetic Gradient

It has been realized that both magnetic inhomogeneity and eddy-currents can cause phase angle distortions. But to evaluate their effects separately is not possible under the normal operational condition of a cryostat by means of the instrument currently available. This experiment is devised to measure the phase distortions which is produced by the magnetic inhomogeneity without any eddy current in the cryostat. To eliminate the effect of the eddy current on the phase distortion in a measurement, consequently to evaluate the effect of the magnetic inhomogeneity on the phase distortion, the main source of vibration, the cold head, is stopped, while instead of the structural vibration of the cryostat an MR probe, which is isolated from the cryostat, is excited by a shaker to generated a relative vibration between the probe and the magnet of the cryostat. The probe is fixed on a wooden beam. The experimental set-up has already been shown in Figure 8-5.

9.2.1 Effect of Magnetic Gradient on MR Phase Angle

Sinusoidal excitations at frequency near 9Hz with peak-to-peak values of 5 μm , 10 μm ,15 μm and 20 μm are respectively applied to the wooden beam on which an MR probe is tightly bound. The measurements of phase distortions under the different amplitudes of vibration and various positions (offsets of X+0cm, X+10cm and X+20cm) are illustrated in Figure 9-4.

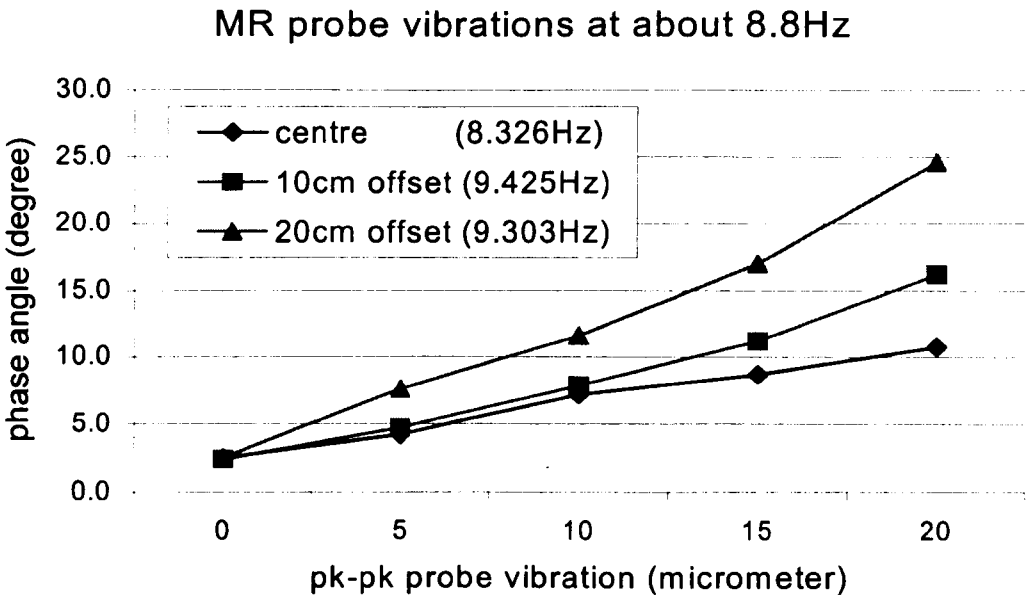

Figure 9-4 The phase distortions against the pk-pk vertical vibrations of the probe at the centre, 10cm offset and 20cm offset in the y-axis.

Significant phase distortions can be observed from the figure. Since there was not any relative vibration between the shield (or any part of the cryostat) and the magnetic field, the eddy-current must not exist in the shield during the experiment, hence the measured phase distortions cannot be due to eddy-currents. The figure also indicates that the phase distortion increases monotonously from the centre to 20cm offset in x-axis. The phase distortion under vibrations with peak-to-peak value of 10 micrometers is about 11 degrees, which is very close to the phase distortion of 12 degrees measured in the same cryostat but under fridge excitation with vibration amplitude of peak-to-peak value of 10 micrometers. Therefore the main contribution to the phase distortion can be seen as from the change of magnetic field due to the vibration of inhomogeneous magnetic field. This conclusion is further supported in section 9.4 and 9.5 by comparing the magnetic gradients measured with two different methods.

9.3 Structural Vibration of OR70#28

Experiments on structural vibrations of cold and warm OR70#28 have been carried out with the swept sine excitations, fridge excitations, and transient excitations. According to the theoretical analysis discussed in the previous chapter, the eddy current is proportional to the relative velocity between the shields and magnet, while the effect of the magnetic inhomogeneity on the phase angle is proportional to the displacement of the magnet vibration. Tested results of displacement and velocity due to vibrations are presented in this chapter.

9.3.1 FRF of Helium Can and 20K Shield by the Swept Sine Experiments

The functions of frequency responses of displacements and velocities of the magnet (the Helium Can) and the 20K shield are illustrated in the following figures. The displacements and velocities have been normalized with the amplitudes of excitations of the cold-head forces, which are displayed in Figure 9-11. The notation, "PE X" represents the location of test point at the patient end of the cryostat in x-axis.

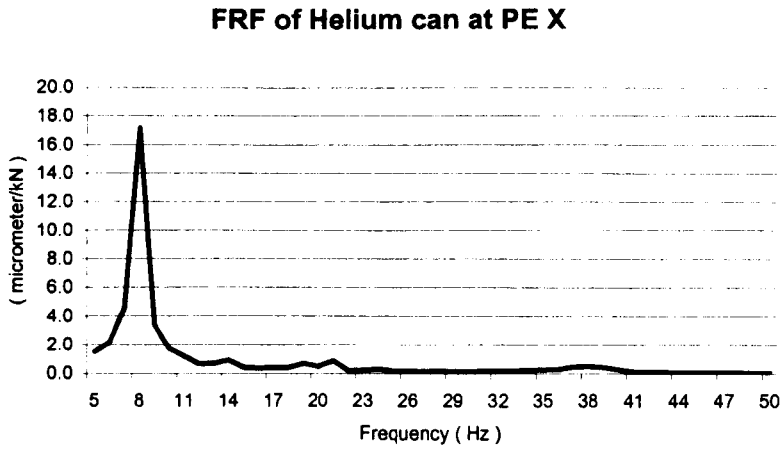

Figure 9-5 Frequency responses of the Helium can displacements measured in x-axis at PE against to the cold head force.

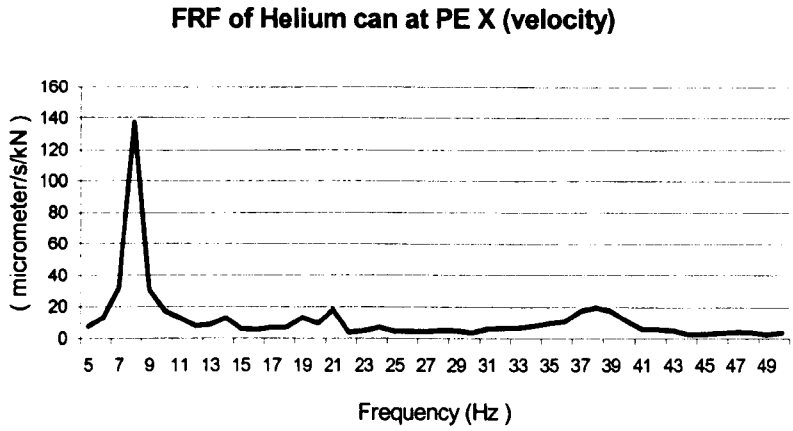

Figure 9-6 Frequency responses of the Helium can velocities measured in x-axis at PE against to the cold head force.

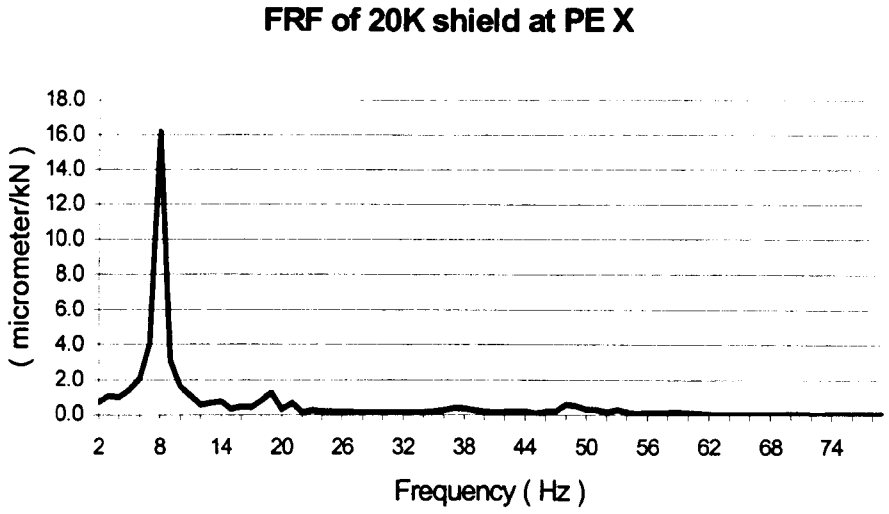

Figure 9-7 Frequency responses of the 20K shield displacements measured in x-axis at PE against to the cold head force.

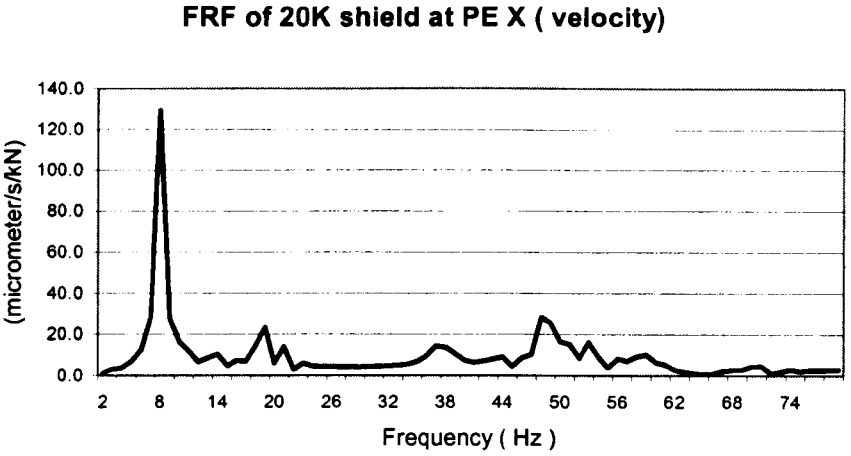

Figure 9-8 Frequency responses of the 20K shield velocities measured in x-axis at PE against to the cold head force.

In the figures above, the vibrations of the Helium Can and 20K shield are dominant at 8Hz at the patient end along the x-axis. Similar responses of the Helium Can are

reflected under the fridge excitations, that are presented in Figure 9-12 and Figure 9-13 in section 9.3.3.

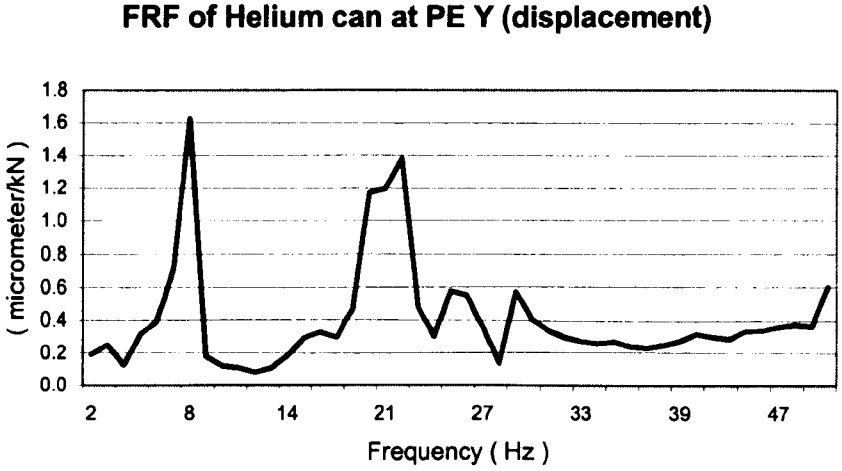

Figure 9-9 Frequency responses of the Helium can displacements measured in y-axis at PE against to the cold head force.

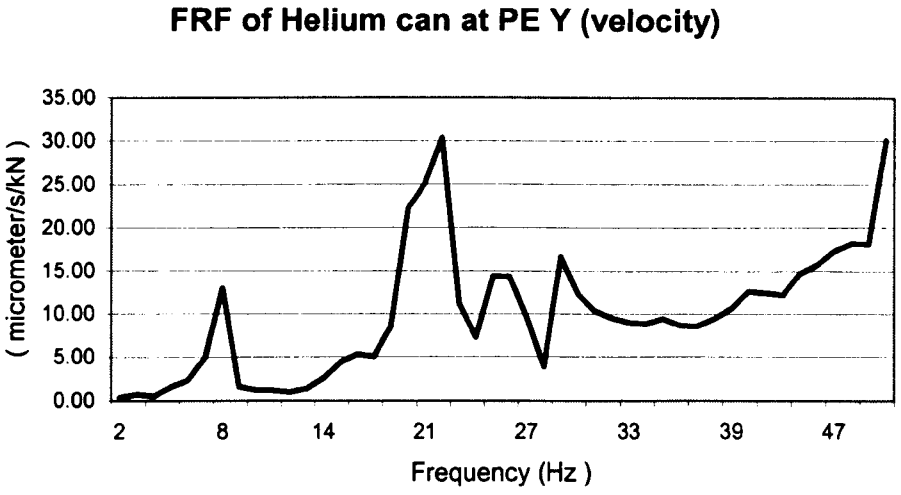

Figure 9-10 Frequency responses of the Helium Can velocities measured in y-axis at PE against to the cold head force.

In Figure 9-9 and Figure 9-10, the responses at 8Hz in y-axis are still considerable compared to the responses at the other frequencies, but their amplitudes are much less than that measured in the direction of x-axis (Figure 9-7 and Figure 9-8). The velocities around 20Hz take dominant roles in y-axis, although their amplitudes are at the same level as they are in x-axis. This indicates that the vibrations of Helium Can and 20K shield in the direction of x-axis are greater than that in y-axis at 8 Hz, while at 20 Hz, the amplitudes of the vibrations in y-axis are comparable with that in x-axis.

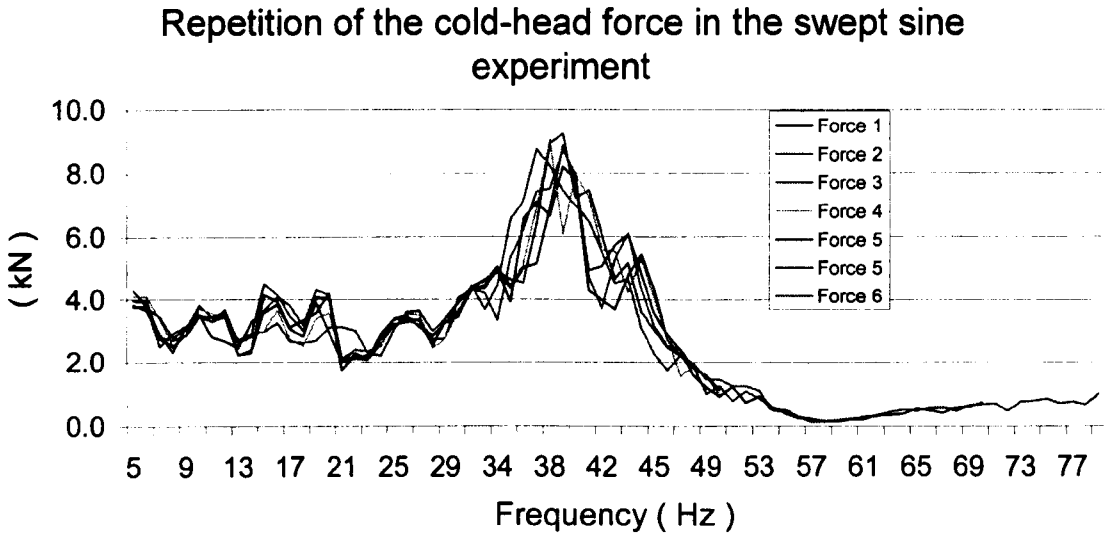

Figure 9-11 The cold head forces applied in the swept sine experiment.

This figure displays the forces measured in the connection between the cold-head and the shaker. It shows a good repetition in six experiments of swept sine excitation. The forces are particularly high around 40Hz, this is due to the resonant frequency of 40Hz of the cold-head. At about 59 Hz the forces are particularly low whilst the structural vibrations (Figure 9-7 and Figure 9-8) and the phase distortions are normal. This must be the main reason, that high values of normalized phase distortions are displayed around 59 Hz in Figure 9-2.

9.3.2 Mechanical Resonance Under Swept Sine Excitations

To measure rigid modals of structural vibrations of cryostat OR70#28, the vibrations of the Helium can and 20K shield are tested at patient end (PE) and service end (SE) in directions of x-axis and y-axis respectively. Since the shapes of the OVC, shields and Helium can are all cylindrical, their rolling modals (rotation about z-axis) are not measured. The vibration modals of translation and rotations are derived from the phase differences between the two ends, the patient end and the service end. Table 9-1 summarizes the vibration modals, which is derived from Table 9-2, Table 9-3 and Table 9-4. All the experimental data displayed in these tables are the same as that used to generate the figure 9.11.

Table 9-1 Important vibration modals of cold cryostat OR70#28.

Frequency (Hz)	Description
8	Whole body lateral vibration with big response amplitude of displacement to the shaker force.
19	(1) Vertically rotational vibration of the Helium can. (2) Helium can is in phase with OVC, 80K and 20K at PE, but somewhat out of phase with 80K at SE.
39	(1) Resonance of the cold head and its mounting system. (2) Translation of the Helium can and 20K shield which are tightly fixed with each other.

The following three tables give the amplitudes and phases of the structural vibrations of the Helium can and 20K shield in x-axis and y-axis at PE and SE.

The following terms are used in the tables:

1. Mechanical phase shift: vibration transfer delay of the tested point to the reference, the cold head force.
2. Pk-pk displacement: peak-to-peak displacement at the tested point.
3. Response gain: the response gain of tested point to the reference, the cold head force.

Resonance at 8Hz

Table 9-2

	Helium can PE		20K shield PE		Helium can SE		20K SE
	X	Y	X	Y	X	Y	X
Mechanical phase shift (degree)	151.00	331.00	151.00	319.00	151.00	331.00	151.00
Pk-pk displacement (micrometer)	123.97	13.29	130.00	3.44	125.10	9.79	115.91
Response gain (micrometer/KN)	17.15	1.63	16.18	0.25	17.40	1.21	16.19
Frequency (Hz)	8.06	8.06	8.06	8.06	8.06	8.06	8.06

The mechanical phase shifts in this table explain that the vibrations of the Helium can and 20K shield are in phase between PE and SE in the same direction, either in x-axis or in y-axis. The 20K shield moves in phase to the vibration of the Helium can both in x-axis and y-axis respectively. It can be concluded that the Helium can and 20K shield translate as one rigid body at 8Hz.

Resonance at 19Hz

Table 9-3

	Helium can PE		20K shield PE		Helium can SE		20K SE
	X	Y	X	Y	X	Y	X
Mechanical phase shift (degree)	151.00	192.00	278.00	195.00	54.90	291.00	68.60
Pk-pk displacement (micrometer)	7.43	12.40	12.48	13.88	4.69	16.17	4.38
Response gain (micrometer/KN)	0.69	1.17	1.25	1.44	0.27	1.55	0.30
Frequency (Hz)	19.05	19.05	19.05	19.05	19.05	19.05	19.05

Resonance at 39Hz

Table 9-4

	Helium can 9.3.2.1 PE		20K shield PE		Helium can SE		20K SE
	X	Y	X	Y	X	Y	X
Mechanical phase shift (degree)	309.00	0.00	276.00	355.00	287.00	5.80	276.00
Pk-pk displacement (micrometer)	7.98	7.24	7.37	5.73	8.74	4.22	6.72
Response gain (micrometer/KN)	0.45	0.27	0.28	0.22	0.41	0.17	0.29
Frequency (Hz)	38.96	38.96	39.08	38.96	39.08	39.08	38.96

9.3.3 Mechanical Vibration Under Fridge Excitation

The spectrum of a fridge excitation has been discussed in Chapter 6. Most of the energy of the fridge excitation is distributed in the range between 40 Hz and 70Hz, while a particularly dominant vibration of the Helium Can at frequency of 8Hz is tested in the direction of x-axis under the fridge excitation, and at the frequency of 20Hz in the direction of y-axis as displayed in the following figures. These results of measurements correspond with the results of swept sine experiments presented in section 9.3.1. The matching of the results gives further evidence of the conclusions summarised in Table 9-1.

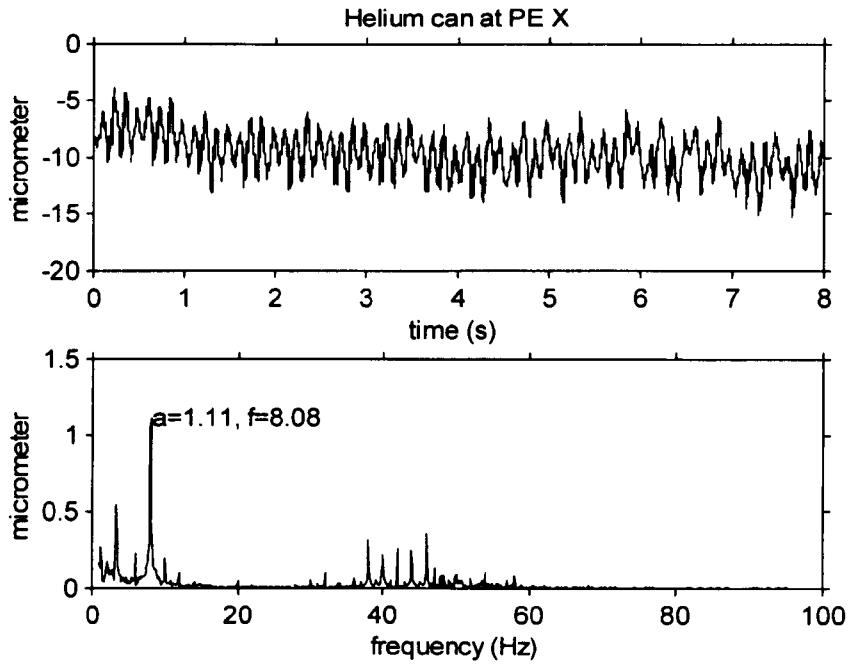

Figure 9-12 The displacement and its spectrum of the Helium can at the patient end (PE) horizontal offset.

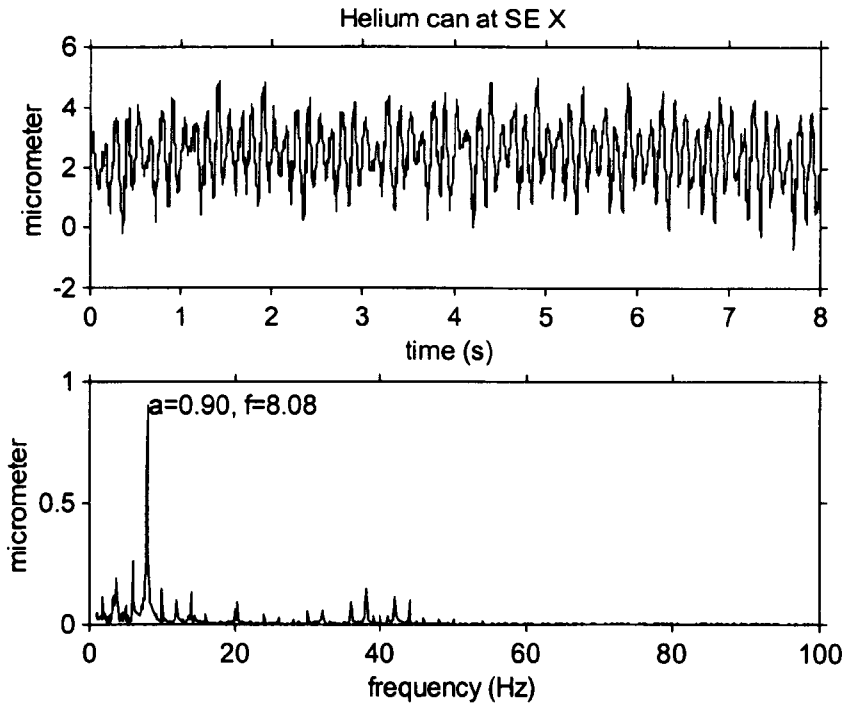

Figure 9-13 The displacement and its spectrum of the Helium can at the service end (SE) horizontal offset.

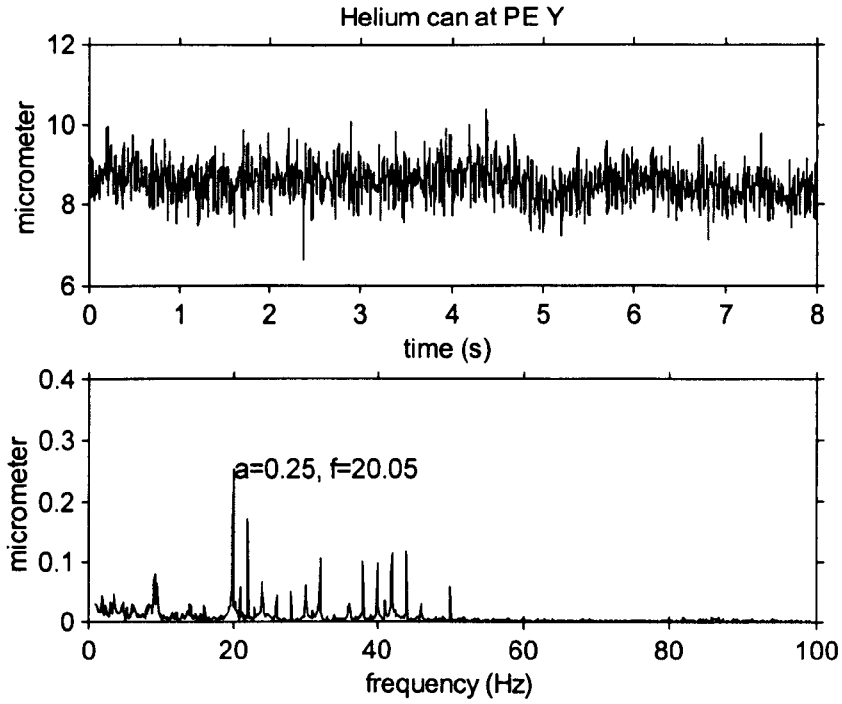

Figure 9-14 The displacement and its spectrum of the Helium can at the patient end (PE) vertical offset.

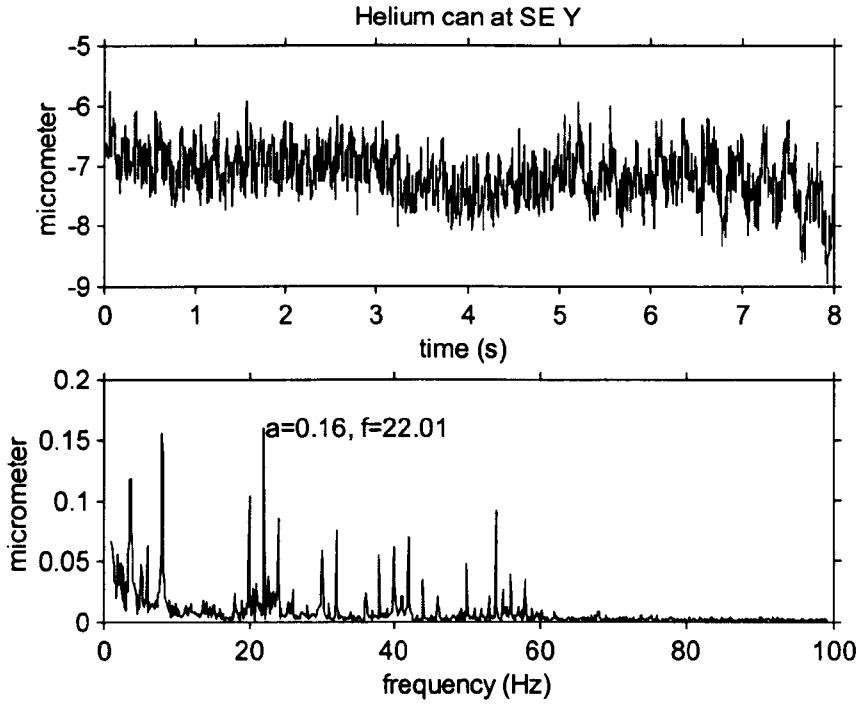

Figure 9-15 The displacement and its spectrum of the Helium can at the service end (SE) vertical offset.

9.4 Magnetic Gradient Analysis of OR70

This section calculates the magnetic gradient of cryostat Type OR70 from two different kinds of experiments in two different ways. One is based on the theory of surface harmonic and corresponding experiment as it has been presented in section 2.3.3. Another one is based on the theory and corresponding experiments, which are developed and presented by author in section 4.3 and 8.4.

9.4.1 Gradient Estimation by Legendre Extention

The following figures show the magnetic gradients of the magnets, OR70-415p01 and OR70-414p02 along their radius in x- and y-axes respectively. The coefficients of Legendre polynomial are obtained from the OMT's standard test of magnetic inhomogeneity.

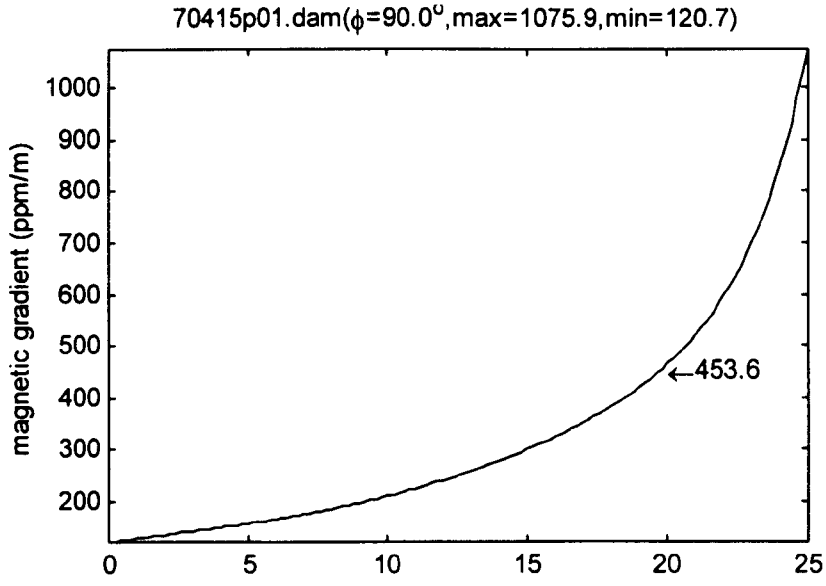

Figure 9-16 The magnetic gradient distribution of OR70-415p01 from the centre to the offset, Y+25cm.

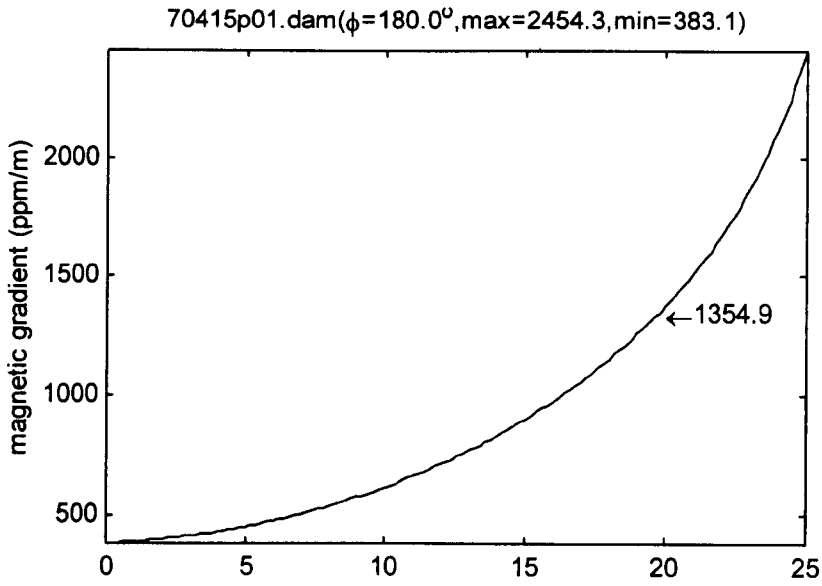

Figure 9-17 The magnetic gradient distribution of OR70-415p01 from the centre to the offset, X+25cm.

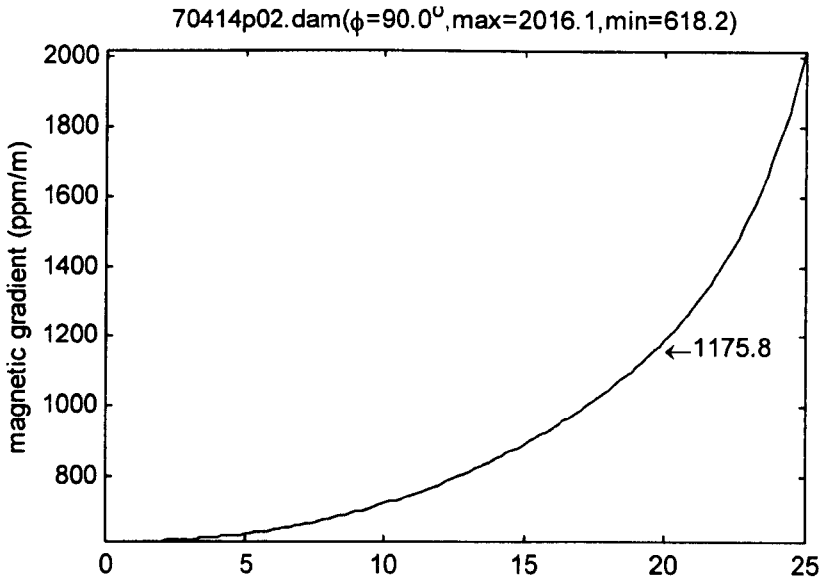

Figure 9-18 The magnetic gradient distribution of OR70-414p02 from the centre to the offset, Y+25cm.

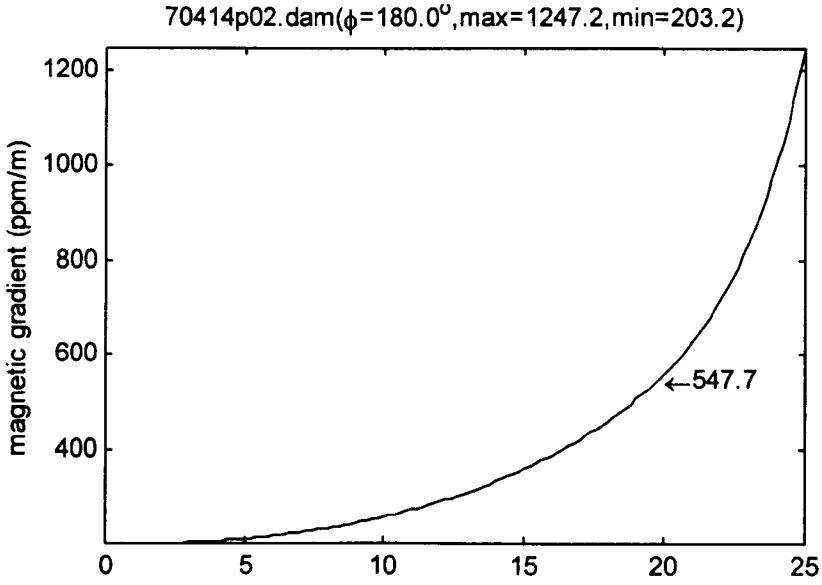

Figure 9-19 The magnetic gradient distribution of OR70-414p02 from the centre to the offset, X+25cm.

9.4.2 Gradient Calculation by Probe Vibration Experiment

The magnetic gradient of a cryostat can be measured by means of the experiment of probe vibration. Denoting **r** and Δr as the mechanical offset and vibration displacement of the probe, the magnetic gradient along the vibration direction of the probe can be calculated by the equation,

$$G(\mathbf{r}) = \frac{1}{\gamma} \cdot \frac{\Delta\Phi_{pk-pk}}{\max\limits_{n} \Delta S(n) - \min\limits_{n} \Delta S(n)}, \tag{9.1}$$

where $\Delta\Phi_{pk-pk}$ is the phase distortion measured, and $\Delta S(n)$ represents the area difference given by the equation,

$$\Delta S(n) = -\int_{nT_R}^{T_E/2+nT_R} \Delta r(t)dt + \int_{T_E/2+nT_R}^{T_E+nT_R} \Delta r(t)dt, \quad n = 0,1,2,\cdots,N. \tag{9.2}$$

Table 9-5 gives the phase distortions measured when the probe is mechanically excited by sinusoidal force. The results of magnetic gradient by equation (9.1) are presented in Table 9-6.

Table 9-5 Phase angle distortion in the probe vibration experiment

Peak-to-peak MR probe vibration (micrometer)	Phase angle measured $\Delta\Phi_{pk-pk}$ (degree)		
	Centre	Y+10cm offset	Y+20cm offset
5	3.37	4.04	7.18
10	6.75	7.53	11.33
15	8.33	10.94	16.82
20	10.51	16.02	24.47

Table 9-6 Magnetic gradient measured by the probe vibration experiment

Peak-to-peak MR probe vibration (micrometer)	Estimation of magnetic gradient $G(\mathbf{r})$ (ppm/m)		
	Centre	Y+10cm offset	Y+20cm offset
5	1607	1616	2871
10	1298	1505	2312
15	1244	1519	2402
20	1155	1586	2399
Average	1326	1557	2496

9.5 Comparison of Experiment with Simulation

9.5.1 Phase Distortion Under Sine Excitation

As the magnetic gradients were calculated from the experiment of probe vibration in section 9.2, the phase distortion due to the magnetic inhomogeneity can also be evaluated with that magnetic gradient and the displacement of the magnet. Table 9-7 shows the estimations of the phase distortions due to the magnetic inhomogeneity, and compares it with the direct measurement of phase angle distortions when the cold head is excited by same sinusoidal forces.

Table 9-7 Comparison of the tested phase angle with that caused by the magnetic inhomogeneity and sinusoidal vibration of the magnet at 8.08Hz.

Laser vibrometer test point	Helium can	
	PE X	PE Y
MR probe position	X-20cm	Y+20cm
Magnetic gradient at Y+20cm (ppm/m)	2496 (assumed the same as it is at PE Y)	2496 (it is measured and calculated from the probe vibration experiment)
Measured MR phase angle (degree)	93.4	13.7
Estimated MR phase angle due to magnetic gradient (degree)	**130.7**	**12.5**

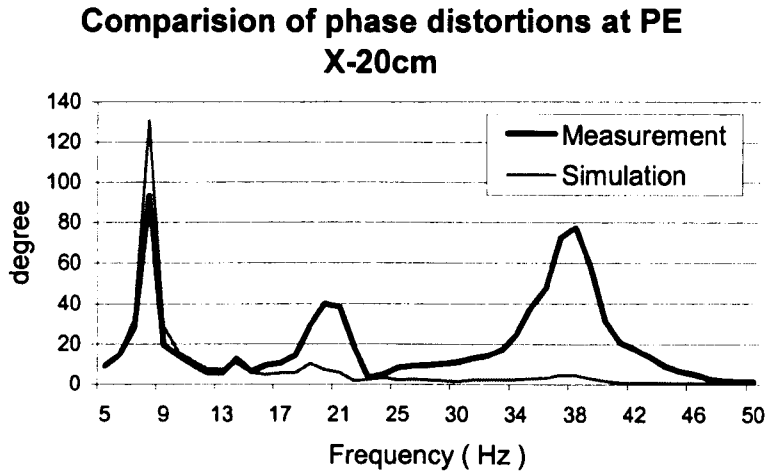

Figure 9-20 Comparison of phase distortions between the direct measurement and the simulation with the magnetic inhomogeneity.

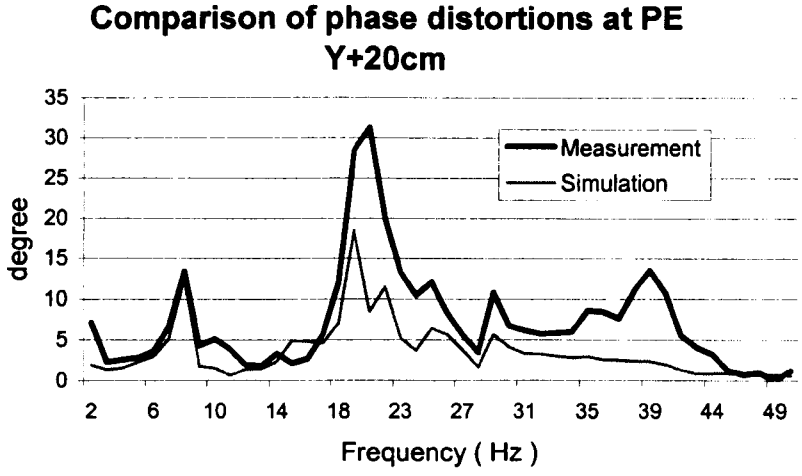

Figure 9-21 Comparison of phase distortions between the direct measurement and the simulation magnetic inhomogeneity.

In Figure 9-20, the simulated phase angles are calculated from the magnetic gradients and the lateral vibrations of the Helium can, while in Figure 9-21, the simulated phase angles are calculated from the magnetic gradients and the vertical vibrations of the Helium can. The calculations are based on equation (7.31), which is presented in section 7.3. Apart from the phase angle distortions at 8 Hz and 21Hz, a high value was also observed at 39Hz, which is found to be the resonant frequency of Cold Head.

The phase distortions due to the Helium can vibrations and the magnetic gradients are numerically estimated using computer simulations developed by the author. The comparison of the simulation results with the tested phase distortion indicated in Table 9-7, Figure 9-20 and Figure 9-21 shows that the phase angle distortions are mostly contributed by the motion of the inhomogeneous magnetic field.

9.5.2 Phase Distortion under Fridge Excitation

Similar to the phase distortion under swept sine excitation, the phase angle distortion under the fridge excitation is calculated from the estimated magnetic gradient and the peak-to-peak value of the Helium-can vibration. This phase distortion is compared with that directly tested under the same fridge excitation. The result is shown in the following table. It can be seen from the table that phase angle distortions are mainly contributed by the motion of the inhomogeneous magnetic field.

Table 9-8 Comparison of the tested phase angles with that caused by the magnetic inhomogeiteity and the vibrations of the magnet under the fridge excitation.

Laser vibrometer test point	Helium can	
	PE x-axis	PE y-axis
MR probe position	X-20cm	Y+20cm
Measured MR phase angle with fridge on, $\Delta\phi_{on}$ (degree)	7.8	3.0
Measured MR phase angle with fridge off $\Delta\phi_{off}$ (degree)	2.4	2.4
Measured pure phase angle $\Delta\phi = \sqrt{\Delta\phi_{on}^2 - \Delta\phi_{off}^2}$ (degree)	7.4	1.8
Magnetic gradient at Y+20cm (ppm/m)	2496.0	2496.0
Estimated Phase angle due to magnetic gradient (degree)	**5.5**	**1.6**

10 Summary and Further Work

10.1 Overall Conclusions

This thesis has studied the distortion problems of MRI super-conductive magnets. Such MRI magnets generally consist of a Helium-can containing super-conductive coils, one or two thermal anti-radiation shields and an outer vacuum chamber with a cooling pump on it. The distortion problems include the MR phase angle distortions, the magnetic field disturbances, the structural vibrations and their interactions. The research is to find the mechanism and a mathematical model which disclose how the magnetic field and MR phase angles are disturbed from the structural vibrations, such that: the problems are clear; the main sources of the phase distortions are located; the phase distortion is predictable; the scheme of improvement is feasible; the phase angle distortion is minimized; and the total development cost is reduced.

The investigation covers theoretical analysis, computational simulation and experiments. An overall system analysis has been deployed on a typical cryostat. From this systematic approach three different magnetic disturbances have been found to be the sources which impact the MR phase angles, i.e. the directional change of magnetic field, the eddy-current and the motion of inhomogeneous magnetic field. Among the vibratory modals of a cryostat, three of them have been regarded as the corresponding sources of the magnetic disturbances, i.e. the rotational vibration of the Helium-can, relative rotational vibration between the Helium-can and the shields, lateral motion of the Helium-can. Mathematical models have been created for the structural vibrations, magnetic disturbances, phase angle distortions and their relationships. It has been found out from the theoretical analysis and the computer simulations that rotational vibration of magnetic field almost does not affect the MR phase angles at all. The considerable

changes of phase angle distortions measured across the image volume have shown that the directional change of magnetic field cannot be the main contributor of the phase angle distortions. The eddy-current is not the main source of the MR phase angle distortions shown from the characteristics of the eddy-current distribution. The experiment of the probe vibration has been created to eliminate any eddy currents in the cryostat while the phase angle is being experimentally obtained. With this experiment there have still been considerable phase angle distortions discovered which obviously are not due to any eddy-currents in the cryostat. These phase distortions have been shown to be the main contributor to the phase distortions. Significant magnetic gradients have been introduced and they have been the main source of phase angle distortion. The corresponding properties of structural vibrations and MR phase distortions are summarized from the experiments and listed as follows:

1. A large local magnetic gradient has been observed in OR70#28 from the probe vibration experiments and the OMT's standard measurements of the magnetic inhomogeneity.
2. 8Hz whole body lateral vibration of OR70#28 has been the strongest response of displacement to the force of the cold head.
3. The displacement responses of OR70#28 have tested sensitive to the frequencies of 19-22Hz and 39Hz, but the susceptibilities are much less than that at 8Hz.
4. 8Hz whole body lateral vibration of OR70#28 has been found being the most significant vibration in OR70#28.
5. The phase distortions measured have been particularly susceptible to the mechanical vibrations at 8Hz, 19~22Hz, 39Hz and 59Hz.
6. Most of the phase distortions at horizontal offset X-20cm have been discovered to be caused by the magnetic inhomogeneity and 8Hz vibration of OR70#28 when excited by the fridge.
7. The phase distortions at vertical offset Y+20cm, are mainly contributed by the 19~22Hz vertical vibrations when excited by the fridge, but much less than that at

horizontal offset. The magnetic inhomogeneity is the main source of the phase distortions.

8. Other sources except for the magnetic inhomogeneity have been found affecting the phase distortions particularly at frequencies higher than 35Hz according to the swept sine experiment.

It is concluded that magnetic inhomogeneity is a significant factor of MR phase distortion, while eddy current has limited influence

10.2 Summary of Main Contributions

These contributions made to the theory and experiments of the research subject all original advances over existing work and have resulted in simulation software for disturbance problems of commercial MRI super-conductive magnets together with application to design and optimization of products for Oxford Magnet Technology and a number of internal reports and presentations.

1. Provided an overall review of relating subjects and existing work for current and future research on disturbance problems of a MRI cryostat.
2. Developed a systematic method to find problem domains relating to the phase angle distortions. Provided a hierarchical structure subjected to the problems.
3. Developed mathematical models of structural vibrations, magnetic disturbances, phase angle distortions and their relationships to provide the fundamentals for deriving structural vibration modals from experiment data, for deriving evaluations of magnetic disturbances and for deriving quantitative estimation of phase angle distortions due to the structural vibrations.
4. Developed theory and algorithms for novel measurements of phase angle distortion and magnetic disturbance. Deployed novel measurement schemes for experiments with NMR spectrometer and search-coil sensor based on the theory and algorithm.

5. Created a novel experimental scheme to eliminate eddy-current effects when measuring phase angle distortion due to the magnetic inhomogeneity.
6. Developed and implemented software for modal analysis, calculation of magnetic field distribution, simulation of spin precession and optimization of measurements.
7. Concluded that magnetic inhomogeneity is a significant factor of phase angle distortion, while eddy current has limited influence.

10.3 Recommendation for Structural Modification

To reduce the phase angle distortions the following structural modification of a cryostat are recommended:

Improve the cooling pump to reduce its vibration.

To reduce the vibration of the cooling pump is always in the first consideration as it has been found to be the main source of the vibrations causing the phase angle distortions. Developing a new type of cryo-pump with a low vibration has been an ongoing approach and has already achieved significantly. Ideally eliminating the main source of vibration reduces most of the distortions without modifying any other parts of a cryostat. To develop a new pump is technically challenging, therefore it is unlikely to be achieved in the near future. Alternatively much effort has been put to isolate the vibration transmitted from the cooling pump by rectifying the natural frequency of the cold-head. Theoretically the transmissibility can be as small as possible as long as the natural frequency is much less than all frequencies of the disturbing forces. That means for a given mass of the cold-head the stiffness should be very small so that the system be very flexible. Two problems will be encountered with this approach. The first problem is that the cold-head cannot be mounted onto the OVC with a very soft suspension. The second problem is that a pulse force is generally applied for the operation of a cryo-pump and it generates force with wide range of frequencies. As

shown from numerous experiments, the phase angle is mainly caused by low frequency. Therefore this kind of vibratory isolation has very limited effectiveness in this particular application. An active isolator could be an option whilst its complexity and high cost must be considered carefully.

Constrain lateral vibration by changing the positions of suspension rods.

Experiments have shown that the 8Hz lateral vibration of the Helium-can is the dominant source of the phase angle distortions. It is because of the positions and shapes of the suspension rods which fix the Helium-can inside the OVC. The suspension rods are designed very thin and long to reduce any thermal transmission along them, and their connections on the OVC are very close to the vertical central line of the cryostat. This architecture of the suspensions causes more freedom of motion relative to the OVC on horizontal direction than on vertical direction. Any unbalanced forces between upper two rods or between lower two rods (a net lateral force) from the OVC will produce a considerable a lateral motion of the Helium-can. A modified suspension architecture, for instance putting the four rods along two 45 degree cross lines, should give a better performance on constraining the lateral vibration whilst a trade-off must be taken between the structural stability and the thermal transmission due to shortening the length of each rod.

Lower the mass centre of a cryostat and/or increase the distance between the two base suspension beams to increase the stability of the cryostat

A net lateral motion of the OVC is obviously the source of lateral vibration of the Helium-can. From the principle of structural vibration, the higher the OVC is from its base, the less the stiffness it has laterally. Both a low mass centre and a wide base suspension beams will improve the lump stiffness of the cryostat as illustrated in Figure

10-1. This change of the suspension beams will use more suspension material but the overall cost should not increase much.

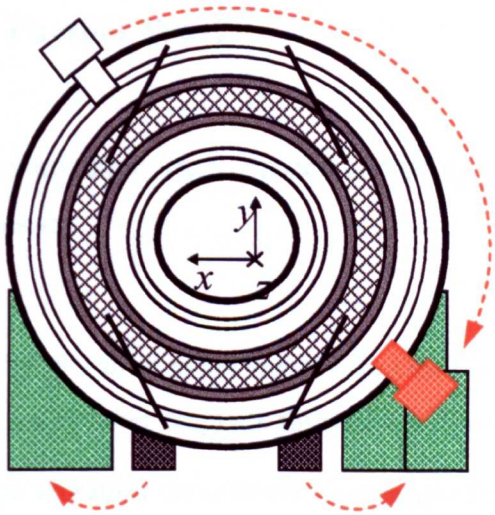

Figure 10-1 Modification of position of the cold-head and base suspension beams.

Move the Cold Head down to the bottom from the current position at the top and fix it to the ground together with the base suspension beams. At the same time reduce the rigidity of connection between the Cold Head and the OVC

Moving the cold-head down and fixing it to the ground increases the mass of the vibration source while the stiffness of the vibration transmission decreases with reduced rigidity of the connection between the cold-head and the OVC. These changes of both mass and stiffness will reduce the transmissibility of vibration significantly, hence will solve the limitation of the stiffness mentioned previously where only the change of the stiffness was considered. Other benefit from this modification is to maintain the cold-

head more conveniently, since there will be not any need to climb a ladder to repair the cold-head.

10.4 Suggestion for Further Work

The following further investigation are suggested according to the research, which has been presented in this thesis:

1. Compare the probe vibration experiment with OMT's standard measurement of magnetic field in many other magnets shimmed and not shimmed.
2. Improve the probe vibration experiment to measure the magnetic gradient more precisely.
3. Improve the magnetic field homogeteity along the horizontal direction in which the Helium-can has been found vibrating most significantly.
4. Develop an experiment to measure the spectrum of magnetic disturbances with MR spectrometer more reliably and precisely by optimising the echo time, repetition time and data acquisition period as it has been described in Section 7.2.
5. More investigation of structural vibration and phase distortion at frequencies of 38~40Hz and 59Hz to find and evaluate the existing sources of the phase distortions except for the magnetic inhomogeneity.

Appendices

Appedix A Approximation of Magnetic Disturbance

A.1 Magnetic Modular Change due to a Small Vertical field

Suppose a static magnetic field $\mathbf{B}_0$ is affected by a very small perpendicular magnetic field $\mathbf{B}_{Ix}$, as shown in Fig A.1.

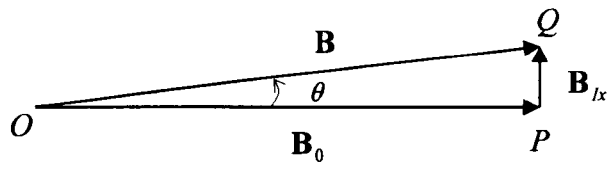

Figure A-1 Perpendicular magnetic disturbance.

The magnetic field **B** fluctuates from its equilibrium $\mathbf{B}_0$ both in magnitude and direction, can be given respectively by

$$B = \sqrt{B_0^2 + B_{Ix}^2} \tag{A.1}$$

and

$$\theta = \tan^{-1}\left(\frac{B_{Ix}}{B_0}\right). \tag{A.2}$$

Because $B_{Ix} << B_0$, equation (A.1) and (A.2) can be approximated as

$$B = B_0 + \frac{B_{Ix}^2}{2B_0} \tag{A.3}$$

and

$$\theta = \frac{B_{Ix}}{B_0}. \tag{A.4}$$

From the above two equations, a scalar increment of the magnetic field can be described as

$$\Delta B = B - B_0 = \frac{1}{2} B_0 \theta^2. \tag{A.5}$$

Let $\theta(t) = \theta_0 \sin(\Omega t)$, in which Ω represents the frequency of the structural vibration. Then Equation (A.5) becomes

$$\Delta B = \frac{1}{2} B_0 \theta_0^2 \sin^2(\Omega t) \tag{A.6}$$

or

$$\Delta B = \frac{1}{4} B_0 \theta_0^2 - \frac{1}{4} B_0 \theta_0^2 \cos(2\Omega t). \tag{A.7}$$

Omitted the static term on right-hand-side, Equation (A.7) is converted into

$$\Delta B = -\frac{1}{4} B_0 \theta_0^2 \cos(2\Omega t). \tag{A.8}$$

A.2 Disturbances of magnetic components due to the magnetic field rotation

Suppose that a static magnetic field $\mathbf{B}_0$ vibrates rotationally in sinusoidal wave, as shown in Figure A.2, where the rotation angle θ is assumed very small, for instance, $\theta \leq 1.5 \times 10^{-5}$ (rad).

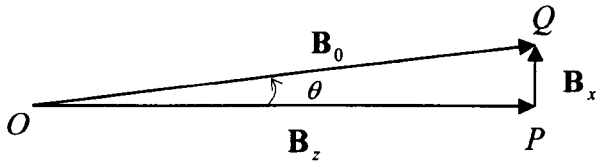

Figure A.2 Magnetic Variation of horizontal component.

Then the horizontal component is described as

$$B_z = B_0 \cos\theta, \tag{A.9}$$

and the scalar change of the z-axis component can be described as

$$\Delta B_z = B_0 - B_0 \cos\theta \tag{A.10}$$

Since the rotation angle, θ, is very small, Equation (A.10) can be approximated into

$$\Delta B_z = \frac{1}{2} B_0 \theta^2. \tag{A.11}$$

Equation (A.11) is the same formulation as Equation (A.5). Let $\theta(t) = \theta_0 \sin(\Omega t)$, and manipulate as previous section, then the same results are obtained,

$$\Delta B_z = \frac{1}{4} B_0 \theta_0^2 - \frac{1}{4} B_0 \theta_0^2 \cos(2\Omega t). \quad \text{(A.12)}$$

Omitting the static term on right-hand-side, Equation (A.12) is converted into

$$\Delta B_z = -\frac{1}{4} B_0 \theta_0^2 \cos(2\Omega t). \quad \text{(A.13)}$$

Appedix B Formulas for Eddy Current Calculation

Structural vibration is described in equation

$$\theta(t) = \theta_0 \sin(\Omega t), \qquad \text{(B.1)}$$

assuming that the cryogenic magnet rotates about the y-axis relative to a shield at angular of $\theta(t)$. That is illustrated in Fig B.1, in which $Ox'y'z'$ and $Oxyz$ are references of the magnet and shield respectively.

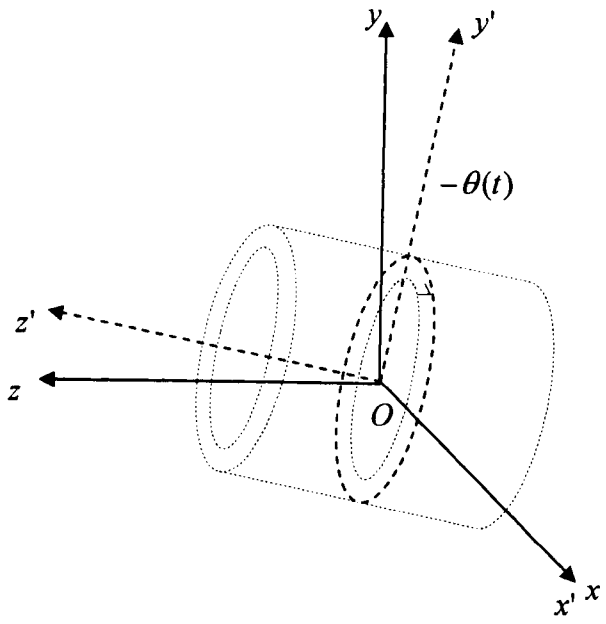

Fig B.1 Vibration of magnet relative to shield.

The relationship of coordinates between these two references are given by

$$y = y'\cos\theta - z'\sin\theta\,, \tag{B.2a}$$

and

$$z = y'\sin\theta + z'\cos\theta\,. \tag{B.2b}$$

The eddy currents and magnetic field obey the Maxwell's equations,

$$\nabla \times \mathbf{J} = -\frac{\partial \mathbf{B}}{\partial t}\,, \tag{B.3a}$$

$$\nabla \times \mathbf{B} = \mu_0 \mathbf{J}\,, \tag{B.3b}$$

$$\nabla \times \mathbf{B} = 0\,, \tag{B.3c}$$

$$\nabla \times \mathbf{J} = 0\,, \tag{B.3d}$$

$$\mathbf{B} = \mathbf{B}_{ex} + \mathbf{B}_r\,. \tag{B.3e}$$

The notations are given as

$\mathbf{J}$	Vector of the current density,
$\mathbf{B}$	Total magnetic flux density,
$\mathbf{B}_r$	Reaction magnetic flux density,
$\mathbf{B}_{ex}$	Excitation magnetic flux density,
$\mathbf{B}_0$	Static magnetic flux density,
S	Surface of the shield,
$\delta = \frac{1}{\sqrt{\pi f \mu \sigma}}$	Skin depth.

The field of the magnet is described in Cartesian and cylindrical coordinates of the body reference of the magnet as

$$\mathbf{B}_0 = B_{0r'}\mathbf{a}_{r'} + B_{0\phi'}\mathbf{a}_{\phi'} + B_{0z'}\mathbf{a}_{z'} = B_{0x'}\mathbf{a}_{x'} + B_{0y'}\mathbf{a}_{y'} + B_{0z'}\mathbf{a}_{z'}. \quad \text{(B.4)}$$

When the magnet vibrates relative to a shield in Equation (B.1), as shown in Fig B.1, the magnetic flux density of it is given by

$$\mathbf{B}_{ex} = B_{0x'}\mathbf{a}_x + \left(B_{0y'}\cos\theta(t) - B_{0z'}\sin\theta(t)\right)\mathbf{a}_y + \left(B_{0y'}\sin\theta(t) + B_{0z'}\cos\theta(t)\right)\mathbf{a}_z, \quad \text{(B.5)}$$

in reference of the shield and the reaction magnetic field produced by eddy currents is

$$\mathbf{B}_r(r,z,\phi) = \frac{\mu_0}{2\pi}\oint_S \frac{\mathbf{J}\times\mathbf{R}}{R^3}ds, \quad \text{(B.6)}$$

in which

$$\mathbf{R} = (x_s - x)\mathbf{a}_{x'} + (y_s - y)\mathbf{a}_{y'} + (z_s - z)\mathbf{a}_{z'}, \text{ and } (x_s, y_s, z_s) \subset S. \quad \text{(B.7)}$$

Skin depths of 20K and 80K shields are 5.16 (mm) and 3.43 (mm) at frequency of 20Hz respectively.

A numerical method of 2-D eddy current must be developed to calculate the eddy current $\mathbf{J}$ and reaction magnetic field $\mathbf{B}_r$.

Appedix C Phase Variation across Imaging Volume

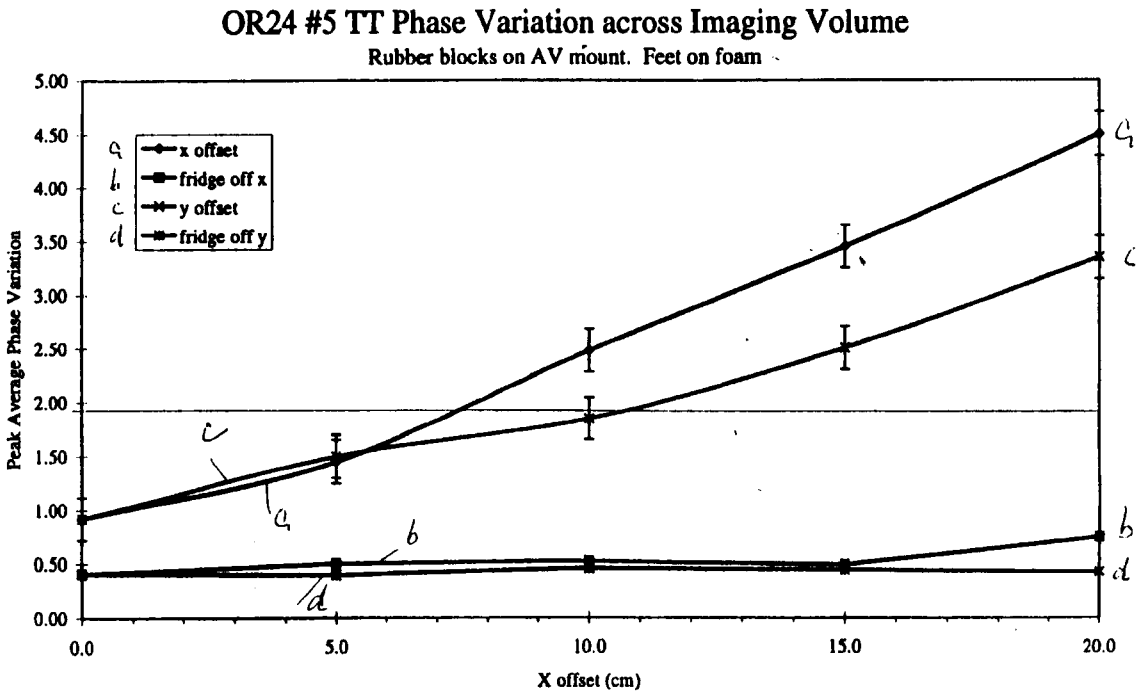

Figure C-1 Phase variation of OR24 #5

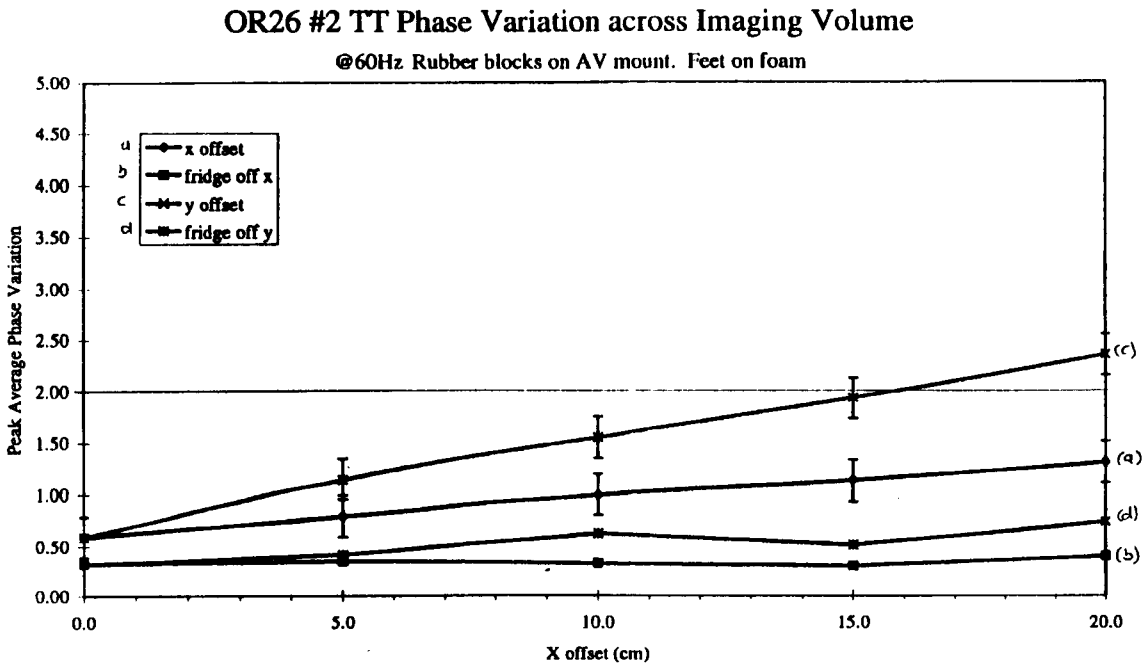

Figure C-2 Phase variation of OR26 #2

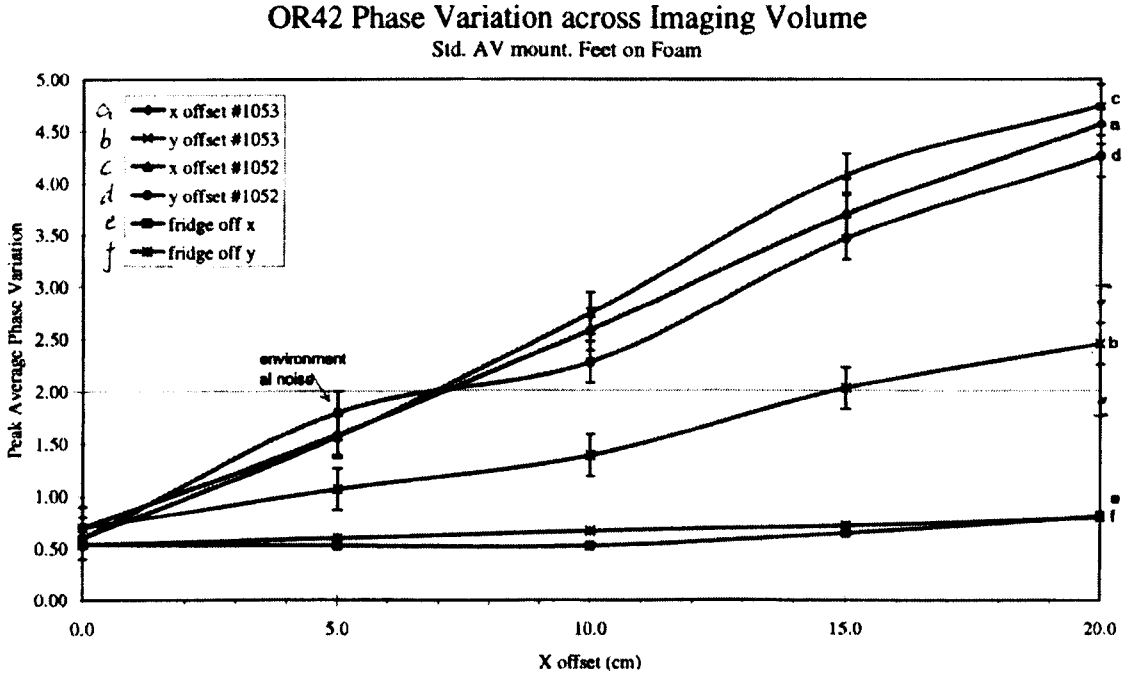

Figure C-3 Phase variation of OR42 #1053 and #1052

Appedix D Associated Legendre Polynomials

Associated Legendre Polynomials $P_n^m(\mu)$ (n=0,1,2,...; m=0,1,2,...n) are defined by the functions,

$$P_n^m(\mu)=(1-\mu)^{\frac{m}{2}}\frac{d^m}{d\mu^m}P_n(\mu), \tag{D.1}$$

where $P_n(\mu)$ (n=0,1,2,...) is known as the Legendre polynomials written in the form,

$$P_n(\mu)=\sum_{s=0}^{m}(-1)^s\frac{(2n-2s)!}{2^n(s)!(n-s)!(n-2s)!}\mu^{n-2s}. \tag{D.2}$$

In Equation (D.2) $m=\frac{1}{2}n$ or $m=\frac{1}{2}(n-1)$, whichever is an integer, and $\mu=\cos\theta$. The values of n<9 are

$$P_0(\mu)=1,$$

$$P_1(\mu)=\mu,$$

$$P_2(\mu)=\tfrac{1}{2}(2\mu^2-1),$$

$$P_3(\mu)=\tfrac{1}{2}(5\mu^3-3\mu),$$

$$P_4(\mu)=\frac{(35\mu^4-30\mu+3)}{8},$$

$$P_5(\mu)=\frac{(63\mu^5-70\mu^3+15\mu)}{8},$$

$$P_6(\mu)=\frac{(231\mu^6-315\mu^4+105\mu^2-15)}{16},$$

$$P_7(\mu)=\frac{(429\mu^7-639\mu^5+315\mu^3-35\mu)}{16},$$

$$P_8(\mu)=\frac{(6435\mu^8-12012\mu^6+6930\mu^4-1260\mu^2)}{128}.$$

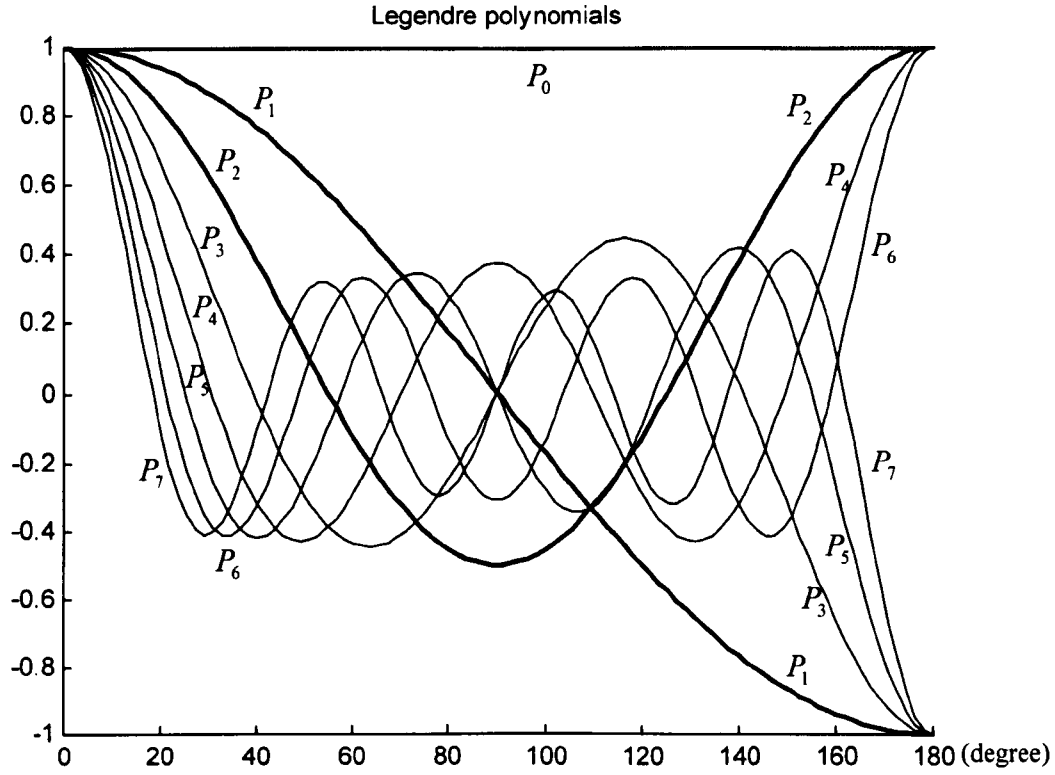

Figure D-1 Legendre polynomials $P_n(\cos\theta)$, n=0,1,2,3,4,5,6,7.

Table D-1 Constants A_n^m and B_n^m for magnetic field calculation. LMS00001.dam

Axial term	As Plotted	Axial term	As Plotted	Z-X terms	As Plotted	X-Y terms	As Plotted
A(1,0)	23.5396	A(10,0)	-2.17214	A(1,1)	-98.9041	B(1,1)	12.9357
A(2,0)	238.684	A(11,0)	-6.97595	A(2,1)	49.2595	B(2,1)	-22.5135
A(3,0)	-49.997	A(12,0)	-25.2837	A(3,1)	45.8849	B(3,1)	23.5955
A(4,0)	-72.2843	A(13,0)	3.75004	A(4,1)	-10.6086	B(4,1)	12.0925
A(5,0)	16.7363	A(14,0)	14.2541	A(5,1)	-9.83153	B(5,1)	-6.87892
A(6,0)	-9.04555	A(15,0)	-1.09102	A(6,1)	-0.366306	B(6,1)	-3.50773
A(7,0)	-4.86792	A(16,0)	-4.05541				
A(8,0)	4.1884	A(17,0)	-0.0103378				
A(9,0)	1.55407	A(18,0)	0.793295				

Peak to Peak=533.326 ppm.

Appedix E Cross Section of Cryostat

E.1 Cryostat and Magnetic Field

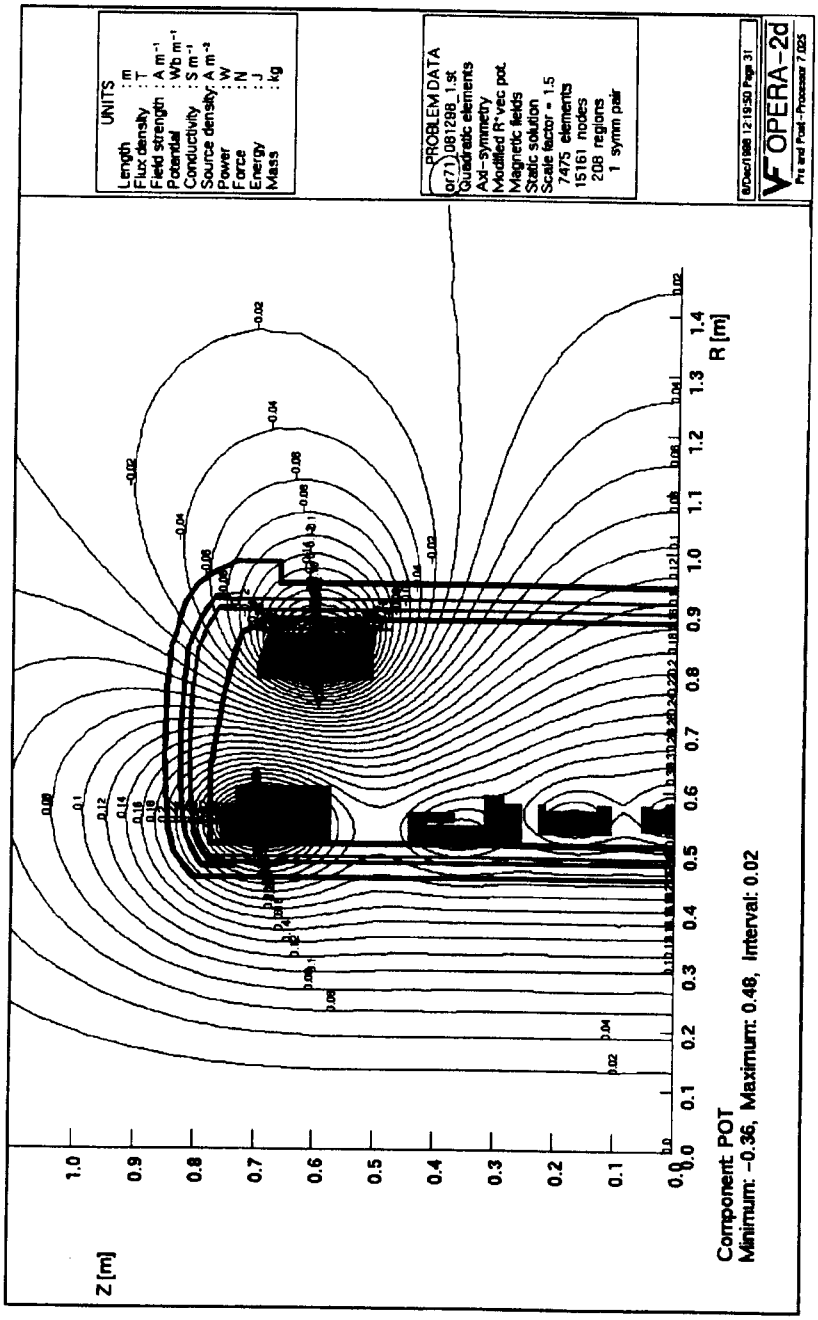

E.2 Diagram of Cold Head

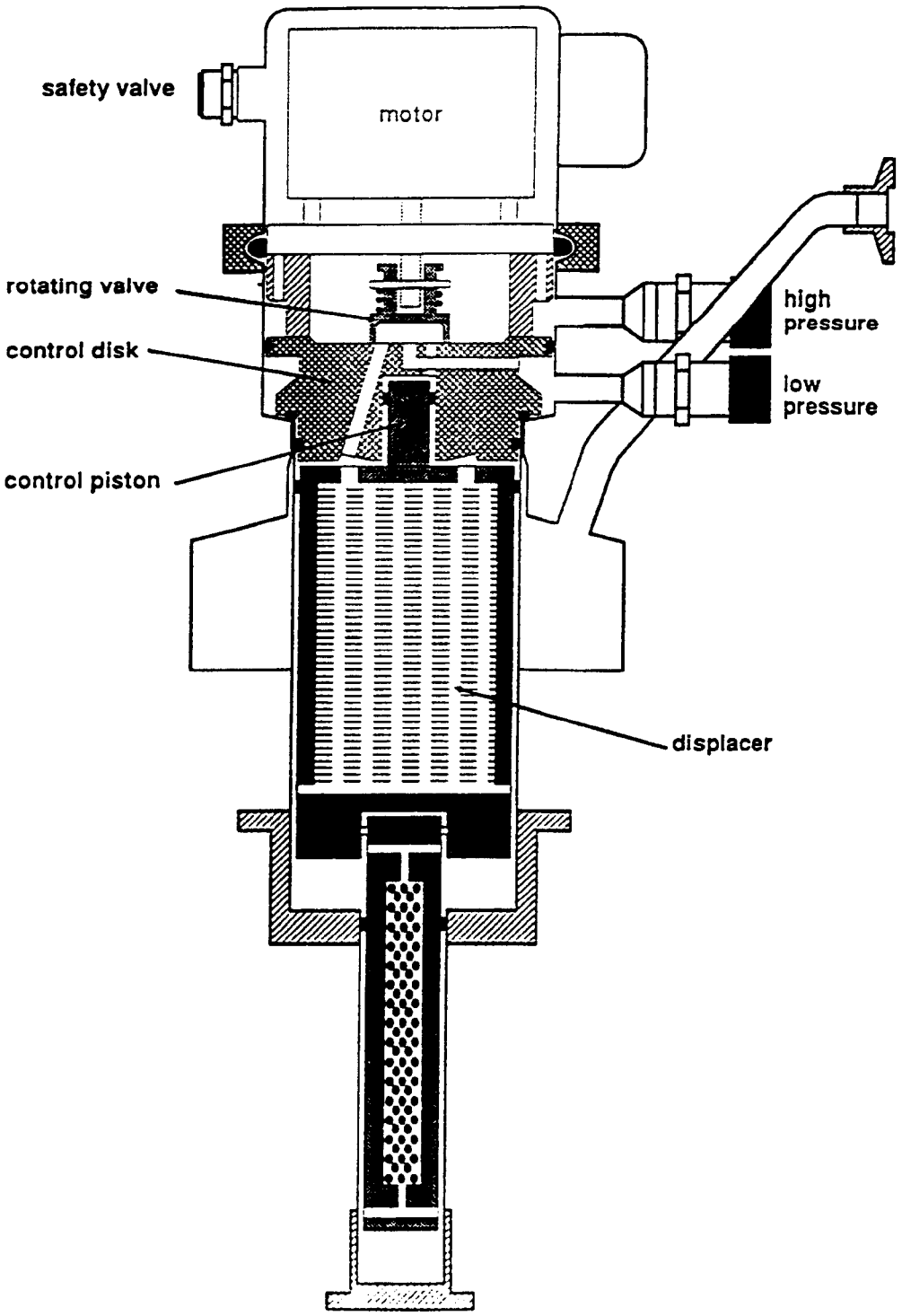

E.3 Section through 'Unisock' Cold Head Turret

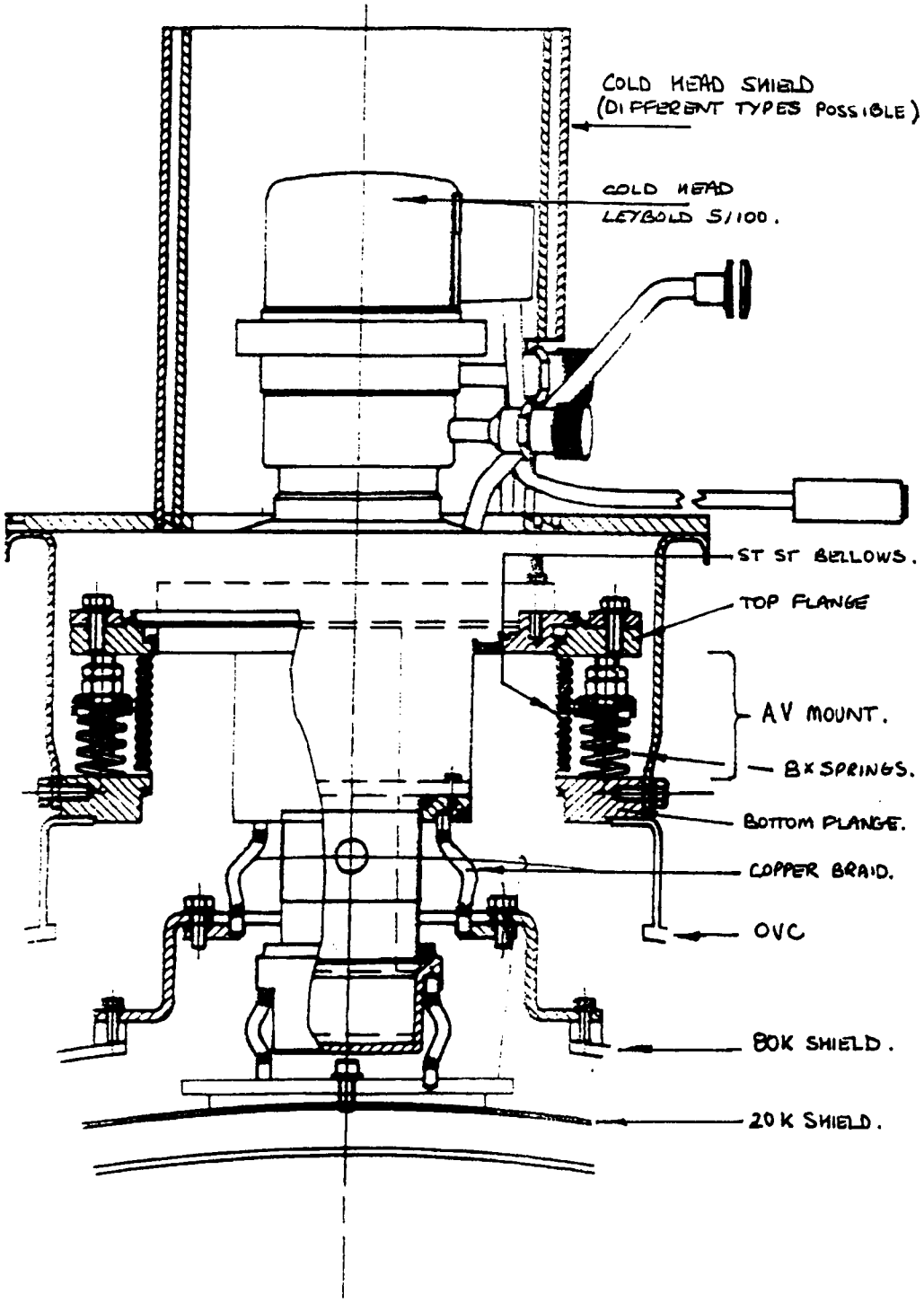

E.4 Section through Integrated Turret

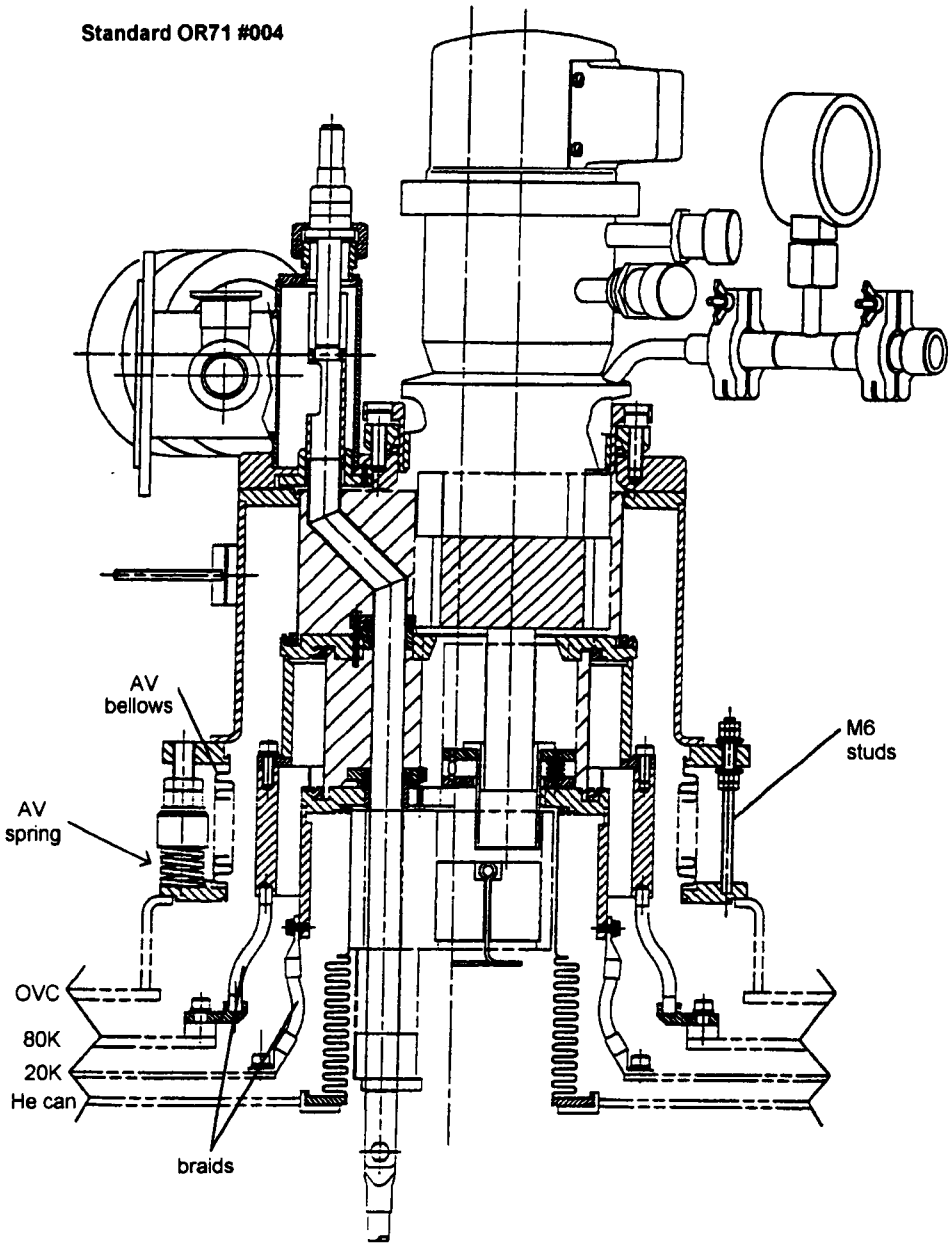

Appedix F Measurements with Search Coil Sensor and Accelerometer

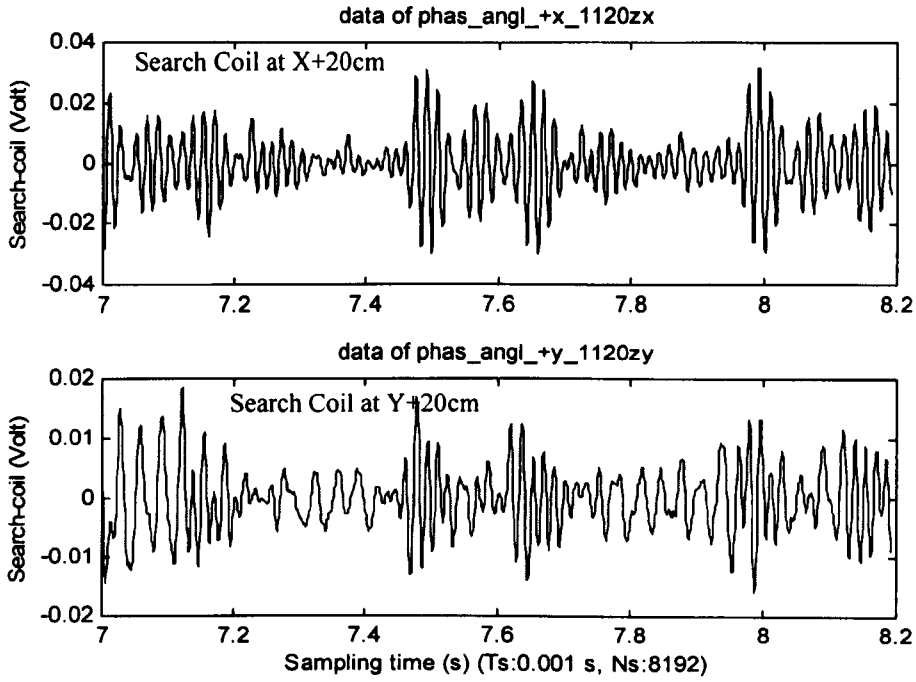

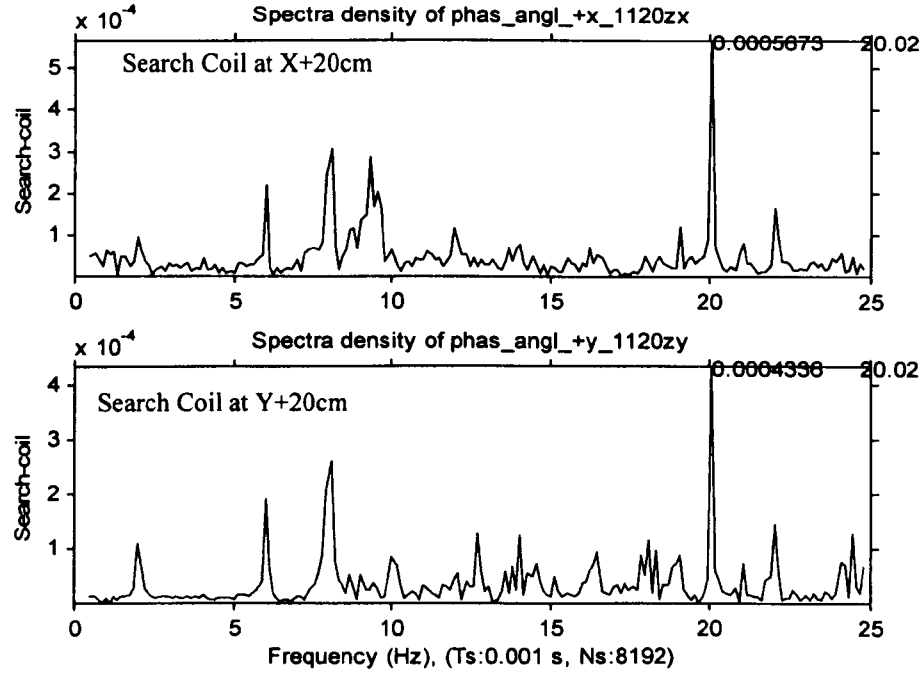

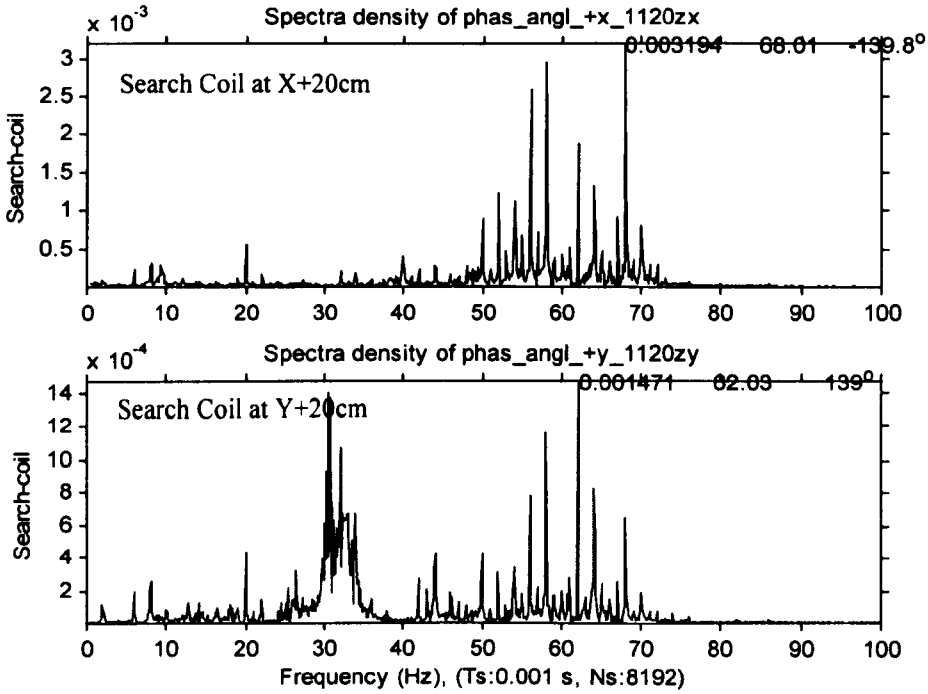

Figure F-1 Measurements of magnetic disturbances with search-coil sensor along z-axis.

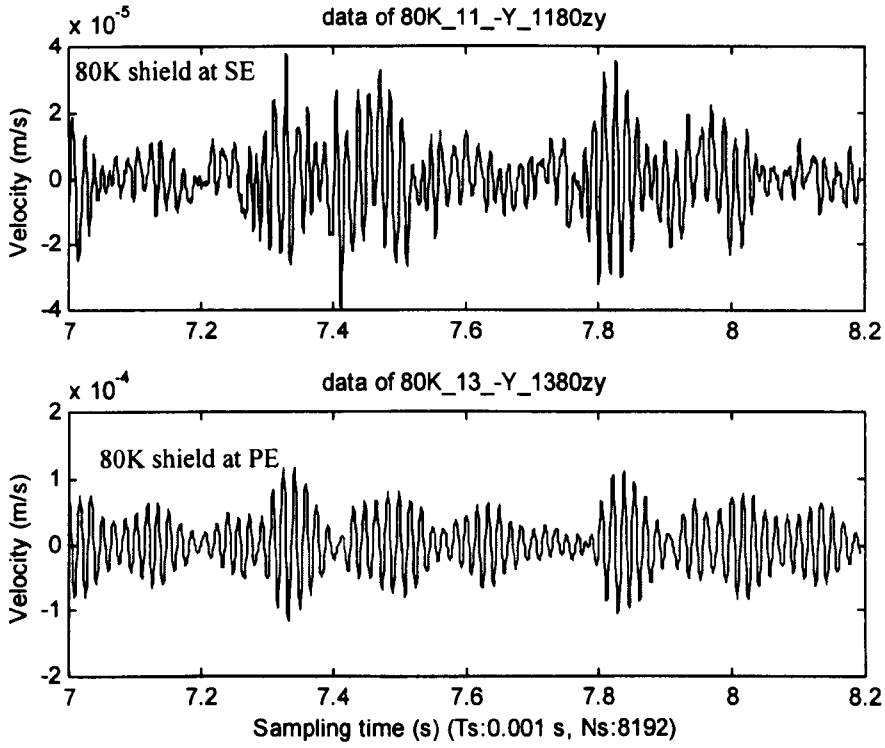

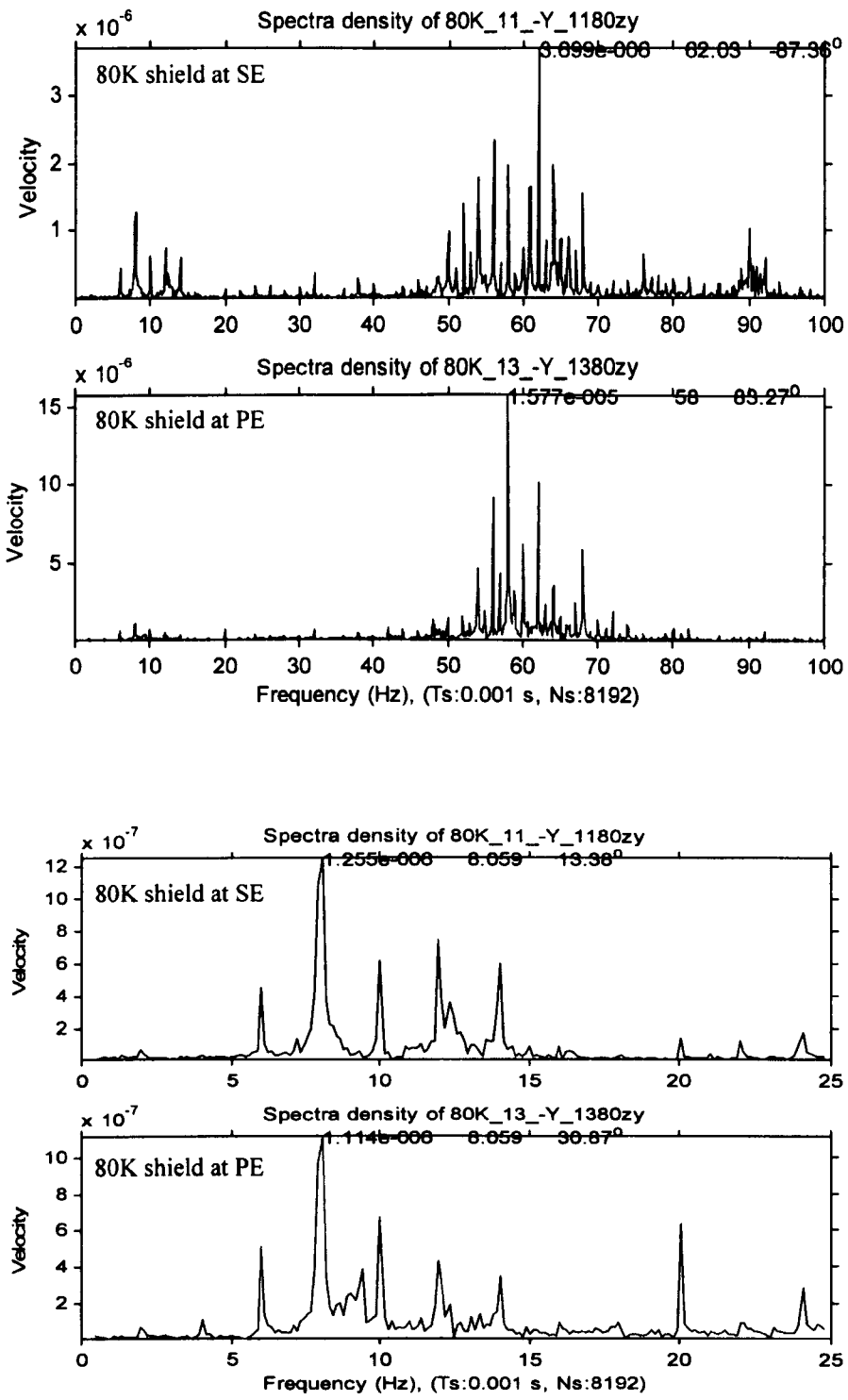

Figure F-2 Measurements of 80K shield vibrations with accelerometers.

Appedix G Phase Distortions under Swept Sine Excitation

Following figures illustrate original phase angle distortions measured with a NMR spectrometer.

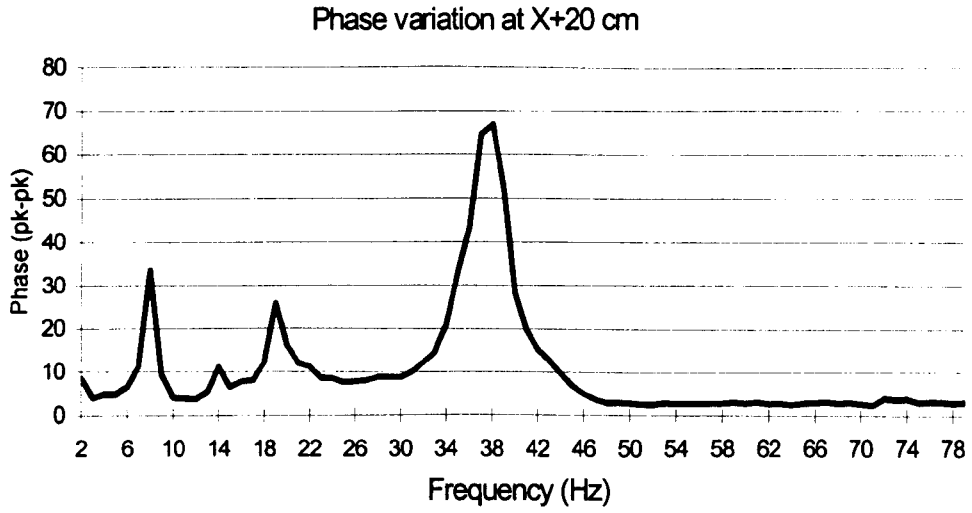

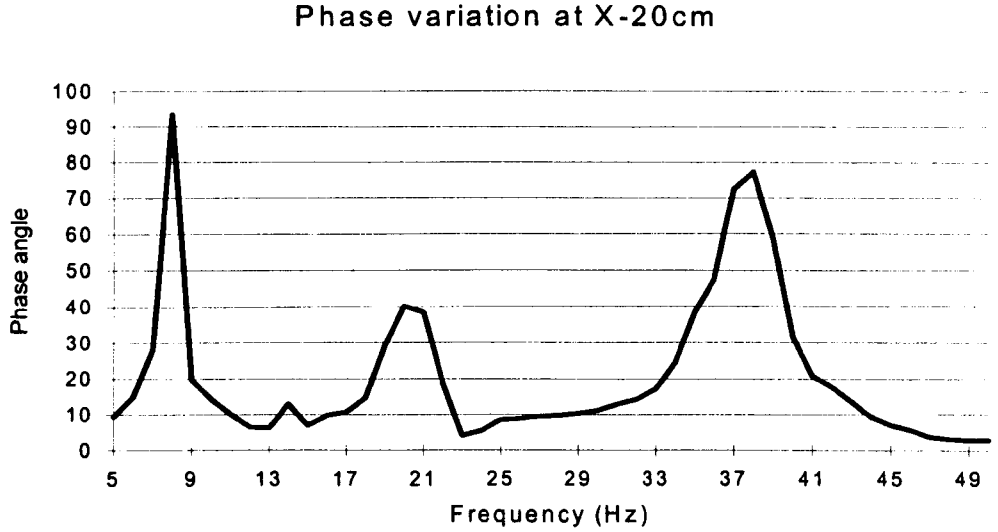

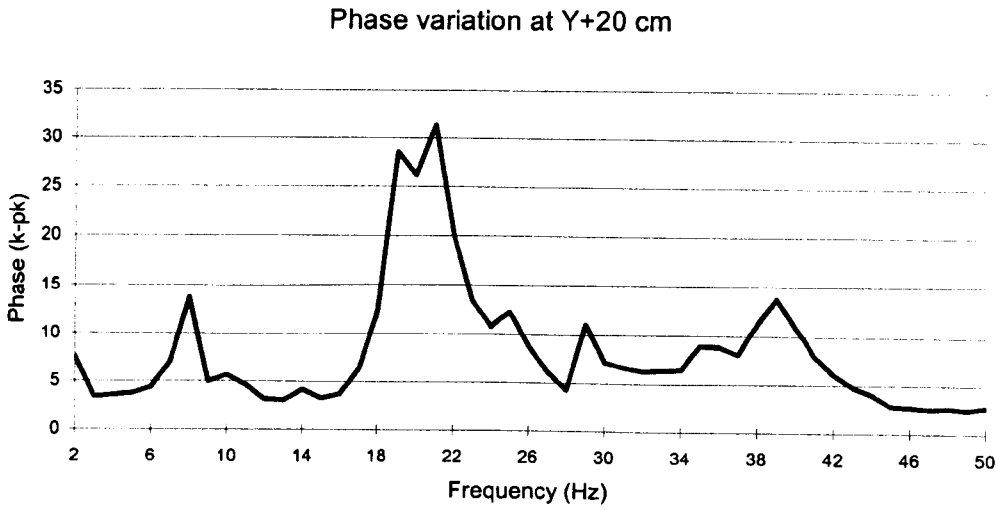
Phase variation at Y+20 cm
Phase (k-pk)
35
30
25
20
15
10
5
0
2
6
10
14
18
22
26
30
34
38
42
46
50
Frequency (Hz)

Appedix H Program Source Codes

H.1 Introduction

A huge amount of data has been obtained from experiments. Data sources include those from the experiments of the investigator, LMS' measurements and OMT's tests. Those measurements cover structural vibrations (with DASYLab and LMS's data acquisition system), MR phase angles (with IAG's spectrometer) and magnetic field maps (data converted from METROLAB's data into data of surface harmonic coefficients with software package named Kufu). LMS has their own data format and it is not open to their clients. But part of the data has been converted into MATLAB data format by LMS. DASYLab has three different data formats, which can be converted into one of the formats, ASCII file. METROLAB gives ASCII data files directly. More than 6000 lines of MATLAB program have been designed for data format transformations, for data reconstruction from multi data files and for data analyses.

H.2 Software for Data transformation

ASCII formats of DASYLab and IAG spectrometer are respectively shown in Table H-1 and 9-3. Most of the experimental data are of structural vibrations and phase angles, and most of analyses are carried out on those data. To reduce time of programming and calculations, MATLAB programs of data transformations were built up before designing a large amount of software for analyses. The transformations are available by executing MATLAB software Dasy2Matlab.m and IAG2Matlab.m respectively, assigning the source file path to variable SourcePath, the destination file path to variable DestinationPath and source file names to variable SearchFiles, as shown in Table H-2

and 9-4. In Table H-1 the data delimiter either can be a space, comma or semicolon, which the program identifies automatically.

Table H-1 Data file format of DASYLab

```
DASYLab - V 4.01.11
WORKSHEET          : HXR01
Recording Date     : 30/05/99, 07:41:47
Block Length       : 4096
Delta              : 0.002000 sec.
Number of Channels : 05
Time;Write 0;Write 1;Write 2;Write 3;Write 4;
0.000;1.3339;-2.5076;0.4929;-10.0000;-0.0073;
0.002;1.3339;-2.5098;0.4895;-10.0000;-0.0073;
0.004;1.3333;-2.5116;0.4239;-10.0000;-0.0073;
0.006;1.3339;-2.5143;0.3903;-10.0000;-0.0058;
0.008;1.3324;-2.5174;0.4120;-10.0000;-0.0061;
.
.
.
8.186;1.3217;-2.5290;0.3983;-10.0000;-0.0046;
8.188;1.3211;-2.5278;0.4102;-10.0000;-0.0024;
8.190;1.3214;-2.5259;0.4071;-10.0000;-0.0043;
```

Table H-2 A header of MATLAB Program for data transformation from DASYLab's to MATLAB's

```
%%%%%%%%%%%%%%%% DASY2M.M %%%%%%%%%%%%%%
% Convert the ASCII format of DASYLab  %
% into matlab format                   %
%%%%%%%%%%%%%%%%%%%%%%%%%%%%%%%%%%%%%%%
close all;clearl;clc
%%%%%%%%%%%%%%%%%%%%%%%%%%%%%%%%
SourcePath='..\data\NMR\DS\';
DestinationPath='..\data\NMR\DS\';
SearchFiles='ds*h.asc';
.
.
.
```

Table H-3 File format of IAG spectrometer

```
Block 1, 256 points, BLOCK1
Point,          Real
1,              1033
2,              -1781
3,              2530
.
.
.
255,            4544
256,            -4601

Block 2, 256 points, BLOCK1
Point,          Real
1,              -3551
2,              2842
3,              -1741
.
.
.
255,            2749
256,            -3360


Method,             Frequency Sweep (alter params.txt
file)
File name,          C:\QT\METHODS\FREQSWEP.MET
User,               Tim Hunt
Last saved,         30/05/1999 06:59:04
Analysis start,     30/05/1999 07:34:25
Analysis end,       30/05/1999 07:36:05
Start delay (s),    0.00
Time reference,     Point number
NMR Freq (MHz),     63.743985
Pulse 90 (uS),      26.3
Seq gain (dB),      26
Channels,           1
Method Notes:
```

Program Dasy2Matlab.m converts DASYLab data into a MATLAB array with dimensions of Block Length by Number of Channels, and saves the data in MATLAB interior data format with extended file name ".mat". Program IAG2Matlab.m converts

phase angle data of IAG's spectrometer into a MATLAB array with dimension of Number of Points (256 in this example) by two (Blocks), and also saves the data in MATLAB interior data format with extended file name ".mat".

Table H-4 A header of MATLAB Program for data transformation from the DASYLab's to the MATLAB's

```
%%%%%%%%%%%%%%% IAG2Matlab.M %%%%%%%%%%%%%
% Convert ASCII format of IAG data  %
% into matlab format                %
%%%%%%%%%%%%%%%%%%%%%%%%%%%%%%%%%%%%%%%%%
close all;clear;clc
%%%%%%% Data Conversion %%%%%%%
SourcePath='..\data\nmr\phase\';
DestinationPath='..\data\nmr\mat\';
SearchFiles='p*.dat';
.
.
.
```

H.3 Software of Data synchronization

Not all the experimental data were acquired simultaneously that is because there was only one laser vibrometer to test structural vibrations. To deliver rigid vibration modals of the Helium-can and 20Kshield, those data of structural vibrations at different positions of a body with single laser vibrometer need to be synchronized. For instance, data files named as "D1F08" and "D5F08" include vibration data of Helium-can at its two different ends measured at different time respectively. To deliver its rotational vibration about y-axis these two data would be synchronized according to a reference vibration. The synchoronization has been realized by applying MATLAB program NMRCROSS.m, with which delays of the vibrations to the reference was calculated using cross-correlation and the delays were saved in the save data files with variable "Delay". With those reconstructed data, a relative vibration between Helium-can and

20K shield or between two different ends of a Helium-can was able to be analyzed. A part of the program is shown in Figure 9-5.

Table H-5 A header of MATLAB program for data synchronization

```
%%%%%%%%%%%%%%% NMRCROSS.M %%%%%%%%%%%%%%%%%%
% Cross-correlation for Data Synchronization %
%%%%%%%%%%%%%%%%%%%%%%%%%%%%%%%%%%%%%%%%%%%%%
clear;clc;close all
%%%%%%%%%%%%%%%%%%%%%%%%%%%%%%%%%%%%
Save='y';       % save file in the Destination path?
SourcePath='..\DATA\NMR\dtbmat\';
DestinationPath='..\DATA\NMR\dtbdly\';
%%%%%%%%%%%%%%%%%%%%%%%%%%%%%%%%%%%%%%%%%%%%%%%%%%%%
% the following three lines define a data file      %
% names which is composed of  strings given by      %
% Fname, Period and  one of Frq                     %
%%%%%%%%%%%%%%%%%%%%%%%%%%%%%%%%%%%%%%%%%%%%%%%%%%%%
Fname='D';
Period='*';     % 1,2,3... or * (all).
Frq=[ {'08'} {'19'} {'39'}];  %frequencies (Hz)
.
.
.
```

In this program, the file name of a source data is divided into three parts represented by the Matlab variables "Fname", "Period" and "Frq". '*' represents all arguments could be in the file names. The format of a file name is already defined in Chapter 8 .

H.4 Software of Data Analysis

Data were analyzed on experimental results and computer simulation. Fast Fourier Transform was the most frequently applied method. The program, NMRFFT.m, is a common FFT for all DASYLab data, as shown partly in Table H-6. Replacement "*" and "?" are valid in the MATLAB variable 'SearchFiles'. For convenient use of FFT in

various DASYLab's data obtained from different experiments, this program has been modified into different versions with more specific information and functions added in. For example, NMRD.m is specially designed for data files D?F??.mat and D?Head.mat as displayed in Table 8-1, NMRDTB.m for DTB??, DTB??F??.mat and DTB??H as displayed in Tabel 8-2, Beamfft.m for DG????? as shown in Table 8-4.

Table H-6 A header of MATLAB program, NMRFFT.m

```
%%%%%%%%%%%%%%%%%%%%%%%%%%%%%%%%%%%%%%%%%%%%%%%%%%%%%%%
%  Fast Fourier Transform  for DASYLab data file   %
%%%%%%%%%%%%%%%%%%%%%%%%%%%%%%%%%%%%%%%%%%%%%%%%%%%%%%%
clear;clc;close all
SourcePath='..\DATA\NMR\ds\';
%%%%%%%  Instruction to Add or delete  %%%%
%%%%%%%  file names in the cell array  %%%%
%  DFileName=[...                           %
%  {'ds*f19.mat'};                          %
%  {'ds01f39.mat'};                         %
%  %Delete above file names                 %
%  % or add new file names bellow           %
%  ];                                       %
%%%%%%%%%%%%%%%%%%%%%%%%%%%%%%%%%%%%%%%%%%%%%%
DFileName=[...
{'ds*f19.mat'};        %replacement '*' and '?' are valid
{'ds01f39.mat'};
%Delete above file names
% and/or add new file names bellow
];
%%%%%%%%%%%%%%%%%%%
IRef=[3 4];     %Channels of a DASYLab's data file
dTs=0.002;      %sampling rate (second)
Ns=4096;        %length of data
.
.
.
```

Program NMREL.m, as shown partly in Table H-7, was designed to obtain modals of translations and rotations of cryostat parts from the synchronized DASYLab data, saving produced data in files prefixed with 'Tr' and 'Ro' respectively. These data files

were analyzed in program NMRREL.m to produce data of relative vibrations between two different parts of a cryostat, as shown partly in Table H-8.

Table H-7 A header of MATLAB program for analyses of translations and rotations of a cryostat part.

```
%%%%%%%%%%%%%%%%%%% NMREL.m %%%%%%%%%%%%%%%%%%
%  Produce data of translation and rotation  %
%  from DASYLab data files D?F??.mat         %
%%%%%%%%%%%%%%%%%%%%%%%%%%%%%%%%%%%%%%%%%%%%%%
clear;clc;close all
%%%%%%%%%%%%%%%%%%%%%%%%%%%%%%%%%%%
SourcePath='..\DATA\NMR\mat\Adjusted\';
DestinationPath='..\DATA\NMR\mat\TrRo\';

Ff=[{'08'}     {'19'}      {'39'}];    %Frequencies
PE=[{'1'}      {'2'}       {'3'}];     %Positions at PE
SE=[{'5'}      {'6'}       {'7'}];     %Positions at SE
SN=[{'HecX'}   {'20KX'}    {'HecY'}]; %Prompts
%  Helium-can  20K shield  Helium-can
%  in x-axis   in x-axis   in y-axis
```

Table H-8 A header of MATLAB program for analyses of relative vibrations between two different parts of a cryostat.

```
%%%%%%%%%%%%%%%% NMRREL.M %%%%%%%%%%%%%%%%%%%%%%%%%%%%%%
% Produce data of Relative translations and rotations %
% between different parts of a cryostat              %
%%%%%%%%%%%%%%%%%%%%%%%%%%%%%%%%%%%%%%%%%%%%%%%%%%%%%%%%%
clear;clc;close all
%%%%%%%%%%%%%%%%%%%%%%%%%%%%%%%%%%%
SourcePath='..\DATA\NMR\mat\Adjusted\';
DestinationPath='..\DATA\NMR\mat\Adjusted\';
%%%%%%%%%%%%%%%%%%%%%%%%%%%%%%%%%%%%%%%%%%%%%%%%%%%%
% destination file names are composed as      %
% ['Rel' TR{i} 'F' Ff{j} '.mat']              %
%%%%%%%%%%%%%%%%%%%%%%%%%%%%%%%%%%%%%%%%%%%%%%%%%%%%
Ff=[{'08'} {'19'} {'39'}]; %frequencies
SN=[{'HecX'} {'20KX'}];
TR=[{'Tr'} {'Ro'}];  %prefixes of destination file names
```

MATLAB program VBPhase.m is to simulate spectrum recovery or calculate magnetic field spectrum from alias data of IAG' phase angle measurements. Theoretical descriptions of the spectrum recovery have been discussed in section 7.2 and 7.3. This program can also be invoked by Visual Basic program, which will be discussed in next section. MATLAB program Proc01.m and Proc02.m are designed to simulate Bloch's Equation under directional changes of magnetic field, which theory was discussed in Section 4.3.3. VBOmtField3.m is designed to calculate magnetic field and gradients from data of METROLAB magnetic field camera using surface harmonic theory, which were reviewed in Section 2.3.3. This program is also can be invoked by the Visual Basic program, OMT.vbp or OMT.exe. A full list of program names and descriptions are presented in the following table. All original codes of the programs are saved in a floppy disk.

Table H-9 List of Matlab programs.

Program Name	Functionality	Input	Output
Dasy2Matlab.m	Convert the ASCII format of DasyLab data files into Matlab format.	DasyLab ASCII data files	Matlab data files
IAG2Matlab.m	Convert ASCII format of IAG data into Matlab format.	Data files of Phase angle distortions acquired with IAG spectrometer	Matlab data files
LegFun.m	Calculate and draw Legendre polynomials.	Degrees and orders of	Coefficients of Legendre

		Legendre polynomials	polynomials
OmtFieldMap.m	Calculate magnetic field and magnetic gradient with experimental data of surface harmonics.	Data file of field and harmonics (Siemens Convention) for example, '70421.dat'	Magnetic field and gradient along a radius or a circle.
NmrCross.m	Synchronize all the measurements of structural vibrations to the measurement of the Cold Head vibration.	A delay adjusted data files, 'DTB??F??.mat' or 'D?F??.mat'	Synchronized data files.
TransRot.M.m	Calculate vibration modals of translation and rotation of Helium-can, 20K-shield or 80K-shield.	Vibratory frequencies, locations of optical test holes, data files 'D?F??.mat'	Vibration data files: File names are prefix "Tr" for translation and "Ro" for rotation.
NmrDtb2.m	Display data and spectrum of structural vibrations.	Data file 'DTB??F??.mat'	Graphic display of data and spectrum
FRF.m	Calculate frequency responses of displacement and search-coil to the force of the cold head.	Data files 'D?F??.mat'	Frequency to the force of cold head
NmrPg.m	Display real signal and spectrum of MR phase angle	'pg*.mat'	Graphic display of data

	distortions.		and spectrum
NmrShift.m	Phase shift between any two different measurements. Original measurement data should be adjusted by applying NMRCross.m to generate an adjusted data before this program is used.	Delay adjusted 'D?F??.mat"D?F??.mat'	Vibratory phase difference
LmsCross.m	Calculate and display spectra and cross-correlation and relative vibration of two measurements from LMS's experiments.	Any data file of LMS experimental data	Cross-correlation, spectrum, relative vibration
PhaseCal.m	Calculate MR phase distortion from Helium Can vibrations and magnetic gradients.	Data file 'D?F??.mat', Magnetic gradient	Peak-to-peak value of phase angles
PhaseDtb.m	Calculate MR phase distortion from dtb data source.	Data file 'DTB??F??.mat'	Peak-to-peak value of phase angles
Disp2VeloFRF.m	Convert FRF of displacement into FRF of velocity.	'D?F??.mat1	
Precession.m	Simulation of precession of magnetization.	Angular vibration of magnetic field, Larmor frequency	Change of amplitude of magnetic field

SenseCoilAngl.m	Calculate susceptibility of search coil to its orientation angles.	Orientation angles of search coil sensor	Variation of reading from the search coil sensor
SenseProbeEcho.m	Calculate and draw the sensitivity of MR phase distortion to various frequencies against different echo times.	Different echo times	Phase angle distortions

H.5 Source Codes

H.5.1 BeamCross.m

```
%%%%%%%%%%%%%%%%%%%%%%%%%%%%%%%%%%%%%%%%%%%%
% Display phase distortions
% Cross-corelation of beam vibratin    %
%%%%%%%%%%%%%%%%%%%%%%%%%%%%%%%%%%%%%%%%%%%%
clear
clc
close all
%%%%%%%%%%%%%%%%%%%%%%%%%%%%%%%%%%%%%%%%%%%%
RunCross='n';
SPath='..\data\NMR\mat\';
TPath='';
Prefix='P';
Sufix='f19.mat';
Delay=0;
dTs=0.1915002;          %sampling period
Ns=256;
TR=[191 192];
IRef=[0 1]; %Index
Idx=[{'1'} {'2'} {'3'} {'4'} {'5'} {'6'}];
Idx=[{'2'} {'3'} {'4'}];       %for Off
Idx=[{'1'} {'2'} {'3'} {'4'}];
```

```
Symbol=[{'P X-20cm'} {'P X+20cm'} ...
      {'P Y+20cm'} {'P X+20cm'} ...
      {'P O+00cm'} {'P x+20, y+10cm'}];
Offph=[0 0 0 0 0 0 0 ];

t=[0:(Ns-1)]*dTs;
fH=1/dTs/2;
f=linspace(0,1,Ns/2)*fH;

%%%%%%%%%%%%%%%
Dt0=0;                    %Second
Dt1=10000;
Df0=1;                    %Hz
Df1=1;
%%%%%%%%%%%%%%%
NDt0=1+floor(Dt0/dTs);
NDt1=min(1+floor(Dt1/dTs),Ns);

NDf0=1+floor(Df0/fH*Ns/2);
NDf1=1+floor(Df1/fH*Ns/2);

%%%%%%%%%%%%5

for nIdx=Idx
   nnIdx=str2num(nIdx{:});
   Name=[Prefix nIdx{:} Sufix ];
   load([SPath Name]);
   x=phase(1:Ns,:)/100;
   [nx mx]=size(x);
   %x02=x;
   figure
   for nRef=IRef
      if nRef<=mx
            x2=x(1:Ns,nRef+1);
         subplot(2,1,nRef+1)
         [Pmax Imax]=max(x2);
         [Pmin Imin]=min(x2);
            Pk=Pmax-Pmin;
         x3=x2;
         x3(Imax)=0;
         x3(Imin)=0;
         OMTPk=max(x3)-min(x3);
         plot(t(NDt0:NDt1),x2(NDt0:NDt1))
         set(gca,'TickDir','out')
         if findstr(lower(Name), lower(SPath))>0
            sName=Name(length(SPath)+1:length(Name));
         else
            sName=Name;
         end
         if nRef==0
            title([sName ': probe position:' ...
                  Symbol{nnIdx} ', Tr=' ...
                  num2str(TR,'%3.0fms ')]);
         end
            xlabel(['time (s)  ( real pk-pk:' ...
               num2str(Pk)  ', OMT pk-pk:' ...
            num2str(OMTPk) ' )'])
```

```
            end
      end
end
```

H.5.2 Correlate.m

```
%%%%%%%%%%%%%%%%%%%%%%%%%%%%%%%%%%%%%%%%%%%%
%     Correlate all the signals to the
%   reference signal of cold head and
%   generate a delay adjusted file for
%   further used in NmrShift.m
%%%%%%%%%%%%%%%%%%%%%%%%%%%%%%%%%%%%%%%%%%%%
clear all
clc
close all
%%%%%%%%%%%%%%%%%%%%%%%%%%%%%%%%%%%%%%%%%%%%
RunRelative='y'
Test='n';
RunCross='y';
PlotCross='n';
PlotDisplacement='y';
PlotVelocity='y';
Save='n';
SPath='..\data\NMR\dtbmat\';
TPath='';
Delay=0;
dTs=0.002;          %sampling period
Ns=1024*4;
IRef=[6];    %Index
IRef1=[9];
Unit4=[1 5 1 20];
Unit16=[1 1 1 20 1 1 1 1 1 20 1 1 1 1 1];
Unitv=5;            %5 for dtb 1 for d
Delta=dTs*0;
Prefix='DTB';
Sufix='H';          %'H' or 'F'
IdxRef=[{'09'}];
Idx=[{'12'}];
Frq=[{'08'} {'19'} {'39'}];
Frq=[{'08'}];
Symbol=[{'He41'} {'20K41'} {'80K41'} {'OVC41'} ...
      {'He43'} {'20K43'} {'80K43'} {'OVC43'} ...
      {'He13'} {'20K13'} {'80K13'} {'OVC13'} ...
      {'He11'} {'20K11'} {'80K11'} {'OVC11'} ...
      {'OvcZ'}{'He41'} {'20K41'}];
Link=[0 1 2 3 4 5 6 7 8 9];
Write16=[{'write:00'} {'write:01'} ...
      {'write:02'} {'write:03'} ...
      {'write:04'} {'write:05'} ...
      {'w06 c/d force'} {'write:07'} ...
      {'(w08 generated signal'} {'displacement'} ...
      {'write:10'} {'write:11'} ...
```

```
      {'write:12'} {'write:13'} ...
      {'write:14'} {'write:15'}];

Write4=[{'w00 c/h force'} {'w01 velovity'} {'w02 function generator
signal'} {'w03 displacement'}];
t=[0:(Ns-1)]*dTs;
fH=1/dTs/2;
f=linspace(0,1,Ns/2)*fH;


%%%%%%%%%%%%%%%
D00=0;
Dt0=0+D00;              %Second
Dt1=.2+D00;
Df0=1;                  %Hz
Df1=70;
%%%%%%%%%%%%%%%
NDt0=1+floor(Dt0/dTs);
NDt1=min(1+floor(Dt1/dTs),Ns);
NDf0=1+floor(Df0/fH*Ns/2);
NDf1=1+floor(Df1/fH*Ns/2);

%%%%%%%%%%%%5

if Sufix=='H'
   sFrq='';
end

nRef=IRef;
nnIdx=str2num(IdxRef{:});
nnIdx1=nnIdx;
      if (nnIdx>6 & nnIdx<18)
         if nRef==9
            nRef=3;
         elseif nRef==6
            nRef=0;
         end
         nv=1;
         write=Write4{nRef+1};
         Unit=Unit4;
      else
         nv=7;
         write=Write16{nRef+1};
         Unit=Unit16;
      end

Name1=[Prefix IdxRef{1} Sufix sFrq '.mat'];
load([SPath Name1]);
x1=x(1:Ns,nRef+1)*Unit(nRef+1);
v1=x(1:Ns,nv+1)*Unitv;
nIdx=Idx;
   Name=[Prefix nIdx{:} Sufix sFrq '.mat'];
   load([SPath Name]);
   x0=x(1:Ns,:);
   [nx mx]=size(x0);
   %x02=x;
   nnIdx=str2num(nIdx{:});
```

```
        if (nnIdx>6 & nnIdx<18)
           if nRef==9
              nRef=3;
           elseif nRef==6
                 nRef=0;
           end
           write=Write4{nRef+1};
           Unit=Unit4;
        else
           write=Write16{nRef+1};
           Unit=Unit16;
        end

        if nRef<=mx
           x2=x0(1:Ns,nRef+1)*Unit(nRef+1);
           v2=x0(1:Ns,nv+1)*Unitv;

           if Test=='y'
              f=50; %hz
              dt1=0;
              dt2=+pi/8;
              dt=(dt1-dt2)/f/2/pi
              x1=sin(2*pi*f*t+dt1);
              x2=sin(2*pi*f*t+dt2);
           end
                    if RunCross=='y'

                          clear x0
              [c l]=xcorr(x1,x2);

              [Y I]=max(c);
              NDelay=l(I);
              Delay=NDelay*dTs;
              [nIdx{:} num2str(Delay,'--> %2.3f (s)')]
              if PlotCross=='y'
                 figure
                 plot(l,c);
                 title([Name1 ' to ' Name])
                 xlabel(['Delay=' ...
                       num2str(Delay,'%2.3f (s)')])
              end
           end
        end          % if nRef
        if Save=='y'
           if Test~='y'
              save([SPath Name],'x','Delay')
           end
        end
end
end    %for nFrq

figure
subplot(2,1,1)
plot(t(NDt0:NDt1),x1(NDt0:NDt1),'r',...
   t(NDt0:NDt1),x2(NDt0:NDt1),'b');
Delay=Delay+Delta;
NDelay=floor(Delay/dTs);
```

```
if Delay<0
   x1=x1(-NDelay+1:Ns);
else
   x2=x2(NDelay+1:Ns);
end
Ns0=min(length(x1),length(x2));
x1=x1(1:Ns0);
x2=x2(1:Ns0);
subplot(2,1,2)
plot(t(NDt0:NDt1),x1(NDt0:NDt1),'r',...
   t(NDt0:NDt1),x2(NDt0:NDt1),'b');
Ns=min(Ns0,1024*2);
Ns=Ns0;
if RunRelative=='y'
   NDf0=1+floor(Df0/fH*Ns/2);
      NDf1=1+floor(Df1/fH*Ns/2);
   x2=x1-x2;
      f=linspace(0,1,Ns/2)*fH;
   FFT=fft(x2);
   Fx=abs(FFT)/Ns*2;
   Ax=angle(FFT);

   if PlotDisplacement=='y'
            figure
            subplot(2,1,1)
            Pk=max(x2)-min(x2);
         plot(t(NDt0:NDt1),x2(NDt0:NDt1))
         set(gca,'TickDir','out')

         title(['Relative displacement: ' Symbol{nnIdx1} ...
               ' via ' Symbol{nnIdx}]);
            xlabel(['time (s), pk-pk:' ...
                  num2str(Pk)])
         ylabel('micrometer')
         [Y I]=max(Fx(NDf0:NDf1));
            AxD=Ax(NDf0:NDf1)*180/2/pi;
            subplot(2,1,2)
            plot(f(NDf0:NDf1),Fx(NDf0:NDf1))
         set(gca,'TickDir','out')
         xlabel('frequency (hz)')
         ylabel('micrometer')
            text(f(I+NDf0),Y,['a=' ...
                  num2str(Fx(I+NDf0-1),'%0.3f')...
               ', f=' num2str(f(I)+Df0,'%0.3f')])
      end
      %%%%%%%%%%%%%%%%%%%%%%%%%%%%%%%%

if PlotVelocity=='y'
figure
subplot(2,1,1)
plot(t(NDt0:NDt1),v1(NDt0:NDt1),'r',...
   t(NDt0:NDt1),v2(NDt0:NDt1),'b');

if Delay<0
   v1=v1(-NDelay+1:Ns);

else
```

```
   v2=v2(NDelay+1:Ns);
end
Ns0=min(length(v1),length(v2));
v1=v1(1:Ns0);
v2=v2(1:Ns0);
subplot(2,1,2)
plot(t(NDt0:NDt1),v1(NDt0:NDt1),'r',...
   t(NDt0:NDt1),v2(NDt0:NDt1),'b');
         nRef=nv;
         x2=v1-v2;
                  f=linspace(0,1,Ns/2)*fH;
               FFT=fft(x2);
               Fxx=abs(FFT)/Ns*2;
            figure
            subplot(2,1,1)
            Pk=max(x2)-min(x2);
         plot(t(NDt0:NDt1),x2(NDt0:NDt1))
         set(gca,'TickDir','out')

         title(['Relative velocity: ' Symbol{nnIdx1} ...
               ' via ' Symbol{nnIdx}]);
            xlabel(['time (s), pk-pk:' ...
                  num2str(Pk)])
         ylabel('micrometer/s')
         [Y I]=max(Fxx(NDf0:NDf1));
            AxD=Ax(NDf0:NDf1)*180/2/pi;
            subplot(2,1,2)
            plot(f(NDf0:NDf1),Fxx(NDf0:NDf1))
         set(gca,'TickDir','out')
         xlabel('frequency (hz)')
         ylabel('micrometer')
            text(f(I+NDf0),Y,['a=' ...
                  num2str(Fxx(I+NDf0-1),'%0.3f')...
               ', f=' num2str(f(I)+Df0,'%0.3f')])
      end
end
```

H.5.3 Dasy2Matlab.m

```
%%%%%%% Data Conversion %%%%%%%%
% Convert the ASCII format of DasyLab
% into matlab format
%%%%%%%%%%%%%%%%%%%%%%%%%%%%%%%
close all
clear
clc
%%%%%%%%%%%%%%%%%%%%%%%%%%%%%%%
SPath='..\data\NMR\DS\'
SSPath=SPath;
TPath='..\data\NMR\DS\'
TTPath=TPath;
TSufix='.mat';
SearchFiles='ds07h.asc';
```

```
SFn=dir([SPath SearchFiles]);
[S R]=strtok(SearchFiles,'.');
TSearchF=[S TSufix];

TFn=dir([TPath TSearchF]);
Nsf=length(SFn);
Ntf=length(TFn);
tic
for Nsf1=1:Nsf
   SFname=SFn(Nsf1).name;
   n=findstr(lower(SFname),lower(SPath));
   if n
      Lf=length(SFname);
      Lp=length(SPath);
      SFname=SFname(n+Lp:Lf);
   end

   FileExist=0;
   for Ntf1=1:Ntf
      TFname=TFn(Ntf1).name;
      n=findstr(lower(TFname),lower(TPath));
      if n
         Lf=length(TFname);
         Lp=length(TPath);
         TFname=TFname(n+Lp:Lf);
      end
      [SS R]=strtok(SFname,'.');
      SS=lower([SS TSufix]);
      TS=lower(TFname);
      FileExist=strcmp(SS,TS);
      if FileExist==1
         ['the file: ' TFname ...
               ' has been converted']
         break;
      end
   end
   if FileExist==0;
         [S R]=strtok(SFname,'.');
          TFname=[S TSufix];
         ['Source file:' num2str(Nsf1)...
               '/'num2str(Nsf) '  ' SFname]
         Fid=fopen([SPath SFname]);
         if Fid==-1
            ['File ' SFname ' nod found!!!']
            pause
         end
            for i=1:4
            s=fgets(Fid);
            end                                    %Block Lengrh
            [T R]=strtok(s,':');
            [T R]=strtok(R,' ');
            Row=str2num(R);
            s=fgets(Fid);
            s=fgets(Fid);
            [T R]=strtok(s,':');     %Sampling Period
            [T R]=strtok(R,' ');     %Number of Channels
            Col=str2num(R);
```

```
        x=zeros(Row,Col);
        s=fgets(Fid);                %Time Write0..
        Dlm=s(5);
           for i=1:Row
              R=fgets(Fid);          %Data
        [S R]=strtok(R,Dlm);
        for n=1:Col
           [S R]=strtok(R,Dlm);
                 x(i,n)=str2num(S);
              end       % end of Column
     end          % end of row
     fclose(Fid);
        save([TPath TFname],'x');
        ['Elapsed time' num2str(toc) 's']
     end          %end if no file exists
end               % end of file list
```

H.5.4 Disp2VeloFRF.m

```
%%%%%%%%%%%%%%%%%%%%%%%%%%%%%%%%%%%%%%%%%%%%
%     Converte d1f**.mat d2f**.mat into vfrf
% Col01:Frequency,      Col02:C/D force,
% Col03:Displacement,Col04:Search-coil
%%%%%%%%%%%%%%%%%%%%%%%%%%%%%%%%%%%%%%%%%%%%
clear all
clc
close all
%%%%%%%%%%%%%%%%%%%%%%%%%%%%%%%%%%%%%%%%%%%%

RunCross='y';
Plot='n';
Plotvfrf='y';
LogX='n';
Save='y';
SPath='..\data\NMR\Dmat\';
TPath='..\data\nmr\dmat\';
Delay=0;
dTs=0.002;          %sampling period
Ns=1024*4;
IRef=[0 1 2];       %Index
Unit=[1 20 1 1];
Prefix='D';
Sufix='f';          %'H' or 'F'
Idx=[{'3'} {'4'} {'5'} {'6'}];
Symbol=[{'Hecan PE X'} {'20K PE X'} ...
      {'Hecan PE Y'} {'20K PE Y'} ...
      {'Hecan SE X'} {'20K SE X'} {'He SE Y'}];
Link=[0 1 2 3 4 5 6 7 8 9];
Write16=[{'write:00'} {'write:01'} ...
      {'write:02'} {'write:03'} ...
      {'write:04'} {'write:05'} ...
      {'w06 c/d force'} {'write:07'} ...
```

```
      {'(w08 generated signal'} {'displacement'} ...
      {'write:10'} {'write:11'} ...
      {'write:12'} {'write:13'} ...
      {'write:14'} {'write:15'}];
t=[0:(Ns-1)]*dTs;
fH=1/dTs/2;
f=linspace(0,1,Ns/2)*fH;

%%%%%%%%%%%%%%%
ConstrictF='y';
Dt0=0;                    %Second
Dt1=1;
Df0=1;                    %Hz
Df1=100;
Pfmin=0.9;
Pfmax=1.1;
%%%%%%%%%%%%%%%
NDt0=1+floor(Dt0/dTs);
NDt1=min(1+floor(Dt1/dTs),Ns);
NDf0=1+floor(Df0/fH*Ns/2);
NDf1=1+floor(Df1/fH*Ns/2);

%%%%%%%%%%%%5
LIRef=length(IRef);
slegend=0;

for nIdx=Idx
   nnIdx=str2num(nIdx{:});
   s=[Prefix nIdx{:} Sufix];
   SFn=dir([SPath s '*.mat']);
   LFrq1=length(SFn);
   vfrf=zeros(LFrq1,2*LIRef+1);
for nFrq1=1:LFrq1

   Name=SFn(nFrq1).name;
   l=length(s);
   sFrq=Name(l+1:l+2);
   a=str2num(sFrq);

   vfrf(nFrq1,1)=a;
   load([SPath Name]);

   oFrq=str2num(sFrq);
   if ConstrictF=='y'
   %%%%%%%%%%%%%%%
      Dt0=0;                  %Second
      Dt1=1;
   %%%%%%%%%%%%%%%
   Df0=oFrq*Pfmin;                  %Hz
      Df1=oFrq*Pfmax;
      %%%%%%%%%%%%%%%
      NDt0=1+floor(Dt0/dTs);
      NDt1=min(1+floor(Dt1/dTs),Ns);
      NDf0=1+floor(Df0/fH*Ns/2);
      NDf1=1+floor(Df1/fH*Ns/2);
   %%%%%%%%%%%%%%%%%%%%%%
   end
```

```
   for InRef=1:LIRef
     nRef=IRef(InRef);
     write=Write16{nRef+1};
        x2=x(1:Ns,nRef+1)*Unit(nRef+1);
      end
end   %for nFrq1
if Save=='y'
save([TPath 'FRF' nIdx{:} '.txt'],...
   'vfrf','-ascii');
end
end
%for nIdx
```

H.5.5 FRF.m

```
%%%%%%%%%%%%%%%%%%%%%%%%%%%%%%%%%%%%%%%%%%%%
%     Calculate the frequency response of
%   displacement from d?f??.mat
% Col01:Frequency,      Col02:C/D force,
% Col03:Displacement,Col04:Search-coil
%%%%%%%%%%%%%%%%%%%%%%%%%%%%%%%%%%%%%%%%%%%%
clear all
clc
close all
%%%%%%%%%%%%%%%%%%%%%%%%%%%%%%%%%%%%%%%%%%%%

RunCross='y';
Plot='n';
Plotvfrf='y';
LogX='n';
Save='y';
SPath='..\data\NMR\Dmat\';
TPath='..\data\nmr\dmat\';
Delay=0;
dTs=0.002;          %sampling period
Ns=1024*4;

IRef=[0 1 2];       %Index
Unit=[1 20 1 1];
Prefix='D';
Sufix='f';          %'H' or 'F'
Idx=[{'3'} {'4'} {'5'} {'6'}];

Symbol=[{'Hecan PE X'} {'20K PE X'} ...
      {'Hecan PE Y'} {'20K PE Y'} ...
      {'Hecan SE X'} {'20K SE X'} {'He SE Y'}];
Link=[0 1 2 3 4 5 6 7 8 9];

Write16=[{'write:00'} {'write:01'} ...
      {'write:02'} {'write:03'} ...
      {'write:04'} {'write:05'} ...
```

```
      {'w06 c/d force'} {'write:07'} ...
      {'(w08 generated signal'} {'displacement'} ...
      {'write:10'} {'write:11'} ...
      {'write:12'} {'write:13'} ...
      {'write:14'} {'write:15'}];
t=[0:(Ns-1)]*dTs;
fH=1/dTs/2;
f=linspace(0,1,Ns/2)*fH;

%%%%%%%%%%%%%%%
ConstrictF='y';
Dt0=0;                    %Second
Dt1=1;
Df0=1;                    %Hz
Df1=100;
Pfmin=0.9;
Pfmax=1.1;
%%%%%%%%%%%%%%%
NDt0=1+floor(Dt0/dTs);
NDt1=min(1+floor(Dt1/dTs),Ns);
NDf0=1+floor(Df0/fH*Ns/2);
NDf1=1+floor(Df1/fH*Ns/2);

%%%%%%%%%%%%5
LIRef=length(IRef);
slegend=0;

for nIdx=Idx
   nnIdx=str2num(nIdx{:});
   s=[Prefix nIdx{:} Sufix];
   SFn=dir([SPath s '*.mat']);
   LFrq1=length(SFn);
   vfrf=zeros(LFrq1,2*LIRef+1);
for nFrq1=1:LFrq1
   Name=SFn(nFrq1).name;
   l=length(s);
   sFrq=Name(l+1:l+2);
   a=str2num(sFrq);
   vfrf(nFrq1,1)=a;
   load([SPath Name]);
   oFrq=str2num(sFrq);
   if ConstrictF=='y'
   %%%%%%%%%%%%%%%
      Dt0=0;                  %Second
      Dt1=1;
   %%%%%%%%%%%%%%%
   Df0=oFrq*Pfmin;                  %Hz
      Df1=oFrq*Pfmax;
      %%%%%%%%%%%%%%%
      NDt0=1+floor(Dt0/dTs);
      NDt1=min(1+floor(Dt1/dTs),Ns);
      NDf0=1+floor(Df0/fH*Ns/2);
      NDf1=1+floor(Df1/fH*Ns/2);
   %%%%%%%%%%%%%%%%%%%%%%%
   end

   for InRef=1:LIRef
```

```
      nRef=IRef(InRef);
      write=Write16{nRef+1};
         x2=x(1:Ns,nRef+1)*Unit(nRef+1);
      FFT=fft(x2);
      Fx=abs(FFT)/Ns*2;
      Ax=angle(FFT);
      Pk=max(x2)-min(x2);
      [Y I]=max(Fx(NDf0:NDf1));
      AxD=Ax(NDf0:NDf1)*180/2/pi;

      vfrf(nFrq1,InRef+1)=Fx(I+NDf0-1);
      vfrf(nFrq1,LIRef+1+InRef)=f(I)+Df0;
       end
end    %for nFrq1

figure
plot(vfrf(:,1),vfrf(:,2:2*LIRef))
legend('cold head force','displacement','search coil')
title(['Index' nIdx{:} ':' ])

%%%%%%%%%%FRF of Displacement to force
figure
if LogX=='y'
   plot(vfrf(:,1),10*log10(vfrf(:,3)/vfrf(:,2)))
   DB='DB'
else
   DB='';
   plot(vfrf(:,1),vfrf(:,3)/vfrf(:,2))
end
title(['FRF of diaplacement of ' Symbol{nnIdx}])
ylabel(['micrometer/KN  ' DB]);
xlabel('Frequency (Hz)');
%%%%%%%%%%FRF of search-coil to force
figure
if LogX=='y'
      plot(vfrf(:,1),10*log10(vfrf(:,4)/vfrf(:,2)))
else
      plot(vfrf(:,1),vfrf(:,4)/vfrf(:,2))
end
%vfrf1=vfrf';
%set(gca,'YScale','log')
title(['FRF of search-coil of ' Symbol{nnIdx}])
ylabel(['micrometer/KN  ' DB]);
xlabel('Frequency (Hz)');
if Save=='y'
save([TPath 'FRF' nIdx{:} '.txt'],...
   'vfrf','-ascii');
end
end
%for nIdx
```

H.5.6 IAG2Matlab.m

```
%%%%%%%%%%%%%%%%%%%%%%%%%%%%%%%%
% Convert ASCII format of IAG data
% into matlab format
%%%%%%%%%%%%%%%%%%%%%%%%%%%%%%%%

close all
clear
clc

%%%%%%% Data Conversion %%%%%%%%

SourcePath='..\data\nmr\phase\'
DestinationPath='..\data\nmr\mat\'
SearchFiles='p*.dat';

SFn=dir([SourcePath SearchFiles]);
[S R]=strtok(SearchFiles,'.');

TFn=dir([DestinationPath S '.mat']);
Nsf=length(SFn);
Ntf=length(TFn);
tic
for Nsf1=1:Nsf
   SFname=SFn(Nsf1).name;

   FileExist=0;
   for Ntf1=1:Ntf
      [SS R]=strtok(SFname,'.');
      [TS R]=strtok(TFn(Ntf1).name,'.');
      FileExist=strcmp(SS,TS);
      if FileExist==1
         ['the file: ' SFname ...
               'has been converted']
         break;
      end
   end
   if FileExist==0;

         [S R]=strtok(SFname,'.');
          TFname=[S '.mat'];
         ['Source file:' num2str(Nsf1)...
               '/'num2str(Nsf) '  ' TFname]
         Fid=fopen([SourcePath SFname]);
         if Fid==-1
            ['File ' SFname ' nod found!!!']
            pause
         end
         s=fgets(Fid);              %First record
      [T R]=strtok(s,' ');
            [T R]=strtok(R,' ');
            [T R]=strtok(R,' ');
            Row=str2num(T);         %Row=256
            s=fgets(Fid);                 %Second record
            Col=2;
         phase=zeros(Row,Col);
         Dlm=' ';
```

```
      for j=1:Col
                  for i=1:Row
                  R=fgets(Fid);            %Data record
                  [S R]=strtok(R,Dlm);
                  phase(i,j)=str2num(R);
            end
            R=fgets(Fid);
            R=fgets(Fid);
            R=fgets(Fid);
            end          % end of row
            fclose(Fid);
         save([DestinationPath TFname],'phase');
         ['Elapsed time' num2str(toc) 's']
      end          %end if no file exists
end                % end of file list
```

H.5.7 LegFun.m

```
%%Associated Legendre Fuctions%%%
clear
clc
close
%%%%%%%%%%%%%%%%%%%%
InMultiWin='n';          %degree n and order 0
%%%%%%%%%%%%%%%%%%5
Degree=8;                        %degree     n=0,1,...Degree.
Order=0;                               %order      m=0,1,...,n.
%% 1. Calculate
Order=Order+1;
Degree=Degree+1;
theta=linspace(-pi,pi,100);
Mm=1;
Mu=cos(theta);

for n=1:Degree;
   P=legendre(n-1,Mu);
   m=Order;
   Nn=n-Order+1;
   if Nn>0
      P0(Nn,:)=P(Order,:);
      if InMultiWin=='n'
         hold on
      plot(theta,P0(Nn:Nn,:));
      title('Associated Legendre Fuctions');
      xlabel(['Degree n=' num2str(n-1,2) ...
            ', Order m=' num2str(Order-1,2)]);
         end
      end
end
```

H.5.8 LmsCross.m

```
%%%%%% Spectra, cross-correlation from LMA data file %%%%%%%%%%
clc
clear
close
%%%%%File of Data%%%%%%%%%%%%%%%%
file_path='..\data\tap\';
file01='80K_11_-Y_1180zy.mat';
file02='80K_13_-Y_1380zy.mat';
file01=strtok(file01,'.');
file02=strtok(file02,'.');
%%%%%%Flag%%%%%%Flag%%%%%%Flag%%%%%%Flag
RawDat='v';
RunCross='n';                    % run cross-correlation if 'y'
RelativeMotion='n';      % run relative motion if 'y'
a1_to_a_v_d='v_to_v';    % 'a_to_v' or 'v_to_d' or
                                          % 'a_to_d' or not
a2_to_a_v_d='v_to_v';    % 'a_to_v'/'v_to_d'/
                                          % 'a_to_d'/search coil or
not
IsVelToDis2='n';         % Velocity to displacement
IsLaser='y';                     %
ProduceRelativeMotion='n';
XLogScale='n';                   %
YlogScale='n';
%%%%%%%%%%%%%%%%%%%%%%%%%%%%%%%%%%%%%%%%%%%%%%%%
aFs0=0.5;          %Hz   Minimum frequency to plot
aFs=25;            %Hz   Maximum frequency to plot
N0=0;                    %Sart point of data to be read
TT=120;            %basic length of data (second).
dT=1e-3;           %basic sampling period (second)
Fs=1/dT;           %basic sampling rate (Hz)
Fs1=1000;          %Nyquist frequency (Hz)
                         % or practical sampling rate
dN=Fs/Fs1;  %
dTs=dT*dN;  %practical sampling period
Nf0=0;             %Start position of ploting spectra
Nf1=0;             %End position of ploting spectra
Nsk=8;             %Re-sampling data
Ts0=7;             %Start time of data to plot
Ts1=0;             %End time of data to plot

%%%%%%%%%%%%%%%%%%%%%%%%%%%%%%%%%%%%%%%%%%%%%%%%

Ns=65536/Nsk;
hNs=Ns/2;
aNs=Ns/dN;
Nafs0=floor(Ns*aFs0/Fs1);
Nafs=floor(Ns*aFs/Fs1);
n=fix(log2(aNs));
aNs2=2^n;
f=linspace(0,1,aNs2/2)'*Fs1/2;
TTc=dTs*aNs2;      %practical length of data (second)
t=linspace(0,1,aNs2)*TTc;
Nts0=fix(Ts0/TTc*aNs2);
```

```
%%%%%%%%%%%%%%%%%%%%%%%%%%%%%%%%%%%%%%%%%%%%%%%%%%%%%%%%%%%%%%%%5

%%%%%%%Load data of time lag and Find time lag%%%%%%%
load OMT_TimeLag FileCold;
%%%%%%%%Find Time lag%%%%%%%%%%%%%%%
aa1=find(file01=='~');
aa2=find(file02=='~');

if isempty(aa1)==0
   s1=strrep(file01,'.mat','');
      s01=strtok(s1,'_');
else
   r1=strrep(file01,'.','_');
      [s01 r1]=strtok(r1,'_');
      for n=1:3
         [s1 r1]=strtok(r1,'_');
      end
      s1=['cold_head_+Z_' s1];
end

if isempty(aa2)==0
   s2=strrep(file02,'.mat','');
      s02=strtok(s2,'_');
else
   r2=strrep(file02,'.','_');
      [s02 r2]=strtok(r2,'_');
      for n=1:3
         [s2 r2]=strtok(r2,'_');
      end
      s2=['cold_head_+Z_' s2];
end

Inx01=findcel(FileCold(:,1),s1)
Inx02=findcel(FileCold(:,1),s2)

if Inx01>0
   Lag01=FileCold{Inx01,2};
else

   ['Check the first file name!!!',7,13]
   pause
end

if Inx02>0
   Lag02=FileCold{Inx02,2};
else
   ['Check the second file name!!!',7,13]
   pause
end
Delay=Lag02-Lag01;

%%%%%%%%%%Types of data%%%%%%%%%%%%%%%%%%%
% L-Laser, A-Accelaration, S-Search coil  %
%%%%%%%%%%%%%%%%%%%%%%%%%%%%%%%%%%%%%%%%%%
Dis='Displacement (m)';
Vel='Velocity (m/s)';
Acc='Acceleration (m/s^2)';
```

```
Coil='Search-coil (Volt)';
switch lower(s01)
case '20k'
   DataUnit1=Vel;
case '80k'
   DataUnit1=Vel;
case 'mdo'
   DataUnit1=Vel;
case 'cold'
   DataUnit1=Acc;
case 'vesi'
   DataUnit1=Acc;
case 'phas'
   DataUnit1=Coil;
      a1_to_a_v_d='coil';
otherwise
   DataUnit1='???';
end

switch lower(s02)
case '20k'
   DataUnit2=Vel;
case '80k'
   DataUnit2=Vel;
case 'mdo'
   DataUnit2=Vel;
case 'cold'
   DataUnit2=Acc;
case 'vesi'
   DataUnit2=Acc;
case 'phas'
   DataUnit2=Coil;
      a2_to_a_v_d='coil';
otherwise
   DataUnit2='???';
end

if strcmp(DataUnit1,DataUnit2)==0
   RelativeMotion='n';
end

%%%01%%%%%%%01%%%%%%%01%%%%%%%01%%%%
%%%01%%%%%%%01%%%%%%%01%%%%%%%01%%%%
if Delay<0
   dT21=Delay;
else
   dT21=0;
end

dN21=floor(abs(dT21/dTs));
file1=file01;
load(['..\data\tap\' file01]);            %Load data one
mean_x=mean(x)
file1=strrep(file1,'_','\_');
file1=strrep(file1,'.mat','');
x=x(1+dN21+N0:dN:Ns+dN21+N0);
x1=x(1:aNs2);
```

```
y=fft(x1);
Y1=abs(y(1+Nafs0:Nafs))/aNs2;
f1=f(1+Nafs0:Nafs);
alf1=angle(y(1+Nafs0:Nafs));

figure(1)   %Plot Spectra density of acc/vel/dis/coi
switch a1_to_a_v_d
case 'a_to_v',
   Y1=Y1./(f1+eps)/(2*pi);
   Ylabel_acc1=Vel;
case 'a_to_d',
   Y1=Y1./(f1+eps)./(f1+eps)/(2*pi)^2;
   Ylabel_acc1=Dis;
case 'v_to_d',
   Y1=Y1./(f1+eps)/(2*pi);
   Ylabel_acc1=Dis;
case 'v_to_v'
   Ylabel_acc1=Vel;
case 'coil'
   Ylabel_acc1=Coil;
otherwise
   Ylabel_acc1=Acc;
end

subplot(2,1,1);
if YlogScale=='y'
   Y1=10.*log10(Y1);
end

plot(f1,Y1,'b')
set(gca,'TickDir','Out')
set(gca,'Ylim',[min(Y1) max(Y1)]);
if YlogScale=='y'
   set(gca,'YScale','Log');
end

[y1 I1]=max(Y1);
alf1(I1)*180/pi
text(f1(I1),y1,[num2str([y1 f1(I1) alf1(I1)*180/pi],4) '^o']);
title(['Spectra density of ' file1]);
s=strtok(Ylabel_acc1);
ylabel(s);

%%%02%%%%%%%02%%%%%%%02%%%%%%%02%%%%
if Delay>0
   dT12=Delay;
else
   dT12=0;
end

dN12=floor(abs(dT12/dTs));

file2=file02;
load(['..\data\tap\' file02]);            %Load data two
%x=x-mean(x);
file2=strrep(file2,'_','\_');
file2=strrep(file2,'.mat','');
```

```
x=x(1+dN12+N0:dN:Ns+dN12+N0);
x2=x(1:aNs2);
y=fft(x2);
Y2=abs(y(1+Nafs0:Nafs))/aNs2;
f2=f(1+Nafs0:Nafs);
alf2=angle(y(1+Nafs0:Nafs));

switch a2_to_a_v_d
case 'a_to_v',
   Y2=Y2./(f2+eps);
   Ylabel_acc2=Vel;
case 'a_to_d',
   Y2=Y2./(f2+eps)./(f2+eps);
   Ylabel_acc2=Dis;
case 'v_to_d',
   Y2=Y2./(f2+eps);
   Ylabel_acc2=Dis;
case 'v_to_v'
   Ylabel_acc2=Vel;
case 'coil'
   Ylabel_acc2=Coil;
otherwise
   Ylabel_acc2=Acc;
end
subplot(2,1,2);
if YlogScale=='y'
   Y2=10.*log10(Y2);
end

plot(f2,Y2,'r')
set(gca,'TickDir','Out')
set(gca,'Ylim',[min(Y2) max(Y2)]);
if YlogScale=='y'
   set(gca,'YScale','Log');
end

[y2 I2]=max(Y2);
alf2(I2)*180/pi

text(f2(I2),y2,[num2str([y2 f2(I2) alf2(I2)*180/pi],4) '^o']);
title(['Spectra density of ' file2]);
xlabel(['Frequency (Hz), (Ts:'num2str(dTs)...
      ' s, Ns:' num2str(aNs2) ')']);
s=strtok(Ylabel_acc2);
ylabel(s);
%%%%%%%%%%%%%%%%%%%%%%%%%%%
format long
Lag=(alf2(I2)-alf1(I1))/f2(I2),I1,I2
format

%%%%%%%%Invers FFT%%%%%%%%%%%%%%%


%%% Cross correlation%%% Cross correlation%%% Cross correlation
if RunCross=='y'

      clear x y Y
```

```
      [c l]=xcorr(x1,x2);
      figure(3)
      plot(l,c);
      [Y I]=max(c);
   X_cross=l(I)*dTs
end

%%%%%%%data figure(2)%%%%%%%data%%%%%%%data
figure(2)   %Sampling data of acc/vel/dec/coil

subplot(2,1,1);
plot(t(1+Nts0:aNs2),x1(1+Nts0:aNs2),'b')
title(['data of ' file1]);
ylabel(DataUnit1);

subplot(2,1,2);
plot(t(1+Nts0:aNs2),x2(1+Nts0:aNs2),'r')
title(['data of ' file2]);
xlabel(['Sampling time (s) (Ts:'num2str(dTs)...
      ' s, Ns:' num2str(aNs2) ')']);
ylabel(DataUnit2);

%%%%%%%Relative motion%%%%%%%Relative motion
if RelativeMotion=='y'
   figure(4);
      x=x1(1:aNs2)-x2(1:aNs2);
      y=fft(x);
      Y3=abs(y(1+Nafs0:Nafs));
   f3=f(1+Nafs0:Nafs);

   subplot(2,1,1)
   plot(t(1+Nts0:aNs2),x2(1+Nts0:aNs2),'b')
      title(['Relative motion of ' file1 ' and ' file2]);
   ylabel(DataUnit1);
   xlabel(['                                          '...
         'Smpling time (s)']);
      switch a1_to_a_v_d
      case 'a_to_v',
         Y3=Y3./(f3+eps);
         Ylabel_acc1='Velocity (m/s)';
      case 'a_to_d',
         Y3=Y3./(f3+eps)./(f3+eps);
         Ylabel_acc1='Displacement (m)';
      case 'v_to_d',
         Y3=Y3./(f3+eps);
         Ylabel_acc1='Displacement (m)';
      case 'v_to_v'
      Ylabel_acc1='Velocity (m/s)';
      case 'coil'
         Ylabel_acc1='Search coil (volt)';
      otherwise
         Ylabel_acc1='Acceleration (m/s^2)';
      end

      subplot(2,1,2)
      plot(f3,Y3)
      [Y I]=max(Y3);
```

```
      alf1(I)*180/pi
   text(f3(I),Y,[num2str([Y f3(I) alf1(I)*180/pi],4) '^o']);
      title('Spectra density');
   xlabel(['Frequency (Hz), (Ts:'num2str(dTs)...
         ' s, Ns:' num2str(aNs2) ')']);
   ylabel(strtok(Ylabel_acc1));
end

%%%%%%%%%%%Save data of lelative motion%%%%%%%%%
if ProduceRelativeMotion=='y';
   load(['..\data\tap\' file01]);          %Load data one
   x1=x(1+dN12:length(x));
   load(['..\data\tap\' file02]);          %Load data two
   x2=x(1+dN12:length(x));
   n=min(length(x1),length(x2));
   x=x1(1:n)-x2(1:n);
   Fname=['..\data\tap\' strrep(file01,'.mat','')...
         '~' strrep(file02,'.mat','')]
   save(Fname, 'x');
end
```

H.5.9 Nmr2Dbt2.m

```
%%%%%%%%%%%%%%%%%%%%%%%%%%%%%%%%%%%%%%%%%%%%
%     Display
%%%%%%%%%%%%%%%%%%%%%%%%%%%%%%%%%%%%%%%%%%%%
clear
clc
close all
%%%%%%%%%%%%%%%%%%%%%%%%%%%%%%%%%%%%%%%%%%%%

RunCross='n';
Chaz='y';

SPath='..\data\NMR\dtbmat\';
TPath='';
iPlot=0;
Delay=0;
dTs=0.002;          %sampling period
Ns=1024*4;

IRef=[9];    %Index
Unit4=[1 5 1 20];
Unit16=[1 1 1 20 1 1 1 1 1 20 1 1 1 1 1];

Prefix='DTB';
Sufix='H';          %'H' or 'F'
Idx=[{'03'} {'04'} {'05'} ...
      {'06'} {'07'} {'08'} {'09'} {'10'} ...
      {'11'} {'12'} {'13'} {'14'} {'15'} ...
```

```
      {'16'} {'17'} {'18'} {'19'}];

Frq=[{'08'} {'19'} {'39'}];
Frq=[{'08'}];

Symbol=[{'Helium can at SE Y'} {'20K shield at SE Y'} {'80K shield at
SE Y'} {'OVC at SE Y'} ...
      {'Helium can at PE Y'} {'20K shield at PE Y'} {'80K shield at PE
Y'} {'OVC at PE Y'} ...
      {'Helium can at PE X'} {'20K shield at PE X'} {'80K shield at PE
X'} {'OVC at PE X'} ...
      {'Helium can at SE X'} {'20K shield at SE X'} {'80K shield at SE
X'} {'OVC at SE X'} ...
      {'Ovc at SE Z'}{'Helium can at SE Y'} {'20K shield at SE Y'}];
Link=[0 1 2 3 4 5 6 7 8 9];
Write16=[{'write:00'} {'write:01'} ...
      {'write:02'} {'write:03'} ...
      {'write:04'} {'write:05'} ...
      {'w06 c/d force'} {'write:07'} ...
      {'(w08 generated signal'} {'displacement'} ...
      {'write:10'} {'write:11'} ...
      {'write:12'} {'write:13'} ...
      {'write:14'} {'write:15'}];

Write4=[{'w00 c/h force'} {'w01 velovity'} {'w02 function generator
signal'} {'w03 displacement'}];
t=[0:(Ns-1)]*dTs;
fH=1/dTs/2;
f=linspace(0,1,Ns/2)*fH;

fz=12;              %Font Size
pz=[50 50 560 420];     %gcf position
a=1;
b=0.015;
az1=[0.1300    0.5811+b    0.7750    0.3439*a];
az2=[0.1300    0.1100+b    0.7750    0.3439*a];

%%%%%%%%%%%%%%%
Dt0=0;                  %Second
Dt1=8;                  %dTs*(Ns-600);
Df0=1;                  %Hz
Df1=99;
%%%%%%%%%%%%%%%
NDt0=1+floor(Dt0/dTs);
NDt1=min(1+floor(Dt1/dTs),Ns);

NDf0=1+floor(Df0/fH*Ns/2);
NDf1=1+floor(Df1/fH*Ns/2);

%%%%%%%%%%%%%5
for nFrq=Frq
      sFrq=nFrq{:};
   if Sufix=='H'
         sFrq='';
      end
for nIdx=Idx
   Name=[SPath Prefix nIdx{:} Sufix sFrq '.mat'];
```

```
load([Name]);
x=x(1:Ns,:);
[nx mx]=size(x);
nnIdx=str2num(nIdx{:});
for nRef=IRef
   if (nnIdx>6 & nnIdx<18)
      if nRef==9
         nRef=3;
      elseif nRef==6
            nRef=0;
      end
      write=Write4{nRef+1};
      Unit=Unit4;
   else
      write=Write16{nRef+1};
      Unit=Unit16;
   end

   if nRef<=mx
         x2=x(1:Ns,nRef+1)*Unit(nRef+1);
      FFT=fft(x2);
         Fx=abs(FFT)/Ns*2;
         Ax=angle(FFT);

      iPlot=iPlot+1;

      figure(iPlot)
               set(gcf,'Position',pz);
      subplot(2,1,1)
         Pk=max(x2)-min(x2);
      plot(t(NDt0:NDt1),x2(NDt0:NDt1))
      set(gca,'TickDir','out',...
         'FontSize',fz)
      if Chaz=='y'
         set(gca,'Position',az1)
      end

      if findstr(lower(Name), lower(SPath))>0
         sName=Name(length(SPath)+1:length(Name));
      else
         sName=Name;
      end

      title([Symbol{nnIdx} ...
            ],'FontSize',fz);
         xlabel(['time (s) ' ],'FontSize',fz)
      ylabel('micrometer','FontSize',fz);
         [Y I]=max(Fx(NDf0:NDf1));
         AxD=Ax(NDf0:NDf1)*180/2/pi;
         subplot(2,1,2)
      set(gca,'TickDir','out','FontSize',fz)
      if Chaz=='y'
         set(gca,'Position',az2)
      end
         plot(f(NDf0:NDf1),Fx(NDf0:NDf1))
      set(gca,'TickDir','out','FontSize',fz)
      xlabel('frequency (Hz)','FontSize',fz)
```

```
          ylabel('micrometer','FontSize',fz);
             text(f(I+NDf0),Y,['a=' ...
                   num2str(Fx(I+NDf0-1),'%1.2f')...
                ', f=' num2str(f(I)+Df0,'%1.2f')]...
             ,'FontSize',fz)
             Dn01=max(Fx)-min(Fx);

figure(20)
iPlot
subplot(2,2,iPlot)
             Pk=max(x2)-min(x2);
          plot(t(NDt0:NDt1),x2(NDt0:NDt1))
          set(gca,'Xlim',[t(NDt0) t(NDt1)])
          set(gca,'TickDir','out',...
             'FontSize',fz)
          if Chaz=='y'
%              set(gca,'Position',az1)
          end

          if findstr(lower(Name), lower(SPath))>0
             sName=Name(length(SPath)+1:length(Name));
          else
             sName=Name;
          end

          title([Symbol{nnIdx} ...
             ],'FontSize',fz);
          if iPlot>2
             xlabel(['time (s) ' ],'FontSize',fz)
          end

             ylabel('micrometer','FontSize',fz);
             [Y I]=max(Fx(NDf0:NDf1));
             AxD=Ax(NDf0:NDf1)*180/2/pi;

          figure(40)
          subplot(2,2,iPlot)
          set(gca,'TickDir','out','FontSize',fz)
          if Chaz=='y'
%              set(gca,'Position',az2)
          end
             plot(f(NDf0:NDf1),Fx(NDf0:NDf1))
          set(gca,'TickDir','out','FontSize',fz)
          title([Symbol{nnIdx} ...
             ],'FontSize',fz);
          if iPlot>2
             xlabel('frequency (Hz)','FontSize',fz)
          end

          ylabel('micrometer','FontSize',fz);
             text(f(I+NDf0),Y,['a=' ...
                   num2str(Fx(I+NDf0-1),'%1.2f')...
                ', f=' num2str(f(I)+Df0,'%1.2f')]...
             ,'FontSize',fz)
             Dn01=max(Fx)-min(Fx);

             end
```

```
      end


end
end   %for nNFrq
```

H.5.10 NmrCross.m

```
%%%%%%%%%%%%%%%%%%%%%%%%%%%%%%%%%%%%%%%%%%%%%%%%
% Cross-correlation for Data Synchronization    %
%%%%%%%%%%%%%%%%%%%%%%%%%%%%%%%%%%%%%%%%%%%%%%%%
clear;clc;close all
%%%%%%%%%%%%%%%%%%%%%%%%%%%%%%%%%%%%%%%
Save='n';             % save file in the Destination path?
SourcePath='..\data\NMR\dtbmat\';
DestinationPath='..\data\NMR\dtbdly\';
%%%%%%%%%%%%%%%%%%%%%%%%%%%%%%%%%%%%%%%%%%%%%%%%%%%%%%%
% the following three lines define a data file        %
% names which is composed of  strings given by        %
% Fname, Period and     one of Frq
     %
%%%%%%%%%%%%%%%%%%%%%%%%%%%%%%%%%%%%%%%%%%%%%%%%%%%%%%%
Fname='Dtb';          % 'D' or other prefixes of data files
Period='*';           % 1,2,3... or * (all).
Frq=[ {'08'} {'19'} {'39'}];  %frequencies

dTs=0.002;            %sampling rate (second)
for nFrq=Frq
RefFile=[Fname  '01F' nFrq{:} '.mat']; %Reference files
DFile=[Fname Period 'F' nFrq{:} '.mat'];
OtherFiles=dir([SourcePath DFile]);
NF=length(OtherFiles);
Ns1=1024;
load([SourcePath RefFile]);
x01=x;
[nx mx]=size(x);
if mx>6
   IRef=6;
else
   IRef=0;
end
Nf0=10;
x1=x(1:Ns1,IRef+1);
t=[0:(length(x)-1)]*dTs;
Fx=abs(fft(x1));
Ns=Ns1;%length(Fx);
fH=1/dTs/2;
f=linspace(0,1,Ns/2)*fH;
[Y I]=max(Fx(Nf0:Ns/2));
f1=f(Nf0+I-1);
t1=1/f1
```

```
tic
for n=1:NF
   Name=OtherFiles(n).name;
   if findstr(lower(Name), lower(SourcePath))>0
      sName=Name(length(SourcePath)+1:length(Name));
   else
      sName=Name;
   end

   load([SourcePath sName]);

   [nx mx]=size(x);
      if mx>6
         IRef=6;
      else
      IRef=0;
      end

      %x02=x;
      x2=x(1:Ns1,IRef+1);
   Fx=abs(fft(x2));
      [Y I]=max(Fx(Nf0:Ns/2));
   f2=f(Nf0+I-1);
   t2=1/f2

      [c l]=xcorr(x1,x2);
      [Y I]=max(c);
   Delay=l(I)*dTs
   if Save=='y'
      save([DestinationPath sName],'x','Delay');
   end

end
end
```

H.5.11 NmrPg.m

```
%%%%%%%%NMRPG.m %%%%%
% Display real signal and its FFT, Recover
% spectrum from the undersampled signals. %
%%%%%%%%%%%%%%%%%%%%%%%%
%figure;plot(1,1);xlabel(['VB000=' VB 'Adjust=' Adjust 'test=' Test
'Ts1=' num2str(Ts1) 'FPath=' FPath Fname]);pause

VB = 'n';

if VB~='y'
      clear all
      clc
   close all
   VB='n';
      %%%%%%%%%%%%%%%%%%%%%%%%
```

```
      Rectify1='n';
   Adjust='y';
   Test='n';
      Plot='y';
      PlotSample='y'
      Ts1=0.197;
      Ts2=0.198;
   stepT=0.05;
   Ntest=256*8
   if Adjust=='y'
      Ftest=[0:stepT:60];
   else
      Ftest=[ 20.9 30 60];% 8 9 17 18 19 20 21 37 38 39 40 41];
      Ftest=[50];
   end
      FSch0(1,:)=[0.0   0.2   0.45];
      FSch1(1,:)=[0.5   0.3   0.5];
      FSch0(2,:)=[0.0   0.2   0.45];
      FSch1(2,:)=[0.5   0.3   0.5];
end
%stepT=Ftest(2)-Ftest(1);
TR=[Ts1 Ts2]*1000;
dTs=Ts2-Ts1;
Fs1=1/Ts1;
Fs2=1/Ts2;
NFtest=length(Ftest);
nFf0=1;

LFS=length(FSch0(1,:));
PFS=zeros(2,LFS);
IFS=PFS;
Fs=Fs1;

if VB~='y'
      if Test~='y'
            FPath='f:\beam\mat\';
            Fname='pghead1';
      load([FPath Fname]);
   end
end

%%%%%%%%%%%%%%%%%%%%%
LFtest=length(Ftest);
if LFtest>30
   Plot='n';
end

%%%%test sampling%%%%%
if Test=='y'
   Fname=num2str(Ftest,'%2.1fHz ');
   clear('phase');
      Row=Ntest;
   phase=zeros(Row,3);
   tt=[1:Row]';
   Tnoise=zeros(Row,1);
   N=50;
   for n=1:N
```

```
      Tnoise=Tnoise+rand(Row,1);
      end
   Tnoise=(Tnoise/N*-0.5);

   Anoise=0;
      for f0=Ftest
      phase(:,1)=phase(:,1)+sin(2*pi*f0*Ts1*tt)+Anoise*Tnoise;
      phase(:,2)=phase(:,2)+sin(2*pi*f0*Ts2*tt)+Anoise*Tnoise;
   end
   phase(:,3)=sin(2*pi*0.02*tt);
end   % if Test=='y'

%%%%%%%%%%%%%%%%%%%%%%
Ntest=' num2str(Ntest) ' Ftest=' num2str(888) ' plot=' Plot]);pause
%%%%%%%%%%%%%%%%%%%%%%%%%%%%%%
if Adjust=='n'
Row=length(phase);
tt=[1:Row]';
Ntest=Row;
Nt=min(Row,300);
LW=2;
F=linspace(0,1,Row);%*pi;
nF0=1;
nF1=min(Row/2);
   RowFcal=1;
      Fcal=zeros(RowFcal,LFS);
nFSch0=fix(1+FSch0*nF1*2);
nFSch1=fix(FSch1*nF1*2);
      if Plot=='y'
            figure
      end
   for n=1:2;
            xFF=fft(phase(:,n));
            xF=abs(xFF)/Ntest*2;
         if Plot=='y'
            subplot(LW,1,n)
            plot(F(nF0:nF1),xF(nF0:nF1))
         end

         for m=1:LFS
               [PFS(n,m) I]=max(xF(nFSch0(n,m):nFSch1(n,m)));
            I=I+nFSch0(n,m)-1;
            IFS(n,m)=I/Ntest;%F(I);
            if Plot=='y'
                     text(IFS(n,m),PFS(n,m),[char(96+m) ...
                     num2str(IFS(n,m),'%1.3f')],...
                  'Color','k','Fontsize',12)
            end
            end %end m
            if Plot=='y'
               set(gca,'TickDir','out','Fontsize',12)
            title([Fname ': FFT of pahse angle' ...
            '(T_R_' num2str(n,1) '=' ...
            num2str(TR(n),3) 'ms)'],'Fontsize',13)
            end % end of if Plot
      end         %end n
```

```
      M=0;
      F0=zeros(2*M+1,LFS);
      sF0='';
      for m=-M:M
         Ff0=abs((IFS(2,:)-IFS(1,:)+m)...
         /(Ts2-Ts1));
         F0(m+M+1,:)=Ff0;
         for n=1:LFS
               sF0=[sF0 char(96+n) num2str(abs(F0(m+M+1,n)),...
               ' %4.2f; ')];
         end
   end %m
      nFf0=nFf0+1;
      if Plot=='y'
            xlabel(['The recovered frequencies: ' sF0 '(Hz)'],...
         'Color','r')
      end
   if PlotSample=='y'
         figure
      subplot(2,1,1)
         plot(tt(1:Nt),phase(1:Nt,1),'b')
         title([Fname ': Undersamplings' ...
           ' (TR1=' num2str(Ts1*1000,3) 'ms)'],...
            'FontSize',13)
      set(gca,'FontSize',12)

         subplot(2,1,2)%   hold on
            plot(tt(1:Nt),phase(1:Nt,2),'r')
      title([Fname ': Undersamplings' ...
            ' (TR2=' num2str(Ts2*1000,3) 'ms)'],...
         'FontSize',13)
            xlabel(['Sampling Points ( the real number of samplings='
...
            num2str(Ntest) ' )'],'FontSize',12)
      set(gca,'FontSize',12)
      end %PlotSample
end %if Adjust=='n'
%num2str([Ftest Fcal],'%02.2f\n ')

Ntest=' num2str(Ntest) ' Ftest=' num2str(888) ' plot=' Plot]);pause

%%%%%%%%%%%%%%%%%%%%%%%%%%%%%%%%%%%%%%%%%%%%
%%%% Spectrum rectifying
%%%%%%%%%%%%%%%%%%%%%%%%%%%%%%%%%%%%%%%%%%%%

if Adjust=='y'
      Delta01=zeros(1,NFtest);
      Delta02=zeros(1,NFtest);
      f1=zeros(1,NFtest);
      f2=zeros(1,NFtest);
      Row=Ntest;
   phase=zeros(Row,3);
   tt=[1:Row]';
   FS=zeros(1,2);
   nFf0=1;
   Fcal=zeros(1,NFtest);
   for f0=Ftest
```

```
                phase(:,1)=sin(2*pi*f0*Ts1*tt);
                phase(:,2)=sin(2*pi*f0*Ts2*tt);
            for n=1:2;
        Fname=num2str(f0,'%2.1fHz ');
                xFF=fft(phase(:,n));
                xF=abs(xFF)/Ntest*2;
              [Y I]=max(xF(1:Ntest/2-1));
        FS(n)=I/Ntest;%F(I);
    end
    Ff0=abs((FS(2)-FS(1))/(Ts2-Ts1));
    Fcal(nFf0)=Ff0;
          a=Ts1*f0;
          Delta01(nFf0)=a-fix(a);
          a=Ts2*f0;
          Delta02(nFf0)=a-fix(a);
          f1(nFf0)=FS(1);
          f2(nFf0)=FS(2);
          Ff00=(FS(2)+FS(1))/(Ts2-Ts1);
          Ff01=(1-FS(2)-FS(1))/(Ts2-Ts1);
%%%%%%%%%%%%%%%%%%%%%5
%%%% Rectify frequencies

          if Rectify1=='y'
             k=0;flag1=1;flag2=1;
             n1=2;
             while n1<=NFtest
                fa=Ftest(n1);
                while (fa<=k/Ts1) & (fa>=k/Ts2)
                   Fcal(n1)=Ff00(n1);
                   n1=n1+1;
                   if n1>NFtest,break,end
                      fa=Ftest(n1);
             end

                while (fa<=(k+0.5)/Ts1) & (fa>=(k+0.5)/Ts2)
                   Fcal(n1)=Ff01(n1);
                   n1=n1+1;
                   if n1>NFtest,break,end
                      fa=Ftest(n1);
             end

                if fa>(k+0.5)/Ts1
                k=k+1;
                else
                   n1=n1+1;
                end
             end
    end %if Rectify
    nFf0=nFf0+1;
    end % f0
    %%%%%%%%%%%%%%%%%%%%%%%%%%%%%%%%%%%%%%%%%%%%
    % Plot recovery of frequency
    %%%%%%%%%%%%%%%%%%%%%%%%%%%%%%%%%%%%%%%%%%%%
    k0=0;
    k1=0;
    figure
    set(gca,'Fontsize',12)
```

```
        set(gca,'XLim',[0 Ftest(NFtest)],...
           'YLim',[0 Ftest(NFtest)]);
        %plot(Ftest,[Ftest; Ftest*k0-k1;Fcal])
        plot(Ftest,Ftest,'g','LineWidth',1.5)
        hold on
    plot(Ftest,Fcal,'b')

        title(['Recovery of frequency from
undersamplings'],'FontSize',13)
        legend('original frequency','calculated frequency')
        xlabel(['frequency (Hz) (Sampling points=' ...
              num2str(Ntest) ', T_R_1=' ...
              num2str(TR(1),'%3.0fms') ', T_R_2=' ...
              num2str(TR(2),'%3.0fms') ')'],'FontSize',12)
        ylabel('frequency (Hz)','FontSize',12)

        %%%%%%%%%%%%%%%%%%%%%%%%%%%%%%%%%%
        %%%%%%%%%%%%%%%%%%%%%%%%%%%%%%%%%%
        N=length(Fcal);
        m=0;
        %%%%%%%%%%%%%%%%%%%%
figure
        subplot(2,1,1)
        plot(Ftest,Delta01,'g','LineWidth',1.5)
        hold on
        plot(Ftest,f1,'b')

        subplot(2,1,2)
        plot(Ftest,Delta02,'g','LineWidth',1.5)
        hold on
        plot(Ftest,f2,'b')
        %%%%%%%%%%%%%%%%%%%%%%%%%%%%%%%%%%%%%%%%%%%
end %if Adjust=='n'

Ntest=' num2str(Ntest) ' Ftest=' num2str(Ftest) ' plot=' Plot]);
```

H.5.12 NmrShift.m

```
%%%%%%%%%%%%%%% NMRshift.m%%%%%%%%%%%%%%%%%%%%%%%%%%%%%%%%%%
%      Phasse shift between two measurements for example      %
%      for exp.  Hecan and 20K or Hecan13 and Hecan11  %
%%%%%%%%%%%%%%%%%%%%%%%%%%%%%%%%%%%%%%%%%%%%%%%%%%%%%%%%%%%%%%
clear;clc;close all
%%%%%%%%%%%%%%%%%%%%%%%%%%%%%%%%%%%%
Save='n';          % save file in TPath?
SourcePath='..\data\NMR\mat\Adjusted\';
%%%%%%%%%%%%%%%%%%%%%%%%%%%%%%%%%%%%%%%%%%%%%%%%%%%%%%%%%%%%%%
% first file name is ['D' F1{n} 'F' Ff{m} '.mat'];     %
% second file name is ['D' F2{n} 'F' Ff{m} '.mat'];    %
%%%%%%%%%%%%%%%%%%%%%%%%%%%%%%%%%%%%%%%%%%%%%%%%%%%%%%%%%%%%%%
```

```
IRef=9;                                                    %channel to be
compared
Ff=[{'08'} {'19'} {'39'}];     %frequencies
%periods for first source files
F1=[{'1'} {'2'} {'3'} {'1'} {'5'} {'3'}];
%periods for second source files
F2=[{'5'} {'6'} {'7'} {'2'} {'6'} {'4'}];
%corresponding prompts
SN=[{'He13'} {'20K13'} {'He43'} {'20K43'} ...
   {'He11'} {'20K11'} {'He41'}];

%%%%%%%%%%%%%%%
dTs=0.002;          %sampling period
fH=1/dTs/2;
Dt0=0;                      %Second
Dt1=7.5;
Df0=1;                      %Hz
Df1=100;
NF=length(F1);

for m=1:3
      for n=1:NF
      %   n,toc
      SFname1=['D' F1{n} 'F' Ff{m} ...
            '.mat'];
      load([SourcePath SFname1])
      x1=x(:,IRef+1);
      SFname2=['D' F2{n} 'F' Ff{m} ...
            '.mat'];
      load([SourcePath SFname2])
      x2=x(:,IRef+1);
      clear x;
      Len=min(length(x1),length(x2));
      x1=x1(1:Len);
      x2=x2(1:Len);
            [c l]=xcorr(x1,x2);
            [Y I]=max(c);
         Delay=l(I)*dTs

      %%%%%%%%%%%%%%%
Ns=Len-1;
t=[0:(Ns-1)]*dTs;
f=linspace(0,1,Ns/2)*fH;
NDt0=1+floor(Dt0/dTs);
NDt1=1+floor(Dt1/dTs);
NDf0=1+floor(Df0/fH*Ns/2);
NDf1=1+floor(Df1/fH*Ns/2);
NDt0=min(NDt0,Ns);
NDt1=min(NDt1,Ns);
NDf0=min(NDf0,Ns/2);
NDf1=min(NDf1,Ns/2);


      %%%%%%%%%%%Plot%%%%%%%%%%
      FFT=fft(x1);
      Fx=abs(FFT);
      Ax=angle(FFT);
```

```
        figure
        subplot(2,1,1)
        Pk=max(x1)-min(x1);
        plot(t(NDt0:NDt1),x1(NDt0:NDt1))
        k1=str2num(F1{n});
        k2=str2num(F2{n});
        title([SN{k1} '~' SN{k2}])
        [Y I]=max(Fx(NDf0:NDf1));
        AxD=Ax(NDf0:NDf1)*180/2/pi;
        frq=f(I)+Df0;
        xlabel(['time (s)' ...
              ', pk-pk=' num2str(Pk) ...
              ',A=' num2str(Fx(I+NDf0-1)) ...
              ',f=' num2str(frq,3)])
        FFT=fft(x2);
        Fx=abs(FFT);
        Ax=angle(FFT);
        subplot(2,1,2)
        Pk=max(x2)-min(x2);
        plot(t(NDt0:NDt1),x2(NDt0:NDt1))
        [Y I]=max(Fx(NDf0:NDf1));
        AxD=Ax(NDf0:NDf1)*180/2/pi;
        frq=f(I)+Df0;
        sft=mod(Delay,1/frq);
        xlabel(['pk-pk=' num2str(Pk) ...
              ',A=' num2str(Fx(I+NDf0-1)) ...
              ', f=' num2str(frq) ...
              ', T=' num2str(1/frq,4) ...
              ',delay=' num2str(Delay) ...
              ',shift=' num2str(sft)])
        end
end
```

H.5.13 OmtFieldMap.m

```
%%%%OMT Magnetic Field Distribution Calculation%%%%%%%%
%%% File Name OMTField3
clc
clear
close all
%%%%%%%%%%%%%%%%%%%%%%%

SPath='..\data\homo\kufu\';
SFname='70421.dat';
SFile1='a70400.dat'; %D2f39.mat';
SFile2='aD3f08.mat'; %'D3f39.mat';
SFile3='aD4f08.mat'; %'D4f39.mat';
O1=dir([SPath SFile1]);
O2=dir([SPath SFile2]);
O3=dir([SPath SFile3]);
```

```
Files=dir([SPath SFname]);
Files=[Files;O1;O2;O3];
NF=length(Files);

Magnet=zeros(1,NF);
PkPk=Magnet;
Phase=zeros(NF,5);
if findstr(lower(Files(1).name),...
      lower(SPath))
   SPath='';
elseif NF<1
   'NO File !!!'
   pause
end

%%%%%%%%%%%%%%%%%%%%%%%%%%%%%%%%%%%
Col=[1 2 3 4 5 6 7 8 9 10 ...
      11 11 11 11 11 11 11 11 11 11 ...
      11 11 11 11];
A=zeros(24,11);
B=A;
nL=24;
mL=11;
%%%%%%%%%%%%%%%%%%%%%%%%%%%%%%%%%%%
%%%%%%%%%%%%%%%%%%%%%%%%%%%%%%%%%%%
%%%%%%%%%%%%%%%%%%%%%%%%%%%%%%%%%%%
GyatY=zeros(1,NF);
GxatY=GyatY;
GzatY=GyatY;
GxatX=GyatY;
GyatX=GyatY;
GzatX=GyatY;
GxatXm=GyatY;
GyatXm=GyatY;
GzatXm=GyatY;
%%%%%%%%%%%%%%%%%%%%%%%%%%%%%%%%%%%
%%%%%%%%%%%%%%%%%%%%%%%%%%%%%%%%%%%
tic
for nFile=1:NF

   Name=Files(nFile).name;
   Fid=fopen([SPath Name]);
   if Fid==-1
          ['File ' SFname ' is not found!!!']
       pause
    end     %if Fid==-1

    n=findstr(Name,'70');
    l=length(Name);
    Magnet(nFile)=str2num(strtok(Name(n:l),'.'));
      for nR=1:161
            s=fgets(Fid);
      end                          %Block Lengrh
   [T R]=strtok(s,':');
      [T R]=strtok(R,' ');
      [T R]=strtok(R,' ');
   PkPk(nFile)=str2num(T);
```

```
      for nR=1:10
            s=fgets(Fid);
      end   %for nR=1:10            %Block Length
   for nR=1:24
      for mR=1:Col(nR)
         s=fgets(Fid);
         a=str2num(s(15:25));
         A(nR,mR)=a;
         b=str2num(s(43:55));
         B(nR,mR)=b;
      end   %for mR=1:Col(nR)

      s=fgets(Fid);
            s=fgets(Fid);
      s=fgets(Fid);

   end      %for nR=1:24


%%%%%%%%%%%%%%%%%%%%%%%%%%
%
% Legendre Polynomials
%
%%%%%%%%%%%%%%%%%%%%%%%%%%

RunTest='n';
PlotField='y';
PlotGradient='y';
PlotR='y';
PlotTheta='y';
PlotPhi='y';
Plotor70='n';
Degree_a=24;      %degree of field in axial direction
Degree_r=11;            %degree of field in radial direction
R0=1;%0.25;
Phi=pi/2;
ThetaForR=pi/2;

%%%%%%%% B vs theta %%%%%%%%%
if PlotTheta=='y'
stepTheta=0.01;
Theta=[-1:stepTheta:1]*pi;
R=[0.01 0.1 0.2 0.25]';

Mu=cos(Theta);

Bz=zeros(length(R),length(Mu));
Br=Bz;

for n=1:Degree_a              %for m=0; n=1~18
   Pmn=legendre(n-1,Mu);
   Rx=(R/R0).^(n-1);
   for m=1:Col(n)

%      if A(n,m)==0 | B(n,m)==0
            Bz=Bz+Rx*Pmn(m,:)*...
         (A(n,m)*cos((m-1)*Phi)+...
```

```
                    B(n,m)*sin((m-1)*Phi));
  %     end

    end       %for m=1:Col(n)

 end   %for n=1:Degree_a

 L=length(R);
 for n=1:L
    sR{n}=['radius ' num2str(R(n),'%0.2f') 'm'];
 end   %for n=1:L

 if PlotField=='y'
 figure
 plot(Theta,Bz)
 legend(sR{:})
 title(Magnet(nFile))
 ylabel('Magnetic fields (ppm)')
 xlabel(['colatitude angle \theta,  pk-pk=' ...
       num2str(max(Bz')-min(Bz'),'%5.1f    ')])
 end   %if PlotField=='y'
 %%%%%%%%% Gradient vs theta %%%%%
 %gradient at theta1
 %%%%%%%%%%%%%%%%%%%%%%%%%%%%%%%%
 for n=1:L
    g=diff(Bz')';
    GrdBz(n,:)=g(n,:)/(stepTheta*pi*R(n));
 end   %for n=1:L
 LBr=length(g);
 %Theta=[-1:stepTheta:1]*pi;
 ii=floor(length(Theta)*(0.5+0.25));
 GzatY(nFile)=GrdBz(ii);

 if PlotGradient=='y'

 figure
 plot(Theta(1:LBr),GrdBz)
 legend(sR{:})
 [Grdmax I]=max(GrdBz,[],2);
 %text('');
 title(Magnet(nFile))
 ylabel('Magnetic gradient (ppm/m)')
 xlabel(['colatitude angle \theta, max=' ...
    num2str(Grdmax','%5.1f    ')])
 for n=1:L
    text(Theta(I(n)),Grdmax(n),...
          [' ' num2str(Grdmax(n),'%5.1f    ')])
 end   %for n=1:L
 end   %if PlotGradient=='y'
 end   %if PlotTheta=='y'


 %%%%%%%%%%%%%%%%%%%%%%%%%%%%
 %%%%%%%%% B vs radius %%%%%
 %%%%%%%%%%%%%%%%%%%%%%%%%%%%
 if PlotR=='y'
 Theta=pi/2*0;     %ThetaForR;% pi/4 pi/2];
```

```
Phi=0;
StepR=0.002;
R=[0:StepR:.25]';
Mu=cos(Theta);


Bz=zeros(length(R),length(Mu));
Br=Bz;
G=Bz;
Gr=G;

for n=1:Degree_a                % for m=0,1
   Pmn=legendre(n-1,Mu);
   Rx=(R/R0).^(n-1);
   Gx=(n-1)./R0.*(R/R0).^(n-2);
   for m=1:Col(n)
 %     if A(n,m)~=0 | B(n,m)~=0

            Bz=Bz+Rx*Pmn(m,:)*...
          (cos((m-1)*Phi)*A(n,m)+...
          sin((m-1)*Phi)*B(n,m));
            Gr=Gr+Gx*Pmn(m,:)*...
          (cos((m-1)*Phi)*A(n,m)+...
          sin((m-1)*Phi)*B(n,m));
  %    end
   end       %for m=1:Col(n)
end   %for n=1:Degree_a

%%GGG
GyatY(nFile)=Gr(floor(0.2/StepR));

if RunTest=='y'
%%%%%%%%%test
figure
L=length(Theta);
for n=1:L
   g=diff(Bz);
   GrdBz(n,:)=g(n,:)/StepR;
end   %for n=1:L
LBr=length(g);

plot(R(1:LBr)*100,-g/StepR)%GrdBz(1:LBr))
title(Magnet(nFile))
%%%%%%%%%test%%%%%%%%%
end   %if RunTest=='y'

N=length(R);
if PlotField=='y'
figure
plot(R*100,Bz')
ylabel('magnetic field (ppm)')
axis([0 R(N)*100 min(Bz) max(Bz)]);
set(gcf,'Position',[0 0 450 300])
title([Magnet(nFile) ...
      '(\phi=' num2str(Phi*180/pi,'%2.1f^o ') ...
      ',max=' num2str(max(Bz),'%4.0f') ...
      ',min=' num2str(min(Bz),'%5.1f   ') ')'])
```

```
end   %if PlotField=='y'

if PlotGradient=='y'
figure;%%%Gradien
plot(R*100,Gr')
ylabel('magnetic gradient (ppm/m)')
axis([0 R(N)*100 min(Gr) max(Gr)]);
set(gcf,'Position',[0 0 450 300])%250])
title([Magnet(nFile) ...
      '(\phi=' num2str(Phi*180/pi,'%2.1f^o ') ...
      ',max=' num2str(max(Gr),'%5.1f   ') ...
      ',min=' num2str(min(Gr),'%5.1f   ') ')'])
Y=Gr(floor(0.2/StepR));
text(20,Y,['\leftarrow' num2str(Y,'%5.1f   ')])
end   %if PlotGradient=='y'
end   %if PlotR=='y'

%%%%%%%%%%%%%%%%%%%%%%%%%
%%%%%%%% B vs Phi %%%%%%%%%
%%%%%%%%%%%%%%%%%%%%%%%%%
if PlotPhi=='y';

StepPhi=0.01;
Phi=[-1:StepPhi:1]*pi;
R=[0.01 0.1 0.2 0.25]';
%R=[0.2]';
Theta=pi/2;
Mu=cos(Theta);
Bz=zeros(length(R),length(Phi));
Br=Bz;

for n=1:Degree_a              %for m=0; n=1~18

   Pmn=legendre(n-1,Mu);
   Rx=(R/R0).^(n-1);
   for m=1:Col(n)
      Bz=Bz+Rx*Pmn(m,:)*...
         (cos((m-1)*Phi)*A(n,m)+...
         sin((m-1)*Phi)*B(n,m));
   end      %for m=1:Col(n)

end   %for n=1:Degree_a

L=length(R);
for n=1:L
   sR{n}=['radius ' num2str(R(n),'%0.2f') 'm'];
end

if PlotField=='y'
figure
plot(Phi,Bz)
legend(sR{:})
title([Magnet(nFile) ...
      '\theta=' num2str(Theta*180/pi,...
      '%2.1f^o ')])
ylabel('Magnetic fields (ppm)')
xlabel(['longitude angle \phi,  pk-pk=' ...
```

```
      num2str(max(Bz')-min(Bz'),'%5.1f    ')])
end   %if PlotField=='y'
%%%%%%%%% Gradient vs theta %%%%%
%gradient at theta1
N=3;
for n=1:L
   g=diff(Bz')';
   GrdBz(n,:)=g(n,:)/(StepPhi*pi*R(n));
end   %for n=1:L
LBr=length(g);

%%GGG
ii=floor(length(Phi)*(0.5+0.25));
GxatY(nFile)=GrdBz(ii);

if PlotGradient=='y'

figure
plot(Phi(1:LBr),GrdBz)
legend(sR{:})
[Grdmax I]=max(GrdBz,[],2);
%text('');
Magnet(nFile)
title(['*' Magnet(nFile) ' (theta=' ...
      num2str(Theta*180/pi,'%2.1f^o )')])
ylabel('Magnetic gradient (ppm/m)')
xlabel(['longitude angle \phi, max=' ...
   num2str(Grdmax','%5.1f    ')])
for n=1:L
   text(Phi(I(n)),Grdmax(n),...
         [' ' num2str(Grdmax(n),'%5.1f    ')])
end   %for n=1:L
end   %if PlotGradient=='y'
end   %if PlotPhi=='y';


toc

end   %for nFile=1:NF


%%%%%%%%%%%%%%%%%%%%%%%%%
if Plotor70=='y'

L=length(or70(:,1));

for n=1:NF
   a=Magnet(n);
   for m=1:L
      if or70(m,1)==a
         Phase(n,:)=or70(m,:);
      end
   end
end
L=length(PkPk);
figure
subplot(2,1,1)
```

```
plot(PkPk,'k')
subplot(2,1,2)
plot(Phase(:,2),'r')
end
```

H.5.14 PhaseCal.m

```
%%%%%%%%%%%%%%%%%%%%%%%%%%%%%%%%%%%%%%%%%%%%
%     Calculate phase distortion
%from He can vibration                                    %
%%%%%%%%%%%%%%%%%%%%%%%%%%%%%%%%%%%%%%%%%%%%
clear
clc
close all
%%%%%%%%%%%%%%%%%%%%%%%%%%%%%%%%%%%%%%%%%%%%
Test='n';
SPath='..\data\NMR\dmat\';
SSPath=SPath;
TPath='';
Delay=0;
dTs=0.002;          %sampling period
if Test=='y'
   dTs=0.002;
end

Ns=4096;

Unit=[1 1 1 20 1 1 1 1 1 20 1 1 1 1 1];

Prefix='D';
Sufix='F59';              %'H' or 'F'
sFrq='';
Idx=[{'2'}];% {'2'} {'7'}];
Symbol=[{'He13'} {'20K13'} {'He43'} {'20K43'} ...
      {'He11'} {'20K11'} {'He41'}];
Write16=[{'write:00'} {'write:01'} ...
      {'write:02'} {'write:03'} ...
      {'write:04'} {'write:05'} ...
      {'w06 c/d force'} {'write:07'} ...
      {'(w08 generated signal'} {'displacement'} ...
      {'write:10'} {'write:11'} ...
      {'write:12'} {'write:13'} ...
      {'write:14'} {'write:15'}];

IRef=1;     %Index Displacement

t=[0:(Ns-1)]*dTs;
fH=1/dTs/2;
f=linspace(0,1,Ns/2)*fH;
```

```
%%%%%%%%%%%%%%%
TE=0.04;
Ts1=0.191;
Ts2=0.192;
TR=[Ts1 Ts2]*1000;
Nph=256;
Nsmp1=Ts1/dTs;
Nsmp2=Ts2/dTs;
Kdis=1.0;
B0=1.5;                                 %Static field (Tesla)
Grd0=672/0.232;                         %Gradient (ppm/m)
Grd=B0*Grd0*1e-6;
Gyro=2.675e8;
   theta1=zeros(1,Nph);
   theta2=theta1;
   NTEh=floor(TE/dTs/2);
   t1=[0:Nph-1]*Ts1;
   t2=[0:Nph-1]*Ts2;
%%%%%%%%%%%%5
Unit=20e-6;
step=Ns*dTs;
%%% Test
disT=5;                 %micrometers
disV=disT/20;     %Voltage
fT=8;                   %Hz
wT=2*pi*fT;       %Radian
tT=[0:dTs:50]';
alfaT=pi/2*0.8;
K0=Gyro*Kdis*Grd*Unit*180/pi;

if Test=='y'
   NF=1;
   Name='Test';
   [{'The  possible maximum value of phase distortion'};...
         {num2str(8*disV*K0/wT,'%3.2f (degrees)')}]

end

%%% Test
for nIdx=Idx
   nnIdx=str2num(nIdx{:});
   if Test=='n'
      Name=[Prefix nIdx{:} Sufix ...
            sFrq '.mat'];
      load([SSPath Name]);
         x2=x(1:Ns,IRef+1);
      [nx mx]=size(x);
         x2=[x2;x2;x2;x2;x2;x2;x2];
      else
         x2=disV*sin(wT*tT+alfaT);  %Voltage
   end
      dB=(x2);
      NdB=length(dB);

   for nP=1:Nph
      mx1s=floor(mod((nP-1)*Nsmp1,NdB))+1;
      mx2s=floor(mod((nP-1)*Nsmp2,NdB))+1;
```

```
        theta1(nP)=(sum(dB(mx1s+NTEh:mx1s+NTEh*2-1))-...
            sum(dB(mx1s:mx1s+NTEh-1)))*K0*dTs;
        theta2(nP)=(sum(dB(mx2s+NTEh:mx2s+NTEh*2-1))-...
            sum(dB(mx2s:mx2s+NTEh-1)))*K0*dTs;
    end
    pK1=max(theta1)-min(theta1);
    pK2=max(theta2)-min(theta2);

    if findstr(lower(Name), lower(SPath))>0
      sName=Name(length(SPath)+1:length(Name));
    else
       sName=Name;
    end

    figure
    subplot(2,1,1)
    plot(t1,theta1)
    xlabel(['pk-pk: ' num2str(pK1,'%3.1f') ...
          ' (Tr=' num2str(TR(1)) 'ms, Te=' ...
          num2str(TE*1000) 'ms, mag gradient=' ...
          num2str(Grd0,'%3.1fppm/m ') ')'])
    ylabel('phase angle (degree)')
    title(['Simulation of phase distortion from ' ...
          strrep(lower(sName),'.mat','') ' ' ...
       Symbol{nnIdx} ' ' Write16{IRef+1}])
    subplot(2,1,2)
    plot(t2,theta2)
    xlabel(['pk-pk: ' num2str(pK2,'%3.1f') ...
          ' (Tr=' num2str(TR(2)) 'ms, Te=' ...
          num2str(TE*1000) 'ms, mag gradient=' ...
          num2str(Grd0,'%3.1fppm/m ') ')'])
   ylabel('phase angle (degree)')
end
```

H.5.15 PhaseDtb.m

```
%%%%%%%%%%%%%%%%%%%%%%%%%%%%%%%%%%%%%%%%%%%%
% Calculate phase distortion
% from dtb matlab data                  %
%%%%%%%%%%%%%%%%%%%%%%%%%%%%%%%%%%%%%%%%%%%%
clear
clc
close all
%%%%%%%%%%%%%%%%%%%%%%%%%%%%%%%%%%%%%%%%%%%%
Gradient='y';
Test='n';
SPath='..\data\NMR\dtbmat\';
SSPath=SPath;
TPath='';
Delay=0;
```

```
dTs=0.002;          %sampling period
iPlot=0;
if Test=='y'
   dTs=0.002;
end

Ns=4096;

pKOff=[2.7 2.7 2.7  2.7 2.7 2.7 2.7  2.7 ...
       2.7 2.7 2.7  2.7 2.7 2.7 2.7  2.7 ...
       2.7 2.7 2.7  2.7 2.7 2.7 2.7  2.7 ...
       2.7 2.7 2.7  2.7 2.7 2.7 2.7  2.7 ];

IRef=[9];   %Index
Unit4=[1 5 1 20];
Unit16=[1 1 1 20 1 1 1 1 1 20 1 1 1 1 1];

Prefix='DTB';
Sufix='H';          %'H' or 'F'
Idx=[{'03'} {'04'} {'05'} ...
       {'06'} {'07'} {'08'} {'09'} {'10'} ...
       {'11'} {'12'} {'13'} {'14'} {'15'} ...
       {'16'} {'17'} {'18'} {'19'}];
Idx=[{'09'} {'13'} {'05'} {'18'}];

Frq=[{'08'} {'19'} {'39'}];
Frq=[{'08'}];

Symbol=[{'He41'} {'20K41'} {'80K41'} {'OVC41'} ...
       {'He43'} {'20K43'} {'80K43'} {'OVC43'} ...
       {'He13'} {'20K13'} {'80K13'} {'OVC13'} ...
       {'He11'} {'20K11'} {'80K11'} {'OVC11'} ...
       {'OvcZ'}{'He41'} {'20K41'}];
Link=[0 1 2 3 4 5 6 7 8 9];
Write16=[{'write:00'} {'write:01'} ...
       {'write:02'} {'write:03'} ...
       {'write:04'} {'write:05'} ...
       {'w06 c/d force'} {'write:07'} ...
       {'(w08 generated signal'} {'displacement'} ...
       {'write:10'} {'write:11'} ...
       {'write:12'} {'write:13'} ...
       {'write:14'} {'write:15'}];

Write4=[{'w00 c/h force'} {'w01 velovity'} {'w02 function generator
signal'} {'w03 displacement'}];
Unit=[1 1 1 20 1 1 1 1 1 20 1 1 1 1 1];
if Sufix=='H'
   Frq=[{''}];
end
t=[0:(Ns-1)]*dTs;
fH=1/dTs/2;
f=linspace(0,1,Ns/2)*fH;

%%%%%%%%%%%%%%%%
TE=0.04;
Ts1=0.191;
Ts2=0.192;
```

```
TR=[Ts1 Ts2]*1000;
Nph=256;
Nsmp1=Ts1/dTs;
Nsmp2=Ts2/dTs;
Kdis=1.0;
B0=1.5;                                %Static field (Tesla)
Grd0=672/0.232;                        %Gradient (ppm/m)
Grd=B0*Grd0*1e-6;
Grd10=[0:3000];                %ppm
Gyro=2.675e8;
   theta1=zeros(1,Nph);
   theta2=theta1;
   NTEh=floor(TE/dTs/2);
   t1=[0:Nph-1]*Ts1;
   t2=[0:Nph-1]*Ts2;
%%%%%%%%%%%%%5
Unit=20e-6;
step=Ns*dTs;
%%% Test
disT=5;                    %micrometers
disV=disT/20;      %Voltage
fT=8;                      %Hz
wT=2*pi*fT;        %Radian
tT=[0:dTs:50]';
alfaT=pi/2*0.8;
K0=Gyro*Kdis*Grd*Unit*180/pi;

if Test=='y'
   NF=1;
   Name='Test';
   [{'The  possible maximum value of phase distortion'};...
         {num2str(8*disV*K0/wT,'%3.2f (degrees)')}]

end
%%%%%%%%%%%%%%%%%%%%%%%%%%%%%
Nl=length(Idx);
GradA=zeros(Nl);
%%%%%%%%%%%%%%%%%%%%%%%%%%%%%
%%% Test
for nIdx=Idx
   nnIdx=str2num(nIdx{:});
   sFrq=Frq{:};          % Will be used when sine sweeping is applied
   nRef=IRef;
   if (nnIdx>6 & nnIdx<18)
      if nRef==9
         nRef=3;
      end
      write=Write4{nRef+1};
      Unit=Unit4;
   else
      write=Write16{nRef+1};
      Unit=Unit16;
   end
   if Test=='n'
      Name=[Prefix nIdx{:} Sufix ...
            sFrq '.mat'];
      load([SSPath Name]);
```

```
      x2=x(1:Ns,nRef+1);
   [nx mx]=size(x);
      x2=[x2;x2;x2;x2;x2;x2;x2];

   else
      x2=disV*sin(wT*tT+alfaT);  %Voltage
end
   dB=(x2);
   NdB=length(dB);

for nP=1:Nph
   mx1s=floor(mod((nP-1)*Nsmp1,NdB))+1;
   mx2s=floor(mod((nP-1)*Nsmp2,NdB))+1;
   theta1(nP)=(sum(dB(mx1s+NTEh:mx1s+NTEh*2-1))-...
      sum(dB(mx1s:mx1s+NTEh-1)))*K0*dTs;
   theta2(nP)=(sum(dB(mx2s+NTEh:mx2s+NTEh*2-1))-...
      sum(dB(mx2s:mx2s+NTEh-1)))*K0*dTs;
end

[Pmax Imax]=max(theta1);
[Pmin Imin]=min(theta1);
pK1=Pmax-Pmin;
theta1(Imax)=0;
theta1(Imin)=0;
OMTpK1=max(theta1)-min(theta1);
PurepK1=(pK1^2-pKOff(nnIdx)^2)^0.5;

[Pmax Imax]=max(theta2);
[Pmin Imin]=min(theta2);
pK2=Pmax-Pmin;
theta2(Imax)=0;
theta2(Imin)=0;
OMTpK2=max(theta2)-min(theta2);
PurepK2=(pK2^2-pKOff(nnIdx)^2)^0.5;
if findstr(lower(Name), lower(SPath))>0
  sName=Name(length(SPath)+1:length(Name));
else
   sName=Name;
end
figure
subplot(2,1,1)
plot(t1,theta1)
xlabel(['pk-pk:' num2str(pK1,'%3.1f, OMT pk-pk:') ...
      num2str(OMTpK1,'%3.1f')...
      ' (Tr=' num2str(TR(1)) 'ms )'])
ylabel('phase angle (degree)')
title(['Simulation from ' ...
      strrep(lower(sName),'.mat','') ' ' ...
      Symbol{nnIdx} ' ' Write16{IRef+1} ...
      ' ( Te=' num2str(TE*1000) 'ms, grad:' ...
      num2str(Grd0,'%3.0fppm/m')')])
subplot(2,1,2)
plot(t2,theta2)
xlabel(['pk-pk:' num2str(pK2,'%3.1f, OMT pk-pk:') ...
               num2str(OMTpK1,'%3.1f')...
      ' (Tr=' num2str(TR(2)) 'ms )'])
ylabel('phase angle (degree)')
```

```
    if Gradient=='y'
          PkPk=(pK1+pK2)/2;
       figure(10)
       iPlot=iPlot+1;
       subplot(2,2,iPlot)
       plot(Grd10,Grd10*PkPk/Grd0)
          title(['Phase distortion:' ...
             ' ' Symbol{nnIdx} ' ' ...
             ' ( Te=' num2str(TE*1000) 'ms, ' ...
             ')']))
       if iPlot>2
          xlabel('Magnetic gradient (ppm/m)')
       end
       GradA(iPlot)=PkPk/Grd0;
       ylabel('(degrees)')
       end
end

%%%%%%%%%%%%%%%%%%%%%%
% Magnetic gradient     %
%%%%%%%%%%%%%%%%%%%%%%
figure

plot(Grd10,Grd10*GradA(1),'g')
hold on
P1=plot(Grd10,Grd10*GradA(2),'r')
set(P1,'LineWidth',3)
hold on
plot(Grd10,Grd10*GradA(3),'--b')
hold on
plot(Grd10,Grd10*GradA(4),':k')
legend('He can PE X','He can SE X',...
   'He can PE Y','He can SE Y')

title(['Estimation of phase distortion:' ...
      ' ( Te=' num2str(TE*1000) 'ms, ' ...
      ')']))

xlabel('Magnetic gradient (ppm/m)')
ylabel('(degrees)')
```

H.5.16 Precession.m

```
%Precession of Magnetization
%dM/dt=Gama*MxB
%B0(x,y,z,t)=By*sin(theta)*ay+Bz*cos(theta)*az
%Initail values of magnetization
clc
clear
hold off
```

```
'--------START--------'
Mx=1;
My0=0;
My=My0;
Mz0=1;
Mz=Mz0;
%%%%%%%%%%%%%%
GyM=2.675e0/2;          %Gryomagnetic ratio
B0=1.5;                 %tesla
Th0=1e-3;          %Angular of rotation of the magnet
k0=1/2/pi;
Vb=120;            %Frequency of vibration
V0=2400;    %B0*GyM          %Static Speed of Angular
Vmin=1e30;%V0*k0;
Vmax=-1e30;%V0*k0;
Div=100;
dT=2*pi/V0/Div
%%%%%%%%%%%%%%%%%%%%%%%%
N=(2*pi/Vb)/dT
S1=zeros(N,1);
i=0;
t=0;
%%%%%%Calculate max and min frequencies
%V1=V0*cos(Th0)/(cos(V0t)^2+sin(V0t)^2*cos(Th0)^2)

V0t=linspace(0,2*pi,Div);
V1=V0.*cos(Th0)./(cos(V0t).^2.+sin(V0t).^2.*cos(Th0).^2);
Max_V1=max(abs(V1))
Min_V1=min(abs(V1))
dV1=Max_V1-Min_V1
T=clock;
format long;
My00=0;
Mn0=1;
Mn=Div;
while(i<N)
   i=i+1;
   Tht=Th0*sin(Vb*t);
   a=sin(Tht);
   My01=Mz0*a;
   Vy=V0*a;
   Vz=V0*cos(Tht);
   dMx=My*Vz-Mz*Vy;
   dMy=-Mx*Vz;
   dMz=Mx*Vy;
   Myy=My-My01;
   V=-(Mx*dMy-Myy*dMx)/(Mx*Mx+Myy*Myy);
   S1(i)=V;

      Mx=Mx+dMx*dT;
      My=My+dMy*dT;
      Mz=Mz+dMz*dT;

   t=t+dT;
end
'--------END--------'
[Vmax,I1]=max(S1)
```

```
[Vmin,I2]=min(S1)
dV=Vmax-Vmin
dVV=V0*(1/cos(Th0)-cos(Th0))
etime(clock,T)

h=figure(1);
h1=get(h,'Position');
set(h,'Position',[h1(1) h1(2) h1(3)*1.2 h1(4)]);
F=1:N;
plot(F,S1(1:N),'-b')
%hold on
%plot(S1,'-b')


xmin=1
xmax=N
dmax=Vmax-V0;
dmin=Vmin-V0;
ymin=V0+dmin*1.15
ymax=V0+dmax*1.15
axis([xmin xmax ymin ymax]);

title('Simulation of Bloch''s Equation');
title('')
ylabel('Angular velocity (rad)');
format short
Sdt=num2str(dT);
Fqc=num2str(V0);
xlabel(['(\theta_0=' num2str(Th0) ...
      'rad, \Omega=' num2str(Vb) ...
      'rad, \omega=' num2str(V0) ...
      'rad)' '    X-axis:sampling points of time'] ...
   );
s=[num2str(V0) '+' num2str(dmax)];

text(I1+10,Vmax+0.05*dmax,s,'FontSize',12);
s=[num2str(V0) '-' num2str(-dmin)];
text(I1+10,Vmin+0.05*dmin,s,'FontSize',12);
d=2*pi/V0/dT/2;
x0=I1-d/2
xe=I1+d
S=S1(x0:xe);
[y1,x1]=min(abs(S-V0));
x1=x1+x0-1
y1
S=S1((x1+d/10):xe);
[y2,x2]=min(abs(S-V0));
x2=x2+x1+d/10-1
y2
S=S1(x2+d/10:xe);
[y3,x3]=min(abs(S-V0));
x3=x3+x2+d/10-1
y3
t=x1:x3;
hold on
S1(x1)=V0;
S1(x2)=V0;
```

```
S1(x3)=V0;
fill(t,S1(x1:x3),'r')
set(gcf,'Position',[0 0 550 300])
set(gca,'FontSize',12);
set(gca,'Position',[0.25 0.15 0.7 0.815])
set(gca,'XTick',[0 500 1000 1500 2000])
line([0 2000],[2400 2400])
clear
```

H.5.17 SenceCoilAngle.m

```
%sensitivity of serch coil to its angle
clc
clear all
close all
%%%%%%Flag%%%%%%Flag%%%%%%Flag
Figure2ToMulti='n';
PlotSpectra='n';
PlotSpectraVariation='n';
%%%%%%%%%%%%%%%%%%%%%%%%%%%%%
B0=1.5;
Beta=3e-8;
th0=1e-5;               %rad vibration angle of B
Tra0=12e-6;             %10 micro meter displacement
Grd=7e-3;               %4mT/m magnetic gradient
frq=20;                       %structural vibration frequancy (Hz)
T0=1/frq;               %sampling period
Af=frq*2*pi;            %structural vibration frequency (rad)
T=20*T0;                                %simulation period
N1=1024;                                %sampling number
t=linspace(0,T,N1);           %discrete sampling time
dTs=T/(N1-1);                       %sampling period
Fs=1/dTs;                           %Nyquist frequency
Ntp=round(2*T0/dTs);          %2*T0, ploting period of signal
N2=N1/2;                                %
Fp=50;      %Hz                     %maximum ploting frequency
NFp=round(Fp/Fs*N1+0.5);%
ft=(0:N2-1)/N1*Fs;            %ploting frequency ranging

Sin1=sin(Af.*t);        %
Cos1=cos(Af.*t);

i=0;
c=['k' 'r' 'b' 'g' 'y' 'm' 'k' 'r'];
thS=[0 1000 2000 3000 4000 5000 6000 ]*th0/1;   %orientation
theta_s=0.0;                  %degree
thS=thS+theta_s*pi/180;


n=size(thS);
```

```
PofY=zeros(1,n(2));
IofY=PofY;
PofZ=zeros(1,n(2));
IofZ=PofZ;
PofFFT1=zeros(1,n(2));
IofF1=PofFFT1;
PofFFT2=zeros(1,n(2));
IofF2=PofFFT2;
PofP=zeros(1,n(2));
IofP=PofP;
PofTr=zeros(1,n(2));
IofTr=PofTr;


for th1=thS
   i=i+1;
%%Z-axis
V=-Cos1.*(Beta-B0*th0*th1-B0*th0*th0*Sin1);
V=V;
   figure(1);
   plot(t(1:Ntp),V(1:Ntp),c(i))
   [Y I]=max(V(1:fix(Ntp/1.5)));
   PofZ(i)=Y;
   IofZ(i)=th1;
   format long
   text(t(I),Y,['\leftarrow    \theta_s= '
num2str(th1*180/pi,2)],'FontSize',18);
   hold on;
%%Y-axis
V1=Cos1.*(Beta.*th1+Beta.*th0.*Sin1+th0.*B0);
V1=V1;
   [YV1 I]=max(V1(1:Ntp))
      PofY(i)=YV1;
      IofY(i)=th1;

   n=1;
      if Figure2ToMulti=='y'
      n=i;
   end

   figure(1+n);                %Figure 2

   plot(t(1:Ntp),V1(1:Ntp),c(i))

   hold on;


   format
   %%%%%%FFT Spectra%%%%%%Spectra
   F=fft(V);
   FF=abs(F)/N2;
   iF1=round(frq/Fs*N1+0.5);
   PofFFT1(i)=FF(iF1);

   iF2=round(frq*2/Fs*N1+0.5);
   PofFFT2(i)=FF(iF2);
```

```
    if PlotSpectra=='y'
    figure(i+2)
    plot(ft(1:NFp),FF(1:NFp),c(i))
    xlabel(['Frequency (Hz) ( \theta_0=' num2str(th0) '  \Omega=2\pi*'
num2str(frq) 'rad )  \theta_s= ' num2str(th1)])
       end
    %%%%%%%%%%%%% translatin%%%%%%%%
    Tran=cos(Af.*t)*Af*Tra0*Grd*cos(th1);
    [PofTr(i) I]=max(Tran);
    figure(30)
    plot(t(1:Ntp),Tran(1:Ntp),c(i))
    hold on
end

%%%%%%%%%%%%%%%%%%%%%%%%%%
figure(2)


text(t(1),YV1,['\leftarrow  all the curves are overlapped']);
Le=length(thS);
for I=1:Le
   text(t(1),YV1-2*YV1/Le*I,['     \theta_s= '...
         num2str(thS(I)*180/pi,2) ', V=' num2str(YV1,4)]);
end




figure(1)
title('Simulation of induced signal in search coil','FontSize',18)
xlabel(['Time (s) ( \theta_0=' num2str(th0) '  \Omega=2\pi*'
num2str(frq) 'rad )'],'FontSize',18)
ylabel('Induced voltage','FontSize',18)
set(gca,'FontSize',16)


figure(2)
title('Induced signal in vertical search coil','FontSize',18)
xlabel(['Time (s) ( \theta_0=' num2str(th0) '  \Omega=2\pi*'
num2str(frq) 'rad )'],'FontSize',18)
ylabel('Induced magnetic field','FontSize',18)
set(gca,'FontSize',16)
%%%%%%%%%%plot signal peaks of Y seach coil%%%%%%
figure(20)
thD=thS*180/pi;
plot(thD,PofY,'k')
a=max(PofY)-min(PofY);
axis([min(thD) max(thD) min(PofY) max(PofY)+a/10]);

title('Signal changes of a vertical search coil','FontSize',18)
xlabel(['Orientatin of the search coil,\theta_s (degree) (\theta_0='
num2str(th0) ')'],'FontSize',18)
ylabel('Induced signal Y(\theta_s)','FontSize',18)
set(gca,'FontSize',16)
n=size(thS);
text(thD(2)+(max(thD)-min(thD))/5,PofY(2),['\Delta%=[Y(\theta_s)-
Y(0)]/Y(0)'],'FontSize',18)
```

```
text(0,PofY(1)-a(1)/2,['  Y(0)=' num2str(Y(1),16)],'FontSize',18)
n=size(thS);
for i=1:n(2)
   text(thD(i),PofY(i),['\leftarrow ' num2str((PofY(i)-
PofY(1))/PofY(1)*100,3) '%'],'FontSize',16)
end

%%%%%%%%%%plot signal peaks of Z seach coil%%%%%%
figure(21)
thD=thS*180/pi;
plot(thD,PofZ,'k')
hold on
a=zeros(1,length(thD))+Beta;
plot(thD,a,'--b');
title('Axial search coil readings','FontSize',18)
xlabel('Orientation angle of search coil,\theta_s
(degree)','FontSize',18)
ylabel('Induced signal Y(\theta_s)','FontSize',18)
set(gca,'FontSize',16)

n=size(thS);

%%%%%%%%%%plot spectra variation due to search coil orientation
thD=thS*180/pi;
if PlotSpectraVariation=='y'
figure(22)
thD=thS*180/pi;
subplot(2,1,1)
plot(thD,PofFFT1,'k')
title('Susceptibility of axial search coil to the orientation')
ylabel(['Magnitude of ' num2str(frq) ' Hz'])

subplot(2,1,2)
plot(thD,PofFFT2,'r')
xlabel(['Search coil orientation,\theta_s( ^o ) ( \theta_0='...
      num2str(th0) '  \Omega=2\pi*' num2str(frq) 'rad )'])
ylabel(['Magnitude of ' num2str(frq*2) ' Hz'])
ymax=max(PofFFT2);
ymin=min(PofFFT2);
y11=ymin+4*(ymax-ymin)/5;
format
text(0,y11,['  max-min=' num2str(ymax-ymin) '=' ...
      num2str((ymax-ymin)/ymin*100) '%']);
y11=ymin+1.5*(ymax-ymin)/5;
text(0,y11,['  min=' num2str(ymin,10)]);

hold off

end


%%%%%signal due to gradient%%%%%%
figure(30);
title('Gradient induced signal');
ylabel('induced signal')
xlabel(['Time (s) ( d_0=' num2str(Tra0*1e6,2) '\mum,'...
      '\Omega=2\pi*' num2str(frq,3) 'rad )'])
```

```
%%%%%%%%%compare rotation%%%%%%%
figure(31);
subplot(2,1,1)
thD=thS*180/pi;
plot(thD,PofY,'k')
a=max(PofY)-min(PofY);
axis([min(thD) max(thD) min(PofY) max(PofY)+a/10]);

title('Signal due to magnetic filed rotation(z-axis)')
ylabel('Amplitude of signal')

subplot(2,1,2)
plot(thD,PofTr);

title('Signal due to magnetic gradient and translation')
xlabel(['search coil orientation,' ...
   '\theta_s(^o) (rotation:\theta_0=' num2str(th0)...
      ',translation:d_0=' num2str(Tra0*1e6,2) '\mum,'...
      '\Omega=2\pi*' num2str(frq,3) 'rad )'])
```

H.5.18 SenseProbeEcho.m

```
%%%%%%Sensitivities with different echo time
echo off
clc
clear
close all

f=0:0.5:100;
%f(1)=eps;
Om=f*2*pi;
Si=linspace(0,2,100)*pi;
Si0=0;
Gama=2.675e8;
dB=17e-9/2;
aa=5.73;          %compensation
dB=dB/aa*3.45;
C=Gama*dB*180/pi;
C=1/4;
Te40=0.04;
Te60=0.06;
Te80=0.08;
N=length(Om);
Pk=Om;

%%%%%%Sensitiveity of peak to peak
for n=1:N
   O=Om(n);
```

```
    %CC=C./O;
    CC=C;
    Dis=CC.*(2.*sin(O*Te40/2+Si)-sin(O*Te40+Si)...
        -sin(Si));
    Pk40(n)=max(Dis);%-min(Dis);
    %Dis=C/O
    Dis=CC.*(2.*sin(O*Te60/2+Si)-sin(O*Te60+Si)...
        -sin(Si));
    Pk60(n)=max(Dis);%-min(Dis);

    Dis=C/O.*(2.*sin(O*Te80/2+Si)-sin(O*Te80+Si)...
        -sin(Si));
    Pk80(n)=max(Dis)-min(Dis);
end

figure(1)
CCC=1;
H1=plot(f,Pk40*CCC,'k');
set(H1,'LineWidth',1);
hold on
H2=plot(f,Pk60*CCC,':b');%,f,Pk80,'r')
set(H2,'LineWidth',1);
legend('T_E=40ms','T_E=60ms')

set(gcf,'Position',[0 0 400 200])
%%%%%%%%%%%%%%%%%%%%%%%%%%%%%%%%%
ccc=8;
Sen40=Pk40./Om*ccc;
Sen60=Pk60./Om*ccc;
figure(2)
H1=plot(f,Sen40,'k');
set(H1,'LineWidth',1);
hold on
H2=plot(f,Sen60,':k');%,f,Pk80,'r')
set(H2,'LineWidth',1);
a=get(gca,'Position')
set(gcf,'Position',[0 0 270 140])
set(gca,'Position',[a(1)*1.5 a(2:4)])
set(gca,'XTick',[0 25 50 75 100])
set(gca,'YTick',[0 0.02 0.04 0.06 0.08 0.10])
legend('T_E=40ms','T_E=60ms')

%set(gcf,'Position',[0 0 400 200])
```

H.5.19 TransRot.m

```
%%%%%%%%%%%%%%%% NMRREL.M %%%%%%%%%%%%%%%%%%%%%%%%%%%%%%%%
% Produce data of Relative translations and rotations %
% between different parts of a cryostat                 %
%%%%%%%%%%%%%%%%%%%%%%%%%%%%%%%%%%%%%%%%%%%%%%%%%%%%%%%%%%%
clear;clc;close all
```

```
%%%%%%%%%%%%%%%%%%%%%%%%%%%%%%%%%%%%%%%
SourcePath='..\data\NMR\mat\Adjusted\';
DestinationPath='..\data\NMR\mat\Adjusted\';
%%%%%%%%%%%%%%%%%%%%%%%%%%%%%%%%%%%%%%%%%%%%%%
% destination file names      are composed as    %
% ['Rel' TR{i} 'F' Ff{j} '.mat']                            %
%%%%%%%%%%%%%%%%%%%%%%%%%%%%%%%%%%%%%%%%%%%%%%
Ff=[{'08'} {'19'} {'39'}];    %frequencies
SN=[{'HecX'} {'20KX'}];
TR=[{'Tr'} {'Ro'}];     %prefixes of destination file names

dTs=0.002;         %sampling period
Ns=4096;
IRef=9;
Delay=0;
Unit=20;                    %micrometers
PEtoSE=1.25;       %meters
for NFRQ=1:3
   for n=1:2
      SFname=[TR{n} SN{1} 'F' Ff{NFRQ} ...
            '.mat'];
      load([SourcePath SFname])
      x1=x;

      SFname=[TR{n} SN{2} 'F' Ff{NFRQ} ...
            '.mat'];
      load([SourcePath SFname])
      x2=x;
      clear x
      L=min(length(x1),length(x2));
      x1=x1(1:L);
      x2=x2(1:L);

      x=(x1-x2);
      DestinationFileName=['Rel' TR{n} 'F' Ff{NFRQ} ...
            '.mat']
      save([DestinationPath DestinationFileName],'x','Delay');
   end

end
```

H.5.20 UnderSamp.m

```
%%%%%%%%Undersamp.m %%%%%%%%%%%%
% Calculate frequency ranges of spikes
% in different repetetin times
%%%%%%%%%%%%%%%%%%%%%%%
clear all
clc
close all
%%%%%%%%%%%%%%%%%%%%%%%
```

```
Kk=11;

Tr=[
   0.191    0.192
   0.197    0.198
%   0.219   0.220
];

Y=[0.2:0.2:1];
C={'k'} {'r'} {'g'} {'y'} {'b'}];
[n m]=size(Tr);


Overlap=zeros(Kk*2,2);
figure
set(gca,'XLim',[0 65]);
for k=1:Kk

   for nTr=1:n
      x1=k/Tr(nTr,2);
      x2=k/Tr(nTr,1);
      x=[x1 x2 x2 x1];
      y=[0 0 Y(nTr) Y(nTr)];
      fill(x,y,'g')%C(nTr));
      n0=k*n*2+nTr*2-n*2;
      Overlap(n0-1,1)=x1;
      Overlap(n0-1,2)=x2;
      hold on

      x1=(k+0.5)/Tr(nTr,2);
      x2=(k+0.5)/Tr(nTr,1);
      x=[x1 x2 x2 x1];
      y=[0 0 Y(nTr) Y(nTr)];
      fill(x,y,'g')%C(nTr));
      Overlap(n0,1)=x1;
      Overlap(n0,2)=x2;
      hold on
   end
end
set(gca,'TickDir','out');

save 'Ovlap.txt' Overlap -ASCII
```

References

1. HENNEL, J.W. and KLINOWSKI, J. (1993). *Fundamentals of Nuclear magnetic Resonance*. Longman Scientific & Technical, England.
2. CALLAGHAN, P.T.(1995). *Principles of Nuclear Magnetic Resonance Microscopy*. Lcarendon Press, Oxford.
3. THOMSON, W.T. (1993 forth edition). *Theory of Vibration whith Applications*. Chapman & Hall, London.
4. NEWLAND, D.E. (1993). *An Introduction to Random Vibrations, Spectral & Wavelet Analysis*. Longman Scientific & technical, England.
5. ZAHN, Markus (1979). *Electromagnetic Field theory, a problem solving approach*. John Wiley & Sons, Inc., USA.
6. SMYTHE, William R. (1968). *Static and Dynamic electricity*. McGrow-Hill, London.
7. CHORLTON, F. (1969). *Boundary Value Problems in Physics and Engineering*. Van Nostrand reinhold.
8. ERNST, Richard R.(1991). *Principles of Nuclear Magnetic Resonance in One and Two Dimensins*. Clarondon Press, Oxford, UK.
9. EDWARD, J., HAUG (1992). Intermediate Dynamics. Englewood Cliffs, N.J.
10. TAYLOR, N.J., DOYLE V.L., FOX R.A. and LEACH M.O. (1998). *A Simple Phantom to Locate The Origin of MRI Ghost Artefacts*. Magnetic Resonance Imaging, Vol. 16, No. 1, pp 73-76.
11. SIJBERS, J., DEKKER, A.J., and AUDEKERKE J. (1998). *Estimation of the Noise in Magnitude MR Images*. Magnetic Resonance Imaging, Vol. 16, No. 1, pp 87-90.
12. HORNAK, Joseph P. (1996). *The Basics of MRI*. http://www.cis.rit.edu/htbooks/mri.

13. HANS-JORGEN SMITH, M.D. (1989). *A Non-mathematical Approach to Basic MRI.* Medical Physics Publishing Corporation, Madison, Wisconsin.

14. SHAW, Derek (1984). *Fourier Transform NMR Spectroscopy.* Elsevier Science Publishers, New York.

15. RAO, Signiresu S. (1995). *Mechanicl Vibrations.* Addison-Wesley Publishing Company.

16. CHENG, David K. (1989). *Field and Wave Electromagnetics.* Addison-Wesley Publishing Company, Inc.

17. KORENEV, Boris G. and REZNIKOV, Leonid M. (1993). *Dynamic Vibration Absorbers-Theory and Technical applications.* John Wiley & sons Ltd., England.

18. BEARDS, C.F. (1996). *Structural Vibration-Analysis and Damping.* Arnold, a member of the Hodder Headline Group.

19. CHARI, M.V.K. and SILVESTER, P.P. (1980). *Finite Elements in Electrical and Magnetic Field Problems.* John Wiley & Sons.

20. ZHOU, Pei-bai (1993). *Numerical Analysis of Electromagnetic Fields.* Springer-Verlag Berlin Heidelberg. Printed in USA.

21. STEEL, Charles W.(1997). *Numerical Computation of Electric and Magnetic Fields.* Chapman &Hall, ITP International Thomson Publishing. Printed in USA.

22. JOHN,K Carl T.A. (1975). *Engineering Electromagnetic Fields & Waves.* John Wiley & Sons, Inc. Printed in USA.

23. JIN, Jianming (1998). *Electromagnetic analysis and design in Magnetic resonance Imaging.* CRC Press.

24. HENDRICX, Wim and SEGERS Luc (1 July 1998). OMT Vibration Analysis Cryogenic Magnet Experimental Analysis, Report. LMS International.

25. HENDRICX, Wim, DAMME Koen and SEGERS Luc (29 April 1998). OMT Vibration Analysis Cryogenic Magnet Intermediate Report. LMS International.

26. DEWDNEY, Andrew (1996). *NMR Phase Variation Measurements*, Report No:S/02/001. Oxford Magnet Technology Ltd.

27. DEWDNEY, Andrew (1996). *NMR Phase Data on OR71*, Report No:S/02/002. Oxford Magnet Technology Ltd.

28. DEWDNEY, Andrew (1996). *OR24 Twin Turret Data in K4/6*, Report No:S/02/003. Oxford Magnet Technology Ltd.
29. DEWDNEY, Andrew (1998). *Site Measurements at Oldchurch and Lens*, Report No:S/02/005. Oxford Magnet Technology Ltd.
30. DEWDNEY, Andrew (1997). *Phase Angle & Ghosting Correlation with Picker*, Report No:S/02/006. Oxford Magnet Technology Ltd.
31. DEWDNEY, Andrew (1997). *Phase Angle & Ghosting Correlation*, Report No:S/02/007. Oxford Magnet Technology Ltd.
32. DEWDNEY, Andrew (1997). *Phase Angle Measurements on Site (Part I)*, Report No:S/02/008. Oxford Magnet Technology Ltd.
33. DEWDNEY, Andrew (1997). *Magnet Vibrational Modes and Phase Angle Frequency Response*, Report No:S/02/009. Oxford Magnet Technology Ltd.
34. DEWDNEY, Andrew (1997). *Phase Angle Measurements on Site (Part II)*, Report No:S/02/010. Oxford Magnet Technology Ltd.
35. THEIN, H. (1997). *The Effect of the Turrent Heater Band (and PSU) on Imag Quality*, Report No:S/02/011. Oxford Magnet Technology Ltd.
36. DEWDNEY, Andrew (1997). *IAG Calibration and Acceptance Criteria*, Report No:S/02/012. Oxford Magnet Technology Ltd.
37. DEWDNEY, Andrew (1997). *Phase Angle Variation Across the Imaging Volume*, Report No:S/02/013. Oxford Magnet Technology Ltd.
38. DEWDNEY, Andrew (June 1998). *JR 3T 905 Stability Assessment – Part I*, Report No:S/02/014. Oxford Magnet Technology Ltd.
39. DEWDNEY, Andrew (1998). *The Influence of Bore Diameter on Phase Angle Instability*, Report No:S/02/015. Oxford Magnet Technology Ltd.
40. DEWDNEY, Andrew (1998). *Magnet Vibration Measurement using an NMR Phase Variation Method*, Report No:S/02/016. Oxford Magnet Technology Ltd.
41. DEWDNEY, Andrew (1998). *Low Frequency Whole Body Resonances*, Report No:S/02/017. Oxford Magnet Technology Ltd.
42. BYRNE, A. (1996). *Eddy Current Production as a Source of Phase Angle Shifts due to Vibration in OR71*, Report No:C/019/002. Oxford Magnet Technology Ltd.

43. RAYNER, Edgar (1996). *Structural Dynamic Analysis of an OR71 Magnet System*, Report No:C/019/003. Oxford Magnet Technology Ltd.
44. BYRNW, Alex (1996). *OR71 Mobile Vibration Analysis*, Report No:C/19/007. Oxford Magnet Technology Ltd.
45. RATTY, William (1997). *Vibration across a Cold Head Turret Anti-vibration Mount*, Report No:C/19/009. Oxford Magnet Technology Ltd.
46. SCHNUR, (22 Jan 1992). *Cold head vibratin and Imaging Artifatts.* Memo. SME51, Siemens.
47. SCHNUR, (09 Aug 1994). *Spot Test: Modified OR42 System (Landshut/Germany)*, Report No:C/19/010. Oxford Magnet Technology Ltd.
48. SCHNUR, (01 Mar 1996). *H52 Impact/Expert on Vibration Isolatorsibration*, Report No:C/19/010. Oxford Magnet Technology Ltd.
49. WEIBENBERGER, Volker (21 Mar 1996). *Cold Head Artifacts at K4/6*, Report No:C/19/010. Oxford Magnet Technology Ltd.
50. WEIBENBERGER, Volker (29 Mar 1996). *Cold Head Artifacts at K4/1 (OR70)*, Report No:C/19/010. Oxford Magnet Technology Ltd.
51. SCHNUR, (17 Jun 1996). *CTI Cold Head on H52 Impact/Expert*, Report No:C/19/010. Oxford Magnet Technology Ltd.
52. SCHNUR, (24 Jun 1996). *Cold Head Artifacts at (at K4/6)/Further Results/Part 1*, Report No:C/19/010. Oxford Magnet Technology Ltd.
53. SCHNUR, (25 Jun 1996). *Leybold Cold Head on OR41 Magnets*, Report No:C/19/010. Oxford Magnet Technology Ltd.
54. SCHNUR, (26 Jun 1996). *Shock Sensitivity of Magnets-a comparison between new and old magnet designs*, Report No:C/19/010. Oxford Magnet Technology Ltd.
55. SCHNUR, (27 Jun 1996). *Cold Head Artifacts (at K4/1 OR70)/Further Results/Part 2*, Report No:C/19/010. Oxford Magnet Technology Ltd.
56. SCHNUR, (05 Jul 1996). *Cold Head Artifacts (at K4/6 OR24)/Further Results/Part 3*, Report No:C/19/010. Oxford Magnet Technology Ltd.
57. SCHNUR, (17 Jul 1996). *Cold Head Vibration Problems on OR71 Magnet (at K4/6*, Report No:C/19/010. Oxford Magnet Technology Ltd.

58. WEIBENBERGER, Volker (21 Aug 1996). *Spectrum of Cold Head Field Instabilities at K4/6*, Report No:C/19/010. Oxford Magnet Technology Ltd.

59. WEIBENBERGER, Volker (10 Sep 1996). *Spectrum of Cold Head Field Instabilities at K4/1 (OR70)*, Report No:C/19/010. Oxford Magnet Technology Ltd.

60. RATTY, W. (1998). *OR70 #12, Buid, Vibration Results, Cut Out*, Report No:C/19/026. Oxford Magnet Technology Ltd.

61. STEVENS, G. (1998). *Investigation of the Structural Dynamics of the OMT OR24 Bodyscanner Magnet System*, Report No:C/19/029. Oxford Magnet Technology Ltd.

62. RATTY, W. (1998). *OR91-Pneumatically Damped Cold Head*, Report No:C/19/035. Oxford Magnet Technology Ltd.

63. JONES, Ian (1998). *Anti-vibration Bed for the Transportation of MRI Systems*, Report No:C/19/037. Oxford Magnet Technology Ltd.

64. BARNES, Stuart (1998). *Laser Measurements and Phase Angle Measurements of System OR70#142 and OR70#151*, Report No:C/19/039. Oxford Magnet Technology Ltd.

65. TOYER , J.T. (1996). , Report No:K/01/035. Oxford Magnet Technology Ltd.

66. HAWKSWORTH, David (1990). *OR46 magnet Homogeneity*, Report No:B/08/017. Oxford Magnet Technology Ltd.

67. SHAIKH, A.A. (1991). *Homogeneity Issues*, Report No:B/08/042. Oxford Magnet Technology Ltd.

68. ZHOU, Youhe and MIYA, Kenzo (March 1998). *A Theoretical Prediction of Natural Frequency of a Ferromagnetic Beam Plate with Low Susceptibility in an In-plane Magnetic Field*. Journal of Applied Mechanics, Vol. 65, pp 121-126.

69. TAKIZAWA, T. and SONOBE, T. (1997). *Development of a High Rigidity Superconducting Magnet for the Maglev System*. Cryogenics, Vol. 37, No. 12, pp 777-781.

70. VOLD, Robert L. and VOLD, Regitze R. (1978). *Nuclear Magnetic Relaxation in Coupled Spin systems*. Progress in NMR Spectrometer Vol. 12 pp79-133, printed in Great Britain.

71. BELMONTE, S.B., OLIVEIRA, I.S. and GUIMARAES A.P. (1998). *Graphical Programming for Pulse Automated NMR Experiments.* Measurement Science & Technology. Vol 9 pp1951-1955, printed in the UK.

72. SIEMENS AG BMed. *Magnets, Spins, and Resonances, --An Introduction into the Basics of Magnetic Resonace Imaging.* Siemens, Germany.

73. TEGOPOULOS, J.A. and KRIEZIS, E.E. (1985). *Eddy currents in Linear Conducting Media.* Elsevier Science Publishers, New York.

74. BLOCH, F. (1946). *Nuclear Induction.* Physics Review. Vol. 70, pp460-474.

75. PERCELL, E.M., TORREY, H.C., POUND R.V. (1946). *Resonance Absorption by Nuclear Magnetic Moments in a Solid.* Physics Review. Vol. 69, pp37-83.

76. LAUTERBUR, P.C. (1973). *Image Formation by Indece Local Interactions: Examples employing Nuclear magnetic Resonance.* Nature Vol. 242, pp190-191.

77. CALLAGHAN, Paul T. (1995). Principles of Nuclear magnetic Resonance Microscopy. Oxfort University Press Inc., New York.

78. CHEN, C.H. (1988).Signal Processing Handbook. Marcel Dekker, Inc., New York.

79. GREENWOOD, Donaldt (1988). *Principles of Dynamics.* Prentice-Hall International (UK) Ltd., London.